

---

# Impacts of C<sub>1</sub>-C<sub>3</sub> alkyl nitrates on tropospheric ozone chemistry

---

A thesis submitted to the  
**School of Environmental Sciences**  
of the  
**University of East Anglia**  
in partial fulfilment of the requirements for the degree of  
**Doctor of Philosophy**

**Maria Zamyatina**  
**April 2020**

© This copy of the thesis has been supplied on condition that anyone who consults it is understood to recognise that its copyright rests with the author and that use of any information derived there from must be in accordance with current UK Copyright Law. In addition, any quotation or extract must include full attribution.



# Abstract

Alkyl nitrates (RONO<sub>2</sub>) are important reservoirs of tropospheric reactive nitrogen. They are produced from the oxidation of their parent alkanes (RH) in the presence of NO<sub>x</sub> and emitted from oceanic and biomass burning sources. Due to their relatively long lifetime of a few days to a few months, alkyl nitrates can be destroyed far away from their sources by photolysis or OH oxidation and alter regional tropospheric ozone concentrations.

While C<sub>1</sub>-C<sub>3</sub> RONO<sub>2</sub> chemistry is well understood, information about their oceanic and biomass burning sources is limited. We derived a new estimate of C<sub>1</sub>-C<sub>3</sub> RONO<sub>2</sub> biomass burning emissions from the Global Fire Emissions Database and implemented these emissions into a global 3D chemistry-climate model UM-UKCA, along with C<sub>1</sub>-C<sub>3</sub> RONO<sub>2</sub> chemistry from the Master Chemical Mechanism, dry deposition and oceanic emissions.

We performed six perpetual year UM-UKCA simulations designed to explore the statistical significance of the global and localised impacts of C<sub>1</sub>-C<sub>3</sub> RONO<sub>2</sub> on tropospheric ozone chemistry. We also compared the regional mean vertical profiles of C<sub>1</sub>-C<sub>3</sub> RH and RONO<sub>2</sub>, NO<sub>x</sub> and O<sub>3</sub> observed during the Atmospheric Tomography mission and simulated by UM-UKCA in 8 remote regions in February and August.

We found that C<sub>1</sub>-C<sub>3</sub> RONO<sub>2</sub> oceanic emissions have the largest global impact on tropospheric ozone chemistry among all alkyl nitrate sources considered in this study, while their biomass burning emissions have the smallest impact. The combination of C<sub>1</sub>-C<sub>3</sub> RONO<sub>2</sub> chemistry and emissions increases tropospheric ozone burden by 2.96±0.69 Tg (1.09±0.25%) and decreases methane lifetime by 0.151±0.036 yr (1.56±0.37%). Statistically significant increases in the seasonal mean ozone concentrations of up to 2 ppbv (≤5%) are located within 0-5 km over the Southern Ocean during boreal winter and autumn and within 0-10 km near the equator during boreal winter, summer and autumn.





# Contents

<b>Abstract</b>	<b>iii</b>
<b>Contents</b>	<b>v</b>
<b>List of Figures</b>	<b>ix</b>
<b>List of Tables</b>	<b>xiii</b>
<b>Acknowledgements</b>	<b>xv</b>
<b>1 Introduction</b>	<b>1</b>
1.1 Composition of the atmosphere . . . . .	1
1.2 Role of ozone in the atmosphere . . . . .	2
1.3 Tropospheric ozone chemistry . . . . .	3
1.4 Alkyl nitrates . . . . .	6
1.4.1 Primary sources . . . . .	8
Oceanic sources . . . . .	8
Biomass burning sources . . . . .	9
1.4.2 Secondary sources . . . . .	10
1.4.3 Sinks and lifetimes . . . . .	12
1.4.4 Temporal variability . . . . .	15
Seasonal cycle . . . . .	15
Diel cycle . . . . .	17
1.4.5 Spatial variability . . . . .	17
1.4.6 Modelling . . . . .	19
1.5 Thesis justification and structure . . . . .	20
1.5.1 Scientific rationale . . . . .	20
1.5.2 Thesis aims . . . . .	21
1.5.3 Thesis outline . . . . .	21
<b>2 Chemical mechanism development</b>	<b>23</b>
2.1 Introduction . . . . .	23
2.2 Description of chemical mechanisms . . . . .	24
2.2.1 Master Chemical Mechanism . . . . .	24
2.2.2 CheT chemical mechanism . . . . .	26

2.3	Protocol for comparison of chemical mechanisms . . . . .	28
2.3.1	Overview of previous studies . . . . .	28
2.3.2	Box model setup . . . . .	31
2.3.3	Experiment setup . . . . .	32
2.4	Revision, unification and comparison of chemical mechanisms . . . . .	34
2.4.1	Revision . . . . .	34
2.4.2	Unification . . . . .	35
2.4.3	Comparison . . . . .	36
	Inorganic chemistry . . . . .	37
	Inorganic + methane chemistry . . . . .	37
	Inorganic + C <sub>1</sub> -C <sub>2</sub> alkane chemistry . . . . .	37
	Inorganic + C <sub>1</sub> -C <sub>3</sub> alkane chemistry . . . . .	38
2.4.4	Outcome of the revision and unification of chemical mechanisms	43
2.5	Adding C <sub>2</sub> -C <sub>3</sub> alkyl nitrate chemistry . . . . .	44
2.6	Summary . . . . .	46
<b>3</b>	<b>UM-UKCA model development and validation</b>	<b>47</b>
3.1	Introduction . . . . .	47
3.2	UM-UKCA model description . . . . .	48
3.2.1	Dynamics and chemistry . . . . .	48
3.2.2	C <sub>1</sub> -C <sub>3</sub> alkyl nitrate photolysis . . . . .	51
3.2.3	C <sub>1</sub> -C <sub>3</sub> alkyl nitrate oceanic emissions . . . . .	51
3.2.4	C <sub>1</sub> -C <sub>3</sub> alkyl nitrate biomass burning emissions . . . . .	55
3.3	UM-UKCA model validation . . . . .	58
3.3.1	Description of Atmospheric Tomography mission (ATom) . . . . .	58
3.3.2	Comparison of ATom and UM-UKCA vertical profiles . . . . .	59
3.3.3	Results . . . . .	61
	Methane . . . . .	61
	Ethane . . . . .	63
	Propane . . . . .	66
	Nitrogen oxides . . . . .	66
	Ozone . . . . .	68
	Methyl nitrate . . . . .	68
	Ethyl nitrate . . . . .	73
	Propyl nitrates . . . . .	76
3.4	Summary . . . . .	79
<b>4</b>	<b>Impact of C<sub>1</sub>-C<sub>3</sub> alkyl nitrates on tropospheric ozone chemistry</b>	<b>81</b>
4.1	Introduction . . . . .	81
4.2	Global impact of alkyl nitrates . . . . .	83
4.2.1	CHEM . . . . .	84

4.2.2	MARI . . . . .	84
4.2.3	FIRE . . . . .	86
4.2.4	FULL . . . . .	86
4.3	Localised impacts of alkyl nitrates . . . . .	92
4.3.1	Statistical analysis . . . . .	92
4.3.2	Impact of C <sub>1</sub> -C <sub>3</sub> alkyl nitrate photochemical production . . . . .	92
4.3.3	Impact of C <sub>1</sub> -C <sub>3</sub> alkyl nitrate oceanic emissions . . . . .	93
4.3.4	Impact of C <sub>1</sub> -C <sub>3</sub> alkyl nitrate biomass burning emissions . . . . .	93
4.3.5	Impact of C <sub>1</sub> -C <sub>3</sub> alkyl nitrate photochemical production and direct emissions . . . . .	93
4.4	Summary . . . . .	100
<b>5</b>	<b>Synthesis and conclusions</b>	<b>103</b>
5.1	Future work . . . . .	105
<b>6</b>	<b>Contribution to the OXBUDS project</b>	<b>107</b>
<b>A</b>	<b>Appendix to Chapter 1</b>	<b>109</b>
<b>B</b>	<b>Appendix to Chapter 2</b>	<b>115</b>
B.1	Figures . . . . .	116
B.2	Code . . . . .	124
B.3	MCM-CheT reaction comparison . . . . .	127
<b>C</b>	<b>Appendix to Chapter 3</b>	<b>141</b>
	<b>Bibliography</b>	<b>163</b>



# List of Figures

1.1	Simplified mechanism for the photochemical oxidation of an alkane in the troposphere . . . . .	5
1.2	Atmospheric loss rate constants for MeONO <sub>2</sub> , EtONO <sub>2</sub> and iPrONO <sub>2</sub> as a function of altitude due to OH oxidation and photolysis . . . . .	14
1.3	Photolysis rates of iPrONO <sub>2</sub> as a function of zenith angle at several altitudes calculated using 298 K and temperature dependent cross sections . . . . .	14
1.4	Seasonal cycle and annual mean C <sub>1</sub> -C <sub>5</sub> RONO <sub>2</sub> concentrations observed at different stations . . . . .	16
1.5	Annual mean distribution of MeONO <sub>2</sub> , EtONO <sub>2</sub> , nPrONO <sub>2</sub> and iPrONO <sub>2</sub> at different altitude ranges in GEOS-Chem . . . . .	18
2.1	Flow chart indicating the major reactions, intermediate classes and product classes considered in the MCM protocol . . . . .	25
2.2	Isopleths giving net rate of ozone production as a function of NO <sub>x</sub> and VOCs . . . . .	30
2.3	An example of different speeds of conversion of NO and NO <sub>2</sub> to HNO <sub>3</sub> in different chemical mechanisms . . . . .	31
2.4	Steady state box model schematic . . . . .	32
2.5	O <sub>3</sub> , O( <sup>1</sup> D), O( <sup>3</sup> P), OH, HO <sub>2</sub> and H <sub>2</sub> O <sub>2</sub> in steady state box model runs with the inorganic chemistry before unification . . . . .	39
2.6	As in Fig. 2.5 but after unification . . . . .	39
2.7	As in Fig. 2.5 but for the inorganic and CH <sub>4</sub> chemistry before unification . . . . .	40
2.8	As in Fig. 2.7 but after unification . . . . .	40
2.9	O <sub>3</sub> , OH and HO <sub>2</sub> in steady state box model runs with the inorganic, CH <sub>4</sub> and C <sub>2</sub> H <sub>6</sub> chemistry before unification . . . . .	41
2.10	As in Fig. 2.9 but after unification . . . . .	41
2.11	O <sub>3</sub> , OH and HO <sub>2</sub> in steady state box model runs with the inorganic, CH <sub>4</sub> , C <sub>2</sub> H <sub>6</sub> and C <sub>3</sub> H <sub>8</sub> chemistry before unification . . . . .	42
2.12	As in Fig. 2.11 but after unification . . . . .	42
2.13	Absolute and relative differences in the steady state O <sub>3</sub> , OH and HO <sub>2</sub> concentrations between the MCM and the CheT before and after the revision and unification from box model runs with the inorganic and C <sub>1</sub> -C <sub>3</sub> alkane chemistry . . . . .	43

3.1	$C_1$ - $C_3$ $RONO_2$ absorption cross sections at 298 K recommended by the IUPAC and JPL and the data used in UKCA . . . . .	51
3.2	Chlorophyll <i>a</i> concentrations in seawater from the OC-CCI dataset . . . . .	54
3.3	Total $C_1$ - $C_3$ $RONO_2$ oceanic emissions per year . . . . .	55
3.4	Total $C_1$ - $C_3$ $RONO_2$ biomass burning emissions per year . . . . .	57
3.5	ATom-1 and ATom-2 flight tracks . . . . .	59
3.6	ATom-1 and ATom-2 flight tracks and regions selected for the calculation of mean vertical profiles . . . . .	60
3.7	ATom and UM-UKCA $CH_4$ regional mean vertical profiles . . . . .	62
3.8	As in Fig. 3.7 but for $C_2H_6$ . . . . .	64
3.9	As in Fig. 3.7 but for $C_3H_8$ . . . . .	67
3.10	As in Fig. 3.7 but for $NO_x$ . . . . .	69
3.11	As in Fig. 3.7 but for $O_3$ . . . . .	70
3.12	As in Fig. 3.7 but for $MeONO_2$ . . . . .	72
3.13	As in Fig. 3.7 but for $EtONO_2$ . . . . .	75
3.14	As in Fig. 3.7 but for $nPrONO_2$ . . . . .	77
3.15	As in Fig. 3.7 but for $iPrONO_2$ . . . . .	78
4.1	The relative importance of peroxide, $RONO_2$ and $HNO_3$ formation as termination reactions . . . . .	82
4.2	$O_3$ production efficiency versus $NO_x$ concentration in a steady state box model . . . . .	82
4.3	Impact of $RONO_2$ chemistry on $NO_x$ export in the boundary layer and free troposphere . . . . .	82
4.4	Annual mean surface level distribution of $MeONO_2$ , $EtONO_2$ , $nPrONO_2$ and $iPrONO_2$ from STOCHEM-CRI BASE and UM-UKCA CHEM . . . . .	85
4.5	Annual mean distribution of $MeONO_2$ at different altitude ranges in GEOS-Chem and UM-UKCA . . . . .	87
4.6	As in Fig. 4.5 but for $EtONO_2$ . . . . .	88
4.7	As in Fig. 4.5 but for the sum of $nPrONO_2$ and $iPrONO_2$ . . . . .	88
4.8	Zonal cross sections of seasonal mean distribution of total $C_1$ - $C_3$ $RONO_2$ over the Pacific in GEOS-Chem and UM-UKCA . . . . .	89
4.9	Relative change in annual mean $NO_x$ , $NO_y$ , PAN and $O_3$ caused by adding $C_1$ - $C_3$ $RONO_2$ chemistry to GEOS-Chem and UM-UKCA . . . . .	90
4.10	Seasonal mean distribution of $O_3$ in the boundary layer in the UM-UKCA BASE and CHEM runs . . . . .	94
4.11	As in Fig. 4.10 but in the UM-UKCA BASE and MARI runs . . . . .	95
4.12	As in Fig. 4.10 but in the UM-UKCA SSAN and FIRE runs . . . . .	96
4.13	As in Fig. 4.10 but in the UM-UKCA BASE and FULL runs . . . . .	97
4.14	Zonal seasonal mean distribution of $O_3$ in the troposphere in the UM-UKCA BASE and CHEM runs . . . . .	98

4.15	As in Fig. 4.14 but in the UM-UKCA BASE and MARI runs . . . . .	98
4.16	As in Fig. 4.14 but in the UM-UKCA SSAN and FIRE runs . . . . .	99
4.17	As in Fig. 4.14 but in the UM-UKCA BASE and FULL runs . . . . .	99
A.1	Annual mean distribution of MeONO <sub>2</sub> and EtONO <sub>2</sub> at different altitude ranges in GEOS-Chem . . . . .	112
A.2	As in Fig. A.1 but for iPrONO <sub>2</sub> and nPrONO <sub>2</sub> . . . . .	113
B.1	As in Fig. 2.5 but for NO, NO <sub>2</sub> , NO <sub>3</sub> , HNO <sub>3</sub> , HONO, HO <sub>2</sub> NO <sub>2</sub> and N <sub>2</sub> O <sub>5</sub> before unification . . . . .	116
B.2	As in Fig. B.1 but after unification . . . . .	116
B.3	As in Fig. B.1 but for the inorganic and CH <sub>4</sub> chemistry before unification	117
B.4	As in Fig. B.3 but after unification . . . . .	117
B.5	CH <sub>3</sub> O <sub>2</sub> , HCHO, CH <sub>3</sub> OH and CH <sub>3</sub> OOH in steady state box model runs with the inorganic and CH <sub>4</sub> chemistry before unification . . . . .	118
B.6	As in Fig. B.5 but after unification . . . . .	118
B.7	As in Fig. 2.9 for HCHO, CH <sub>3</sub> OH and CH <sub>3</sub> OOH but before unification .	119
B.8	As in Fig. B.7 but after unification . . . . .	119
B.9	As in Fig. 2.9 but for C <sub>2</sub> H <sub>5</sub> OOH, CH <sub>3</sub> CHO and PAN before unification	120
B.10	As in Fig. B.9 but after unification . . . . .	120
B.11	As in Fig. 2.11 but for CH <sub>2</sub> O <sub>2</sub> , HCHO, CH <sub>3</sub> OH and CH <sub>3</sub> OOH before unification . . . . .	121
B.12	As in Fig. B.11 but after unification . . . . .	121
B.13	As in Fig. 2.11 but for C <sub>2</sub> H <sub>5</sub> OOH, CH <sub>3</sub> CHO and PAN before unification	122
B.14	As in Fig. B.13 but after unification . . . . .	122
B.15	As in Fig. 2.11 for C <sub>2</sub> H <sub>5</sub> CHO, CH <sub>3</sub> COCH <sub>3</sub> , C <sub>2</sub> H <sub>5</sub> CO <sub>3</sub> H and PPN but before unification . . . . .	123
B.16	As in Fig. B.15 but after unification . . . . .	123
C.1	Total C <sub>1</sub> -C <sub>3</sub> RONO <sub>2</sub> oceanic emissions per season . . . . .	142
C.2	Figure C.1 continued . . . . .	143
C.3	Total C <sub>1</sub> -C <sub>3</sub> RONO <sub>2</sub> biomass burning emissions per season . . . . .	144
C.4	Figure C.3 continued . . . . .	145
C.5	Total C <sub>1</sub> -C <sub>3</sub> RONO <sub>2</sub> oceanic and biomass burning emissions per season	146
C.6	Figure C.5 continued . . . . .	147
C.7	As in Fig. 3.7 but for C <sub>2</sub> H <sub>6</sub> and with differing x-axis . . . . .	148
C.8	As in Fig. 3.7 but for C <sub>3</sub> H <sub>8</sub> and with differing x-axis . . . . .	149
C.9	As in Fig. 3.7 but for NO <sub>x</sub> and with differing x-axis . . . . .	150
C.10	As in Fig. 3.7 but for nPrONO <sub>2</sub> and with differing x-axis . . . . .	151
C.11	As in Fig. 3.7 but for iPrONO <sub>2</sub> and with differing x-axis . . . . .	152





## List of Tables

1.1	Nomenclature of monofunctional alkyl nitrates and their parent alkanes . . . . .	7
1.2	Emission factors for species emitted from different types of biomass burning . . . . .	10
1.3	Kinetic data related to the formation of C <sub>1</sub> -C <sub>5</sub> RONO <sub>2</sub> from their parent alkanes . . . . .	11
1.4	Reaction rate coefficients and resultant lifetimes of C <sub>1</sub> -C <sub>5</sub> RONO <sub>2</sub> due to photolysis and OH oxidation . . . . .	14
1.5	Global 3D modelling studies of alkyl nitrates . . . . .	19
1.6	Implementation of processes that control C <sub>1</sub> -C <sub>3</sub> RONO <sub>2</sub> abundance in different global 3D modelling studies . . . . .	20
2.1	Chemical species in the tropospheric part of the CheST mechanism . . . . .	27
2.2	Steady state box model configuration . . . . .	32
2.3	C <sub>1</sub> -C <sub>3</sub> RONO <sub>2</sub> chemistry in UM-UKCA . . . . .	45
3.1	UM-UKCA 10-year perpetual year 2000 experiments for exploring the processes that control C <sub>1</sub> -C <sub>3</sub> RONO <sub>2</sub> abundance . . . . .	50
3.2	Emission factors for species emitted from different types of biomass burning . . . . .	56
3.3	Global oceanic and biomass burning C <sub>1</sub> -C <sub>3</sub> RONO <sub>2</sub> emissions per year . . . . .	58
3.4	Dates of ATom deployments . . . . .	58
3.5	Tropospheric interhemispheric annual mean OH ratio . . . . .	65
4.1	Percentage change in the annual mean tropospheric ozone burden and methane lifetime due to the addition of alkyl nitrate chemistry and/or direct emissions . . . . .	83
4.2	Global mean tropospheric ozone and methane burdens, methane lifetime and interhemispheric annual mean OH ratio . . . . .	100
4.3	Global mean tropospheric MeONO <sub>2</sub> , EtONO <sub>2</sub> , nPrONO <sub>2</sub> and iPrONO <sub>2</sub> burdens . . . . .	100
A.1	Aircraft and ship measurements of alkyl nitrates . . . . .	110
A.2	Ground-based measurements of alkyl nitrates . . . . .	111
B.1	Comparison of the MCM and CheT inorganic reactions and rate coefficients . . . . .	127
B.2	As in Table B.1 but for methane chemistry. . . . .	134
B.3	As in Table B.1 but for ethane chemistry . . . . .	137

B.4	As in Table B.1 but for propane chemistry . . . . .	138
C.1	Correlation coefficient, correlation of determination and root-mean-square error derived from a simple linear regression for CH <sub>4</sub> vertical profiles . .	153
C.2	As in Table C.1 but for C <sub>2</sub> H <sub>6</sub> . . . . .	154
C.3	As in Table C.1 but for C <sub>3</sub> H <sub>8</sub> . . . . .	155
C.4	As in Table C.1 but for NO <sub>x</sub> . . . . .	156
C.5	As in Table C.1 but for O <sub>3</sub> . . . . .	157
C.6	As in Table C.1 but for MeONO <sub>2</sub> . . . . .	158
C.7	As in Table C.1 but for EtONO <sub>2</sub> . . . . .	159
C.8	As in Table C.1 but for nPrONO <sub>2</sub> . . . . .	160
C.9	As in Table C.1 but for iPrONO <sub>2</sub> . . . . .	161

# Acknowledgements

I would like to sincerely thank my supervisor, Claire Reeves, for patiently guiding me through the labyrinth of atmospheric reactions during the five years of my master's and doctoral degrees, and for always being willing to discuss my ideas and give advice. A huge thanks to the members of the OXBUDS project: Alex Archibald, Paul Griffiths, Marcus Köhler and Mike Newland. To Alex, thanks for constantly asking: "So, what is the big picture?" To Paul, thanks for your wholehearted support and encouragement, and especially thanks for our stimulating scientific chats on Slack. Thanks to Marcus for all the time spent together thinking about our favourite  $\text{RONO}_2/\text{RH}$  ratios. Thanks to Mike for explaining the firn air modelling, and to Manoj Joshi for comments on atmospheric circulation. And, of course, I am forever grateful to my examiners, Parvatha Suntharalingam and Paul Young, for an interesting and inspiring viva.

Thanks to the University of East Anglia for welcoming me to the hive of wonderful people and bringing me together with my dear friend Annemarie Eckes-Shephard, as well as awarding me the Lord Zuckerman scholarship and providing financial support to travel to conferences. I also thank the EnvEast Doctoral Training Partnership for providing excellent research training and extra opportunities to disseminate my research.

I would like to acknowledge the contribution of several people to this thesis. Firstly, the contribution of Paul Griffiths, who ran the UM-UKCA experiments and helped me with the model setup and implementation of modifications to the chemistry. I thank and acknowledge the contribution of Jennifer Fisher (University of Wollongong), who provided the data on alkyl nitrate oceanic emissions. I would also like to thank Fiona O'Connor for supporting my application for the access to the Met Office Managed Archive Storage System from the JASMIN super-data-cluster, and Mark Prosser for proofreading my thesis.

My unconventional thanks are going to the cast of Critical Role and Brian W. Foster for keeping me laughing even on the darkest of days. Also, a huge thanks to YouTubers ChristopherOdd and Luckless Lovelocks for producing high-quality let's play content to enjoy after a long working day.

But above all, sincere thanks to my Mum and Grandma for always being there for me no matter how many kilometers apart, and, of course, perpetual hugs and thanks to my husband, Denis, for being my honey-bunny and my ever critical code reviewer, for his infinite patience, love and care.



# 1

## Introduction

### 1.1 Composition of the atmosphere

The atmosphere is a thin gaseous layer around our planet, commonly referred to as air. By volume, dry air (i.e. without water vapour) contains 78.08% of molecular nitrogen ( $\text{N}_2$ ), 20.94% of molecular oxygen ( $\text{O}_2$ ), 0.93% of argon (Ar) and 0.04% of carbon dioxide (407.75 ppmv  $\text{CO}_2$ , global mean as of August 2019<sup>1</sup>). Water vapour ( $\text{H}_2\text{O}$ ) is a major constituent of the Earth's atmosphere too, but in contrast to the other constituents, its concentration varies with temperature. At 30 °C, for example, a volume of air can contain up to 4%  $\text{H}_2\text{O}$ . At -40 °C, however, it can hold no more than 0.2%  $\text{H}_2\text{O}$ <sup>2</sup>. The remaining ~0.01% of the dry atmosphere is made up of so called trace gases, i.e. gases concentrations of which are equal to or smaller than that of  $\text{CO}_2$  (Hungate and Koch, 2015).

Despite their low concentrations, trace gases exert a substantial influence on the thermal and chemical balance of the Earth's atmosphere. Some trace gases trap a part of the thermal infrared radiation emitted by the Earth's surface, causing a warming of the Earth's surface known as the greenhouse effect. Without these so called greenhouse gases, and  $\text{H}_2\text{O}$  and  $\text{CO}_2$ , the Earth's average surface temperature would have been near -18 °C instead of the current 15 °C<sup>3</sup>. Other trace gases like the hydroxyl radical (OH), the nitrate radical ( $\text{NO}_3$ ), atomic chlorine (Cl) and atomic bromine (Br) can react with greenhouse gases and oxidise other reactive trace gases such as carbon monoxide (CO), volatile organic compounds (VOCs), reactive nitrogen gases and reactive sulfur

---

<sup>1</sup><https://www.esrl.noaa.gov/gmd/ccgg/trends/global.html>

<sup>2</sup><https://www.britannica.com/science/humidity>

<sup>3</sup>[https://www.giss.nasa.gov/research/briefs/ma\\_01/](https://www.giss.nasa.gov/research/briefs/ma_01/)

gases. By oxidising reactive trace gases, oxidant trace gases control their abundance and lifetimes, but in turn the abundance of reactive trace gases regulates the supply of oxidants. This means that the composition of the Earth’s atmosphere is determined by a finite supply of internally generated oxidants, or in other words, the Earth’s atmospheric oxidising capacity (Ehhalt et al., 2015).

## 1.2 Role of ozone in the atmosphere

Ozone ( $\text{O}_3$ ) is an inorganic trace gas, which is both an oxidant and a greenhouse gas. As an oxidant, it can harm living cells and corrode construction materials causing respiratory problems in humans and damage to vegetation and built infrastructure (Monks et al., 2015). As a greenhouse gas, it exerts  $0.35$  ( $0.15$  to  $0.55$ )  $\text{W m}^{-2}$  of radiative forcing<sup>4</sup> (Myhre et al., 2013), of which  $0.40$  ( $0.20$  to  $0.60$ )  $\text{W m}^{-2}$  is generated in the lowest part of the atmosphere — the troposphere, and  $-0.05 \pm 0.10$   $\text{W m}^{-2}$  in the layer above the troposphere — the stratosphere. In addition,  $\text{O}_3$  absorbs the Sun’s biologically harmful ultraviolet (UV) radiation, and together with  $\text{N}_2$  and  $\text{O}_2$  prevents most of it from reaching the Earth’s surface.

Since the discovery of ozone in 1839, researchers have been measuring ozone concentrations at a variety of sites around the globe. The oldest measurements, important for understanding trends in tropospheric ozone, were made at the Municipal Observatory at the Parc de Montsouris in Paris between 1876 and 1910. For some time, the Montsouris measurements were considered representative of the pre-industrial or “background” tropospheric ozone levels (e.g. Cooper et al., 2014; Tarasick and Slater, 2008; Vingarzan, 2004; Volz and Kley, 1988). However, they were recently reviewed and excluded from the historical ozone reconstruction because of (a) a significant contamination by interfering pollutants and (b) not being representative of the regional boundary layer. As a result, it is currently thought that tropospheric ozone concentrations increased by 30-70% since 1896 to 2014 in the temperate and polar regions of the Northern Hemisphere (Tarasick et al., 2019). This agrees well with isotopic measurements of oxygen trapped in polar firn and ice that imply an increase in tropospheric ozone burden of <40% between 1850 and 2005 (Yeung et al., 2019). While modern chemistry-climate models estimate a similar ( $\sim 30\%$ ) increase in tropospheric ozone burden between 1850 and 2000 (Young et al., 2013), they are consistently biased high in the Northern Hemisphere and biased low in the Southern Hemisphere (Young et al., 2018). This interhemispheric ozone bias, as well as a factor of  $\sim 1.5$  spread in the model estimates of tropospheric ozone burden, highlight the need for a better understanding and modelling of tropospheric ozone. Exploring the drivers and chemistry of tropospheric ozone is key to achieving that.

---

<sup>4</sup>Radiative forcing “is the net change in the energy balance of the Earth system due to some imposed perturbation” (Myhre et al., 2013).

### 1.3 Tropospheric ozone chemistry

Ozone is produced photochemically throughout the atmosphere. In the stratosphere, it is produced following the photolysis of  $O_2$ . First, an  $O_2$  molecule absorbs a photon ( $h\nu$ ) of wavelength ( $\lambda$ ) shorter than 242 nm and splits into two ground state oxygen atoms ( $O(^3P)$ ) (R1). Then,  $O(^3P)$  combines with  $O_2$  in a three-body reaction to form  $O_3$  (R2), where the third body (M) is  $N_2$  or  $O_2$ :



In the troposphere, however,  $O_3$  is produced by reactions involving free radicals, which are in turn mainly formed from the photolysis of  $O_3$  itself (The Royal Society, 2008). At wavelengths shorter than 320 nm,  $O_3$  photolysis (R3) generates excited oxygen atoms ( $O(^1D)$ ), which then either collide with  $N_2$  and  $O_2$  to reform  $O_3$  ((R4) followed by (R2)) or react with  $H_2O$  to form the OH radicals (R5):

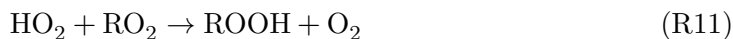


Once formed, the OH radicals can react with CO,  $CH_4$  and other hydrocarbons (RH) and initiate the  $O_3$  formation or removal cycles by producing the hydroperoxy radicals ( $HO_2$ ) and the alkyl peroxy radicals ( $RO_2$ , where R denotes an alkyl group):



Whether the initiated free radical cycles are that of  $O_3$  formation or loss depends on the fate of the  $HO_2$  and  $RO_2$  radicals and the presence of nitrogen monoxide (NO). In fact, the rapid conversion of NO to nitrogen dioxide ( $NO_2$ ) is also crucial for these cycles and is why NO and  $NO_2$  are often referred to together in air pollution literature, and their sum is denoted as  $NO_x$ .

In low- $NO_x$  conditions, typical for the remote regions of the atmosphere, the  $HO_2$  radicals are more likely to react with the other  $HO_2$  radicals to form hydrogen peroxide ( $H_2O_2$ ) or react with the  $RO_2$  radicals to form organic hydrogen peroxide (ROOH):



Because no  $\text{O}_3$  is being produced in the reaction sequence (R3)-(R11) and the sequence starts with  $\text{O}_3$  photolysis, this sequence results in net  $\text{O}_3$  loss. An additional  $\text{O}_3$  loss may also occur because  $\text{O}_3$  can react with the  $\text{HO}_2$  and  $\text{OH}$  radicals. When  $\text{O}_3$  reacts with an  $\text{HO}_2$  radical, an  $\text{OH}$  radical is produced. This  $\text{OH}$  radical can then react with  $\text{O}_3$  to reform an  $\text{HO}_2$  radical. As a result, the sequence of reactions (R12)-(R13) destroys  $\text{O}_3$  by recycling  $\text{HO}_2$  radicals, and is therefore known as an  $\text{O}_3$  depleting  $\text{OH-HO}_2$  inter-conversion cycle:

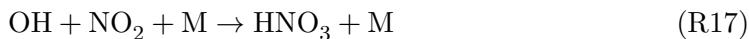


In intermediate  $\text{NO}_x$  conditions, typical for rural areas of most industrialised countries, the peroxy radicals are more likely to react with  $\text{NO}$  than with the other peroxy radicals. The reactions between the peroxy radicals and  $\text{NO}$  ((R14), (R15)) convert  $\text{NO}$  to  $\text{NO}_2$ , which subsequently photolyses generating  $\text{O}_3$  via (R16) followed by (R2):



As shown in Figure 1.1, the reactions (R14) and (R15) are part of the two  $\text{O}_3$  forming cycles, which may occur a number of times before being terminated by the reactions (R10) and (R11). Because these cycles recycle  $\text{HO}_x$  ( $=\text{OH}+\text{HO}_2$ ),  $\text{RO}_x$  ( $=\text{RO}+\text{RO}_2$ ) and  $\text{NO}_x$  and produce  $\text{O}_3$  as a by-product, they catalyse  $\text{O}_3$  production and lead to a net  $\text{O}_3$  gain. This process is sensitive to changes in  $\text{NO}_x$  but is insensitive to changes in  $\text{CO}$  or  $\text{RH}$ , because the  $\text{OH}$  radicals mostly react with  $\text{CO}$  and  $\text{RH}$  under intermediate  $\text{NO}_x$  conditions.

In high- $\text{NO}_x$  conditions, typical of an urban environment, the reactions of the peroxy radicals with  $\text{NO}$  still dominate over their reactions with other peroxy radicals, but  $\text{O}_3$  production is inhibited by further increases in  $\text{NO}_x$ . This happens because the reaction of the  $\text{OH}$  radical with  $\text{NO}_2$  forming nitric acid ( $\text{HNO}_3$ ) becomes the major termination process for the free radical cycles:



The formation of  $\text{HNO}_3$  halts the cycling of radicals and limits the  $\text{O}_3$  production rate.



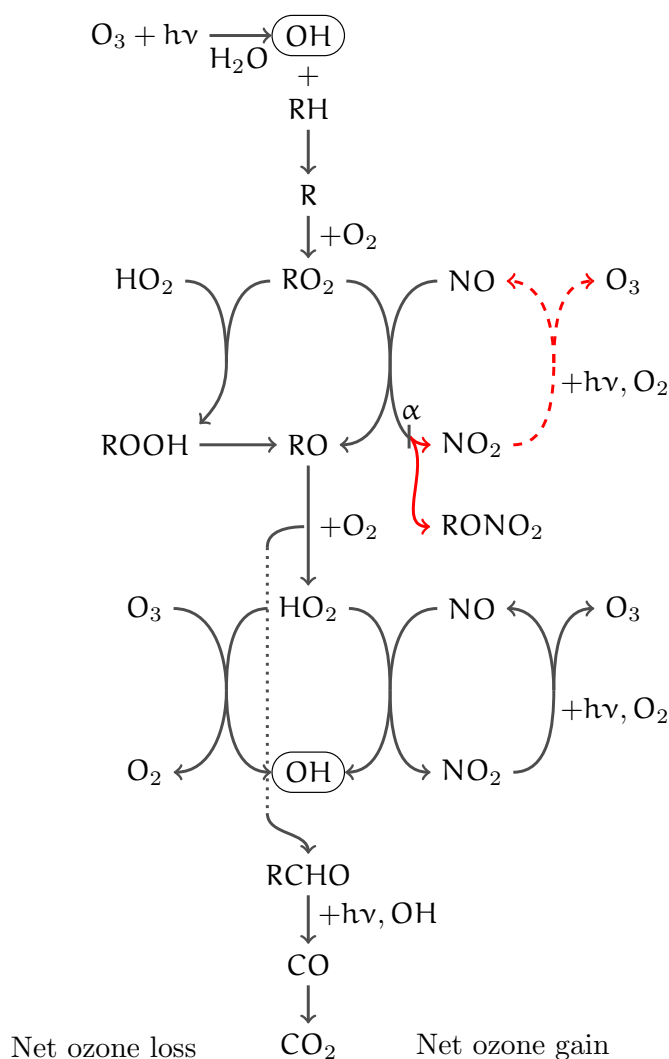


FIGURE 1.1: Simplified mechanism for the photochemical oxidation of an alkane in the troposphere. Highlighted in red is the interaction of alkyl nitrate chemistry with  $\text{O}_3$  chemistry.

However, elevated emissions of CO and RH make the reactions (R6) and (R8) more competitive with the reaction (R17) and increase the  $\text{O}_3$  production rate. Therefore, in high- $\text{NO}_x$  conditions  $\text{O}_3$  production is sensitive to changes in CO and RH but is insensitive to changes in  $\text{NO}_x$ .

Considering the rapid conversion of NO to  $\text{NO}_2$ , and the fact that photolysis of  $\text{NO}_2$  is a major  $\text{O}_3$  production pathway, it is clear that  $\text{NO}_x$  plays a critical role in tropospheric ozone chemistry. However  $\text{NO}_x$  is rather short-lived (with a lifetime of about a day (Jacob, 1999)), because it is rapidly converted into a range of other inorganic and organic species. These species include nitric acid ( $\text{HNO}_3$ ), nitrous acid (HONO), peroxyacetic acid ( $\text{HO}_2\text{NO}_2$ ), dinitrogen pentoxide ( $\text{N}_2\text{O}_5$ ), the nitrate radical ( $\text{NO}_3$ ), chlorine nitrate ( $\text{ClONO}_2$ ) and organic species like peroxyacetyl nitrate (PAN), peroxypropionyl nitrate (PPN) and alkyl nitrates. The collective name for these species, including  $\text{NO}_x$ , is “total reactive nitrogen” or “odd nitrogen” ( $\text{NO}_y$ ). A long-standing

problem in atmospheric chemistry related to  $\text{NO}_y$  is known as the “missing  $\text{NO}_y$ ”. “Missing  $\text{NO}_y$ ” is an unexplained deficit in the  $\text{NO}_y$  budget observed as a difference between the sum of  $\text{NO}_y$  species measured individually and the total  $\text{NO}_y$  measurement. Numerous studies have attempted to close the  $\text{NO}_y$  budget, and in doing so one of them eventually led to the discovery of alkyl nitrates (Atlas, 1988).

## 1.4 Alkyl nitrates

Alkyl nitrates ( $\text{RONO}_2$ ) are organic trace gases that contain an  $-\text{ONO}_2$  group. They belong to a broader group of organic nitrates and are an important component of  $\text{NO}_y$ . Alkyl nitrates are produced from the oxidation of hydrocarbons in the presence of  $\text{NO}_x$  and emitted from oceanic and biomass burning sources. Emissions of alkyl nitrates from industrial sources have been observed too (Roberts, 1990), but the importance of such emissions is uncertain.

In this thesis, I am going to focus on monofunctional alkyl nitrates, i.e. those that contain a single  $-\text{ONO}_2$  group. I will use the nomenclature of alkyl nitrates that is used in the literature together with that used within the Master Chemical Mechanism (Saunders et al., 2003) (Table 1.1). It is also common to refer to a group of alkyl nitrates with the same number of carbon atoms in a carbon chain using  $\text{C}_n \text{RONO}_2$  notation, where  $n$  is the so called carbon number. Thanks to that, one could, for example, use  $\text{C}_3 \text{RONO}_2$  notation to refer to both isomers of propyl nitrate ( $n\text{PrONO}_2$  and  $i\text{PrONO}_2$ ) at the same time.

To facilitate the discussion of the variability and distribution of alkyl nitrates observed during various aircraft, ship and ground-based campaigns, I summarised generic information about these campaigns in Tables A.1 and A.2.

The first direct evidence of alkyl nitrates being present in ambient air was found by Atlas (1988) in the North Pacific Ocean. They identified  $\text{C}_3\text{-C}_7 \text{RONO}_2$  in the local air, and noted that they seemed to be a significant fraction of  $\text{NO}_y$  in the marine troposphere. Later studies revealed that the contribution of alkyl nitrates to  $\text{NO}_y$  varies with time and location and depends on the air mass origin. According to Muthuramu et al. (1994), in the Arctic  $\text{C}_3\text{-C}_7$  and larger  $\text{RONO}_2$  comprised up to 20% of  $\text{NO}_y$  during boreal winter and at least 7% of  $\text{NO}_y$  during boreal spring. Jones et al. (1999) reported that at the Neumayer station, Antarctica,  $\text{MeONO}_2$  and  $\text{EtONO}_2$  contributed 18% and 4% to  $\text{NO}_y$ , respectively, during austral summer. In the tropics Walega et al. (1992) found that  $\text{MeONO}_2$  was 2% of  $\text{NO}_y$  when the air was coming from the free troposphere, and up to 10% of  $\text{NO}_y$  when the air was of tropical origin. The largest contribution of alkyl nitrates to  $\text{NO}_y$  (mainly from  $\text{MeONO}_2$  and  $\text{EtONO}_2$ ) of 20-80% was observed by Talbot et al. (2000) in equatorial and high-latitude regions over the South Pacific. In urban regions, however, the contribution of alkyl nitrates to  $\text{NO}_y$

TABLE 1.1: Nomenclature of monofunctional alkyl nitrates and their parent alkanes. Alternative name for the alkyl group (R) is given in brackets.

RH	R group	RONO <sub>2</sub> name	RONO <sub>2</sub> 2D structure
CH <sub>4</sub>	methyl	MeONO <sub>2</sub>	
C <sub>2</sub> H <sub>6</sub>	ethyl	EtONO <sub>2</sub>	
C <sub>3</sub> H <sub>8</sub>	n-propyl (1-propyl)	nPrONO <sub>2</sub>	
	isopropyl (2-propyl)	iPrONO <sub>2</sub>	
nC <sub>4</sub> H <sub>10</sub>	n-butyl (1-butyl)	nBuONO <sub>2</sub>	
	sec-butyl (2-butyl)	sBuONO <sub>2</sub>	
iC <sub>4</sub> H <sub>10</sub>	isobutyl (2-methylpropyl)	iBuONO <sub>2</sub>	
	tert-butyl	tBuONO <sub>2</sub>	
nC <sub>5</sub> H <sub>12</sub>	n-pentyl	nPeAONO <sub>2</sub>	
	2-pentyl (1-methylbutyl)	nPeBONO <sub>2</sub>	
	3-pentyl	nPeCONO <sub>2</sub>	
iC <sub>5</sub> H <sub>12</sub>	2-methyl-1-butyl	iPeAONO <sub>2</sub>	
	2-methyl-3-butyl (3-methyl-2-butyl)	iPeBONO <sub>2</sub>	
	2-methyl-2-butyl	iPeCONO <sub>2</sub>	

rarely exceeds 10%. [Flocke et al. \(1998\)](#) showed that C<sub>1</sub>-C<sub>8</sub> RONO<sub>2</sub> comprised 0.5-10% of NO<sub>y</sub> at a suburban site in Southern Germany, with higher values occurring in winter. [Simpson et al. \(2006\)](#) found that C<sub>1</sub>-C<sub>5</sub> RONO<sub>2</sub> were 0.3-8% of NO<sub>y</sub> during winter and 1-6% during summer at a site downwind of Hong Kong. Finally, using a broader definition of alkyl nitrates, [Day et al. \(2003\)](#) reported that they contributed 10-20% of NO<sub>y</sub> at a rural site in California.

As evident from above, the contribution of alkyl nitrates to NO<sub>y</sub> has a high spatio-temporal variability. The question is where and when that contribution — irrespective of size — matters. Therefore, characterizing alkyl nitrates in various environments is important and may help us to better understand the distribution of tropospheric ozone.

### 1.4.1 Primary sources

Alkyl nitrates are produced directly from oceanic sources and biomass burning.

#### Oceanic sources

Measurements of high concentrations of shorter-chain alkyl nitrates in the marine boundary layer suggest the presence of an oceanic source near the equator ([Atlas et al., 1993](#); [Blake et al., 2003](#)) and in the southern high latitudes ([Blake et al., 1999](#); [Jones et al., 1999](#); [Talbot et al., 2000](#); [Fischer et al., 2002](#)). In both regions MeONO<sub>2</sub> was found to be the dominant alkyl nitrate, with EtONO<sub>2</sub> and iPrONO<sub>2</sub> concentrations decreasing with increasing carbon number. The idea that the ocean is the source of these high concentrations is supported by the following. (1) These high concentrations could not be fully explained by local photochemical production and long-range transport. (2) MeONO<sub>2</sub> had no significant correlation with tetrachloroethylene<sup>5</sup> (C<sub>2</sub>Cl<sub>4</sub>) in both regions during the PEM-Tropics A and B aircraft campaigns. (3) During the same campaigns EtONO<sub>2</sub> also had no significant correlation with C<sub>2</sub>Cl<sub>4</sub> south of 10°N. (4) Both EtONO<sub>2</sub> and iPrONO<sub>2</sub> were well correlated with MeONO<sub>2</sub> south of 10°N during PEM-Tropics A and B and with bromoform<sup>6</sup> (CHBr<sub>3</sub>) near the equator during the SAGA-3 cruise.

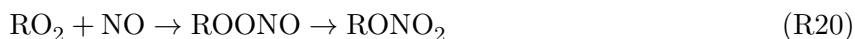
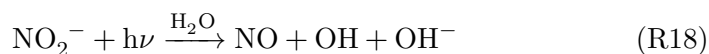
The existence of an equatorial oceanic source of shorter-chain alkyl nitrates has been confirmed by [Chuck et al. \(2002\)](#) and [Dahl et al. \(2005\)](#). [Chuck et al. \(2002\)](#) found high positive saturation anomalies, i.e. high fluxes from sea to air, of MeONO<sub>2</sub> and EtONO<sub>2</sub> (up to 800% for both species) in the equatorial Atlantic that coincided with high atmospheric concentrations of these species. In the more temperate regions, particularly in the Northern Hemisphere, they found that atmospheric and seawater concentrations of MeONO<sub>2</sub> and EtONO<sub>2</sub> were near equilibrium, suggesting a potential oceanic sink. [Dahl et al. \(2005\)](#) reported saturation anomalies of MeONO<sub>2</sub> of up to ~900%, EtONO<sub>2</sub> up to ~1500% and both of C<sub>3</sub> RONO<sub>2</sub> up to 2000% in the

<sup>5</sup>C<sub>2</sub>Cl<sub>4</sub> is often used as a tracer of industrial activity because it is an industrial cleaning solvent.

<sup>6</sup>CHBr<sub>3</sub> is produced by marine organisms such as macroalgae and phytoplankton ([Ziska et al., 2013](#)).

tropical Pacific. The highest saturation anomalies for all alkyl nitrates were found in a region bounded by 0-5°N, 170°E-173°W. Outside the tropics, these anomalies were near zero. The presence of alkyl nitrate oceanic source in the Southern Ocean is more speculative. Hughes et al. (2008) showed that the range of MeONO<sub>2</sub> and EtONO<sub>2</sub> saturation anomalies was -95...220% and -98...174% with medians of -40% and -11%, respectively, in November-December in a region bounded by 36-65°S, 30-70°W. Overall negative saturation anomalies suggest an ocean sink in that region at that time, but occasional supersaturation indicates that some MeONO<sub>2</sub> and EtONO<sub>2</sub> production was taking place.

The mechanism of oceanic alkyl nitrate production is not entirely known. The most studied potential mechanism is the photochemical production in the presence of sunlight, nitrite (NO<sub>2</sub><sup>-</sup>) and coloured dissolved organic matter (CDOM) (Moore and Blough, 2002; Dahl and Saltzman, 2003; Dahl and Saltzman, 2008; Dahl et al., 2012):



This process appears to be dependent on the source of CDOM (Dahl et al., 2012) and is largely limited by the availability of NO<sub>2</sub><sup>-</sup> (Dahl and Saltzman, 2008; Dahl et al., 2012). It is also predominantly applicable to surface waters, because deeper in the water column (in the absence of light) alkyl nitrate production was shown to be bacteria driven (Kim et al., 2015).

Other hypothesis of oceanic alkyl nitrate production include production by algae (Chuck et al., 2002), alkylation of NO<sub>3</sub> (Ballschmiter, 2002; Fischer et al., 2002), catalysed reaction of nitrate with alkyl halides and methyltransferase-catalysed biochemical methylation of nitrate (Ballschmiter, 2002). There also seems to be a large-scale relationship between seawater alkyl nitrate levels and chlorophyll (both are high near the equator and both are low outside the equator) (Dahl et al., 2005) as well as sea surface temperature (higher seawater levels occur at higher latitudes) (Chuck et al., 2002). Also, observations of Blake et al. (2003) indicated that oceanic alkyl nitrate production is not necessarily coupled to the production of CHBr<sub>3</sub>, methyl iodide (CH<sub>3</sub>I) or dimethyl sulfide (DMS), which suggests that alkyl nitrate source might be associated with high-nutrient, low-chlorophyll waters.

### Biomass burning sources

Not much is known about a biomass burning source of alkyl nitrates. One of the first reports about it came from Friedli et al. (2001). They found C<sub>1</sub>-C<sub>5</sub> RONO<sub>2</sub> in temperate forest and sage scrub fire emissions in Western US, and noted that they are linearly correlated with CO, a tracer of biomass burning. Later Simpson et al. (2002)

TABLE 1.2: Emission factors ( $\text{g kg}^{-1}$ ) for species emitted from different types of biomass burning (Akagi et al., 2011). The natural variation of the emission factors is given in parenthesis where available.

RONO <sub>2</sub>	tropical forest	savannah	boreal forest	extratropical forest
MeONO <sub>2</sub>	$8.29 \times 10^{-3}$ ( $1.60 \times 10^{-2}$ )	$5.1 \times 10^{-4}$ ( $3.7 \times 10^{-4}$ )	$2.83 \times 10^{-3}$	$2.83 \times 10^{-3}$
EtONO <sub>2</sub>	$5.70 \times 10^{-3}$	-	$1.78 \times 10^{-3}$	$1.78 \times 10^{-3}$
nPrONO <sub>2</sub>	$3.00 \times 10^{-4}$	-	$3.23 \times 10^{-4}$	$3.23 \times 10^{-4}$
iPrONO <sub>2</sub>	$1.00 \times 10^{-3}$	-	$3.23 \times 10^{-3}$	$3.23 \times 10^{-3}$
sBuONO <sub>2</sub>	$6.00 \times 10^{-4}$	-	$3.84 \times 10^{-3}$	$3.84 \times 10^{-3}$
nPeBONO <sub>2</sub>	-	-	$9.70 \times 10^{-4}$	$9.70 \times 10^{-4}$
nPeCONO <sub>2</sub>	-	-	$7.27 \times 10^{-4}$	$7.27 \times 10^{-4}$
iPeBONO <sub>2</sub>	-	-	$1.15 \times 10^{-3}$	$1.15 \times 10^{-3}$

reported enhancements in C<sub>1</sub>-C<sub>4</sub> RONO<sub>2</sub> of about 47-122 times their local background concentrations in the vicinity of savanna fires in Northern Australia. The compositional distribution of alkyl nitrates was similar in all fires sampled in Western US. In Australian savannah, however, MeONO<sub>2</sub> was mostly emitted during the flaming stage of the fire and C<sub>2</sub>-C<sub>4</sub> RONO<sub>2</sub> mostly during the smoldering stage.

More recent studies revealed that alkyl nitrate biomass burning emissions depend on biomass fuel type (Table 1.2) (Akagi et al., 2011). MeONO<sub>2</sub> dominates in emissions from tropical forest fires, while sBuONO<sub>2</sub> and iPrONO<sub>2</sub> prevail in emissions from boreal and extratropical forest fires. The latter is more or less consistent with findings of Reeves et al. (2007), who found that the combined measurement of nPeBONO<sub>2</sub> and nPeCONO<sub>2</sub> concentrations was the highest (rather than MeONO<sub>2</sub>) among C<sub>1</sub>-C<sub>5</sub> RONO<sub>2</sub> in the air impacted by Alaskan fires sampled over the North Atlantic.

### 1.4.2 Secondary sources

Alkyl nitrates are produced photochemically in a minor channel of the reaction between RO<sub>2</sub> and NO:



RONO<sub>2</sub> formation can serve as a termination step of the propagated O<sub>3</sub> forming cycle (Figure 1.1), and as Roberts et al. (1998) estimated, is more likely to happen when NO mixing ratio increases up to 100-200 ppt. The yield ( $\alpha$ ) of RONO<sub>2</sub> increases with increasing pressure and decreasing temperature (Roberts, 1990) as well as with increasing number of carbons in the alkyl peroxy radical (Atkinson et al., 1982) (Table 1.3).

TABLE 1.3: Kinetic data related to the formation of C<sub>1</sub>-C<sub>5</sub> RONO<sub>2</sub> from their parent alkanes. Values were obtained from the MCM v3.3.1.

RH	k <sub>RH+OH</sub> at 298 K (cm <sup>3</sup> molecule <sup>-1</sup> s <sup>-1</sup> )	α <sub>RO<sub>2</sub></sub>	RO <sub>2</sub>	k <sub>RO<sub>2</sub>+NO</sub> at 298 K (cm <sup>3</sup> molecule <sup>-1</sup> s <sup>-1</sup> )	α <sub>RONO<sub>2</sub></sub>
CH <sub>4</sub>	0.006 × 10 <sup>-12</sup>	1	MeOO	7.69 × 10 <sup>-12</sup>	0.001
C <sub>2</sub> H <sub>6</sub>	0.24 × 10 <sup>-12</sup>	1	EtOO	9.13 × 10 <sup>-12</sup>	0.009
C <sub>3</sub> H <sub>8</sub>	1.07 × 10 <sup>-12</sup>	0.264	nPrOO	9.39 × 10 <sup>-12</sup>	0.020
		0.736	iPrOO	9.04 × 10 <sup>-12</sup>	0.042
nC <sub>4</sub> H <sub>10</sub>	2.35 × 10 <sup>-12</sup>	0.127	nBuOO	9.04 × 10 <sup>-12</sup>	0.033
		0.873	sBuOO		0.090
iC <sub>4</sub> H <sub>10</sub>	2.19 × 10 <sup>-12</sup>	0.206	iBuOO	9.04 × 10 <sup>-12</sup>	0.033
		0.794	tBuOO		0.025
nC <sub>5</sub> H <sub>12</sub>	4.00 × 10 <sup>-12</sup>	0.083	nPeAOO	9.04 × 10 <sup>-12</sup>	0.052
		0.568	nPeBOO		0.129
		0.349	nPeCOO		0.131
iC <sub>5</sub> H <sub>12</sub>	3.70 × 10 <sup>-12</sup>	0.087	iPeAOO	9.04 × 10 <sup>-12</sup>	0.052
		0.297	iPeBOO		0.141
		0.616	iPeCOO		0.047

An alternative photochemical pathway of the formation of alkyl nitrates is the reaction of an alkoxy radical (RO) with NO<sub>2</sub>:



Archibald et al. (2007) showed that this pathway becomes important for MeONO<sub>2</sub> production at 10 ppb NO<sub>2</sub> and dominant over reaction (R21) at 35 ppb NO<sub>2</sub> according to their box model simulations that assumed a European mix of anthropogenic emissions (the authors did not consider other alkyl nitrates). That study was triggered by a finding of Simpson et al. (2006) that high concentrations of MeONO<sub>2</sub> (25 ppt) observed in the outflow from Hong Kong could not be explained by MeONO<sub>2</sub> oceanic emissions or fully accounted for by CH<sub>4</sub> oxidation and the decomposition of longer-chain alkoxy radicals to methoxy radicals. That left CH<sub>3</sub>O+NO<sub>2</sub> as a viable option. Yet, as Simpson et al. (2007) pointed out, the crossover point at which reaction (R22) becomes dominant may occur at a different NO<sub>2</sub> level in China, because of the difference in VOC/NO<sub>x</sub> mix of anthropogenic emissions between China and Europe. Outside heavily polluted environments, RO radicals react rapidly with O<sub>2</sub> and most ≥C<sub>4</sub> RO radicals decompose or isomerise, making alkyl nitrate formation from (R22) relatively unimportant for most organics under atmospheric conditions (Atkinson et al., 1982).

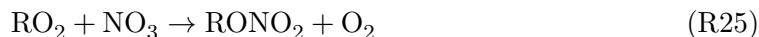
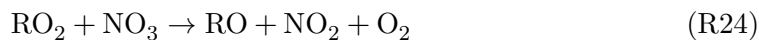
The same (R22) reaction has been invoked by Simpson et al. (2002) to explain the

formation of alkyl nitrates during savannah burning. They proposed that  $\text{RO}_2$  radicals present in abundance in the fire quickly react to form RO radicals. Larger RO radicals decompose into smaller RO radicals that then react with  $\text{NO}_2$  to form alkyl nitrates:



By this pathway, alkyl nitrate formation is not limited by the  $\text{RH}+\text{OH}$  rate coefficient nor by the  $\text{RO}_2+\text{NO}$  branching ratio. At higher temperatures such as those during the flaming stage of the fire, high concentrations of small radicals and  $\text{NO}_x$  lead to the formation of shorter-chain alkyl nitrates. At the lower temperatures of the smoldering stage, the formation of larger radicals is favoured, so it contributes to the production of longer-chain alkyl nitrates.

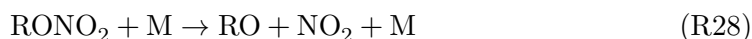
Another pathway of alkyl nitrate photochemical production has been suggested by [Worton et al. \(2010\)](#) as an explanation of the early morning  $\text{MeONO}_2$  maximum observed in south-east England during the Tropospheric Organic Chemistry experiments (TORCH1 and TORCH2). The explanation involved night time  $\text{MeONO}_2$  production from the chemistry of  $\text{NO}_3$ :



and boundary layer dynamics. [Worton et al. \(2010\)](#) also observed that the predominant photochemical source of shorter-chain ( $\leq \text{C}_4$ )  $\text{RONO}_2$  was the photochemical oxidation and decomposition of longer-chain compounds rather than the oxidation of the parent hydrocarbons. This finding is largely consistent with the modelling results of [Sommariva et al. \(2008\)](#), who using a subset of the Master Chemical Mechanism v3.1 concluded that  $\leq \text{C}_4$   $\text{RONO}_2$  can be formed from several precursors, while  $\geq 90\%$  of  $\text{C}_5$   $\text{RONO}_2$  are produced from the oxidation of a single parent alkane.

### 1.4.3 Sinks and lifetimes

Alkyl nitrates can be removed from the atmosphere by (a) photolysis, (b) OH oxidation, (c) thermal decomposition:





and also by (d) wet and (e) dry deposition. Photolysis of alkyl nitrates occurs by the cleavage of the RO–NO<sub>2</sub> bond (Turberg et al., 1990; Zhu and Kellis, 1997), while the reaction with OH proceeds via H-atom abstraction from the alkyl group releasing NO<sub>2</sub> in the process (Talukdar et al., 1997a; Aschmann et al., 2011). The relative importance of each of these loss processes varies from one alkyl nitrate to another and depends on time and location of alkyl nitrate removal from the atmosphere.

The major loss processes for C<sub>1</sub>–C<sub>5</sub> RONO<sub>2</sub> are photolysis and OH oxidation. Photolysis is the dominant sink for ≤C<sub>3</sub> RONO<sub>2</sub> and some higher branched ≥C<sub>4</sub> RONO<sub>2</sub> isomers. OH oxidation is generally slower than photolysis, especially for shorter-chain alkyl nitrates, but its reaction rate increases with increasing number of carbons in an alkyl nitrate (Roberts, 1990) (Table 1.4).

Both photolysis and OH oxidation rates vary with altitude and temperature (Figure 1.2, 1.3). Having a quantum yield of unity and absorption cross-sections increasing with decreasing wavelength (i.e. altitude) (Turberg et al., 1990; Clemitshaw et al., 1997; Zhu and Kellis, 1997), C<sub>1</sub>–C<sub>5</sub> RONO<sub>2</sub> are photolysed most efficiently at high altitudes. However, the fact that their absorption cross-sections also decrease with decreasing temperature (i.e. altitude) (Talukdar et al., 1997b; Zhu and Kellis, 1997) slows down photolysis rates at colder temperatures of high altitudes, making alkyl nitrate loss due to photolysis fairly uniform with height. OH reaction rates decrease with decreasing temperature, but the overall loss due to OH highly depends on the OH concentration.

Alkyl nitrates are believed to be thermally stable at atmospheric temperatures and easily decomposed at the higher temperatures of combustion processes (Roberts, 1990; Talukdar et al., 1997a). Such behaviour distinguishes alkyl nitrates from peroxyacyl nitrates, which decompose quickly as the temperature decreases (Talukdar et al., 1995), potentially increasing the relative contribution of alkyl nitrates to NO<sub>y</sub> in warmer conditions (e.g. in the boundary layer). However, Inomata et al. (2016) recently identified C<sub>1</sub>–C<sub>2</sub> RONO<sub>2</sub> in the exhaust of light-duty trucks with a diesel oxidation catalyst in laboratory conditions. The authors did not provide any information about the observed concentrations, but the Inomata et al. (2016) study and earlier ones mentioned in Roberts (1990) suggest that at least some alkyl nitrates might be stable at high temperatures, and that thermal decomposition reactions of alkyl nitrates need to be re-evaluated.

Dry deposition of alkyl nitrates is rarely considered. However, it was recently discovered that it is important for MeONO<sub>2</sub>. Mean MeONO<sub>2</sub> dry deposition velocities vary from 0.09 cm s<sup>-1</sup> in winter (Abeleira et al., 2018) to 0.13±0.07 cm s<sup>-1</sup> in summer (Russo et al., 2010). An increase in C<sub>1</sub>–C<sub>5</sub> RONO<sub>2</sub> dry deposition velocities with increasing carbon number was also reported (Abeleira et al., 2018). Wet deposition of alkyl nitrates is believed to be slow because of, unlike HNO<sub>3</sub>, low alkyl nitrate solubility (which also decreases with increasing carbon number (Sander, 2015)) and reactivity in water (Robertson et al., 1982; Roberts, 1990). Nevertheless, C<sub>1</sub>–C<sub>5</sub> RONO<sub>2</sub> were

TABLE 1.4: Reaction rate coefficients and resultant lifetimes of C<sub>1</sub>-C<sub>5</sub> RONO<sub>2</sub> due to photolysis and OH oxidation.

RONO <sub>2</sub>	J <sup>1</sup> (10 <sup>-6</sup> s <sup>-1</sup> )	k <sub>OH</sub> at 298 K (10 <sup>-12</sup> cm <sup>3</sup> molecule <sup>-1</sup> s <sup>-1</sup> )	τ <sub>J</sub> (days)	τ <sub>OH</sub> <sup>2</sup> (days)	τ <sup>3</sup> (days)
MeONO <sub>2</sub>	1.13	0.023 <sup>a</sup> , 0.028 <sup>b</sup>	10	503, 413	10.0, 9.9
EtONO <sub>2</sub>	1.34	0.18 <sup>a</sup> , 0.20 <sup>b</sup>	9	64, 58	7.6, 7.5
nPrONO <sub>2</sub>	1.75	0.58 <sup>a</sup> , 0.71 <sup>b</sup>	7	20, 16	5.0, 4.7
iPrONO <sub>2</sub>	2.93	0.29 <sup>a</sup> , 0.41 <sup>b</sup>	4	40, 28	3.6, 3.5
nBuONO <sub>2</sub>	1.75	1.6 <sup>a</sup>	7	7	3.5
sBuONO <sub>2</sub>	2.93	0.86 <sup>a</sup>	4	13	3.0
iBuONO <sub>2</sub>	1.75	0.77 <sup>c</sup>	7	15	4.6
tBuONO <sub>2</sub>	8.19	0.082 <sup>c</sup>	1	141	1.4
nPeAONO <sub>2</sub>	1.75	3.0 <sup>c</sup>	7	4	2.4
nPeBONO <sub>2</sub>	2.93	1.9 <sup>c</sup>	4	6	2.4
nPeCONO <sub>2</sub>	2.93	1.1 <sup>c</sup>	4	11	2.9
iPeAONO <sub>2</sub>	1.75	2.0 <sup>c</sup>	7	6	3.1
iPeBONO <sub>2</sub>	2.93	1.8 <sup>c</sup>	4	6	2.4
iPeCONO <sub>2</sub>	8.19	0.41 <sup>c</sup>	1	28	1.3

<sup>1</sup> Calculated from  $J=1 \cdot \cos^m \cdot e^{-n \cdot \sec x}$ , 21 June 45°N using MCM v3.3.1 photolysis parameters.

<sup>2</sup> Calculated from  $\tau_{OH}=1/(k_{OH}OH)$  for 298 K with  $OH=1 \times 10^6$  molecules cm<sup>3</sup>.

<sup>3</sup> Calculated from  $\tau=1/(J+k_{OH}OH)$ .

<sup>a</sup> Atkinson et al. (2006) (IUPAC), <sup>b</sup> Burkholder et al. (2015) (JPL), <sup>c</sup> MCM v3.3.1.

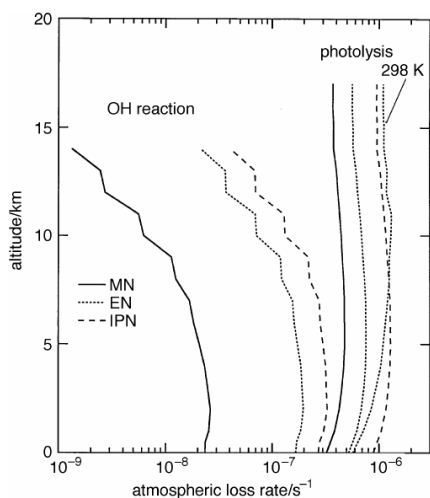


FIGURE 1.2: Atmospheric loss rate constants for methyl (MN), ethyl (EN) and isopropyl (IPN) nitrate as a function of altitude (i.e. temperature) due to OH oxidation and photolysis. The J-value for EN is calculated using constant 298 K absorption cross-sections. From Talukdar et al. (1997b).

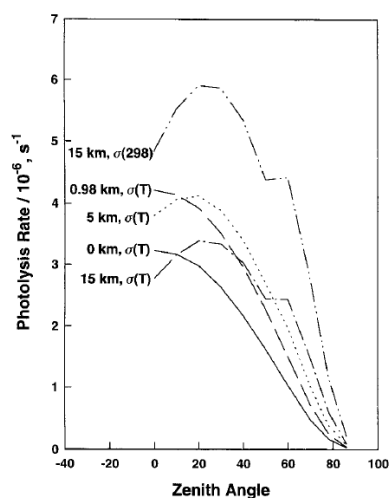


FIGURE 1.3: Photolysis rates of isopropyl nitrate as a function of zenith angle at several altitudes calculated using 298 K and temperature dependent cross sections (US Standard Atmosphere was used as the temperature-altitude profile). From Zhu and Kellis (1997).

detected in rain, snow and surface water (Hauff et al., 1998) and studies of the reactivity of alkyl nitrates in aqueous phase are ongoing (e.g. González Sánchez et al. (2018)).

So, in general, photolysis and OH oxidation are the major atmospheric loss processes for C<sub>1</sub>-C<sub>5</sub> RONO<sub>2</sub>. Photolysis is relatively more important for nitrates with <C<sub>4</sub>, while nitrates with longer chains are photolysed and oxidised by OH at similar rates. Other sinks, i.e. thermal decomposition, dry and wet deposition, are negligible, with the exception of dry deposition for MeONO<sub>2</sub>.

The resultant lifetimes of C<sub>1</sub>-C<sub>5</sub> RONO<sub>2</sub> depend on the seasonality of their two major sinks. These lifetimes vary from hours in the summer tropics to several months during the polar winter which makes these alkyl nitrates important reservoirs of tropospheric reactive nitrogen. Due to such relatively long lifetimes, C<sub>1</sub>-C<sub>5</sub> RONO<sub>2</sub> can be destroyed far away from their sources and release NO<sub>2</sub> back into the local atmosphere. This might change ozone concentrations on regional levels and alter the oxidising capacity of the atmosphere.

#### 1.4.4 Temporal variability

##### Seasonal cycle

Seasonal variations in alkyl nitrate concentrations are influenced by: (1) the strength of primary and (2) secondary sources, (3) photochemical removal, (4) dilution due to atmospheric mixing and (5) the transport from source regions to the sampling site. As a result, seasonal cycles of alkyl nitrates vary with location. Alkyl nitrate concentrations have been measured in a plethora of aircraft campaigns, yet there are not many studies that measured alkyl nitrates in the same location for long enough to obtain information about their seasonality. Data from studies such as these are reproduced in Figure 1.4 and discussed in this section.

At a remote Summit station, Greenland, C<sub>1</sub>-C<sub>4</sub> RONO<sub>2</sub> typically maximise in winter and show a minimum in summer (Swanson et al., 2003). Winter alkyl nitrate maxima are caused by higher winter abundances of their parent alkanes and lower rates of photochemical destruction, while summer alkyl nitrate minima arise out of a combination of lowered alkyl nitrate production due to lower alkane concentrations and increased alkyl nitrate photochemical removal. Similar seasonality was observed at the Schauinsland station, Germany, for C<sub>1</sub>-C<sub>8</sub> RONO<sub>2</sub>, when photochemically aged air arrived at that station. However, when polluted air prevailed over the station, alkyl nitrates maximised in summer rather than winter (Flocke et al., 1998). Simpson et al. (2006) reported a winter maximum and a summer minimum of C<sub>1</sub>-C<sub>5</sub> RONO<sub>2</sub> at the Tai O station, a subtropical coastal site in south-eastern China. There, alkyl nitrate seasonality happened to match that observed in photochemically aged air, but was, in fact, largely determined by local meteorology as polluted air masses were advected to the site predominantly during winter and clean air masses during summer. Long-term data from two temperate suburban North American sites, the University of New

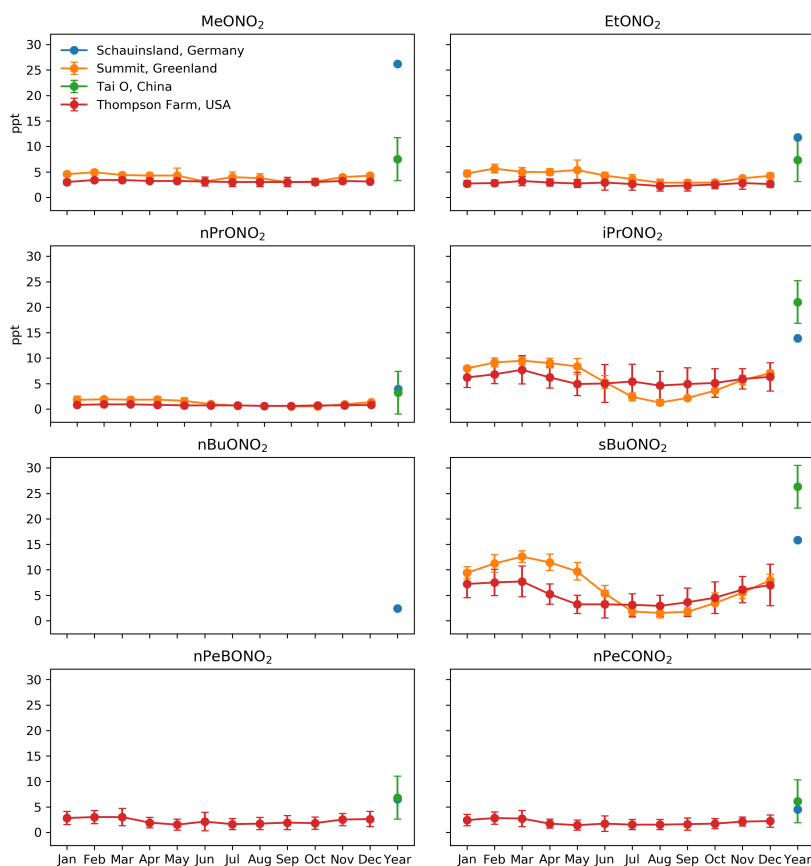


FIGURE 1.4: Seasonal cycle and annual mean  $C_1$ - $C_5$   $RONO_2$  concentrations observed at Schauinsland, Germany (Flocke et al., 1998), Summit, Greenland (Swanson et al., 2003), Tai O, China (Simpson et al., 2006) and Thompson Farm, US (Russo et al., 2010). Data from Schauinsland: 2 June 1990 - 4 May 1991 mean; Summit: June 1997 - June 1998 monthly means with 1-sigma standard deviation; Tai O: 24 August 2001 - 31 December 2002 mean; Thompson Farm: 12 January 2004 - 8 February 2008 monthly means with standard deviation.

Hampshire Atmospheric Observing Station at Thompson Farm, NH (Russo et al., 2010) and the Boulder Atmospheric Observatory, CO (Abeleira et al., 2018), demonstrated again that  $C_1$ - $C_5$   $RONO_2$  have a winter maximum and a summer minimum. However, both of these datasets revealed that the average mixing ratios of alkyl nitrates at these sites were more similar across the seasons than in the other aforementioned suburban locations [Schauinsland, Tai O].

Owing to their longer lifetimes,  $MeONO_2$  and  $EtONO_2$  seasonal cycles are more uniform than those of other alkyl nitrates. For the same reason,  $MeONO_2$  and  $EtONO_2$  dominate the total alkyl nitrate concentration in photochemically aged air and comprise a significant proportion of it in summer (Swanson et al., 2003; Russo et al., 2010). In fairly polluted air and/or during winter (depending on transport patterns),  $iPrONO_2$  and  $sBuONO_2$  are the most abundant (Flocke et al., 1998; Simpson et al., 2006; Russo et al., 2010; Abeleira et al., 2018). This is because they are produced faster and at a higher yield from  $RH+OH$  reactions than shorter-chain alkyl nitrates, and their

lifetimes are longer than those of longer-chain alkyl nitrates. The balance between these factors, i.e. photochemical production and loss, and transport time and dilution, is what generally increases the amplitude of the alkyl nitrate seasonal cycle with increasing carbon number, at least for C<sub>1</sub>-C<sub>5</sub> RONO<sub>2</sub>.

### Diel cycle

Diel cycles of alkyl nitrates have a minimum at night, increase throughout the morning and reach peak levels in the afternoon (Russo et al., 2010) or, in the case of polluted air masses, early evening (Flocke et al., 1998). Abeleira et al. (2018) reported that MeONO<sub>2</sub> concentrations change little throughout the day in all seasons. EtONO<sub>2</sub> and nPrONO<sub>2</sub> exhibit small increases from late morning to late afternoon during summer. In contrast, iPrONO<sub>2</sub> and C<sub>4</sub>-C<sub>5</sub> RONO<sub>2</sub> have a more pronounced diel variability in summer compared to winter or spring. Such variability is consistent with both photochemical production and loss being higher during summer due to higher OH concentrations and photolysis rates.

### 1.4.5 Spatial variability

Spatial variability of alkyl nitrates is determined by their sources and lifetimes. Combining 22 years of aircraft data with model results (Figure 1.5), Fisher et al. (2018) found that MeONO<sub>2</sub> is the dominant alkyl nitrate over much of the globe at the majority of altitudes. At the equator, it is enhanced in the lower troposphere due to the presence of an oceanic source and stays enhanced at higher altitudes due to convection. Atmospheric circulation and a long MeONO<sub>2</sub> lifetime facilitate the spread of this alkyl nitrate over the tropics and across the Southern Ocean.

EtONO<sub>2</sub> distribution generally follows that of MeONO<sub>2</sub> but shows lower concentrations. It is expected because EtONO<sub>2</sub> has a weaker oceanic source and a shorter lifetime. The fact that EtONO<sub>2</sub> yield from RO+NO reaction is smaller than that of propyl nitrates, but ethane is more abundant than propane, might explain why EtONO<sub>2</sub> concentrations are smaller than those of iPrONO<sub>2</sub> but higher than those of nPrONO<sub>2</sub>.

Propyl nitrates display maxima in the continental boundary layer and nearby outflow regions. Such a distribution is determined by the proximity of their precursor emissions, a higher yield of formation from RO+NO than MeONO<sub>2</sub> and EtONO<sub>2</sub> and the shortest lifetimes among C<sub>1</sub>-C<sub>3</sub> RONO<sub>2</sub>. iPrONO<sub>2</sub> occasional concentration maxima in the Arctic might be linked to local biomass burning activity or plumes from Eurasian fossil fuel emissions (Fisher et al., 2010; Shindell et al., 2008) sampled during the flights. The prevalence of iPrONO<sub>2</sub> over nPrONO<sub>2</sub> in terms of abundance is dictated by the higher yield of the iPrOO radical from the C<sub>3</sub>H<sub>8</sub>+OH reaction and a higher branching ratio for the iPrOO+NO reaction.



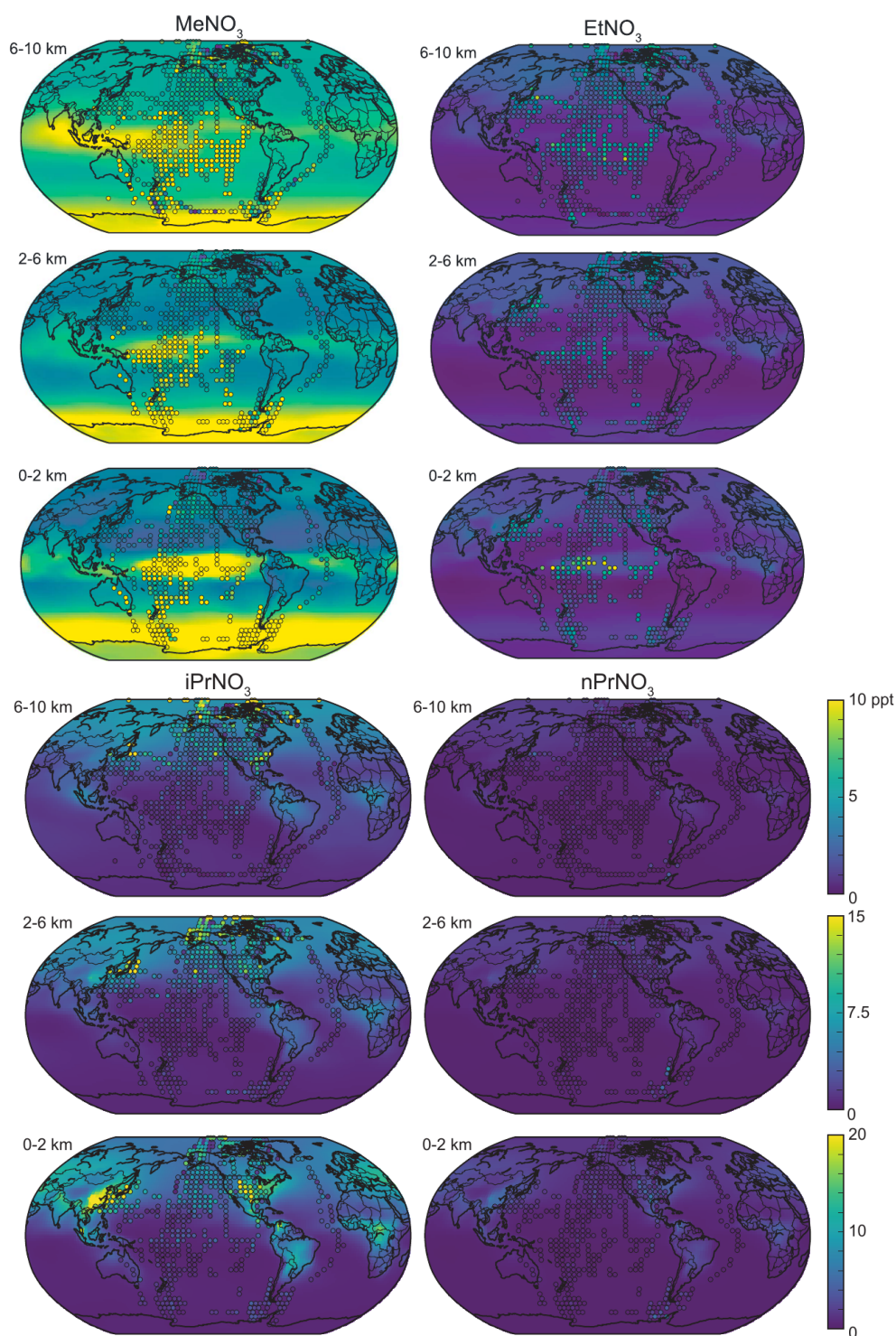


FIGURE 1.5: Annual mean distribution of  $\text{MeONO}_2$ ,  $\text{EtONO}_2$ ,  $\text{nPrONO}_2$  and  $\text{iPrONO}_2$  at different altitude ranges: (bottom) 0–2 km, (middle) 2–6 km, (top) 6–10 km. Background colours show GEOS-Chem model results from 2013 with aircraft observations from 1996–2017 overlaid as filled circles. Observations have been averaged over all flight days and over a horizontal resolution of  $4^\circ \times 5^\circ$  for visibility. Note the difference in colour scale between different altitude ranges and supersaturated colours in the case of  $\text{MeONO}_2$ . See Fig. A.1 for the full  $\text{MeONO}_2$  range. From Fisher et al. (2018).

TABLE 1.5: Global 3D modelling studies of alkyl nitrates.

Study	Model name	Model type	Meteorology	Year	Chemical scheme
Neu et al. (2008)	UCI	CTM	ECMWF	2000	Wild et al. (2003)
Williams et al. (2014)	TM5	CTM	ERA-interim	2008	CB05
Khan et al. (2015)	STOCHEM-CRI	CTM	HadCM	1998	CRI v2-R5
Fisher et al. (2018)	GEOS-Chem	CTM	GEOS-FP	2013	GEOS-Chem
this study	UM-UKCA	CCM	UM-UKCA	2000	CheST

### 1.4.6 Modelling

There has been a significant number of modelling studies that investigated alkyl nitrate chemistry. The majority of them used variations of a simple box model that was designed to simulate the chemistry occurring at a specific location for a certain period of time. Studies like that include Atherton (1989), Reeves et al. (2007), Sommariva et al. (2008), Farmer et al. (2011) and Browne and Cohen (2012). For the sake of brevity, I do not summarise the results from these studies here and direct the reader to Chapter 4 for details.

In this section, I would like to focus on the studies that modelled alkyl nitrate chemistry using more complex, global 3D models. There are only four such studies: Neu et al. (2008), Williams et al. (2014), Khan et al. (2015) and Fisher et al. (2018). The advantage of using a 3D model rather than a box model is that a 3D model can better simulate atmospheric mixing and transport, i.e. processes that are crucial for understanding the fate of alkyl nitrates. However, other processes that control the abundance of alkyl nitrates might be represented in different 3D models differently, if at all. Tables 1.5 and 1.6 summarise the information about the global 3D models used previously, namely their names, types (chemistry transport model (CTM) or chemistry-climate model (CCM)), meteorological data used to force chemical fields, years of simulation, chemical mechanism and processes that control alkyl nitrate sources and sinks.

The strengths and weaknesses of each of these studies are discussed in the following chapters. The important point here is that the study presented in this thesis includes all known sources and sinks of  $C_1$ - $C_3$   $RONO_2$ .

TABLE 1.6: Implementation of processes that control  $C_1$ - $C_3$   $RONO_2$  abundance in different global 3D modelling studies: photochemical production (PP), photochemical loss (PL), dry deposition (DD), wet deposition (WD), oceanic source (OC), biomass burning source (BB).  $\square$  indicates that the process is absent from the model,  $\blacksquare$  that it is present.

Process	Neu2008	Williams2014	Khan2015	Fisher2018	this study
<i>MeONO<sub>2</sub></i>					
PP	$\square$	$\blacksquare$	$\blacksquare$	$\blacksquare$	$\blacksquare$
PL	$\blacksquare$	$\blacksquare$	$\blacksquare$	$\blacksquare$	$\blacksquare$
DD	$\square$	$\blacksquare$ +WD	$\blacksquare$	$\blacksquare$	$\blacksquare$
OC	$\blacksquare$	$\blacksquare$ Neu2008	$\blacksquare$ Neu2008	$\blacksquare$ Fisher2018	$\blacksquare$ Fisher2018
BB	$\square$	$\square$	$\blacksquare$ Simpson2002	$\square$	$\blacksquare$ GFEDs
<i>EtONO<sub>2</sub></i>					
PP	$\square$	$\blacksquare$ <sup>1</sup>	$\blacksquare$	$\blacksquare$	$\blacksquare$
PL	$\blacksquare$	$\blacksquare$ <sup>1</sup>	$\blacksquare$	$\blacksquare$	$\blacksquare$
DD	$\square$	$\blacksquare$ +WD	$\blacksquare$	$\blacksquare$	$\blacksquare$
OC	$\blacksquare$	$\blacksquare$ Neu2008 <sup>2</sup>	$\square$	$\blacksquare$ Fisher2018	$\blacksquare$ Fisher2018
BB	$\square$	$\square$	$\blacksquare$ Simpson2002	$\square$	$\blacksquare$ GFEDs
<i>nPrONO<sub>2</sub></i>					
PP	$\square$	$\blacksquare$ <sup>1</sup>	$\blacksquare$	$\blacksquare$	$\blacksquare$
PL	$\square$	$\blacksquare$ <sup>1</sup>	$\blacksquare$	$\blacksquare$	$\blacksquare$
DD	$\square$	$\blacksquare$ +WD	$\blacksquare$	$\blacksquare$	$\blacksquare$
OC	$\square$	$\blacksquare$ Neu2008 <sup>2</sup>	$\square$	$\blacksquare$ Fisher2018	$\blacksquare$ Fisher2018
BB	$\square$	$\square$	$\blacksquare$ Simpson2002	$\square$	$\blacksquare$ GFEDs
<i>iPrONO<sub>2</sub></i>					
PP	$\square$	$\blacksquare$ <sup>1</sup>	$\blacksquare$	$\blacksquare$	$\blacksquare$
PL	$\square$	$\blacksquare$ <sup>1</sup>	$\blacksquare$	$\blacksquare$	$\blacksquare$
DD	$\square$	$\blacksquare$ +WD	$\blacksquare$	$\blacksquare$	$\blacksquare$
OC	$\square$	$\blacksquare$ Neu2008 <sup>2</sup>	$\square$	$\blacksquare$ Fisher2018	$\blacksquare$ Fisher2018
BB	$\square$	$\square$	$\blacksquare$ Simpson2002	$\square$	$\blacksquare$ GFEDs

<sup>1</sup>  $C_2$ - $C_3$   $RONO_2$  lumped into an ORGNIT species.

<sup>2</sup> An estimate of lumped “other” alkyl nitrate emissions, which is twice the a priori estimate of EtONO<sub>2</sub> oceanic emission calculated by Neu et al. (2008).

## 1.5 Thesis justification and structure

### 1.5.1 Scientific rationale

Monofunctional  $C_1$ - $C_3$  alkyl nitrates are important reservoirs of tropospheric reactive nitrogen. They are produced from the oxidation of their parent alkanes in the presence of  $NO_x$  and emitted from oceanic and biomass burning sources. Due to their relatively long lifetime, they can be destroyed far away from their sources and change ozone concentration on regional levels, altering the oxidising capacity of the atmosphere.

The chemistry of alkyl nitrates is rather well known, but information about their oceanic and biomass burning sources is limited. Dry deposition data on alkyl nitrates has been recently reported, but the data on their wet deposition is practically absent. All of this hinders our understanding of the importance of different alkyl nitrate sources and sinks and their impact on tropospheric chemistry. This work attempts to fill some of these gaps by achieving the following aims.



### 1.5.2 Thesis aims

The aims of this thesis were as follows:

- develop a chemical mechanism that includes C<sub>1</sub>-C<sub>3</sub> RONO<sub>2</sub> photochemical production and loss;
- test this mechanism against a benchmark;
- implement this mechanism into a global 3D chemistry-climate model, UM-UKCA;
- add C<sub>1</sub>-C<sub>3</sub> RONO<sub>2</sub> oceanic emissions into UM-UKCA;
- create a 2D field of C<sub>1</sub>-C<sub>3</sub> RONO<sub>2</sub> biomass burning emissions;
- add C<sub>1</sub>-C<sub>3</sub> RONO<sub>2</sub> biomass burning emissions into UM-UKCA;
- validate UM-UKCA against observations;
- estimate the impact of C<sub>1</sub>-C<sub>3</sub> RONO<sub>2</sub> chemistry and direct emissions on the global distribution and budget of HO<sub>x</sub>, NO<sub>x</sub> and NO<sub>y</sub>.

### 1.5.3 Thesis outline

In Chapter 2 of this thesis, I describe the development of a new chemical mechanism for use in UM-UKCA and the procedure used to test this mechanism against the Master Chemical Mechanism in a box model. In Chapter 3, I describe the UM-UKCA model, derive C<sub>1</sub>-C<sub>3</sub> RONO<sub>2</sub> oceanic and biomass burning emissions and validate the UM-UKCA model against the aircraft data from the Atmospheric Tomography mission. In Chapter 4, I present the results from the UM-UKCA model and discuss the impacts of C<sub>1</sub>-C<sub>3</sub> RONO<sub>2</sub> chemistry and oceanic and biomass burning emissions on tropospheric chemistry. In Chapter 5, I synthesise our findings and present our conclusions. In Chapter 6, I summarise my contribution of the OXBUDS project.



# 2

## Chemical mechanism development

### 2.1 Introduction

Concentrations of all chemical species that comprise the Earth's atmosphere are continually changing over time. Some of these species are produced and destroyed within seconds, some reside in the atmosphere for centuries. The change in species concentration is determined by a series of consecutive, parallel and sometimes competing reactions (Dlugokencky and Houweling, 2015), which together constitute a complex network of pathways that transforms one species into another. In numerical models such a network is called a chemical scheme (or a mechanism), and it is simply a collection of chemical reactions and rate coefficients that describes the chemistry of the atmosphere.

An explicit representation of the inorganic tropospheric chemistry requires about 20 species and 50 reactions (Stockwell et al., 2012). That is the level of complexity that any modern CTM or CCM can afford given the current state of computer technology. However, an explicit representation of the organic tropospheric chemistry requires millions of species and reactions (Aumont et al., 2005; Szopa et al., 2005), solving the equations for which in such models is beyond the computational resources now available. For that reason, CTMs and CCMs use simplified chemical schemes, which are produced by reducing the complexity of an explicit chemical scheme whilst retaining the essential features of the chemistry.

Chipperfield and Arnold (2015) postulate that there are three major methods for reducing the complexity of a chemical scheme: (1) the carbon-bond lumping method (where organic species are separated into common bond groups, e.g. as alkenes with internal double bonds in the Carbon Bond mechanism (Yarwood et al., 2005)), (2) the surrogate species method (where species with similar reactivity are grouped together and solved as one species, e.g. organic peroxy radicals in the Master Chemical Mechanism (Jenkin et al., 1997)), and (3) the lumped species method (where species are grouped together but the reaction rate coefficients for the lumped group are a weighted average of the rate coefficients for the individual species, e.g. MACR species<sup>1</sup> in Pöschl et al. (2000)). Each of these methods aims to produce the best reduced chemical scheme within the capabilities of the method and tailors the scheme for a specific application. Therefore, it is important to know what a chemical scheme was developed for and apply and develop it further accordingly.

In this chapter, I describe the chemical schemes used in this study and present the protocol for the development of (a) an update and (b) an extension to one of the tropospheric chemistry schemes of the UM-UKCA model. I evaluate this new chemical scheme at different stages of development by comparing the output from box model simulations with a new scheme with that from box model simulations with a benchmark scheme. At the end, I list the changes that have been introduced into the scheme.

For box model simulations, I used the Kinetic PreProcessor v2.2 (KPP), which is an open-source software that facilitates the computer simulation of chemical kinetic systems. It translates a set of chemical reactions and their rate coefficients into FORTRAN or C code that computes the time-evolution of chemical species according to the differential law of mass action kinetics. Apart from being computationally efficient, KPP incorporates a comprehensive suite of numerical integration methods, while the modular fashion of the KPP environment provides an ideal framework for rapid prototyping and evaluation of new chemical mechanisms (Damian et al., 2002).

## 2.2 Description of chemical mechanisms

### 2.2.1 Master Chemical Mechanism

The Master Chemical Mechanism (MCM) is a near-explicit chemical mechanism that describes the generation of ozone and other secondary pollutants from the gas-phase degradation of a series of VOCs. The MCM contains about 6700 species and 17000 reactions. Its inorganic chemistry includes 20 species (apart from N<sub>2</sub>, O<sub>2</sub> and H<sub>2</sub>O) and 45 reactions, and its non-aromatic chemistry, that is of interest here, includes 4351 species and 12691 reactions (Saunders et al., 2003), out of which isoprene chemistry now takes 602 species and 1926 reactions (Jenkin et al., 2015).

---

<sup>1</sup>Representing methacrolein, methylvinylketone and other C<sub>4</sub> carbonyls.

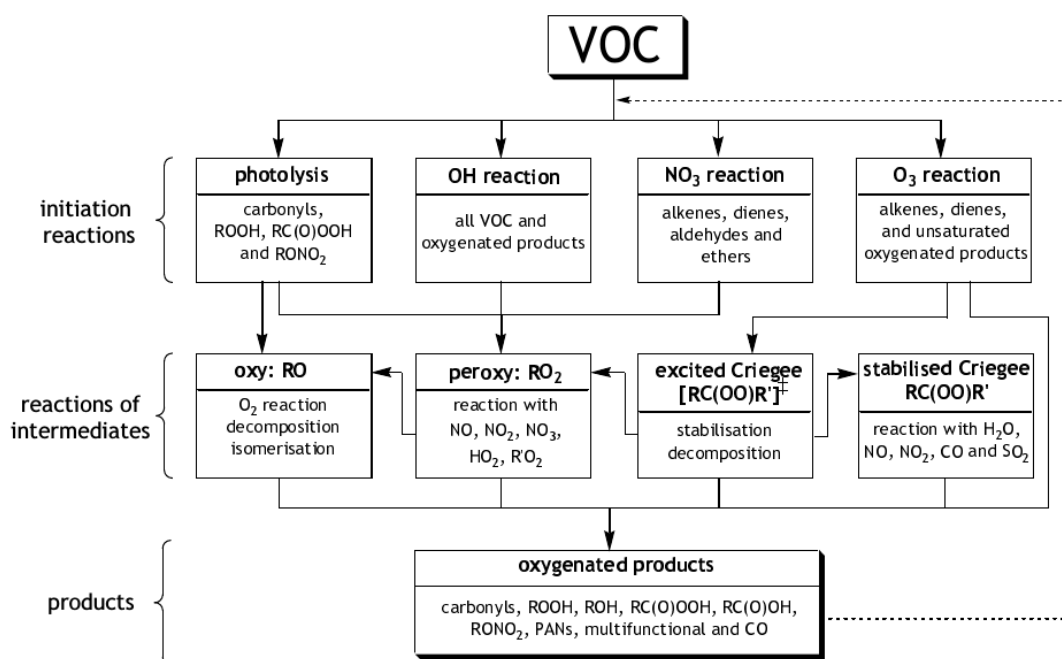


FIGURE 2.1: Flow chart indicating the major reactions, intermediate classes and product classes considered in the MCM protocol. From Saunders et al. (2003).

The MCM protocol is illustrated in Figure 2.1. It summarises the main types of reactions and classes of organic intermediates and products which are potentially generated for a given VOC. The main rules behind the MCM protocol for the degradation of non-aromatic VOCs are:

- Consider degradation of VOCs listed in the UK National Atmospheric Emissions Inventory (Passant, 2002), emphasising those with greater emissions;
- Include reactions important for a single VOC or a class of VOCs:
  - Include photolysis reactions only for those classes of VOCs for which this process is significant, and use generic photolysis rates;
  - Include O<sub>3</sub> or NO<sub>3</sub> initiated chemistry only for those VOCs, for which relationships, formulated based on typical boundary layer concentrations of OH, O<sub>3</sub> and NO<sub>3</sub>, apply;
  - Only include the reactions of NO<sub>2</sub> with acyl peroxy radicals (e.g. CH<sub>3</sub>CO<sub>3</sub>) for which the products are the comparatively stable peroxy nitrates (ROONO<sub>2</sub>); but also include the reactions with the most abundant peroxy radical, the methyl peroxy radical (CH<sub>3</sub>O<sub>2</sub>);
- Assume the general pattern for the reaction mechanism. For example, the reactions of NO<sub>3</sub> with aldehydes are assumed to proceed via abstraction of the aldehydic H-atom, leading to the production of acyl radicals;

- Treat peroxy radicals together:
  - Each organic peroxy radical reacts with all the other organic peroxy radicals and itself at a single, collective rate. This is achieved by defining a parameter  $RO_2$ , the organic peroxy radical pool, which is the sum of the concentrations of all organic peroxy radicals. In the case of ethane chemistry, for example,  $RO_2$  is equal to the sum of the concentrations of  $CH_3O_2$ ,  $C_2H_5O_2$ ,  $HOCH_2CH_2O_2$ ,  $CH_3CO_3$ ,  $HCOCH_2O_2$ ,  $HOCH_2CO_3$  and  $HCOCO_3$ ;
  - Each organic peroxy radical requires only one reaction, which could then branch into up to three channels;
- Simplify the degradation of the first and subsequent generation's products in comparison with the parent VOC (mostly by disregarding the minor OH+VOC reaction channels);
- Simplify the degradation of organic nitrates, peroxy nitrates, hydroperoxides, percarboxylic acids, carboxylic acids and alcohols, since these are usually regarded as minor products;
- Define the kinetics and products of unstudied chemical reactions on the basis of the known reactions by analogy and with the use of structure-reactivity relationships; devise and use generic rate coefficients where necessary.

For further details about this protocol please refer to [Jenkin et al. \(1997\)](#) and [Saunders et al. \(2003\)](#).

I chose the MCM as a benchmark for this study, because (a) this mechanism acted as a reference benchmark for the development and evaluation of many reduced chemical mechanisms before (e.g. [Pöschl et al., 2000](#); [Whitehouse et al., 2004](#); [Jenkin et al., 2008](#)), and (b) the organic chemistry of the CheT mechanism described below was partially based on the data from the MCM. I chose the latest version of the MCM, MCM v3.3.1., because it contains the latest revision of isoprene chemistry ([Jenkin et al., 2015](#)).

### 2.2.2 CheT chemical mechanism

The Met Office Unified Model coupled to the United Kingdom Chemistry and Aerosols sub-model (UM-UKCA) described in depth in Chapter 3, has several chemical mechanisms. Each of these mechanisms was designed for a different UM-UKCA application, which can vary from global climate modelling to assessments of regional air quality. The mechanism explored in this chapter is the tropospheric part of the Chemistry for Stratosphere and Troposphere mechanism (“strat-trop” or CheST), hereafter referred to as CheT. CheT is based on the TOMCAT mechanism ([Law et al., 1998](#)), with the isoprene degradation being based on the Mainz Isoprene Mechanism (MIM) ([Pöschl et al., 2000](#)) and extensions from [Young \(2007\)](#). CheT describes the chemistry

of odd oxygen ( $O_x$ ), hydrogen ( $HO_x$ ), nitrogen ( $NO_y$ ) and carbon monoxide (CO), with near-explicit treatment of methane ( $CH_4$ ), ethane ( $C_2H_6$ ) and propane ( $C_3H_8$ ) and parametrised isoprene. CheT contains 55 species (including  $N_2$ ,  $O_2$  and  $H_2O$ ) (Table 2.1) and 164 reactions of which 11 species and 41 reactions are specific to the isoprene chemistry (O'Connor et al., 2014). Ethane and propane are surrogate species in CheT. Ethane represents a sum of ethane, ethene and ethyne, and propane represents the sum of propane and propene.

TABLE 2.1: Chemical species in the tropospheric part of the CheST mechanism.

Species formula	UKCA name	Species formula	UKCA name
$H_2O$	$H_2O$	$CH_3CHO$	MeCHO
$N_2$	$N_2$	$CH_3COOH$	MeCO2H <sup>1</sup>
$O_2$	$O_2$	$CH_3CO_3H$	MeCO3H <sup>2</sup>
$H_2$	$H_2$	$CH_3COO_2$	MeCO <sub>3</sub>
$O_3$	$O_3$	$CH_3O_3NO_2$	PAN
$O(^3P)$	$O(^3P)$		
$O(^1D)$	$O(^1D)$	$C_3H_8$	$C_3H_8$
OH	OH	n- $C_2H_7O_2$	nPrOO
$HO_2$	$HO_2$	i- $C_2H_7O_2$	iPrOO
$H_2O_2$	$H_2O_2$	n- $C_2H_7OOH$	nPrOOH
NO	NO	i- $C_2H_7OOH$	iPrOOH
$NO_2$	$NO_2$	$CH_3CHO$	EtCHO
$NO_3$	$NO_3$	$CH_3COCH_3$	Me2CO
HONO	HONO	$CH_3COCH_2OO$	MeCOCH2OO
$HO_2NO_2$	$HO_2NO_2$	$CH_3COCH_2OOH$	MeCOCH2OOH
$HNO_3$	$HONO_2$	$CH_3COO_2$	EtCO <sub>3</sub>
$N_2O_5$	$N_2O_5$	$C_2H_5CO_3NO_2$	PPAN
CO	CO		MGLY <sup>3</sup>
$CH_4$	$CH_4$	$C_5H_8$	$C_5H_8$
$CH_3O_2$	MeOO		ISO2
$CH_3OH$	MeOH		MACRO2
$CH_3OOH$	MeOOH		ISOOH
HCHO	HCHO		ISON
$CH_3ONO_2$	MeONO <sub>2</sub>		MACR
			MACROOH
$C_2H_6$	$C_2H_6$		MPAN
$C_2H_5O_2$	EtOO		HACET
$C_2H_5OOH$	EtOOH		NALD
		HCOOH	HCOOH

<sup>1</sup> MeCO2H is produced from  $HO_2+MeCO_3$  and  $MeOO+MeCO_3$ .

<sup>2</sup> MeCO3H is produced from  $HO_2+MeCO_3$ .

<sup>3</sup> MGLY is produced from  $MeCOCH_2OOH+OH$ , MeCOCH2OOH is produced from  $HO_2+MeCOCH_2O$ , MeCOCH2OO is produced from  $NO_3+Me_2CO$ ,  $OH+Me_2CO$  and  $OH+MeCOCH_2OOH$ .

CheT has been used for many climate modelling studies (e.g. [Squire et al. \(2014\)](#) and [Squire et al. \(2015\)](#)), and is, therefore, suitable for our study as well. However, to examine the impacts of C<sub>1</sub>-C<sub>3</sub> RONO<sub>2</sub> chemistry on tropospheric ozone, we needed to add C<sub>2</sub>-C<sub>3</sub> RONO<sub>2</sub> into the CheT as MeONO<sub>2</sub> was already present in it. To determine the best way to describe C<sub>2</sub>-C<sub>3</sub> RONO<sub>2</sub> chemistry for use in UM-UKCA, I conducted a series of box model runs with the MCM and the CheT and compared the results. The protocol for comparison is described below.

## 2.3 Protocol for comparison of chemical mechanisms

### 2.3.1 Overview of previous studies

There are many different approaches to evaluating a chemical mechanism or comparing chemical mechanisms. [Stone et al. \(2012\)](#) recommend focusing on testing the accuracy of chemical mechanisms in simulating OH and HO<sub>2</sub> radicals. These radicals are very short-lived due to their high reactivity, which means that their budgets (and hence concentrations) are controlled by local chemistry, and not by transport. Zero-dimensional “box” models, which solve the chemical continuity equations for a single air mass, can be used for such testing.

From a policy perspective, however, it is often more important to know how well a chemical mechanism can simulate tropospheric ozone, rather than OH and HO<sub>2</sub> radicals. In this case, [Malkin et al. \(2016\)](#) recommend running box models with different mechanisms until all of them reach “ozone steady state” (i.e. when ozone concentration does not change anymore). Comparing results at ozone steady state ensures that each mechanism realises its full ozone creation potential and has enough time to reach steady state. Different chemical mechanisms need a different amount of time to reach steady state, with simpler mechanisms reaching it faster.

From a global modelling perspective, it is usually more important to have a chemical mechanism that is capable of simulating the chemistry both near and far from a pollution source ([Szopa et al., 2005](#)). Near the source, NO<sub>x</sub> and VOC concentrations are typically high, while far away from the source, they are typically low, resulting in different chemical regimes dominating over different regions. However, local chemical regimes are not isolated, but constantly affected by transport of air from other regions, which requires a chemical mechanism to represent the local chemistry well as well as to represent the formation of, and release from, reservoir species well.

An example of a study, where a chemical mechanism was designed for use in a global 3D model, is that of [Pöschl et al. \(2000\)](#), who derived a condensed mechanism of isoprene degradation from the MCM. They tested their mechanism in a box model using more than fifty scenarios and ran a box model in two different modes. Initialisation mode tested the ability of the mechanism to simulate the impact of isoprene and its



oxidation products on the background atmosphere. In this mode, the model was initialised with a range of isoprene, CO, O<sub>3</sub> and NO<sub>2</sub> concentrations at noontime and ran forward without any emissions. That approximated an air mass being transported away from the source, assuming no interaction with the ground or the atmosphere outside the box. Emission mode focused on assessing the impact of the first steps of isoprene oxidation that happens directly over the source. The model was initialised in the same manner as in the initialisation mode, but was started at midnight and ran forward with constant NO emissions and isoprene emissions coupled to the cosine of the solar zenith angle. In both modes, the model was run for 5 days with a low and high NO<sub>x</sub> scenario, diurnally varying photolysis and the same initial concentrations of H<sub>2</sub>O<sub>2</sub>, HNO<sub>3</sub>, H<sub>2</sub>, CH<sub>4</sub> and HCHO. Archibald et al. (2010) used a similar box model setup to that of Pöschl et al. (2000) for emission mode for an intercomparison of isoprene mechanisms used in global 3D models.

Pöschl et al. (2000) extensively tested their mechanism in two extreme scenarios: degradation of isoprene during transport and accumulation of isoprene in stagnant conditions. This provided information about the skill of the mechanism in performing at a lower and upper limit of possible typical atmospheric conditions. However, in the real atmosphere these scenarios are often combined, and not having information about the mechanism's performance in "in-between" scenarios might lead to unforeseen model biases. Testing chemical mechanisms in all possible scenarios is impossible, but seeing at least what species are most sensitive to the change in the representation of the chemistry might soon be possible thanks to recent advances in machine learning and especially in the study of artificial neural networks (e.g. Nicely et al. (2017)).

The choice of a timescale for running a box model, when comparing chemical mechanisms, is often arbitrary, and is nothing more than a trade-off between competing requirements. The length of a run should be long enough for the chemistry to feedback on itself, but not too long so that the model produces chemical environments that are never observed. That is the main reason why Squire et al. (2015) ran their box model for 3 days and not longer when investigating the impact of variations in the representation of isoprene chemistry on ozone. In addition, shorter model run times usually lead to higher model sensitivity to initial conditions (e.g. initial concentrations, start time (night or day)), which may make certain feedbacks seem more important than they really are.

The results from a zero-dimensional box model inevitably deviate from the observations due to many limitations of a box modelling approach. However, if the task is to compare chemical mechanisms (rather than reproduce observations), the primary concern should be in supplying the mechanisms with the same boundary conditions and more importantly with the same drivers.

The main drivers of tropospheric ozone chemistry are NO<sub>x</sub> and VOCs. NO<sub>2</sub> provides the primary tropospheric source of O(<sup>3</sup>P) required for O<sub>3</sub> formation, while RO<sub>2</sub> radicals

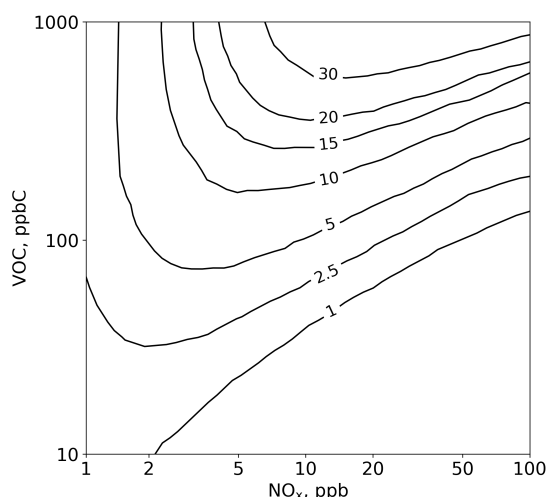


FIGURE 2.2: Isopleths giving net rate of ozone production ( $\text{ppb h}^{-1}$ , daytime average) as a function of  $\text{NO}_x$  and VOCs. Both scales are logarithmic. Adapted from Sillman (1999).

produced during VOCs oxidation assist in converting  $\text{NO}$  to  $\text{NO}_2$ . Depending on the relative amount of  $\text{NO}_x$  and VOCs,  $\text{O}_3$  is either produced or destroyed. In the  $\text{NO}_x$ -sensitive regime (with relatively low  $\text{NO}_x$  and high VOC),  $\text{O}_3$  increases with increasing  $\text{NO}_x$  and changes little in response to increasing VOC. In the  $\text{NO}_x$ -saturated or VOC-sensitive regime,  $\text{O}_3$  decreases with increasing  $\text{NO}_x$  and increases with increasing VOC. The ridge line connecting local  $\text{O}_3$  maxima separates the  $\text{NO}_x$ -sensitive and VOC-sensitive regimes, with  $\text{NO}_x$ -sensitive regime being above the line.

Capturing the non-linearity of the relationship between  $\text{O}_3$ ,  $\text{NO}_x$  and VOCs is an important skill for a chemical mechanism. Therefore, constructing figures like Figure 2.2 is a powerful way of evaluating a chemical mechanism. However, the choice of quantities to plot on such figures is complex. Traditionally, X and Y axes show  $\text{NO}_x$  and VOC emission rates, but if a model does not have emissions, X and Y could show  $\text{NO}_x$  and VOC concentrations. The contours (isopleths) often display the instantaneous rate of ozone production or maximum ozone concentration on a certain day, often the 3<sup>rd</sup> or 4<sup>th</sup> day of simulation, or at steady state.

Using  $\text{NO}_x$  and VOC emission rates as coordinates gives an opportunity to predict the sensitivity of  $\text{O}_3$  to its precursor emissions. Such predictions could be derived from a global 3D model, but having emissions in a box model and no realistic removal processes (e.g. advection, deposition) leads to an accumulation of longer-lived species in a box model, and an inability of the model to reach a steady state.

Using  $\text{NO}_x$  and VOC concentrations as coordinates is problematic too. For example, if the model is run with no emissions but initialised with a value for  $\text{NO}_x$ , the same initial amount of  $\text{NO}_x$  might be converted to a  $\text{NO}_x$  reservoir species (e.g.  $\text{HNO}_3$ ) at different speeds by different mechanisms (Figure 2.3). This means that in spite of  $\text{NO}_x$  being exactly the same at the start of a simulation, it might not be the same at the time of comparison (e.g. on the 3-rd day) or be unrealistically low. A way around

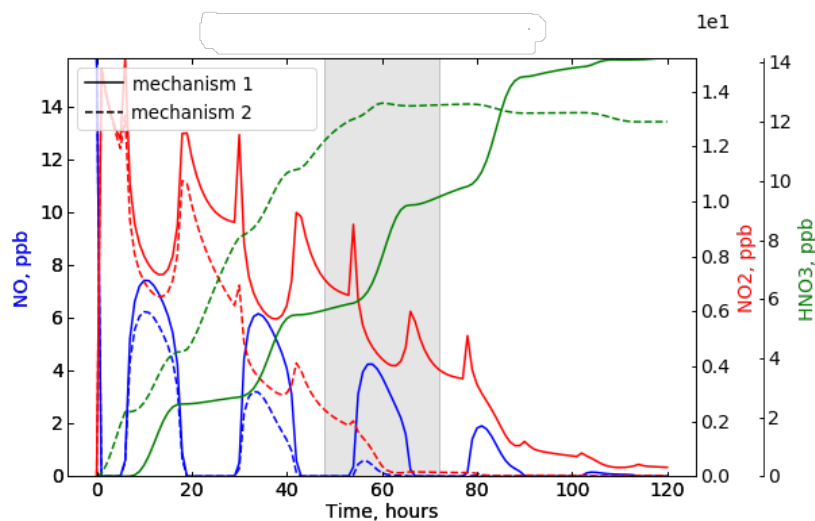


FIGURE 2.3: An example of different speeds of conversion of NO and NO<sub>2</sub> to HNO<sub>3</sub> in different chemical mechanisms. Shaded area highlights the time period when model data could be sampled for comparison.

these problems is running a box model constrained to NO<sub>x</sub> as, for example, was done by Emmerson and Evans (2009). Their box model calculated NO<sub>x</sub> every 24 hours and multiplied NO or NO<sub>2</sub> depending which of the two was constrained by a number so that modelled NO<sub>x</sub> remained in agreement with the value of NO<sub>x</sub> initially input into the model<sup>2</sup>. However, such treatment of NO<sub>x</sub> lessens one of the dominant feedbacks on the chemical system - that between NO<sub>x</sub> and the organic chemistry.

Below I describe how I used the recommendations above in my box model experiments and how my experiments are different from those in other studies.

### 2.3.2 Box model setup

To test the performance of the new CheT mechanism against the MCM, I ran a set of box model runs that covers a range of NO<sub>x</sub>-VOC conditions. The number of box model runs in a set was determined by the number of NO<sub>x</sub>-VOC conditions considered sufficient for constructing an isopleth plot similar to Figure 2.2. I configured the box model in a way described in Table 2.2 and illustrated in Figure 2.4. To ensure that the differences in species concentrations were not caused by the differences in photolysis, I used the MCM photolysis parametrization in both the MCM and the CheT model runs.

<sup>2</sup><https://github.com/barronh/DSMACC/wiki/Inputs-and-initial-conditions>

TABLE 2.2: Steady state box model configuration.

Parameter	Value
Temperature	298 K
Pressure	1000 hPa
Relative humidity	50 %
Cloud cover	No clouds
Julian day	172 (21 June)
Latitude	45°N
Solar declination angle	23.44°
Initial concentrations	O <sub>3</sub> 40 ppb, CO 100 ppb, CH <sub>4</sub> 1800 ppb
Initialised variable species	O <sub>3</sub> , NO
Initialised fixed species	CO, C <sub>1</sub> -C <sub>3</sub> alkanes, N <sub>2</sub> , O <sub>2</sub> , H <sub>2</sub> O
Photolysis	MCM parametrisation with diurnal cycle
Emissions	NO, NO <sub>2</sub> at a ratio computed online
Deposition	O <sub>3</sub> , HNO <sub>3</sub> , H <sub>2</sub> O <sub>2</sub>
Run length	6 months
Output frequency	1 h
Solver	LSODE (Livermore Solver for Ordinary Differential Equations)

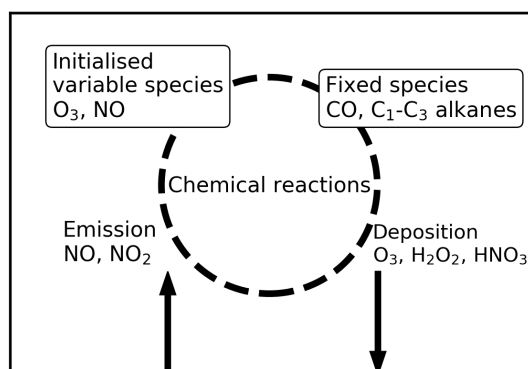


FIGURE 2.4: Steady state box model schematic.

### 2.3.3 Experiment setup

Following the recommendations of Malkin et al. (2016), I designed my box model runs so that they simulated the chemistry in the air that remains over an emission source region for a period of time long enough for ozone to reach steady state. I defined steady state as a state when two consecutive diurnal cycles of ozone did not differ from each other by more than  $\pm 1$  ppt. Runs with the MCM and the CheT reached ozone steady state at different times in different NO<sub>x</sub>-VOC conditions, but through experimentation I found that it takes about 6 months for both mechanisms to reach a steady state in all NO<sub>x</sub>-VOC conditions considered in this study.

Ozone steady state was reached in a box model by keeping the concentrations of species that drive ozone chemistry constant in time:

- CO and CH<sub>4</sub> concentrations were fixed at 100 ppb and 1800 ppb respectively. C<sub>2</sub>H<sub>6</sub> concentration was initialised with a value between 1 ppt to 10 ppb (20 levels) and kept constant. C<sub>3</sub>H<sub>8</sub> initial concentration was 0.58 of that of C<sub>2</sub>H<sub>6</sub> and was also kept constant. The upper limit of C<sub>2</sub>H<sub>6</sub> concentration and the ratio of C<sub>3</sub>H<sub>8</sub> to C<sub>2</sub>H<sub>6</sub> were derived from the data on urban mean concentrations of these species reported by [Baker et al. \(2008\)](#).
- NO<sub>x</sub> concentration was kept constant by replenishing NO and NO<sub>2</sub> consumed by the chemistry with fresh emissions of NO to NO<sub>2</sub> at a NO/NO<sub>2</sub> ratio calculated online. NO<sub>x</sub> concentration was initialised with a value between 1 ppt to 1 ppm (21 levels). The NO/NO<sub>2</sub> ratio was calculated based on (1) the difference between the desired [initial] NO<sub>x</sub> concentration and the sum of NO and NO<sub>2</sub> at the current time step and (2) the relative contribution of NO and NO<sub>2</sub> to NO<sub>x</sub> dictated by the chemistry.

To construct one isopleth plot I ran 420 box model runs. On the X axis of the plots I show the range of NO<sub>x</sub> mixing ratios, and on the Y axis I show the range of the sum of mixing ratios of non-methane alkanes present in a run in ppb of carbon (ppbC). Isopleths show a 24-hour average mixing ratio of a species of interest one day after an ozone steady state is reached. Following the recommendation of [Stone et al. \(2012\)](#), I focused my analysis on OH and HO<sub>2</sub> but also O<sub>3</sub>. However, I also created isopleth plots for others species, if the reactions involving these species were modified in either of the mechanisms.

The difference between the [Emmerson and Evans \(2009\)](#) treatment of NO<sub>x</sub> and that used in this study is that they constrained NO<sub>x</sub> every 24 hours, while I constrained it every internal time step of the LSODE solver. I did this by adding an artificial emission of NO<sub>x</sub> that would release NO<sub>x</sub> in a form of NO or NO<sub>2</sub> once the “real” NO and NO<sub>2</sub> are consumed. Code implementation of that is given in [Appendix B.2](#). By constraining NO<sub>x</sub> in this way I ensured that the chemistry was always exposed to the same amount of NO<sub>x</sub> rather than was exposed to a changing amount of NO<sub>x</sub> throughout the day. As a result, there is no diel cycle in NO<sub>x</sub> in my work (in contrast to the [Emmerson and Evans \(2009\)](#) work), which prevented the transition of the chemistry from one chemical regime to another when NO<sub>x</sub> reacts away. However, by treating NO<sub>x</sub> this way I lessened or even removed the feedback of the rest of the chemistry on NO<sub>x</sub>.

## 2.4 Revision, unification and comparison of chemical mechanisms

The development of an extension to the CheT mechanism was split into two stages:

1. Revision and an update of CheT;
2. Addition of C<sub>2</sub>-C<sub>3</sub> RONO<sub>2</sub> chemistry into CheT.

### 2.4.1 Revision

Chemical mechanisms are periodically updated to incorporate newly published kinetic and photochemical data. CheT was last updated in 2012, while new recommendations are available now [in 2015/19]. In this study, I updated only the inorganic and C<sub>1</sub>-C<sub>3</sub> alkane CheT chemistry, because isoprene chemistry is not directly related to alkyl nitrates. Although, one might say that I updated one reaction from isoprene chemistry, OH+MGLY (O'Connor et al., 2014), but if the origin of MGLY is traced back, MGLY turns out to be a part of propane CheT chemistry (see Table 2.1 for details).

Sometimes it was difficult to decide which CheT reactions did and did not require an update, because two internationally recognised authorities that provide recommendations of the kinetic and photochemical data for use in computer simulations of atmospheric chemistry, the NASA Panel for Data Evaluation in the Jet Propulsion Laboratory (JPL) and the International Union of Pure and Applied Chemistry (IUPAC), provide different recommendations. In fact, Newsome and Evans (2017) recently explored the impact of the differences between JPL and IUPAC recommended inorganic reaction rate coefficients (those for O<sub>x</sub>-HO<sub>x</sub>-NO<sub>x</sub>-CO-CH<sub>4</sub> chemistry) on modelled tropospheric ozone. They found that the uncertainty in the annual mean tropospheric ozone burden, surface ozone, tropospheric OH concentrations and tropospheric methane lifetime in GEOS-Chem model was 10, 11, 16 and 16% respectively, caused by a combined uncertainty in 60 reaction rate coefficients that they studied. They pointed out that these uncertainties were larger than the spread between models in recent model intercomparisons, which highlights the need to refine the recommendations for these supposedly well-known reactions.

Another issue was that historically CheT preferred to use JPL data for the inorganic chemistry and IUPAC data for the organic chemistry, while the benchmark that I used for this study, the MCM, always uses IUPAC data. As a result, the changes that I introduced to the inorganic and C<sub>1</sub>-C<sub>3</sub> alkane CheT chemistry<sup>3</sup> should be considered more as a revision of CheT that incorporates more IUPAC data rather than an update of CheT to the latest recommendations possible.

---

<sup>3</sup>I did this while developing C<sub>4</sub>-C<sub>5</sub> alkane and alkyl nitrate chemistry for the OXBUDS project.

I introduced the following changes to the inorganic and C<sub>1</sub>-C<sub>3</sub> alkane CheT chemistry:

- added CO that was missing from the products of two CheT reactions:
  1.  $\text{OH} + \text{PAN} \rightarrow \text{HCHO} + \text{NO}_2 + \text{H}_2\text{O} \dots + \text{CO}$
  2.  $\text{OH} + \text{PPAN} \rightarrow \text{MeCHO} + \text{NO}_2 + \text{H}_2\text{O} \dots + \text{CO}$
- updated reaction rate coefficients of the following bimolecular CheT reactions:
  1.  $\text{HO}_2 + \text{O}_3 \rightarrow \text{OH} + \text{O}_2 + \text{O}_2$
  2.  $\text{OH} + \text{HO}_2\text{NO}_2 \rightarrow \text{H}_2\text{O} + \text{NO}_2 + \text{O}_2$
  3.  $\text{OH} + \text{HONO} \rightarrow \text{H}_2\text{O} + \text{NO}_2$
  4.  $\text{OH} + \text{OH} \rightarrow \text{H}_2\text{O} + \text{O}({}^3\text{P})$
  5.  $\text{NO}_3 + \text{HCHO} \rightarrow \text{HNO}_3 + \text{HO}_2 + \text{CO}$
  6.  $\text{OH} + \text{CH}_4 \rightarrow \text{H}_2\text{O} + \text{MeOO}$
  7.  $\text{OH} + \text{MeOOH} \rightarrow \text{H}_2\text{O} + \text{MeOO}$
  8.  $\text{HO}_2 + \text{EtCO}_3 \rightarrow \text{O}_2 + \text{EtCO}_3\text{H}$
  9.  $\text{iPrOO} + \text{NO}_3 \rightarrow \text{Me}_2\text{CO} + \text{HO}_2 + \text{NO}_2$
  10.  $\text{nPrOO} + \text{NO}_3 \rightarrow \text{EtCHO} + \text{HO}_2 + \text{NO}_2$
  11.  $\text{OH} + \text{MGLY} \rightarrow \text{MeCO}_3 + \text{CO} + \text{H}_2\text{O}$
- updated reaction rate coefficients of the following termolecular CheT reactions:
  1.  $\text{HO}_2 + \text{NO}_2 + \text{M} \rightarrow \text{HO}_2\text{NO}_2 + \text{M}$
  2.  $\text{NO}_2 + \text{NO}_3 + \text{M} \rightarrow \text{N}_2\text{O}_5 + \text{M}$
  3.  $\text{MeCO}_3 + \text{NO}_2 + \text{M} \rightarrow \text{PAN} + \text{M}$
  4.  $\text{EtCO}_3 + \text{NO}_2 + \text{M} \rightarrow \text{PPAN} + \text{M}$
- added  $\text{HO}_2 + \text{EtCO}_3 \rightarrow \text{EtOO} + \text{OH} + \text{CO}_2$  reaction to CheT.

### 2.4.2 Unification

Revising the inorganic and C<sub>1</sub>-C<sub>3</sub> alkane chemistry in the MCM and the CheT helped to find reactions that are different between mechanisms. However, to determine the best way to describe C<sub>2</sub>-C<sub>3</sub> RONO<sub>2</sub> chemistry for use in UM-UKCA, I had to unify the MCM and the CheT in a way described in Tables B.1-B.4. In brief:

- in the MCM, I:
  - removed gas-particle reactions and those that involve chlorine, sulphur and methoxy nitrate (CH<sub>3</sub>O<sub>2</sub>NO<sub>2</sub>);

– added:

1.  $\text{OH} + \text{OH} \rightarrow \text{H}_2\text{O}_2$
2.  $\text{OH} + \text{OH} \rightarrow \text{O}$
3.  $\text{O}(^1\text{D}) + \text{CH}_4 \rightarrow \text{HCHO} + \text{H}_2$
4.  $\text{O}(^1\text{D}) + \text{CH}_4 \rightarrow \text{HCHO} + \text{HO}_2 + \text{HO}_2$
5.  $\text{O}(^1\text{D}) + \text{CH}_4 \rightarrow \text{OH} + \text{CH}_3\text{O}_2$
6.  $\text{CH}_3\text{CHO} + h\nu \rightarrow \text{CH}_4 + \text{CO}$
7.  $\text{NO}_3 + \text{CH}_3\text{COCH}_3 \rightarrow \text{HNO}_3 + \text{CH}_3\text{COCH}_2\text{O}_2$

• to the CheT, I added<sup>4</sup>:

1.  $\text{NO} + \text{NO} + \text{O}_2 \rightarrow \text{NO}_2 + \text{NO}_2$
2.  $\text{O}(^3\text{P}) + \text{NO} + \text{M} \rightarrow \text{NO}_2 + \text{M}$
3.  $\text{O}(^3\text{P}) + \text{NO}_2 + \text{M} \rightarrow \text{NO}_3 + \text{M}$
4.  $\text{HO}_2 + \text{EtCO}_3 \rightarrow \text{EtOO} + \text{OH} + \text{CO}_2$

- in the inorganic chemistry, I updated old JPL rates to new JPL rates from [Burkholder et al. \(2015\)](#) and replaced IUPAC rates in the MCM with new JPL rates;
- in the organic chemistry, I updated old IUPAC and MCM rates to new IUPAC and MCM rates and did not use any JPL data.

The results of the unification of chemical mechanisms are discussed below. Please note that because there are no new recommendations for  $\text{MeONO}_2$  chemistry, and this chemistry is identical in the MCM and the CheT, I excluded  $\text{MeONO}_2$  chemistry from box model runs with the CheT and  $\text{C}_1$ - $\text{C}_3$   $\text{RONO}_2$  chemistry from box model runs with the MCM that are discussed in the section below.

### 2.4.3 Comparison

To see what subsets of the chemistry caused the predictions of the mechanisms to diverge, I compared the output from box model runs with the MCM and the CheT before and after the unification using the following chemistry subsets:

1. inorganic chemistry (in figures referred to as C0);
2. inorganic + methane chemistry (C0C1);
3. inorganic +  $\text{C}_1$ - $\text{C}_2$  alkane chemistry (C0C2);
4. inorganic +  $\text{C}_1$ - $\text{C}_3$  alkane chemistry (C0C3).

---

<sup>4</sup>The first three of these reactions were absent from the KPP version of CheT but present in UM-UKCA.



i.e. starting from the simplest subset and ending with the most complex.

I considered the MCM and the CheT being in acceptably close agreement when the difference in  $O_3$ , OH and  $HO_2$  steady state concentrations between mechanisms was no more than  $\pm 10\%$  in all  $NO_x$ -VOC conditions considered in the box model. When I was analysing the biases, I was subtracting the MCM values from the CheT values, i.e. the bias was high or positive when the CheT values were higher than the MCM ones.

### Inorganic chemistry

Before the unification (Figures 2.5 and B.1), the differences in concentrations of inorganic species between mechanisms often exceeded the 10% threshold. The bias was especially large (negative or positive depending on a species) in model runs with  $NO_x$  concentrations higher than 1 ppb, mostly due to the influence of the  $NO+NO\rightarrow NO_2+NO_2$  reaction.

After the unification (Figures 2.6 and B.2), the differences in concentrations of inorganic species reduced to less than 0.1% in all  $NO_x$  conditions considered.

### Inorganic + methane chemistry

Before the unification (Figures 2.7, B.3, B.5), the differences in the representation of methane chemistry between mechanisms only had a noticeable effect on  $CH_3OH$  and  $CH_3OOH$ , both of which were biased high.

After the unification (Figures 2.8, B.4, B.6), the differences in concentrations of all species in a subset reduced to less than 0.07% in all  $NO_x$  conditions considered.

### Inorganic + $C_1$ - $C_2$ alkane chemistry

Before the unification (Figures 2.9, B.7, B.9), there were almost no differences in the concentrations of inorganic species. However, concentrations of several organic species were different:  $CH_3OH$  and  $C_2H_5OOH$  were biased low, while PAN was biased high. Low CheT bias in  $CH_3OH$  was caused by the fact that  $CH_3OH$  production in CheT depends only on the concentration of the  $CH_3O_2$  radical, while in the MCM it depends on the total concentration of 7 organic peroxy radicals<sup>5</sup>. I left  $CH_3OH$  production in CheT unchanged, because (a) including the chemistry of the other organic peroxy radicals into CheT would have substantially increased the complexity of the mechanism, which I tried to avoid, (b) including an organic peroxy radical pool was beyond the scope of this study (but it has been recently done by Archer-Nicholls et al. (2019)), (c) the  $CH_3O_2$  radical is the dominant organic peroxy radical in the atmosphere, so having  $CH_3OH$  production being controlled by only the variability in the  $CH_3O_2$  radical should be enough to capture the main variations in  $CH_3OH$  production in a global 3D model.

---

<sup>5</sup> $RO_2=CH_3O_2+C_2H_5O_2+HOCH_2CH_2O_2+CH_3CO_3+HCOCH_2O_2+HOCH_2CO_3+HCOCO_3$ .

After the unification (Figures 2.10, B.8, B.10), the low  $\text{CH}_3\text{OH}$  bias at all  $\text{NO}_x$  levels and VOC levels higher than 10 ppbC remained almost the same, but the biases in  $\text{C}_2\text{H}_5\text{OOH}$  and PAN reduced to less than 10% in almost all  $\text{NO}_x$ -VOC conditions considered thanks to the unification of the reaction rate coefficients controlling their abundance.

### **Inorganic + C<sub>1</sub>-C<sub>3</sub> alkane chemistry**

Before the unification (Figures 2.11, B.11, B.13, B.15), the differences in concentrations of inorganic species and  $\text{CH}_3\text{O}_2$ , HCHO,  $\text{CH}_3\text{OH}$  and  $\text{CH}_3\text{OOH}$  exceeded the 10% threshold, especially in model runs with VOC concentrations higher than 1 ppbC. Concentrations of  $\text{C}_2\text{H}_5\text{OOH}$ ,  $\text{CH}_3\text{CHO}$ , PAN,  $\text{C}_2\text{H}_5\text{CHO}$ ,  $\text{CH}_3\text{COCH}_3$ ,  $\text{C}_2\text{H}_5\text{CO}_3\text{H}$  and PPN exceeded the 10% threshold in all  $\text{NO}_x$ -VOC conditions considered in the box model.

After the unification (Figures 2.12, B.12, B.14, B.16), the disagreement in concentrations of inorganic species between mechanisms disappeared, but biases in several organic species remained. The sign of these biases after the unification was sometimes different from before the unification, but the magnitude was usually smaller. Species for which concentrations differences still exceeded the 10% threshold were:  $\text{CH}_3\text{OH}$  (low at all  $\text{NO}_x$  levels and VOC levels higher than 1 ppbC),  $\text{C}_2\text{H}_5\text{OOH}$  (low at  $\text{NO}_x$  less than 1 ppb and VOC higher than 10 ppbC), PAN (low at  $\text{NO}_x$  levels lower than 1 ppb and all VOC levels),  $\text{C}_2\text{H}_5\text{CO}_3\text{H}$  (high in all  $\text{NO}_x$ -VOC conditions) and PPN (high at  $\text{NO}_x$  levels lower than 1 ppb and all VOC levels).

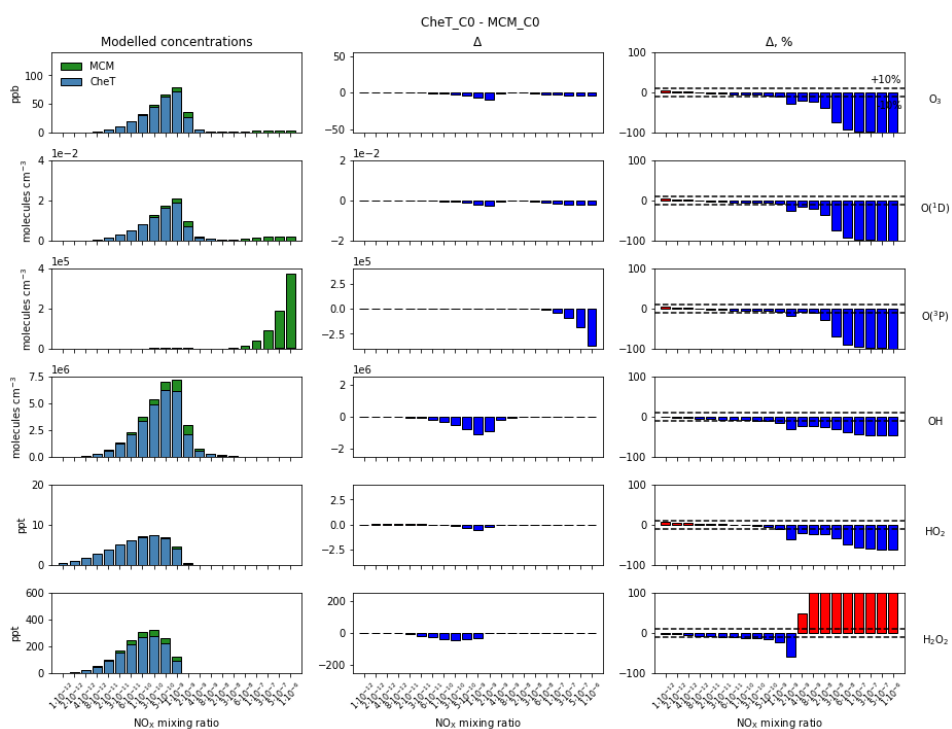


FIGURE 2.5:  $\text{O}_3$ ,  $\text{O}(^1\text{D})$ ,  $\text{O}(^3\text{P})$ ,  $\text{OH}$ ,  $\text{HO}_2$  and  $\text{H}_2\text{O}_2$  in steady state box model runs with the inorganic chemistry. (Left) steady state concentrations, (middle) absolute and (right) relative differences between mechanisms (CheT minus MCM) before unification. Dashed lines mark  $\pm 10\%$  difference.

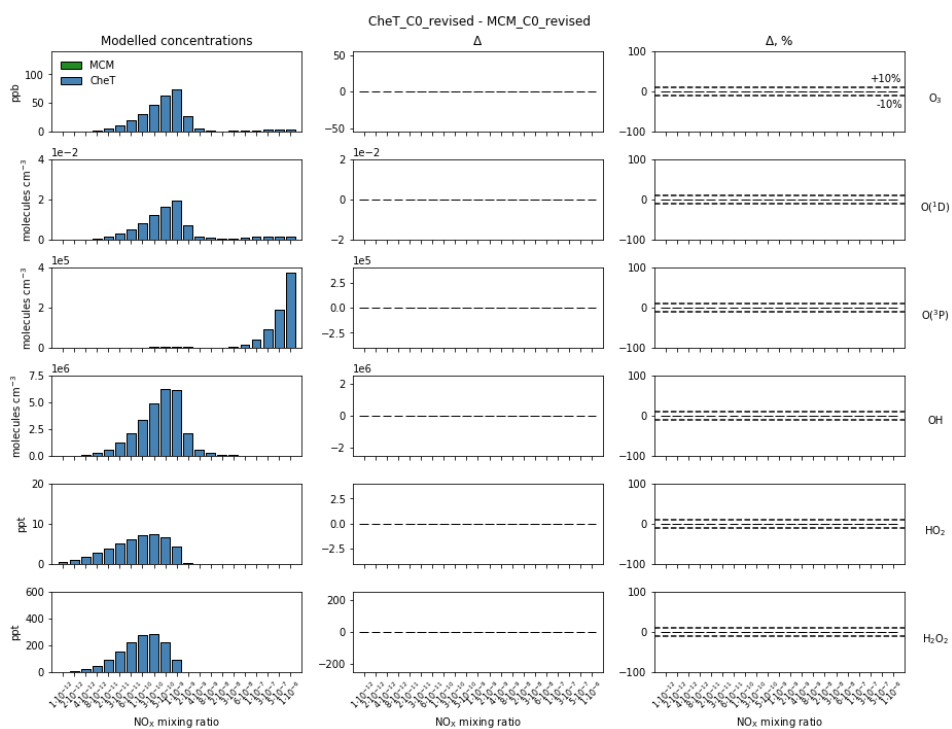


FIGURE 2.6: As in Fig. 2.5 but after unification.

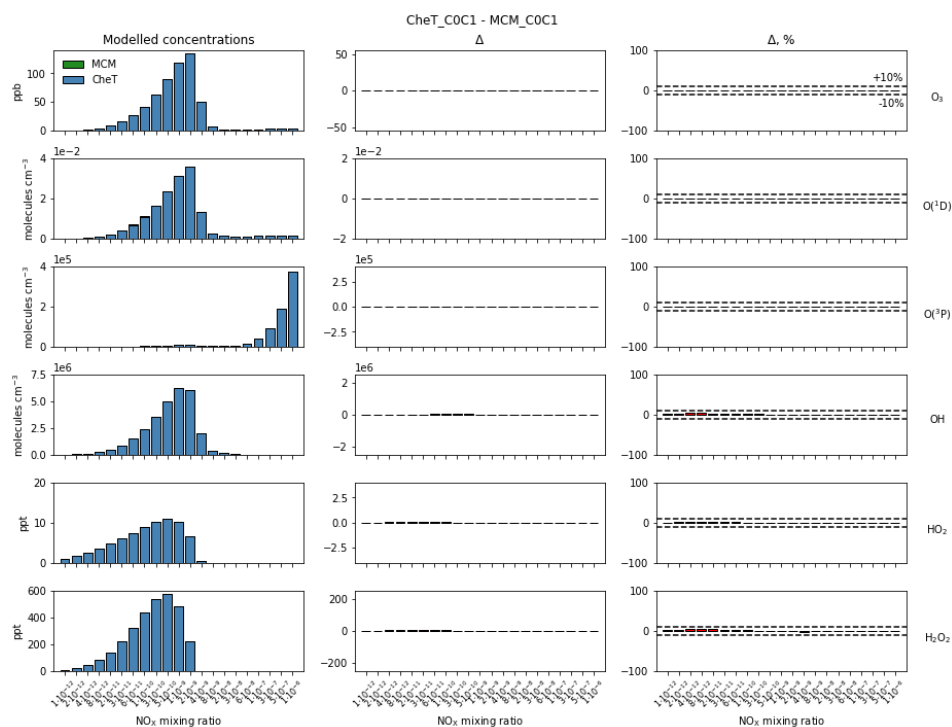


FIGURE 2.7: As in Fig. 2.5 but for the inorganic and  $\text{CH}_4$  chemistry before unification.

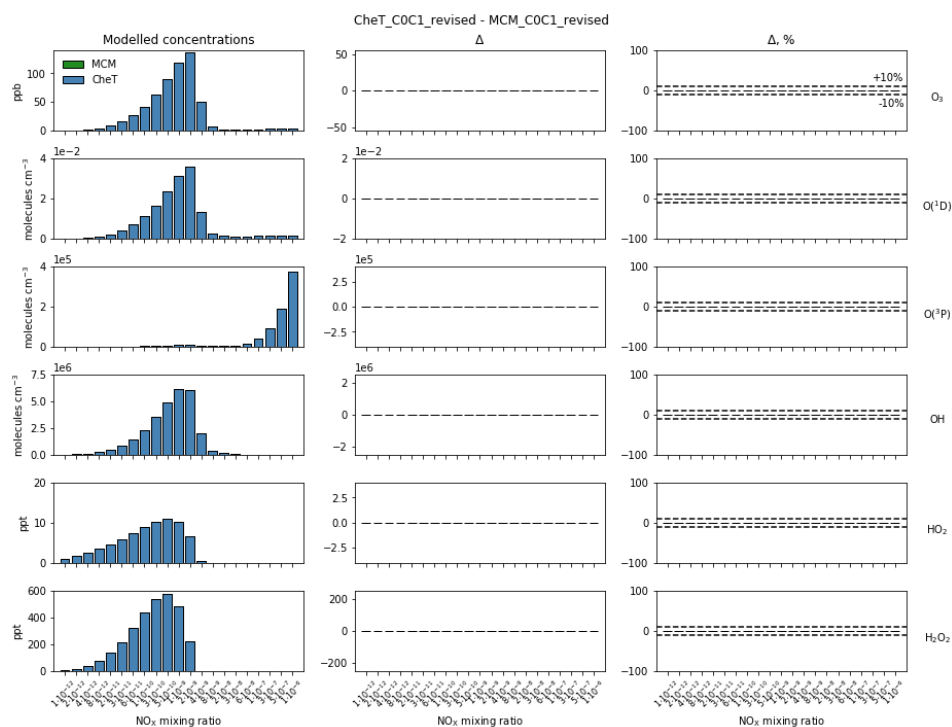


FIGURE 2.8: As in Fig. 2.7 but after unification.

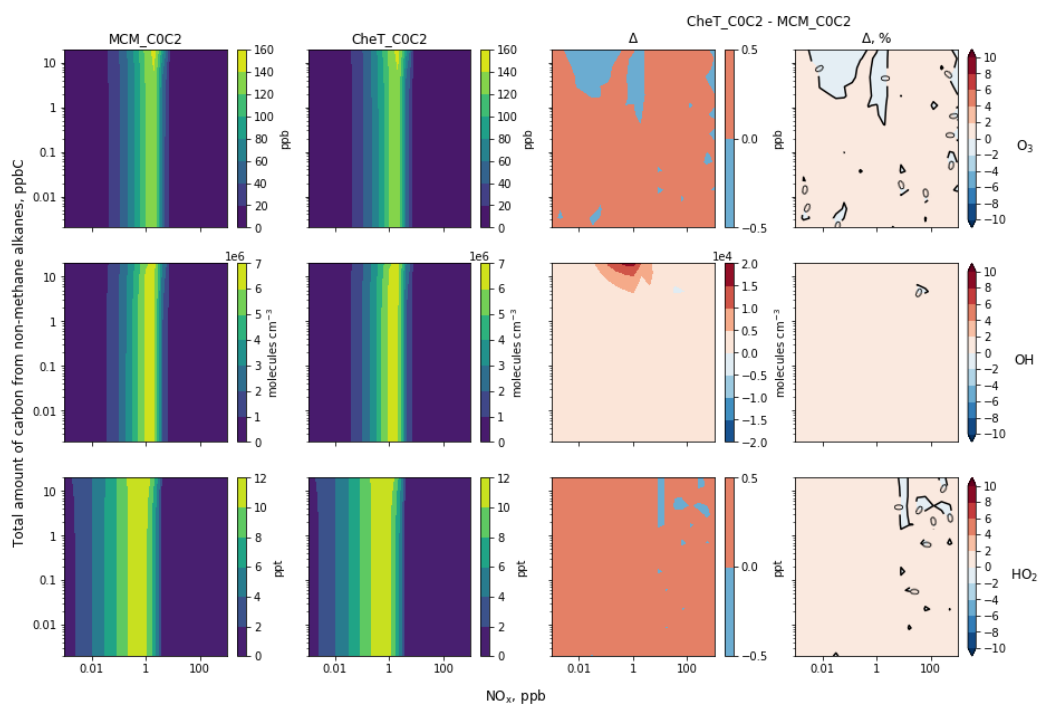


FIGURE 2.9:  $O_3$ , OH and  $HO_2$  in steady state box model runs with the inorganic,  $CH_4$  and  $C_2H_6$  chemistry. (Two left columns) steady state concentrations in the MCM and the CheT, (two right columns) absolute and relative differences between mechanisms (CheT minus MCM) before unification.

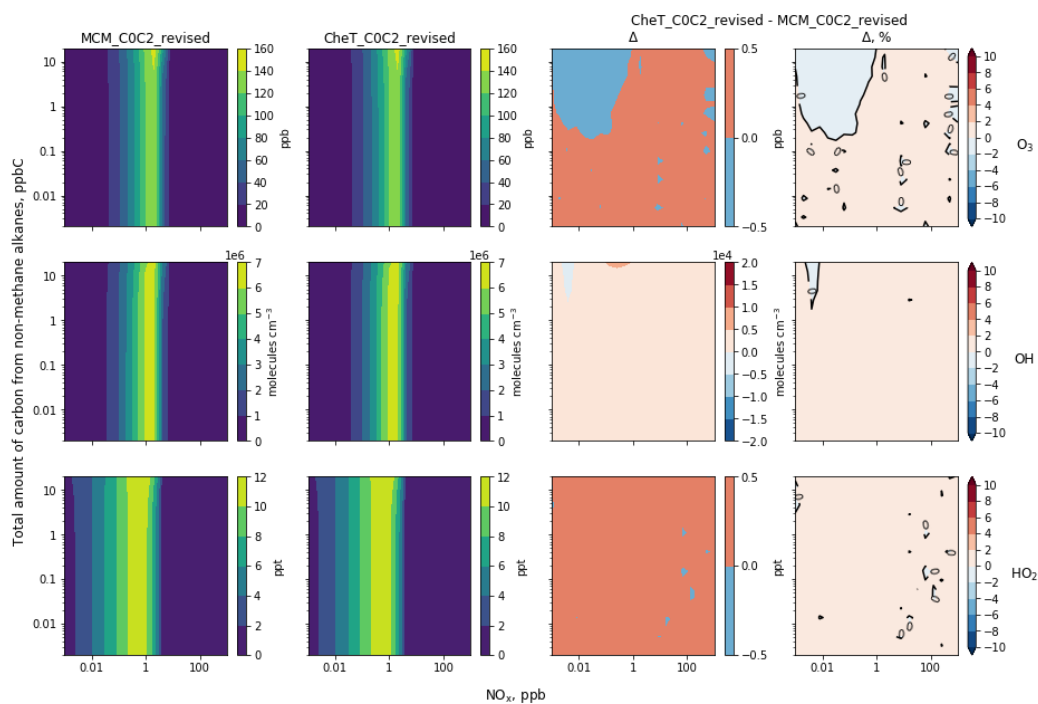


FIGURE 2.10: As in Fig. 2.9 but after unification.

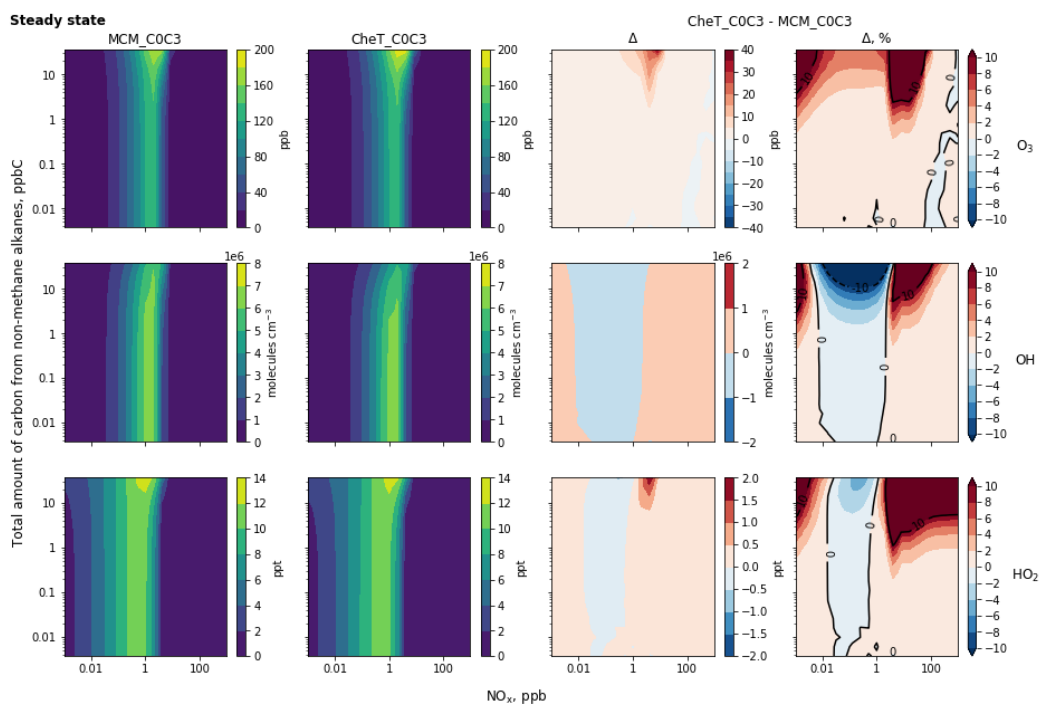


FIGURE 2.11:  $O_3$ , OH and  $HO_2$  in steady state box model runs with the inorganic,  $CH_4$ ,  $C_2H_6$  and  $C_3H_8$  chemistry. (Two left columns) steady state concentrations in the MCM and the CheT, (two right columns) absolute and relative differences between mechanisms (CheT minus MCM) before unification.

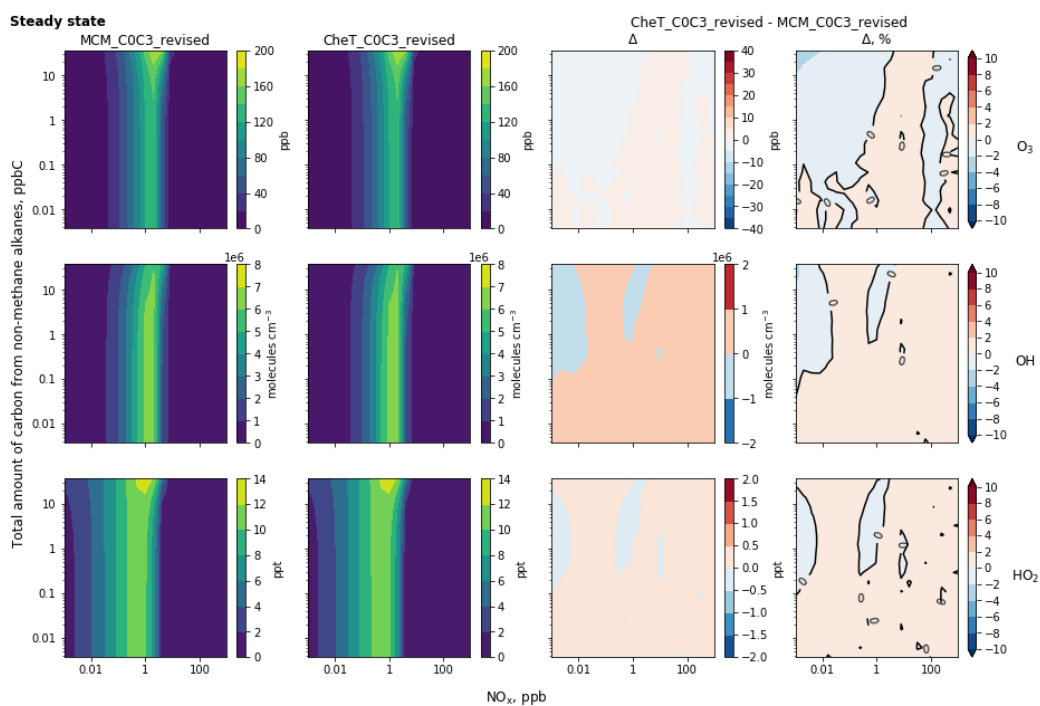


FIGURE 2.12: As in Fig. 2.11 but after unification.

### 2.4.4 Outcome of the revision and unification of chemical mechanisms

So, I revised and unified the inorganic and C<sub>1</sub>-C<sub>3</sub> alkane chemistry in the MCM and the CheT in a way that reduced the differences in their predictions of O<sub>3</sub>, OH and HO<sub>2</sub> steady state concentrations. Figure 2.13 shows that before the revision and unification, the CheT mechanism predicted lower O<sub>3</sub>, OH and HO<sub>2</sub> concentrations by up to 19 ppb, 1 × 10<sup>6</sup> molecules<sup>-1</sup> cm<sup>-3</sup> and 0.6 ppt, respectively, at NO<sub>x</sub> levels ranging from 0.1 ppb to 10 ppb and all VOC levels. At higher NO<sub>x</sub> levels, CheT was predominantly biased low by more than 10%, with an exception of a high bias in OH and HO<sub>2</sub> in high NO<sub>x</sub>-high VOC conditions. After the revision and unification, the differences in O<sub>3</sub>, OH and HO<sub>2</sub> steady state concentrations between the MCM and the CheT became smaller than 5% in all NO<sub>x</sub>-VOC conditions considered in the box model, i.e. even smaller than the 10% threshold.

This revision and unification of chemical mechanisms not only helped us prepare the CheT mechanism to be extended to include new chemistry, but also revealed that the differences in reaction rate coefficients between the MCM and the CheT often had a greater impact on predicted concentrations of inorganic species than the difference in the complexity of the mechanisms. This highlights the importance of and need for conducting more chemical kinetics studies to reduce the uncertainties in reaction rate coefficients, especially of inorganic reactions.

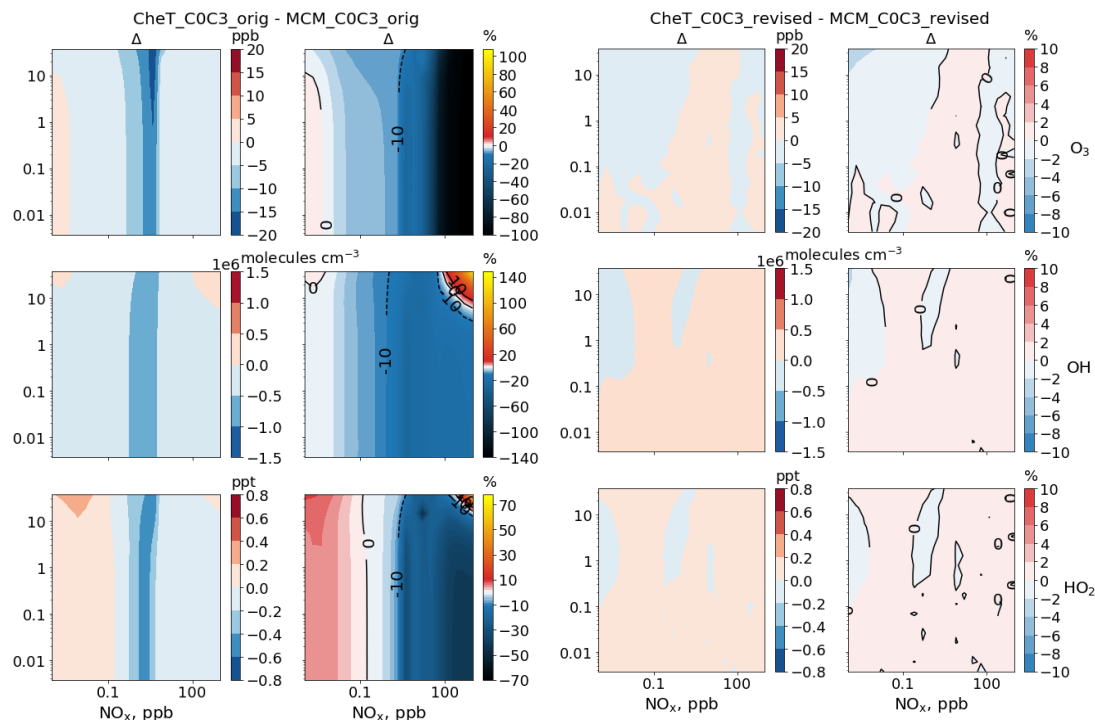


FIGURE 2.13: Absolute and relative differences in the steady state (top row) O<sub>3</sub>, (middle row) OH and (bottom row) HO<sub>2</sub> concentrations between the MCM and the CheT (CheT minus MCM) from box model runs with the inorganic and C<sub>1</sub>-C<sub>3</sub> alkane chemistry. (Two left columns) before the unification, (two right columns) after the unification.

## 2.5 Adding C<sub>2</sub>-C<sub>3</sub> alkyl nitrate chemistry

Having unified the mechanisms, I finally tested what representation of C<sub>2</sub>-C<sub>3</sub> RONO<sub>2</sub> chemistry was most suitable for use in UM-UKCA.

Because MeONO<sub>2</sub> chemistry was already present in the CheT and was identical to that from the MCM, I left it unchanged. EtONO<sub>2</sub> chemistry is very straightforward, so I added it to CheT as it is in the MCM. In the hope of reducing the computational cost of running UM-UKCA with additional chemistry, I tried to develop a simplified version of C<sub>3</sub> RONO<sub>2</sub> chemistry. I tested three versions of it, where:

1. PrONO<sub>2</sub> was a surrogate species. PrONO<sub>2</sub> was produced from both nPrOO+NO and iPrOO+NO reactions and was destroyed as if it were iPrONO<sub>2</sub>:

- nPrOO+NO→PrONO<sub>2</sub> :  $2.90 \times 10^{-12} \exp(350/T) \times 0.020$
- iPrOO+NO→PrONO<sub>2</sub> :  $2.70 \times 10^{-12} \exp(360/T) \times 0.042$
- PrONO<sub>2</sub>+OH→Me2CO+NO<sub>2</sub> :  $6.20 \times 10^{-13} \exp(-230/T)$
- PrONO<sub>2</sub>+hν →Me2CO+NO<sub>2</sub>+HO<sub>2</sub>

2. PrONO<sub>2</sub> was a lumped species. PrONO<sub>2</sub> was produced from both nPrOO+NO and iPrOO+NO reactions and, when destroyed, produced both EtCHO and Me2CO at yields derived from the ratio of the corresponding reaction rate coefficients:

- nPrOO+NO→PrONO<sub>2</sub> :  $2.90 \times 10^{-12} \exp(350/T) \times 0.020$
- iPrOO+NO→PrONO<sub>2</sub> :  $2.70 \times 10^{-12} \exp(360/T) \times 0.042$
- PrONO<sub>2</sub>+OH→0.62\*EtCHO+0.38\*Me2CO+NO<sub>2</sub> :  $5.8 \times 10^{-13}$
- PrONO<sub>2</sub>+hν →0.4\*EtCHO+0.6\*Me2CO+NO<sub>2</sub>+HO<sub>2</sub>

3. Same as version 2 but reaction rate coefficients for PrONO<sub>2</sub> loss were the average of the corresponding reaction rate coefficients for nPrONO<sub>2</sub> and iPrONO<sub>2</sub>:

- nPrOO+NO→PrONO<sub>2</sub> :  $2.90 \times 10^{-12} \exp(350/T) \times 0.020$
- iPrOO+NO→PrONO<sub>2</sub> :  $2.70 \times 10^{-12} \exp(360/T) \times 0.042$
- PrONO<sub>2</sub>+OH→0.62\*EtCHO+0.38\*Me2CO+NO<sub>2</sub> :  $(5.8 \times 10^{-13} + 6.20 \times 10^{-13} \exp(-230/T))/2$
- PrONO<sub>2</sub>+hν →0.4\*EtCHO+0.6\*Me2CO+NO<sub>2</sub>+HO<sub>2</sub>

These simplifications to C<sub>3</sub> RONO<sub>2</sub> chemistry appeared to introduce various biases into O<sub>3</sub> and C<sub>1</sub>-C<sub>3</sub> RONO<sub>2</sub> concentrations in steady state box model runs (not shown). The main reasons for this are as follows:

- at 298 K production rates of nPrONO<sub>2</sub> and iPrONO<sub>2</sub> differ by a factor of 2;



- products of nPrONO<sub>2</sub> and iPrONO<sub>2</sub> photolysis and oxidation are different and have different lifetimes: Me<sub>2</sub>CO produced during iPrONO<sub>2</sub> loss is longer-lived than EtCHO produced during nPrONO<sub>2</sub> loss. As a result, e.g. in version 3, an underestimation of Me<sub>2</sub>CO led to lower MeOO concentrations and therefore lower MeONO<sub>2</sub>, whereas overestimation of EtCHO led to higher EtOO concentrations and higher EtONO<sub>2</sub>.
- iPrONO<sub>2</sub> photolysis is 1.67 times faster than nPrONO<sub>2</sub> photolysis in the MCM photolysis parametrization.

Therefore, I decided to add the MCM representation of nPrONO<sub>2</sub> and iPrONO<sub>2</sub> chemistry into the CheT.

In total, new C<sub>2</sub>-C<sub>3</sub> RONO<sub>2</sub> chemistry required the addition of 3 new species and 9 new reactions (Table 2.3).

TABLE 2.3: C<sub>1</sub>-C<sub>3</sub> RONO<sub>2</sub> chemistry in UM-UKCA. New reactions are listed below the dashed line.

Reaction	Reaction rate coefficient
MeOO + NO → MeONO <sub>2</sub>	$2.30 \times 10^{-12} \exp(360/T) \times 0.001$
MeONO <sub>2</sub> + hν → HCHO + HO <sub>2</sub> + NO <sub>2</sub>	MeONO <sub>2</sub> photolysis
MeONO <sub>2</sub> + OH → HCHO + NO <sub>2</sub>	$4.00 \times 10^{-13} \exp(-845/T)$
EtOO + NO → EtONO <sub>2</sub>	$2.55 \times 10^{-12} \exp(380/T) \times 0.009$
nPrOO + NO → nPrONO <sub>2</sub>	$2.90 \times 10^{-12} \exp(350/T) \times 0.020$
iPrOO + NO → iPrONO <sub>2</sub>	$2.70 \times 10^{-12} \exp(360/T) \times 0.042$
EtONO <sub>2</sub> + hν → MeCHO + HO <sub>2</sub> + NO <sub>2</sub>	MeONO <sub>2</sub> photolysis
nPrONO <sub>2</sub> + hν → EtCHO + HO <sub>2</sub> + NO <sub>2</sub>	MeONO <sub>2</sub> photolysis
iPrONO <sub>2</sub> + hν → Me <sub>2</sub> CO + HO <sub>2</sub> + NO <sub>2</sub>	MeONO <sub>2</sub> photolysis
EtONO <sub>2</sub> + OH → MeCHO + NO <sub>2</sub>	$6.70 \times 10^{-13} \exp(-395/T)$
nPrONO <sub>2</sub> + OH → EtCHO + NO <sub>2</sub>	$5.80 \times 10^{-13}$
iPrONO <sub>2</sub> + OH → Me <sub>2</sub> CO + NO <sub>2</sub>	$6.20 \times 10^{-13} \exp(-230/T)$

## 2.6 Summary

- I developed and used a slightly new methodology for the intercomparison of chemical mechanisms. It involved running a set of box model simulations to ozone steady state with fixed  $\text{NO}_x$  and VOC concentrations and constructing isopleth plots for species of interest in  $\text{NO}_x$ -VOC coordinates.
- I used these isopleth plots to assess the differences between the UKCA's CheT mechanism and the MCM.
- I revised the inorganic and  $\text{C}_1$ - $\text{C}_3$  alkane CheT chemistry using the MCM as a benchmark.
- I unified the inorganic and  $\text{C}_1$ - $\text{C}_3$  alkane chemistry in the MCM and the CheT and showed that it is possible to predict the same  $\text{O}_3$ , OH and  $\text{HO}_2$  concentrations in steady state box model runs with these mechanisms after unification despite the MCM being a more complex mechanism. It highlights the important but detrimental impact of the differences in JPL and IUPAC recommendations on computer modelling of atmospheric chemistry.
- I extended the CheT mechanism to include  $\text{C}_2$ - $\text{C}_3$   $\text{RONO}_2$  chemistry using its representation from the MCM. It required the addition of 3 new species and 9 new reactions.

# 3

## UM-UKCA model development and validation

### 3.1 Introduction

Chemistry-climate models (CCMs) are physical climate models augmented with chemistry and aerosols schemes. In contrast to chemistry transport models (CTMs), CCMs assimilate the computed changes in greenhouse gases and aerosols into their calculation of radiative fluxes, which makes CCMs an excellent tool for investigating the effects of changing atmospheric composition on climate.

CCMs that include tropospheric chemistry are a relatively recent addition to the family of CCMs. The first few such CCMs participated in the Atmospheric Chemistry and Climate Model Intercomparison Project (ACCMIP, Lamarque et al., 2013), conducted in support of the Fifth Assessment Report of the Intergovernmental Panel on Climate Change (IPCC AR5). Tropospheric chemistry in the ACCMIP models was represented to various degrees of complexity: from 16 to 120 species, with this range reflecting the differences in representation of non-methane hydrocarbon (NMHC) chemistry. Because ACCMIP was not able to fully characterise the contribution of ozone and aerosols to the radiative forcing (Collins et al., 2017), a more comprehensive assessment of CCMs was launched as a combined activity of the International Global Atmospheric Chemistry (IGAC) and Stratosphere-troposphere Processes And their Role in Climate (SPARC) projects called the Chemistry-Climate Model Initiative (CCMI, Eyring et al., 2013; Morgenstern et al., 2017). The CCMI models described tropospheric chemistry more explicitly than the ACCMIP models, and although some of them still lacked

NMHC chemistry, the overall models' internal consistency, comprehensiveness and resolution have improved. Many CCMs that participated in CCMI are now submitting simulations to the Aerosol Chemistry Model Intercomparison Project (AerChemMIP, Collins et al., 2017), which will inform the Sixth Assessment report of the IPCC (IPCC AR6).

In this chapter, I describe the CCM used in this study and the experiments run with this CCM to investigate the impacts of C<sub>1</sub>-C<sub>3</sub> RONO<sub>2</sub> on tropospheric chemistry. Then, I describe how C<sub>1</sub>-C<sub>3</sub> RONO<sub>2</sub> photolysis was implemented and how the global oceanic and biomass burning emissions of C<sub>1</sub>-C<sub>3</sub> RONO<sub>2</sub> were derived. Finally, I compare the CCM results with observations and summarise the information about the model performance at the end.

## 3.2 UM-UKCA model description

### 3.2.1 Dynamics and chemistry

For this study, we used the Met Office Unified Model (UM) version 7.3 coupled with the United Kingdom Chemistry and Aerosol sub-model (together referred to as UM-UKCA). UM is the atmospheric dynamics component of the model. It solves the full, deep-atmosphere, non-hydrostatic equations of motion (Davies et al., 2005) and contains parametrisations of model sub-grid scale turbulence, convection, cloud and precipitation formation and radiative transfer. UKCA is the atmospheric chemistry component of the model. It solves chemical equations, calculates photolysis rates and contains parametrisations of dry and wet deposition of chemical species.

UM v7.3 is better known as HadGEM3-A revision 2.0 that was released shortly after HadGEM3-A r1.1 – the Global Atmosphere 1.0 (GA1.0) configuration (Hewitt et al., 2011), but before a major upgrade to the GA2.0 (Arribas et al., 2011; Walters et al., 2011). According to Hewitt et al. (2011), HadGEM3-A r1.1 reproduces the main features of the atmospheric circulation and generates fairly realistic precipitation, and the results from this model were considered scientifically credible.

O'Connor et al. (2014) evaluated the performance of the coupled HadGEM2-UKCA model, where HadGEM2 is an earlier version of the UM. They found that modelled distributions of radon-222, a tracer used to evaluate convective and synoptic-scale processes, are (a) generally in agreement with observations<sup>1</sup> and (b) comparable to those of other models, indicating that the parametrisations of boundary layer mixing and convection perform well in the model. HadGEM2-UKCA also reproduces the observed concentrations of lead-210, a tracer used to evaluate a model's wet scavenging scheme, but tends to underestimate lead-210 geographical and interannual variability in the Northern Hemisphere and does not capture its seasonal cycle at the South Pole.

---

<sup>1</sup>Except that the radon-222 seasonal cycle was not captured at Socorro (US) and Dumont d'Urville (Antarctica).

The modelled timescale for interhemispheric transport, inferred from simulations with krypton-85 tracer, is longer than in other models and was suggested to indicate deficiencies in tropical deep convection and/or insufficient boundary layer mixing. With regard to tropospheric chemistry, HadGEM2-UKCA was reported to reproduce present-day observed surface methane concentrations and tropospheric ozone concentrations very well (O'Connor et al., 2014), and a discussion of which is continued in Section 3.3.3 based on our results.

We ran UM-UKCA in its climate, atmosphere-only configuration, with horizontal resolution of  $3.75^\circ$  longitude by  $2.5^\circ$  latitude and 60 hybrid-height vertical levels extending up to 84 km (i.e. at N48L60 resolution). Because the model was not coupled to the ocean, it was driven with observed sea surface temperatures and sea ice extent from the Hadley Centre for Climate Prediction and Research Sea Ice and Sea Surface Temperature climatology (HadISST1, Rayner et al., 2003).

All simulations were performed with the UKCA's Chemistry for Stratosphere and Troposphere (CheST) chemical scheme. The stratospheric part of this scheme was described in Morgenstern et al. (2009) and the tropospheric part in O'Connor et al. (2014). Online calculation of the photolysis rates was handled by the FAST-JX photolysis scheme (Telford et al., 2013).  $O_3$  was coupled to the radiation scheme, but  $CH_4$  was not. We updated the tropospheric part of the CheST scheme in accordance with the findings in Chapter 2, i.e. updated selected reactions and reaction rate coefficients and included an explicit representation of photochemical production and loss of  $EtONO_2$ ,  $nPrONO_2$  and  $iPrONO_2$ . We also added  $MeONO_2$ ,  $EtONO_2$ ,  $nPrONO_2$  and  $iPrONO_2$  dry deposition and set it to be equal to PAN dry deposition, but did not consider wet deposition of these alkyl nitrates.

Monthly surface emissions of  $NO_x$ , CO, HCHO,  $C_2H_6$ ,  $C_3H_8$ , isoprene ( $C_5H_8$ ), acetone ( $CH_3COCH_3$ ) and acetaldehyde ( $CH_3CHO$ ) for the year 2000 were taken from the set of historical emissions data<sup>2</sup> used to initialise the models that simulated the Representative Concentration Pathways<sup>3</sup>. Monthly methanol ( $CH_3OH$ ) surface emissions were taken from the Model of Emissions of Gases and Aerosols from Nature (MEGAN, Guenther et al., 2012). For  $CH_4$  we used a year 2000 lower boundary condition of 1750 ppbv from the WMO SRES A1b scenario: at the lowest level of the model  $CH_4$  concentration was enforced to be equal to 1750 ppbv, but at higher levels it was determined by the dynamical and photochemical processes.

Table 3.1 summarises our UM-UKCA experiments. All of them were initialised from the Banerjee et al. (2014) "Base" simulation, where tracer concentrations are believed to be in a steady state. The only species not initialised from that simulation was  $MeONO_2$ . It was instead initialised with zero in all simulations but SSAN and FIRE in order to avoid the interference of the steady state concentration of  $MeONO_2$  achieved

<sup>2</sup>[ftp://ftp-ippc.fz-juelich.de/pub/emissions/gridded\\_netcdf](ftp://ftp-ippc.fz-juelich.de/pub/emissions/gridded_netcdf)

<sup>3</sup>[https://sedac.ciesin.columbia.edu/ddc/ar5\\_scenario\\_process/RCPs.html](https://sedac.ciesin.columbia.edu/ddc/ar5_scenario_process/RCPs.html)

TABLE 3.1: UM-UKCA 10-year perpetual year 2000 experiments for exploring the processes that control  $C_1$ - $C_3$   $RONO_2$  abundance: photochemical production (PP), photochemical loss (PL), dry deposition (DD), oceanic emissions (OC) and biomass burning emissions (BB). Wet deposition of alkyl nitrates was not considered.  $\square$  indicates that the process was switched off in the experiment,  $\blacksquare$  that it was switched on. UMUI job names are listed in the second column.

Experiment	UMUI	PP	PL	DD	OC	BB
SSAN <sup>1</sup>	xojnd	$\square$	$\square$	$\blacksquare$	$\square$	$\square$
BASE	xojng	$\square$	$\square$	$\blacksquare$	$\square$	$\square$
CHEM	xojnh	$\blacksquare$	$\blacksquare$	$\blacksquare$	$\square$	$\square$
MARI	xojni	$\square$	$\blacksquare$	$\blacksquare$	$\blacksquare$	$\square$
FIRE <sup>1</sup>	xojnc	$\square$	$\blacksquare$	$\blacksquare$	$\square$	$\blacksquare$
FULL	xojnl	$\blacksquare$	$\blacksquare$	$\blacksquare$	$\blacksquare$	$\blacksquare$

<sup>1</sup> The initial  $MeONO_2$  concentration was a non-zero steady state concentration from the [Banerjee et al. \(2014\)](#) “Base” simulation.

by the model in the presence of only a secondary source of  $MeONO_2$ , with  $MeONO_2$  concentrations computed in the presence of both primary and secondary sources.

Our BASE experiment used the updated CheST scheme, included no sources of  $C_1$ - $C_3$   $RONO_2$  and had the initial  $MeONO_2$  concentration equal to zero. The sensitivity experiments were built upon the BASE experiment so that we could explore the model’s response to (1)  $C_1$ - $C_3$   $RONO_2$  photochemistry in the presence of their secondary source, (2) photochemical processing of their oceanic and (3) biomass burning emissions, and (4)  $C_1$ - $C_3$   $RONO_2$  photochemistry in the presence of their primary and secondary sources. Therefore, the BASE experiment setup was extended to include  $C_1$ - $C_3$   $RONO_2$  photochemical production and loss in the CHEM experiment, oceanic emissions of  $C_1$ - $C_3$   $RONO_2$  and their photochemical loss in the MARI experiment, biomass burning emissions of  $C_1$ - $C_3$   $RONO_2$  and their photochemical loss in the FIRE experiment, and the photochemical production and loss of  $C_1$ - $C_3$   $RONO_2$  and their oceanic and biomass burning emissions in the FULL experiment. All experiments included  $C_1$ - $C_3$   $RONO_2$  dry deposition.

To achieve a new steady state after modifications to the chemistry and facilitate statistical analysis of the impact of alkyl nitrates on atmospheric composition discussed in Chapter 4, we ran perpetual year 2000 simulations, which were 10-year-long simulations with each year representing the year 2000. The output time resolution was monthly.

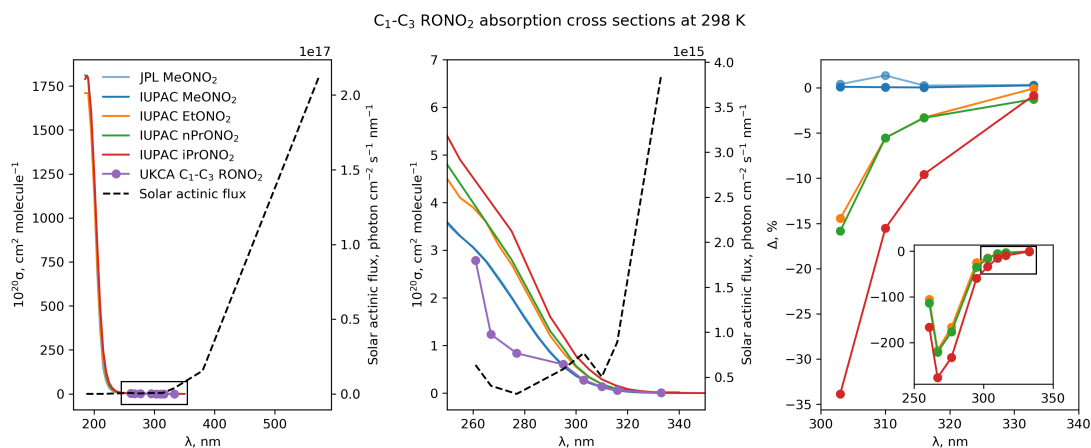


FIGURE 3.1:  $C_1$ - $C_3$   $\text{RONO}_2$  absorption cross sections at 298 K recommended by the IUPAC and JPL and the data used in UKCA (Telford et al., 2013): (left) full wavelengths range, (middle) zoomed in to 250–350 nm. Dashed line indicates the solar actinic flux at the surface in UKCA. Relative differences between UKCA values and either of the recommendations are shown on the right for 300–340 nm and (insert) 250–350 nm.

### 3.2.2 $C_1$ - $C_3$ alkyl nitrate photolysis

Due to various circumstances, we used  $\text{MeONO}_2$  absorption cross section for all  $C_1$ - $C_3$   $\text{RONO}_2$ . This is not ideal as the absorption cross sections of longer-chain alkyl nitrates increase with increasing carbon number (Figure 3.1). However, it is acceptable if the main focus of a study is tropospheric chemistry, because photons corresponding to wavelengths, where the largest discrepancies between cross sections occur (shorter than 300 nm), are absorbed by the atmosphere before these photons reach the surface (as evident from a rapid decrease in the solar actinic flux in Figure 3.1). Wavelengths longer than 300 nm penetrate deeper into the atmosphere and can photodissociate alkyl nitrates. At these wavelengths the difference between the  $\text{MeONO}_2$  cross section recommended by the IUPAC (Atkinson et al., 2006) and the cross section used in UKCA (Telford et al., 2013) is less than 0.3% (it is less than 2% if compared to the JPL data (Burkholder et al., 2015)). However, the differences between UKCA’s  $\text{MeONO}_2$  cross section and the recommended values for  $C_2$ - $C_3$   $\text{RONO}_2$  increase with decreasing wavelength, reaching 35% at 303 nm in the case of  $\text{iPrONO}_2$ . This means that in the troposphere,  $\text{MeONO}_2$  photolytic loss is described well in our model, but in the case of  $C_2$ - $C_3$   $\text{RONO}_2$  it is negatively biased. In the stratosphere,  $C_1$ - $C_3$   $\text{RONO}_2$  photolysis is likely negatively biased too, but the stratosphere is not our region of interest.

### 3.2.3 $C_1$ - $C_3$ alkyl nitrate oceanic emissions

Many previous studies support the hypothesis that alkyl nitrates are produced in seawater. However, lack of observational data and little understanding of the mechanism of alkyl nitrate seawater production makes modelling it a challenge. Neu et al. (2008) were the first to calculate alkyl nitrate oceanic emissions using a global CTM

(UCI). For that, they first calculated an a priori flux of MeONO<sub>2</sub> and EtONO<sub>2</sub> using a single, average equatorial Pacific Ocean value for the air-sea concentration gradient and surface wind speed from [Dahl et al. \(2005\)](#). They imposed this flux in the model as a constant, spatially uniform value over the tropical oceans (10°S-10°N) and the Southern Ocean (south of 45°S). Then, to get an a posteriori flux and emissions, they scaled an a priori flux of MeONO<sub>2</sub> and EtONO<sub>2</sub> separately in both regions so that the CTM reproduced the large scale MeONO<sub>2</sub> and EtONO<sub>2</sub> distribution observed during the PEM-Tropics A and B aircraft campaigns ([Blake et al., 2003](#)). Two later studies, [Williams et al. \(2014\)](#) and [Khan et al. \(2015\)](#), used variants of the [Neu et al. \(2008\)](#) MeONO<sub>2</sub> and EtONO<sub>2</sub> oceanic emissions (hereafter referred to as the [Neu et al. \(2008\)](#) emissions) as input to other CTMs (TM5 and STOCHEM-CRI, respectively).

The [Neu et al. \(2008\)](#) emissions had some limitations. One was that the model [Neu et al. \(2008\)](#) used to derive these emissions did not include a photochemical source of MeONO<sub>2</sub> and EtONO<sub>2</sub>. That might have lead to an overestimation of their oceanic source and inflated the role of this source in two later studies, both of which included a photochemical source in addition to an oceanic one. Another limitation was that the [Neu et al. \(2008\)](#) emissions had neither seasonal nor spatial variability. That might have been enough for simulating equatorial regions since [Blake et al. \(2003\)](#) observed similar MeONO<sub>2</sub> and EtONO<sub>2</sub> concentrations over the equatorial Pacific during PEM-Tropics A (August-October) and B (March-April). Yet, it is not enough for simulating emissions from the Southern Ocean, because (a) [Blake et al. \(1999\)](#) observed a distinct increase in MeONO<sub>2</sub> concentrations from November to December south of Tasmania during the ACE-1 aircraft campaign, and (b) [Hughes et al. \(2008\)](#) confirmed the variability of alkyl nitrate source in the Southern Ocean via saturation measurements.

More recently [Fisher et al. \(2018\)](#) took a completely different approach and developed a parametrisation for alkyl nitrate air-sea exchange. They designed this parametrisation to be driven by changes in wind speed, sea surface temperature and nitrite availability, and implemented it into a global CTM (GEOS-Chem). The gas exchange in this parametrisation followed [Johnson \(2010\)](#) with updated Henry's Law coefficients from [Sander \(2015\)](#). The global distribution of surface seawater nitrite was calculated from observations and was used to find regions with predominantly non-zero nitrite, i.e. regions where alkyl nitrate production was possible. That was justified by the fact that alkyl nitrate photochemical production in seawater was shown to be limited by nitrite availability ([Dahl and Saltzman, 2008](#); [Dahl et al., 2012](#)).

In regions with non-zero nitrate, they set a single, fixed seawater concentration for MeONO<sub>2</sub> based on seawater measurements where possible. EtONO<sub>2</sub> seawater concentration was calculated using a 6:1 ratio of MeONO<sub>2</sub> to EtONO<sub>2</sub> from [Dahl et al. \(2007\)](#). Elsewhere the ocean was considered as an alkyl nitrate sink.

In the tropics, [Dahl et al. \(2007\)](#) found that the surface seawater concentrations of MeONO<sub>2</sub>, EtONO<sub>2</sub> and iPrONO<sub>2</sub> are positively correlated with chlorophyll *a*. That



relationship and another between alkyl nitrates and nitrite prompted Fisher et al. (2018) to link chlorophyll *a* to nitrite. Relying on that link, they used satellite monthly mean chlorophyll *a* concentration data for the year 2003 to further refine the tropical MeONO<sub>2</sub> and EtONO<sub>2</sub> oceanic sources. They found that chlorophyll-derived distribution of seawater alkyl nitrate concentrations improved the simulation of atmospheric alkyl nitrate concentrations in the tropical marine boundary layer relative to a version with nitrite-derived distribution of oceanic sources.

As a result, Fisher et al. (2018) managed to model MeONO<sub>2</sub> and EtONO<sub>2</sub> oceanic sources in a mechanistic way and calculated MeONO<sub>2</sub> and EtONO<sub>2</sub> oceanic emissions with monthly resolution for the entire globe. This is a progress since the Neu et al. (2008) work, which is why we used MeONO<sub>2</sub> and EtONO<sub>2</sub> oceanic emissions from Fisher et al. (2018) (hereafter referred to as the Fisher et al. (2018) emissions) in our study. However, in future studies, it would be desirable to obtain some direct observational evidence for the link between chlorophyll *a* and nitrite seawater concentrations in the tropics.

Regarding the questions (a) how typical the year 2003 chlorophyll *a* distribution was and (b) how different it was relative to year 2013, important because meteorological data for year 2013 was used in the Fisher et al. (2018) GEOS-Chem simulations, there is a growing body of literature. According to the Radenac et al. (2012) classification of El Niño events for the period 1997-2010, an El Niño event occurred during 2002-2003 (September-February) that was categorised as a central Pacific El Niño and associated with an overall decrease of chlorophyll *a* concentrations in the tropical Pacific. They found that the maximum of the negative chlorophyll anomaly equal to  $\sim 0.15 \text{ mg m}^{-3}$  was centred around the dateline and the bands of the anomaly stretched along the equator and north-east towards the North American coast. This agrees with the more comprehensive data on the seawater chlorophyll *a* concentration from the Ocean-Colour Climate Change Initiative dataset v4.2 (OC-CCI, Sathyendranath et al., 2019) that shows an annual mean negative chlorophyll anomaly of  $0.01 \text{ mg m}^{-3}$  that stretches north-east from Papua New Guinea to the North American coast (Figure 3.2b). Therefore, year 2003 chlorophyll *a* concentrations in the tropical Pacific could be considered as anomalously low, but not as low as during El Niño events of the eastern Pacific type. However, because of the high interannual variability of chlorophyll *a* evident from Figures 3.2b-d, oceanic alkyl nitrate emissions in the tropics should be derived for each year individually, if one uses the Fisher et al. (2018) approach.

To add information about nPrONO<sub>2</sub> and iPrONO<sub>2</sub> oceanic emissions into our simulations, I assumed that these emissions are (a) co-located with EtONO<sub>2</sub> emissions and (b) constitute 10% and 20% of EtONO<sub>2</sub> emissions, respectively, according to the ratios reported by Dahl et al. (2007) (0.1:1 nPrONO<sub>2</sub>:EtONO<sub>2</sub>, 0.2:1 iPrONO<sub>2</sub>:EtONO<sub>2</sub>). I applied the same ratios in the tropics and northern and southern high latitudes in the absence of observational data from high latitudes.

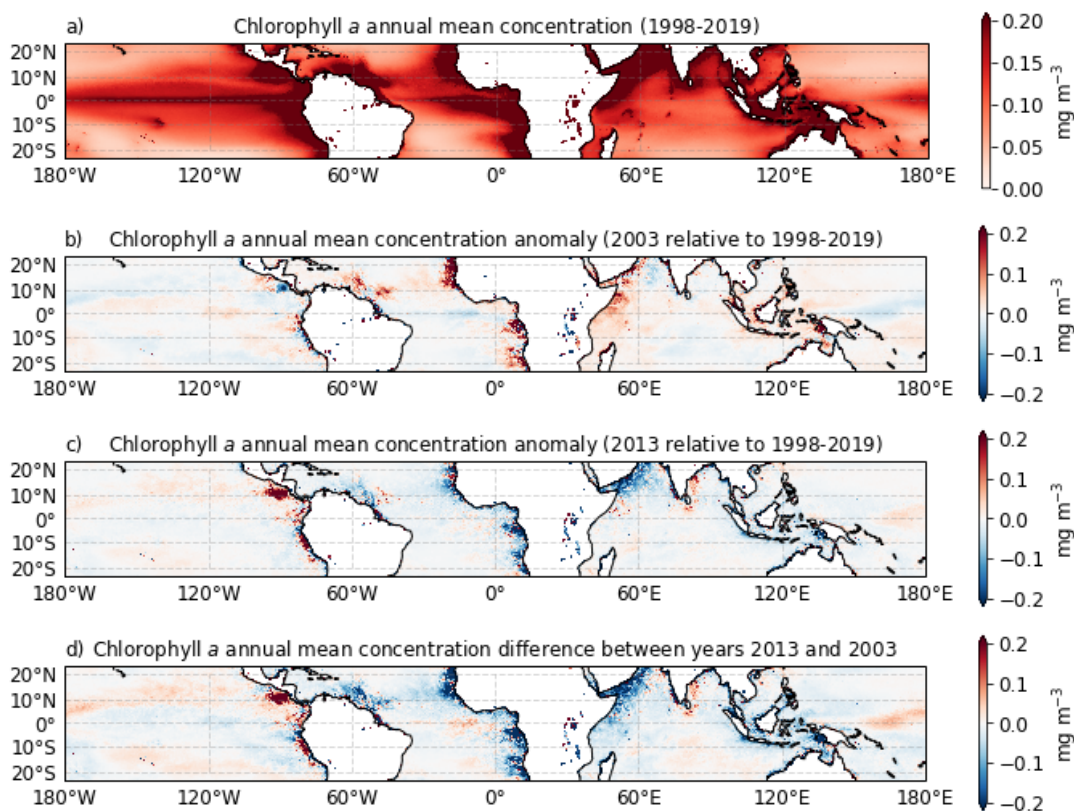


FIGURE 3.2: Chlorophyll *a* concentrations in seawater from the OC-CCI dataset: (a) annual mean for the period 1998-2019, (b) 2003 annual mean anomaly relative to the 1998-2019 period, (c) 2013 annual mean anomaly relative to the 1998-2019 period and (d) the difference between 2013 and 2003 annual means (2013 minus 2003). Note that the colour scales are supersaturated.

The GEOS-Chem data on oceanic emissions had a higher horizontal resolution than the UM-UKCA version used in this study. Therefore, I regridded the GEOS-Chem data onto the UM-UKCA grid. This has led to the global annual oceanic emission of  $\text{MeONO}_2$  and  $\text{EtONO}_2$  to be smaller in UM-UKCA than in GEOS-Chem by about 10%. Most of this difference was caused by the fact that a coarser resolution land mask had to be applied in UM-UKCA over the Indian Ocean, where alkyl nitrate emissions were high throughout the year.

Figure 3.3 shows the distribution of  $\text{MeONO}_2$ ,  $\text{EtONO}_2$ ,  $\text{nPrONO}_2$  and  $\text{iPrONO}_2$  oceanic emissions in UM-UKCA as an annual sum (Figures C.5-C.6 as a seasonal sum). The strongest alkyl nitrate oceanic source is the equatorial oceans. It varies in time following the variability of chlorophyll *a*. High latitude sources of alkyl nitrates are weaker than equatorial ones and have a smaller temporal and spatial variability.  $\text{MeONO}_2$  oceanic emissions are the strongest,  $\text{EtONO}_2$  are second strongest,  $\text{iPrONO}_2$  third and  $\text{nPrONO}_2$  fourth. Fisher et al. (2018) simulations showed that tropical oceans are a small net sink of alkyl nitrates, therefore there are no alkyl nitrate emissions there.

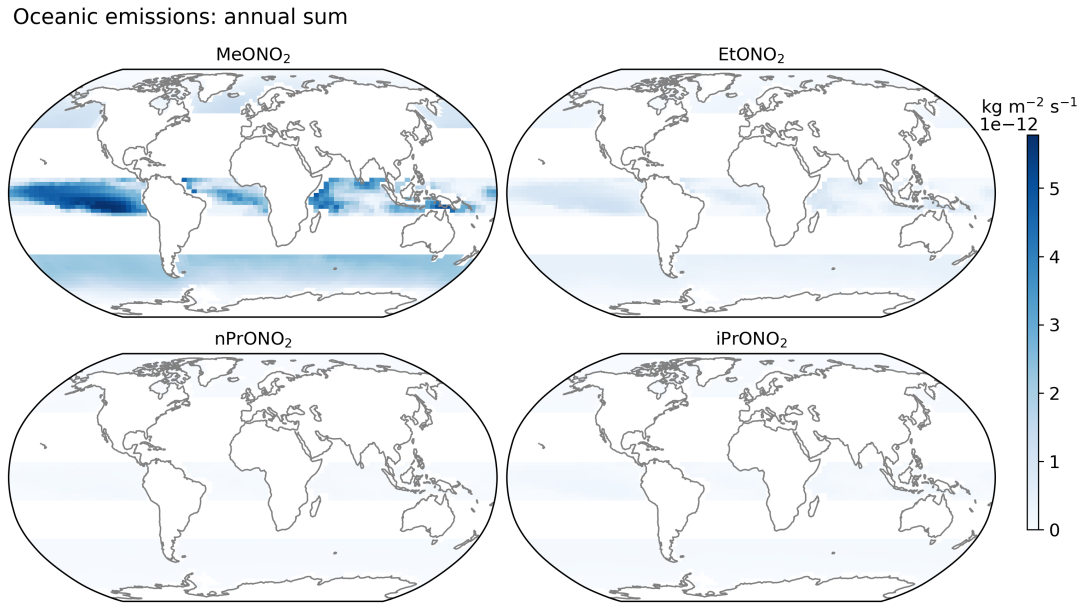


FIGURE 3.3: Total C<sub>1</sub>-C<sub>3</sub> RONO<sub>2</sub> oceanic emissions per year simulated by GEOS-Chem and regridded onto UM-UKCA grid. The white color over the oceans corresponds to regions of small alkyl nitrate uptake by the ocean.

### 3.2.4 C<sub>1</sub>-C<sub>3</sub> alkyl nitrate biomass burning emissions

Biomass burning emissions of C<sub>1</sub>-C<sub>3</sub> RONO<sub>2</sub> were calculated here for the first time using the data from the Global Fire Emissions Database version 4.1 with small fires (GFED4s, Werf et al., 2017). The calculation procedure is described below.

GFED4s provides high resolution (0.25°) monthly data for the 1997-2016 period on burned area, fire carbon emissions, dry matter emissions and the contribution of different fire types to these emissions. The fire types include (1) savannah, grassland, shrubland fires, (2) boreal forest fires, (3) temperate forest fires, (4) tropical forest fires (deforestation and degradation), (5) peatland fires and (6) agricultural waste burning. To calculate trace gas emissions from a certain fire type, one should multiply dry matter emissions by the contribution of that fire type to dry matter emissions and by the emission factor of that trace gas from that fire type. Adding up trace gas emissions from all fire types gives the total trace gas emission from fires.

Even though we use the Fisher et al. (2018) oceanic emissions derived for a combination of years 2003 and 2013, I tried to avoid the bias related to the choice of specific years when calculating alkyl nitrate biomass burning emissions. For that reason, I first calculated a 20-year mean annual cycle of (a) dry matter emissions and (b) the contribution of various fire types to dry matter emissions.

The next step was choosing what emission factors to use with what dry matter emissions. Akagi et al. (2011) provide information about alkyl nitrate emission factors for tropical forest fires, savannah fires, boreal forest fires and extratropical forest fires (Table 3.2). The last two fire types are related in a way that extratropical forest

TABLE 3.2: Emission factors ( $\text{g kg}^{-1}$ ) for species emitted from different types of biomass burning. An estimate of the natural variation is given in parenthesis, where available (Akagi et al., 2011).

RONO <sub>2</sub>	tropical forest	savannah	boreal forest	extratropical forest
MeONO <sub>2</sub>	$8.29 \times 10^{-3}$ ( $1.60 \times 10^{-2}$ )	$5.1 \times 10^{-4}$ ( $3.7 \times 10^{-4}$ )	$2.83 \times 10^{-3}$	$2.83 \times 10^{-3}$
EtONO <sub>2</sub>	$5.70 \times 10^{-3}$	$3.51 \times 10^{-4}$ <sup>a</sup>	$1.78 \times 10^{-3}$	$1.78 \times 10^{-3}$
nPrONO <sub>2</sub>	$3.00 \times 10^{-4}$	$1.85 \times 10^{-5}$ <sup>a</sup>	$3.23 \times 10^{-4}$	$3.23 \times 10^{-4}$
iPrONO <sub>2</sub>	$1.00 \times 10^{-3}$	$6.15 \times 10^{-5}$ <sup>a</sup>	$3.23 \times 10^{-3}$	$3.23 \times 10^{-3}$

<sup>a</sup> in this study

fires are split into boreal and temperate forest fires in the fourth generation of GFED. Knowing that and the fact that (a) there are no data on emission factors for temperate forest fires, but (b) there are data on dry matter emissions from boreal and temperate forest fires, I added up dry matter emissions from boreal and temperate forest fires and multiplied their sum by the emission factor for extratropical forest fires. In the case of savannah fires, Akagi et al. (2011) do not report any data on the emission factors of C<sub>2</sub>-C<sub>3</sub> RONO<sub>2</sub>, but report these for MeONO<sub>2</sub>. Knowing this and the fact that (a) Simpson et al. (2002) observed emissions of C<sub>2</sub>-C<sub>3</sub> RONO<sub>2</sub> from savannah fires and (b) savannah fires have more in common with tropical forest fires than with extratropical forest fires, I calculated C<sub>2</sub>-C<sub>3</sub> RONO<sub>2</sub> emission factors for savannah fires using the relationship between MeONO<sub>2</sub> emissions factors for savannah and tropical forest fires. Future studies would benefit from incorporating the Simpson et al. (2002) estimates of emission ratios of alkyl nitrates relative to CO<sub>2</sub> and CO during different stages of savannah fires (flaming and smoldering), but our study was limited by the GFED4s v4.1 assumption that emission factors are constant in time (Zheng et al., 2018). Lastly, there are GFED4s data on dry matter emissions from agricultural waste burning, but no data on emission factors of alkyl nitrates from that fire type. For that reason, emissions from agricultural waste burning were excluded from our analysis.

The last step was to regrid the resulting 20-year mean monthly data on MeONO<sub>2</sub>, EtONO<sub>2</sub>, nPrONO<sub>2</sub> and iPrONO<sub>2</sub> biomass burning emissions onto the UM-UKCA grid. Regridding to a coarser resolution introduced a small positive bias, but the difference between the original and regridded global annual emission of each of the alkyl nitrates was less than 3%.

Figure 3.4 shows the distribution of MeONO<sub>2</sub>, EtONO<sub>2</sub>, nPrONO<sub>2</sub> and iPrONO<sub>2</sub> biomass burning emissions in UM-UKCA as an annual sum (Figures C.3-C.4 as a seasonal sum). The strongest alkyl nitrate biomass burning source is the tropical forest fires. The second strongest is the savannah fires. Both of these sources emit mostly MeONO<sub>2</sub>, with a smaller amount of EtONO<sub>2</sub> and an even smaller amount for propyl nitrates. Extratropical forest fires predominantly emit iPrONO<sub>2</sub>, and this source is the strongest biomass burning source of iPrONO<sub>2</sub>.

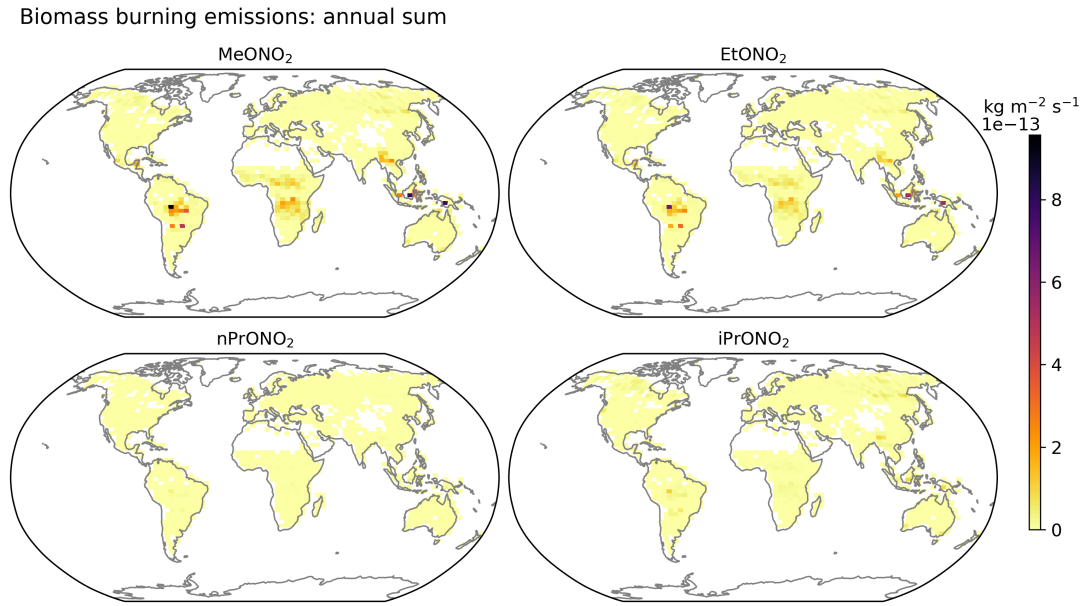


FIGURE 3.4: Total  $C_1-C_3$  RONO<sub>2</sub> biomass burning emissions per year derived from GFEDs and regridded onto UM-UKCA grid.

To better understand the potential impact of  $C_1-C_3$  RONO<sub>2</sub> oceanic and biomass burning emissions on the oxidising capacity of the atmosphere, it is useful to estimate the contribution of these emissions into the global nitrogen budget. Table 3.3 summarises such estimates from this and the other two studies. Oceanic emissions of alkyl nitrates are larger than biomass burning emissions. The sum of  $C_1-C_3$  RONO<sub>2</sub> oceanic emissions is equal to  $171.94 \text{ Gg N yr}^{-1}$  ( $184.08 \text{ Gg N yr}^{-1}$  in the case of  $C_1-C_2$  RONO<sub>2</sub> according to Fisher et al. (2018)), while the GFEDs-derived sum of  $C_1-C_3$  RONO<sub>2</sub> biomass burning emissions is equal to  $16.89 \text{ Gg N yr}^{-1}$ , which is close to the Simpson et al. (2002) estimate of  $18 \text{ Gg N yr}^{-1}$  for  $C_1-C_4$  RONO<sub>2</sub> biomass burning emissions. MeONO<sub>2</sub> biomass burning emissions comprise 6-7% of its oceanic emissions, EtONO<sub>2</sub> 20-23%, nPrONO<sub>2</sub> 15% and iPrONO<sub>2</sub> 38%, and the sum of  $C_1-C_3$  RONO<sub>2</sub> biomass burning emissions is 9-10% of its oceanic equivalent. As NO<sub>x</sub> sources, oceanic and biomass burning emissions of alkyl nitrates are 2-3 orders of magnitude smaller than other NO<sub>x</sub> sources. For example, a recent estimate of NO<sub>x</sub> emissions from lightning is  $2-9 \text{ Tg N yr}^{-1}$  (Nault et al., 2017), while the global total NO<sub>x</sub> source is  $44 \text{ Tg N yr}^{-1}$  with an uncertainty range of  $23-81 \text{ Tg N yr}^{-1}$  (Lee et al., 1997). This then poses the question of whether direct emissions of alkyl nitrates as NO<sub>x</sub> sources matter for the oxidising capacity of the atmosphere. This is explored in the UM-UKCA runs MARI and FIRE discussed in Chapter 4.

TABLE 3.3: Global oceanic (OC) and biomass burning (BB) C<sub>1</sub>-C<sub>3</sub> RONO<sub>2</sub> emissions in Gg N yr<sup>-1</sup>.

Source	MeONO <sub>2</sub>	EtONO <sub>2</sub>	nPrONO <sub>2</sub>	iPrONO <sub>2</sub>	Total	Reference
OC	157.13	26.95	-	-	184.08	Fisher et al. (2018)
BB	-	-	-	-	18.00 <sup>a</sup>	Simpson et al. (2002)
BB	9.52	5.49	0.31	1.57	16.89	GFEDs, this study
OC	141.39	24.25	2.10	4.20	171.94	this study
BB	9.76	5.63	0.31	1.59	17.29	this study
OC + BB	151.15	29.88	2.41	5.79	189.23	this study

<sup>a</sup> The sum of C<sub>1</sub>-C<sub>4</sub> RONO<sub>2</sub> biomass burning emissions.

TABLE 3.4: Dates of ATom deployments.

Deployment	Date range
ATom-1	July 29 - August 23, 2016
ATom-2	January 26 - February 21, 2017
ATom-3	September 28 - October 28, 2017
ATom-4	April 24 - May 21, 2018

### 3.3 UM-UKCA model validation

#### 3.3.1 Description of Atmospheric Tomography mission (ATom)

To validate the newly implemented chemistry, we compared modelled species concentrations with those observed during the NASA Atmospheric Tomography (ATom) mission (Prather et al., 2017). That mission was the most recent aircraft mission that measured C<sub>1</sub>-C<sub>3</sub> RH and RONO<sub>2</sub>, but more importantly, it sampled the remote atmosphere in all meteorological conditions (not only clear skies) without chasing pollution plumes (Strode et al., 2018). The latter allowed ATom to obtain an unbiased climatology of the chemical reactivity of the troposphere, therefore providing an excellent dataset for validating global CTMs and CCMs.

ATom continuously profiled the atmosphere from 0.2 to 12 km altitude over the Pacific and Atlantic Ocean in each of 4 seasons from 2016 to 2018. It had 4 deployments (Table 3.4). In this thesis, we use ATom-1 and ATom-2 data only, because the relevant data from ATom-3 and ATom-4 have not been released at the time of writing. All ATom flights originated from the Armstrong Flight Research Center in Palmdale, California. February 2017 and August 2016 flights then proceeded north to the Western Arctic, south to the South Pacific, east to the Atlantic, north to Greenland and returned to California. January 2017 and July 2016 flights were limited to the West Pacific area (Figure 3.5).

For validation, we used high resolution ATom data on CH<sub>4</sub> (measured by NOAA Picarro) and O<sub>3</sub>, NO and NO<sub>2</sub> (NOAA Nitrogen Oxides and Ozone) and whole air



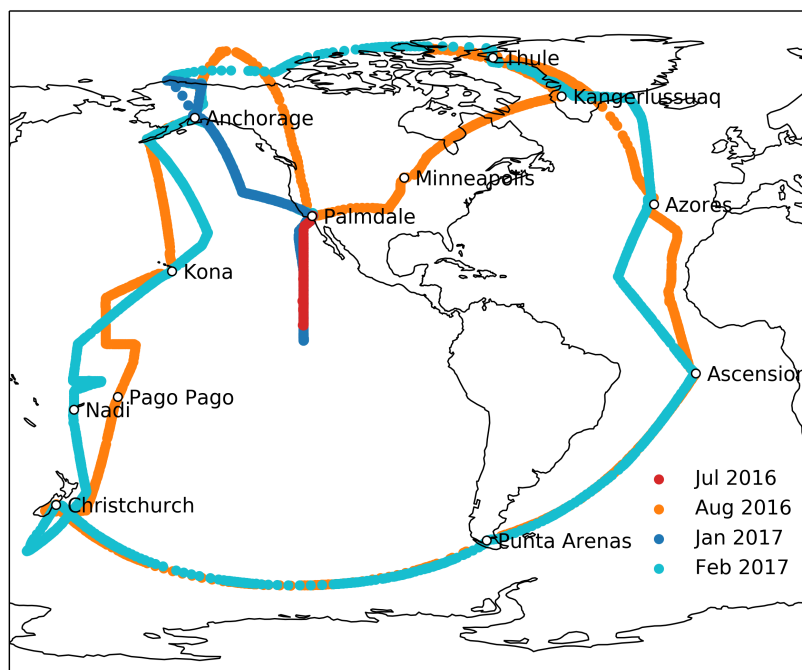


FIGURE 3.5: ATom-1 and ATom-2 flight tracks. ATom-1 July 2016 (red markers): Palmdale, equator, Palmdale; August 2016 (orange markers): Palmdale, Anchorage, Kona, Pago Pago, Christchurch, Punta Arenas, Ascension, Azores, Kangerlussuaq, Minneapolis, Palmdale. ATom-2 January 2017 (blue markers): Palmdale, equator, Palmdale, Anchorage; February 2017 (cyan markers): Anchorage, Kona, Nadi, Christchurch, Punta Arenas, Ascension, Azores, Thule, Anchorage, Palmdale.

sampling data on ethane, ethene ( $C_2H_4$ ), ethyne ( $C_2H_2$ ), propane, propene ( $C_3H_6$ ),  $MeONO_2$ ,  $EtONO_2$ ,  $nPrONO_2$ ,  $iPrONO_2$ , all merged to whole air sampling interval (MER-WAS data, Wofsy et al., 2018).

### 3.3.2 Comparison of ATom and UM-UKCA vertical profiles

To investigate spatial and seasonal biases in modelled  $C_1$ - $C_3$  RH and  $RONO_2$ ,  $O_3$ , NO and  $NO_2$  concentrations, I compared observed and modelled mean vertical profiles of these species over 8 geographical regions in 2 different months. I used monthly mean UM-UKCA data, which is not ideal when comparing to high time resolution observational data, but monthly mean was the lowest output frequency in our 10-year-long simulations. We did a separate simulation with UM-UKCA v10.6 with hourly output over a limited domain (see Chapter 6), and saw that the main conclusions about UM-UKCA bias in  $C_2H_6$ ,  $C_3H_8$  and  $MeONO_2$  relative to ATom were similar to those obtained in this chapter. However, in future studies it would be desirable to run UM-UKCA with hourly resolution in the configuration used in this chapter and compare the results.

The procedure used to calculate regional mean vertical profiles is described below. First, I selected the regions of interest and determined their appropriate size (Figure

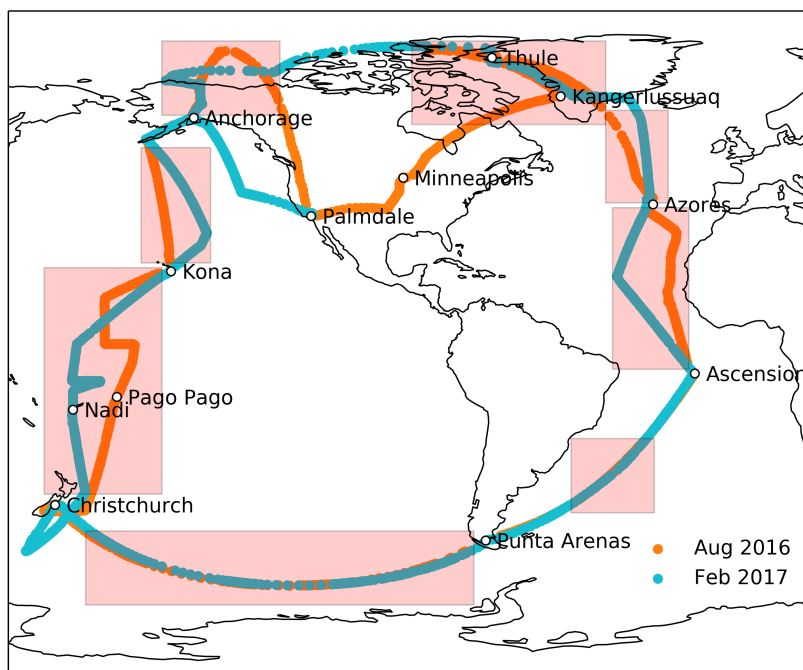


FIGURE 3.6: ATom-1 and ATom-2 flight tracks (coloured markers) and regions selected for the calculation of mean vertical profiles (red shaded boxes).

3.6). The regions should have been big enough to encompass as many areas with ATom measurements as possible, but not too big that variations in general atmospheric circulation (e.g. tropics vs. mid-latitudes) and boundary conditions (land vs. ocean) would have affected the calculation of a regional mean. Next, I extracted ATom and UM-UKCA regional data from their respective global datasets and binned these data by altitude into 500 m layers. In the process, UM-UKCA data had to be (a) re-levelled from the hybrid-height coordinate to absolute height with a 100 m vertical resolution and (b) the first two years of data discarded as a spin-up. Lastly, I calculated the mean and standard deviation for each layer in each region averaged over time. For that, I performed the same spatial averaging calculation on both ATom and UM-UKCA data, but applied a different time averaging. ATom data were averaged over the time period when the flight tracks were within selected regions. UM-UKCA data were averaged over 8 months of the same month. So, it means that the error bars shown in Figures 3.7-3.15 for ATom vertical profiles reflect the variability observed along the ATom flight tracks on different hours/days of a month, while the error bars for the UM-UKCA profiles reflect the modelled variability across entire regions as an 8-year-mean monthly mean.

Before I proceed to the data analysis, I would like to remind the reader that ethane and propane are lumped species in UKCA. Ethane represents the sum of ethane, ethene and ethyne, and propane represents the sum of propane and propene (O'Connor et al., 2014). To obtain equivalents of these UM-UKCA species from ATom, I converted the respective ATom data into pptv of carbon (pptvC) and added them up. Unfortunately,



this procedure greatly reduced the amount of data suitable for comparison, especially in the case of the sum of propane and propene (too few observations of propene). For that reason, to compare UM-UKCA's propane with ATom I used only propane data from ATom.

In the next section, I present the comparison of the regional mean vertical profiles of  $\text{CH}_4$ ,  $\text{C}_2\text{H}_6$ ,  $\text{C}_3\text{H}_8$ ,  $\text{NO}_x$ ,  $\text{O}_3$ ,  $\text{MeONO}_2$ ,  $\text{EtONO}_2$ ,  $\text{nPrONO}_2$  and  $\text{iPrONO}_2$  observed by ATom and simulated in the UM-UKCA FULL run, unless specified otherwise.

### 3.3.3 Results

#### Methane

UM-UKCA generally captures the observed  $\text{CH}_4$  vertical profiles (Figure 3.7, Table C.1). However, high observed  $\text{CH}_4$  variability sometimes leads to low coefficients of determination ( $R^2$ ) and high root-mean-square errors (RMSE) between the observations and the model. Modelled mean  $\text{CH}_4$  concentrations stay mostly within the observed variability, except for the regions of Alaska, Greenland and the North Atlantic. Over Alaska and Greenland in February, the model explains 98% and 92% of the observed profiles, respectively, but underestimates  $\text{CH}_4$  concentrations with an RMSE of 70 and 53 ppbv, respectively. Over Alaska, Greenland and the North Atlantic in August, the model has a positive bias below 8 km (RMSE 89, 89 and 48 ppbv, respectively). Such UM-UKCA's bias has been reported before and was suggested to be caused by an overestimation of wetland emissions in the Northern Hemisphere (O'Connor et al., 2014). However, another possible explanation could be the  $\text{CH}_4$  lower boundary condition. Lower boundary condition is a tool designed to help the model simulate the right global mean concentration of a species without trying to capture its observed surface latitudinal gradient. We used a single, fixed value for the  $\text{CH}_4$  lower boundary condition, while the observed surface  $\text{CH}_4$  concentration varies with latitude<sup>4</sup>. So, in a way, our model is not even expected to capture the  $\text{CH}_4$  latitudinal gradient. A solution to this would be to use a latitudinally varying  $\text{CH}_4$  lower boundary condition or  $\text{CH}_4$  emissions, both of which have their pros and cons. More about these can be found in Heimann et al. (in prep.).

At altitudes higher than 8 km, the model predicts a strong vertical gradient in  $\text{CH}_4$ , but this gradient is stronger than the observed gradient in all regions except for the Central Pacific and Central Atlantic. Such UM-UKCA's bias has also been reported before and was attributed to slow ascent of air in the tropics in the model (O'Connor et al., 2014).

---

<sup>4</sup>[https://www.esrl.noaa.gov/gmd/ccgg/globalview/ch4/ch4\\_description.html](https://www.esrl.noaa.gov/gmd/ccgg/globalview/ch4/ch4_description.html)

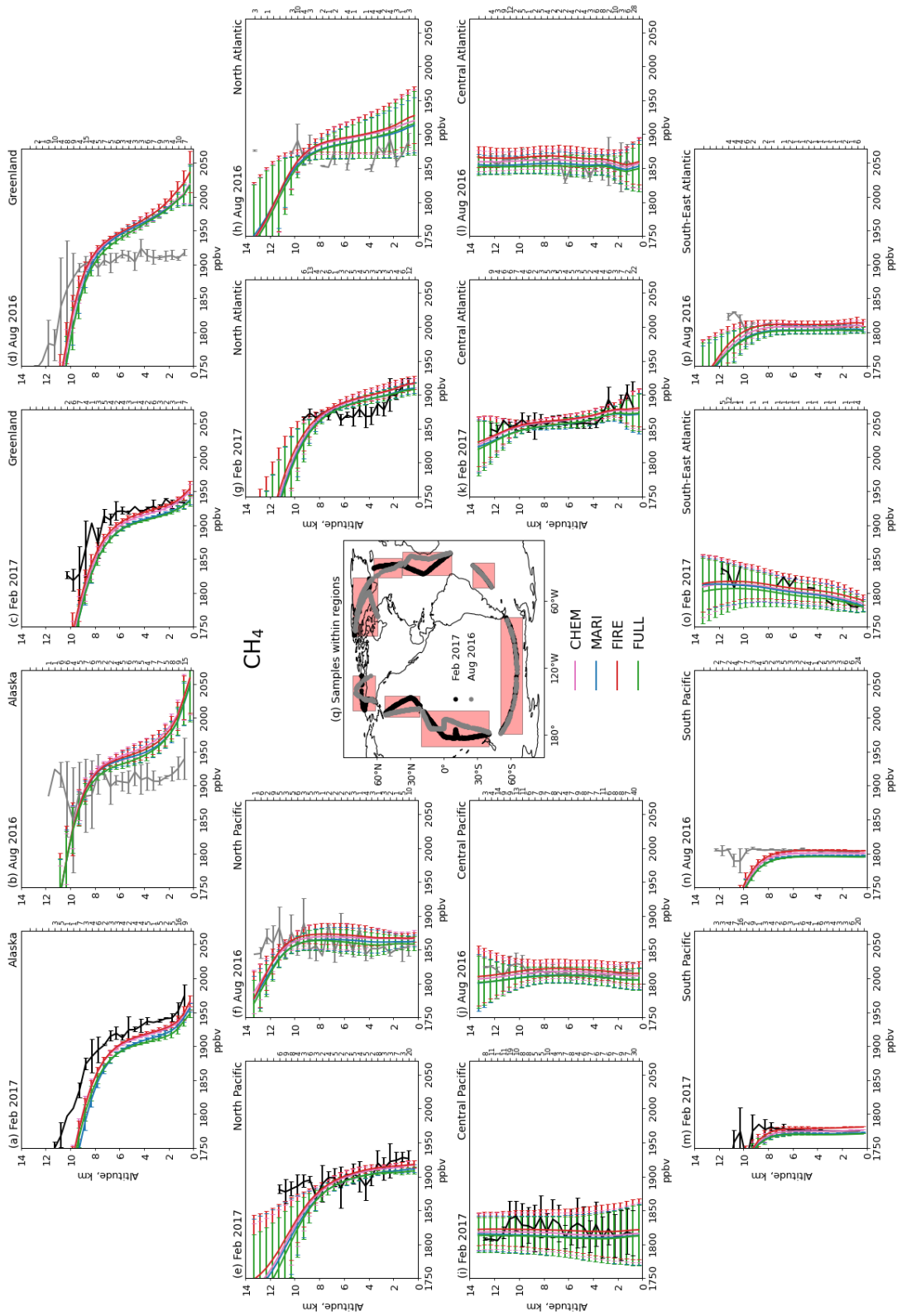


FIGURE 3.7:  $\text{CH}_4$  regional mean vertical profiles: (a)-(p) vertical profiles paired by season (February - left, August - right) and region. Number of ATom observations per level is shown on the right y-axis. For the error bar description see Section 3.3.2. (q) a map showing the coordinates (markers) of ATom observations located within selected regions. ATom data from February 2017 is shown in black and August 2016 in grey. UM-UKCA data from the CHEM run is shown in magenta, MARI in blue, FIRE in red and FULL in green.

## Ethane

UM-UKCA predominantly does not capture the observed vertical profiles of the sum of  $C_2H_6$ ,  $C_2H_4$  and  $C_2H_2$  (Figures 3.8 and C.7 with differing x-axis, Table C.2). In February, the model underestimates this sum with an RMSE of 2.25, 3.16, 2.97, 2.03 and 1.19 ppbvC over the North Pacific, Alaska, Greenland, North Atlantic and Central Atlantic, respectively, and predicts concentrations twice as high as the observed for the South Pacific and South-East Atlantic boundary layer. In August, the model has a smaller negative bias over Alaska, Greenland, the North Atlantic and Central Atlantic (RMSE 1.46, 1.45, 0.56 and 0.82 ppbvC, respectively), but explains a smaller proportion of the observed variability than in February ( $R^2$  for August is lower than for February).

Due to their relatively short lifetimes of hours to months,  $C_2H_6$ ,  $C_2H_4$  and  $C_2H_2$  are more sensitive to the temporal and spatial variability of their sources and sinks than  $CH_4$ .  $C_2H_6$ ,  $C_2H_4$  and  $C_2H_2$  sources and sinks also differ. The dominant source of  $C_2H_6$  and  $C_2H_2$  is fossil fuel and biofuel production (Xiao et al., 2007; Xiao et al., 2008), while the dominant source of  $C_2H_4$  (and  $C_3H_6$ ) is biogenic production from plants (Rhew et al., 2017). The dominant sink of  $C_2H_6$  and  $C_2H_2$  is OH oxidation, while an additional sink of  $C_2H_4$  (and  $C_3H_6$ ) is ozonolysis (Atkinson and Arey, 2003). UKCA simplifies  $C_2H_6$ ,  $C_2H_4$  and  $C_2H_2$  chemistry and lumps  $C_2H_6$ ,  $C_2H_4$  and  $C_2H_2$  emissions by mass<sup>5</sup> into  $C_2H_6$ , which is then oxidised by OH at the rate of the  $C_2H_6+OH$  reaction. Such a simplification extends modelled  $C_2H_6$  lifetime and explains part of the positive model bias over the South Pacific and South-East Atlantic in February. Elsewhere, a negative model bias in  $C_2H_6$  is likely linked to an overestimation of the OH sink and/or an underestimation of  $C_2H_6$ ,  $C_2H_4$  and  $C_2H_2$  emissions.

To better understand the OH sink, I calculated UM-UKCA's air mass weighted annual mean tropospheric OH ratio of Northern to Southern Hemisphere (Table 3.5). It varied between simulations and was on average equal to 1.36, which exceeds observation-derived ratios of 0.98 (Krol and Lelieveld, 2003), 1 (Spivakovsky et al., 2000) and  $0.97\pm 0.12$  (Patra et al., 2014), but stays within 1.13-1.42 range of estimates from ACCMIP models (Naik et al., 2013). The excess in OH in the Northern Hemisphere was noticed in UM-UKCA before and was attributed to an overproduction of OH from the  $O(^1D)+H_2O$  reaction due to an overproduction of  $O(^1D)$  from the photolysis of  $O_3$  (Telford et al., 2013). Nevertheless, the model captures the seasonal variability in the OH sink by simulating higher  $C_2H_6$  (and  $C_3H_8$ ) concentrations in February than in August in the Northern Hemisphere, with this effect present but mirrored in the Southern Hemisphere.

---

<sup>5</sup>[https://www.ukca.ac.uk/wiki/index.php/Emissions\\_for\\_ACSIS](https://www.ukca.ac.uk/wiki/index.php/Emissions_for_ACSIS)

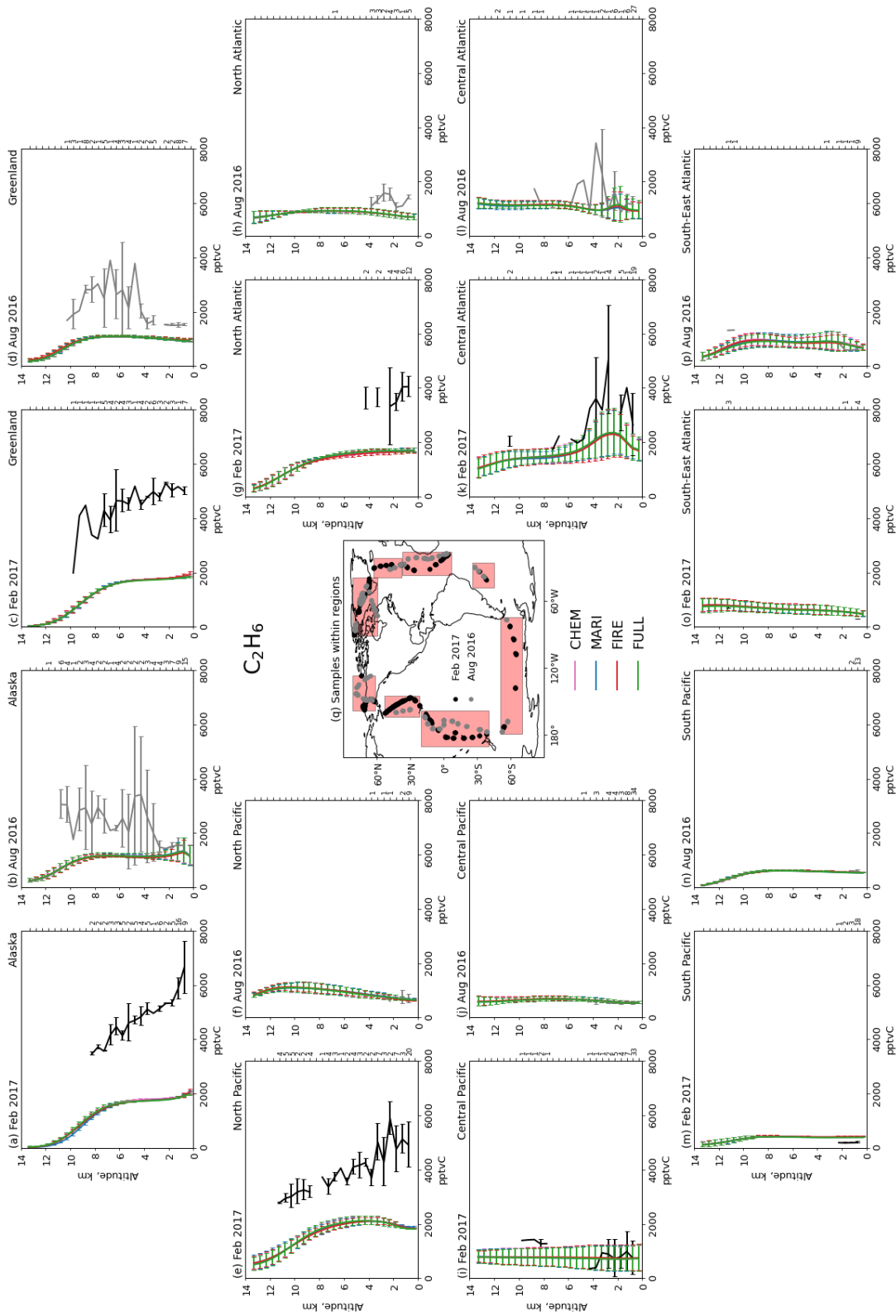
FIGURE 3.8: As in Fig. 3.7 but for  $C_2H_6$ .

TABLE 3.5: Tropospheric interhemispheric annual mean OH ratio computed for 90°N-90°S using 125 ppb ozonepause and averaged over 8 years of UM-UKCA perpetual year 2000 simulation. The standard error of the mean is given in brackets.

Experiment	NH/SH OH ratio
BASE	1.367 (0.005)
CHEM	1.358 (0.003)
MARI	1.340 (0.005)
FIRE	1.366 (0.006)
FULL	1.345 (0.005)

While there is evidence of excessive OH in the model, the situation with the bias in  $C_2H_6$ ,  $C_2H_4$  and  $C_2H_2$  emissions is uncertain. On the one hand, because of the ongoing shift of anthropogenic emissions from North America and Europe to Asia (Gaudel et al., 2018), more recent anthropogenic emissions are different from their year 2000 counterparts. For that reason, we did not expect the model to capture  $C_2H_6$  concentrations, because we used emissions for the year 2000 but are comparing modelled concentrations to those observed in 2016/2017. On the other hand, there is evidence of a recent global increase in  $C_2H_6$  and  $C_3H_8$  hypothesised to be driven by an increase in oil and natural gas production in the USA (Helmig et al., 2016). This recent increase in  $C_2H_6$  and  $C_3H_8$  might partially explain a negative model bias in  $C_2H_6$  and  $C_3H_8$  in the Northern Hemisphere relative to ATom.

Another potential source of model bias in  $C_2H_6$  is the variability in  $C_2H_6$ ,  $C_2H_4$  and  $C_2H_2$  biomass burning emissions. In fact, Strode et al. (2018) reported that in August 2016 plumes of African biomass burning were seen at the beginning of the Ascension Island-Azores flight and plumes of Eurasian biomass burning were seen during the northern part of the Azores-Kangerlussuaq flight. These specific biomass burning events are not captured by the emissions inventory used in our study, but they might explain a part of the negative model bias over the Central Atlantic and Greenland in August.

We did not include biogenic or oceanic  $C_2H_6$  and  $C_2H_4$  emissions in our UM-UKCA v7.3 simulations, but they were included into our UM-UKCA v10.6 simulations nudged with ERA-Interim reanalysis (see Chapter 6). In all of these simulations, however, UM-UKCA showed very similar negative biases in  $C_2H_6$  relative to ATom, which indicates that  $C_2H_6$ ,  $C_2H_4$  and  $C_2H_2$  emissions are likely underestimated in both emission inventories used in our study.

In addition to the biases and uncertainties in emissions, other sources of uncertainty in the model include (a) a well known inability of coarse resolution global models to simulate fine-scale structures observed in pollution plumes and (b) a faster than observed dissipation of pollution plumes due to numerical effects linked to the vertical resolution of such models (Eastham and Jacob, 2017).

## Propane

UM-UKCA shows a similar bias in  $C_3H_8$  as it does in  $C_2H_6$  (Figures 3.9 and C.8 with differing x-axis, Table C.3). In February, the model underestimates  $C_3H_8$  concentrations with an RMSE of 332, 567, 533, 198 and 72 pptv over the North Pacific, Alaska, Greenland, North Atlantic and Central Atlantic, respectively. Over the same regions in August, the bias is smaller (RMSE 23, 86, 60, 116 and 27 pptv, respectively), but the model explains a smaller proportion of the observed variability than in February. An exception to that rule is the North Pacific, where  $R^2$  for the profiles in both months is almost the same. Over the Central Pacific, South Pacific and South-East Atlantic in February, modelled  $C_3H_8$  concentrations stay within the observed variability but are mostly positively biased in August, sometimes by up to a factor of 7.

UKCA simplifies  $C_3H_8$  and  $C_3H_6$  chemistry and lumps  $C_3H_8$  and  $C_3H_6$  emissions by mass into  $C_3H_8$ , which is then oxidised by OH at the rate of the  $C_3H_8+OH$  reaction. Such a simplification extends modelled  $C_3H_8$  lifetime, because  $C_3H_6$  which has a lifetime of hours is lumped in  $C_3H_8$  which has a lifetime of weeks (Atkinson and Arey, 2003). This could lead to an overestimation of  $C_3H_8$  by the model, but it is difficult to find a clear example of this, because to compare UM-UKCA's propane with ATom we used only propane data from ATom.

As mentioned before, the model substantially underestimates  $C_2H_6$  and  $C_3H_8$  concentrations in the Northern Hemisphere, especially in February. February, and the boreal winter in general, is the time when anthropogenic emissions are high and OH concentrations are low, which allows concentrations of hydrocarbons to build up and be transported longer distances into the remote atmosphere. This and the fact that the model underestimates  $C_2H_6$  and  $C_3H_8$  by a larger amount in February than in August leads us to believe that an underestimation of the emissions of either of the hydrocarbons included in UKCA's  $C_2H_6$  and  $C_3H_8$  plays a bigger role in the explanation of this negative model bias than does the model bias in OH. In future studies, it would be useful to run an experiment with, e.g. doubled, emissions of hydrocarbons in question and see if it is enough to close the gap between the model and the observations. One such study was conducted by Dalsøren et al. (2018), where they found that fossil fuel emissions of ethane and propane had to be doubled and tripled, respectively, in order to bring the OsloCTM3 model into agreement with the observations.

## Nitrogen oxides

NO and  $NO_2$  are such short-lived species that the comparison of their monthly mean modelled concentrations with ATom measurements can not serve as a comprehensive test of regional model performance. However, it does give some information about the veracity of the  $NO_x$  emissions used in the model.

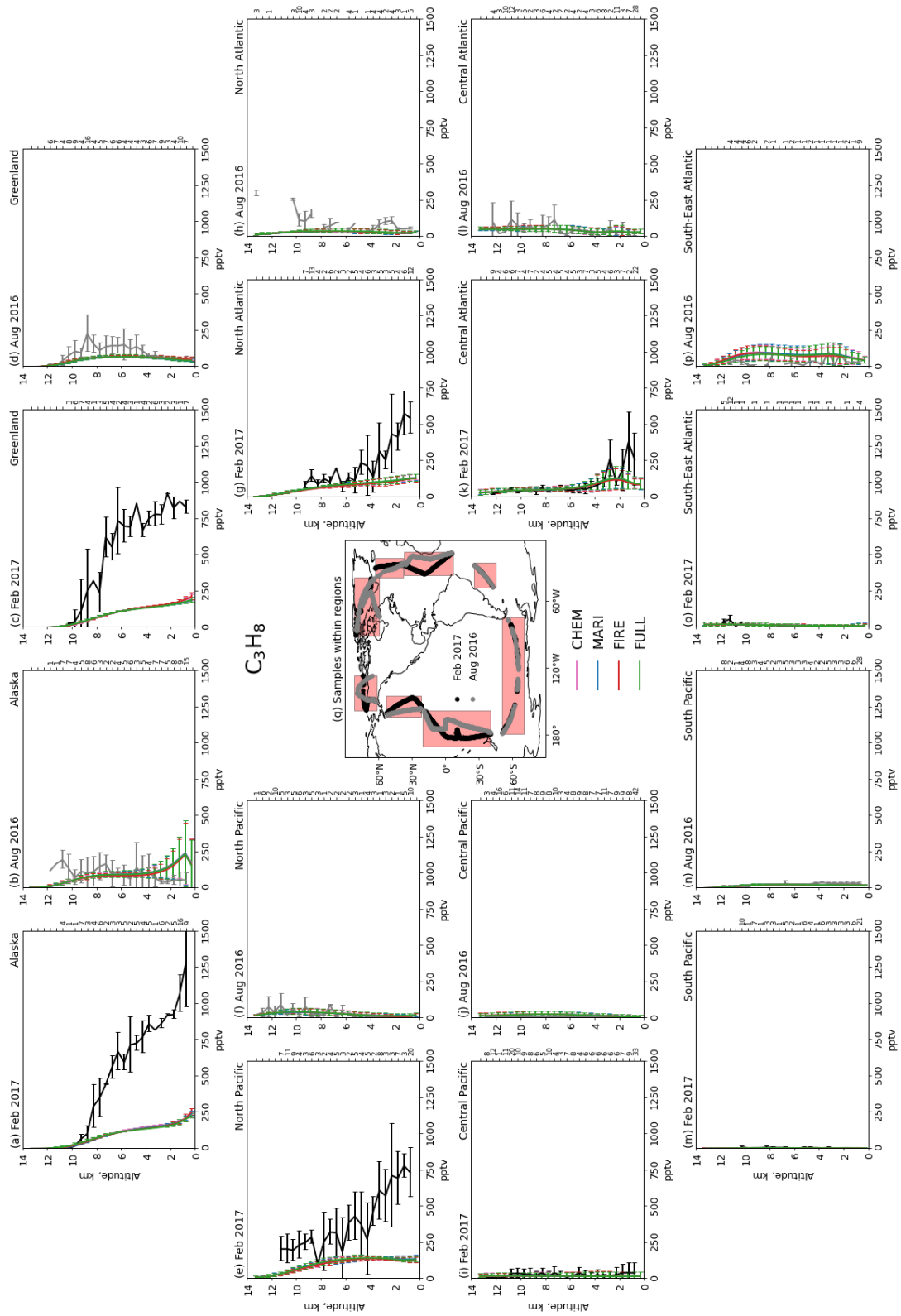


FIGURE 3.9: As in Fig. 3.7 but for  $C_3H_8$ .



Figures 3.10 and C.9 (with differing x-axis) show the observed and modelled  $\text{NO}_x$  vertical profiles for February and August. In both months UM-UKCA tends to underestimate  $\text{NO}_x$  concentrations and simulates profiles that are different in shape from the observed. Some profiles, however, are simulated better than others (Table C.4), namely over the North Atlantic in both months (February  $R^2=0.61$ , August  $R^2=0.78$ ), South Pacific in February ( $R^2=0.78$ ), Central Atlantic in August ( $R^2=0.63$ ) and Greenland in August ( $R^2=0.86$ ). All modelled profiles except those over the Central Pacific in February have a negative bias above 8 km, which was reported to be partially explained by a negative model bias in lightning  $\text{NO}_x$  emissions or related to weak boundary layer mixing and/or lack of convective uplift in the model (O'Connor et al., 2014).

### Ozone

Despite the aforementioned biases in  $\text{O}_3$  precursors, UM-UKCA captures the observed  $\text{O}_3$  vertical profiles reasonably well (Figure 3.11, Table C.5). It reproduces  $\text{O}_3$  seasonality by simulating a faster increase in  $\text{O}_3$  concentrations with height during boreal and austral summer relative to the increase during boreal and austral winter. UM-UKCA generally underestimates  $\text{O}_3$  concentrations below 6-8 km during boreal and austral winter, but stays within the range of observed variability during boreal and austral summer. Exceptions from the latter are the profiles over the North Pacific and North Atlantic showing a positive bias below 6 km (RMSE 28 and 37 ppbv, respectively) and the South Pacific showing a negative bias below 6 km (RMSE 47 ppbv). While the absolute concentrations are not always well captured, the model explains most of the observed variation of the mean  $\text{O}_3$  concentrations over the South Pacific (February  $R^2=0.90$ , August  $R^2=0.68$ ), Greenland (February  $R^2=0.84$ , August  $R^2=0.98$ ), Alaska in February ( $R^2=0.98$ ) and the Central Atlantic in August ( $R^2=0.60$ ), but performs worse in other regions.

### Methyl nitrate

$\text{MeONO}_2$  is the only alkyl nitrate originally present in the UKCA's CheST chemical mechanism. Despite the fact that  $\text{MeONO}_2$  has been present in the model since at least the work of O'Connor et al. (2014), we have not heard of any published studies evaluating the UM-UKCA's skill in simulating  $\text{MeONO}_2$ . Here we present the first such study and, given the fact that the recommended chemical kinetics of  $\text{MeONO}_2$  photochemical production and loss have not changed since  $\text{MeONO}_2$  was introduced into the model, our results from the UM-UKCA CHEM run might be informative for other UM-UKCA studies.

So far in Section 3.3.3 we have been discussing the results from the UM-UKCA FULL run because the differences in  $\text{CH}_4$ ,  $\text{C}_2\text{H}_6$ ,  $\text{C}_3\text{H}_8$ ,  $\text{NO}_x$  and  $\text{O}_3$  concentrations between that run and CHEM, MARI or FIRE were small. However, it is not the case



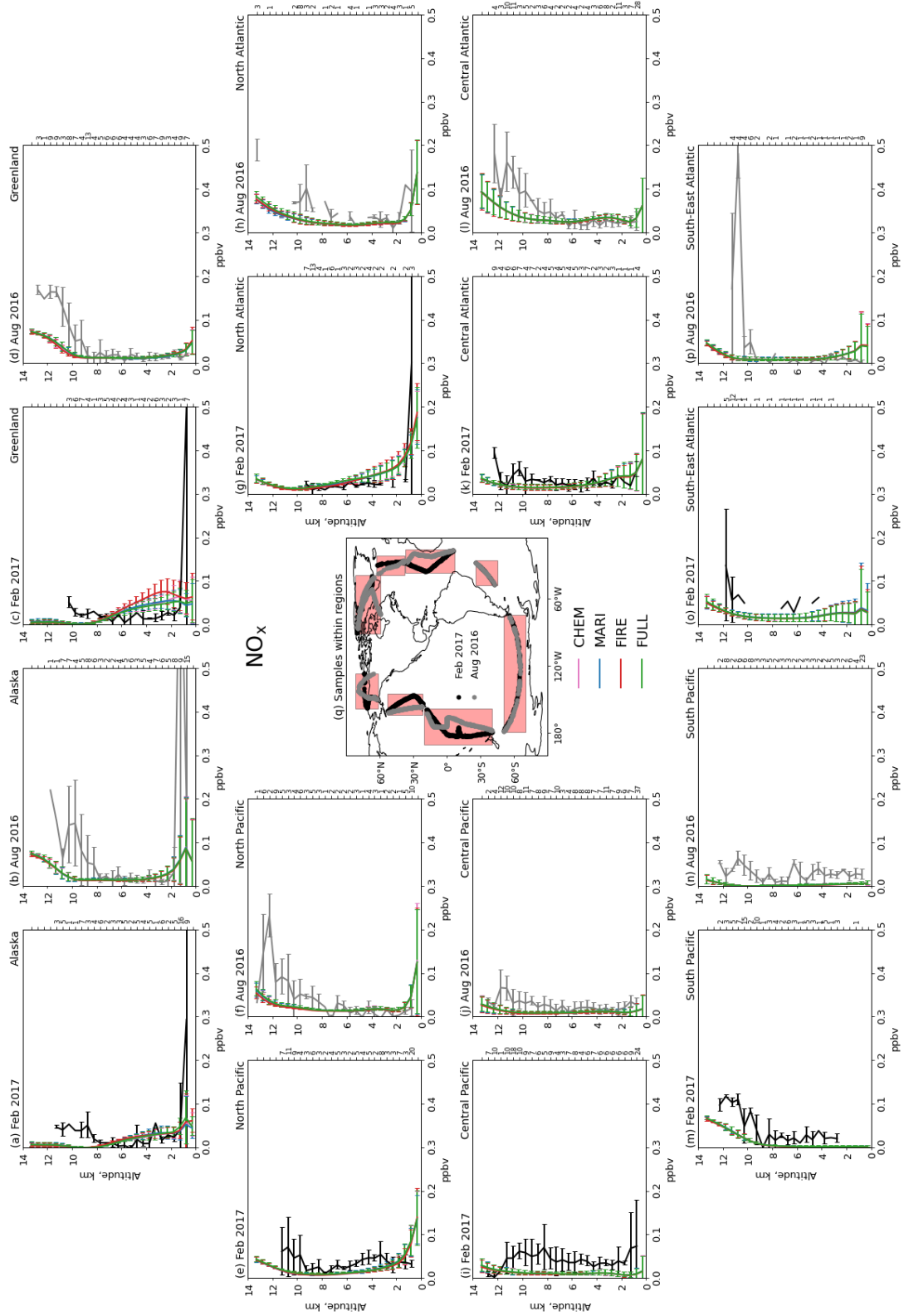
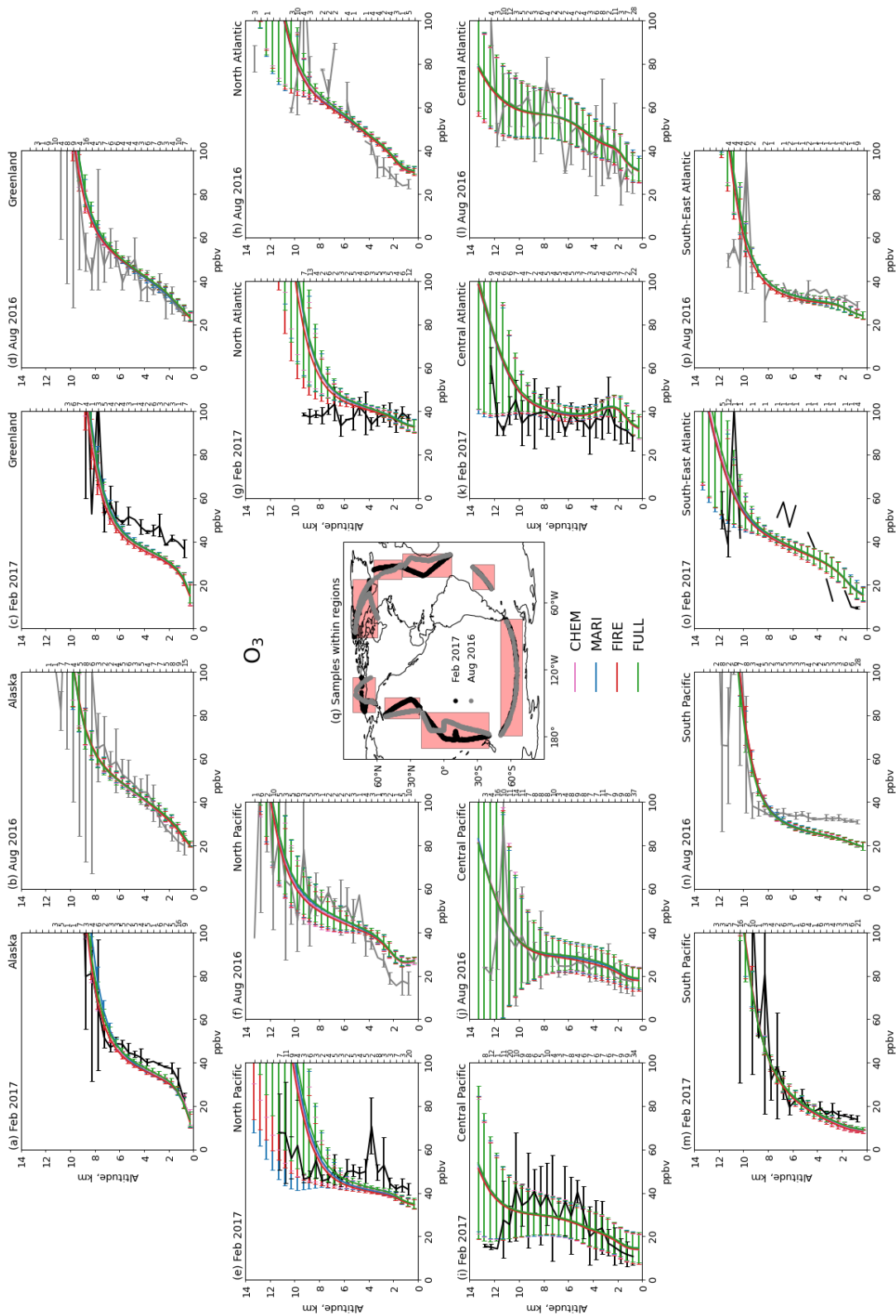


FIGURE 3.10: As in Fig. 3.7 but for  $\text{NO}_x$ .

FIGURE 3.11: As in Fig. 3.7 but for O<sub>3</sub>.

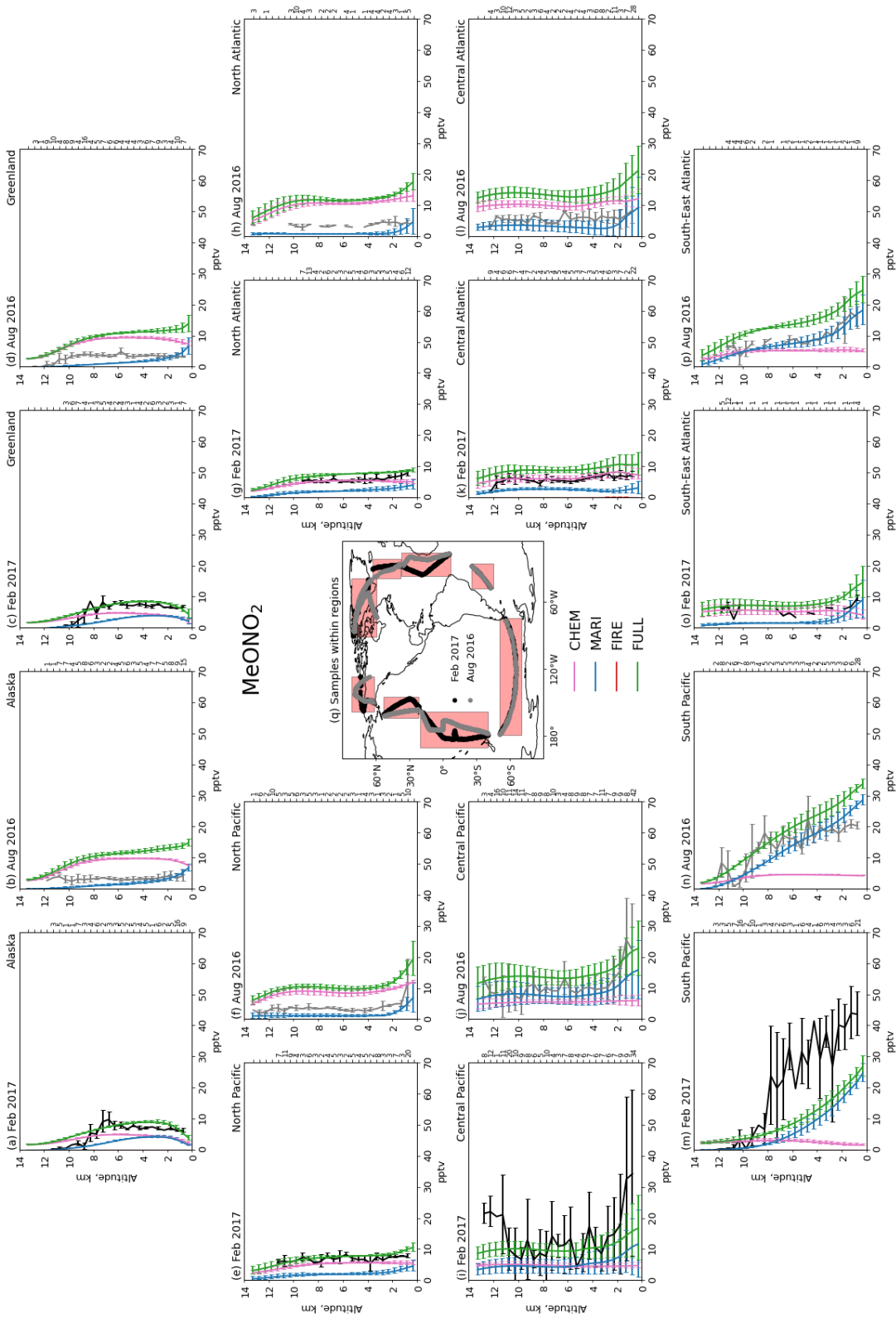
for the profiles of alkyl nitrates discussed below. So, to remind the reader, our sensitivity experiments are (1) CHEM that includes C<sub>1</sub>-C<sub>3</sub> RONO<sub>2</sub> photochemical production and loss, (2) MARI that includes oceanic emissions of C<sub>1</sub>-C<sub>3</sub> RONO<sub>2</sub> and their photochemical loss, (3) FIRE that includes biomass burning emissions of C<sub>1</sub>-C<sub>3</sub> RONO<sub>2</sub> and their photochemical loss and (4) FULL that includes the photochemical production and loss of C<sub>1</sub>-C<sub>3</sub> RONO<sub>2</sub> and their oceanic and biomass burning emissions.

Let us start with a comparison of the CHEM run with ATom (Figure 3.12, Table C.6). In February, the CHEM run explains 68% of the observed MeONO<sub>2</sub> profile over Alaska, but generates R<sup>2</sup> lower than 0.6 for all other regions. In August, the CHEM run predicts MeONO<sub>2</sub> concentrations higher than the observed with an RMSE of 5, 5, 5, 7 and 5 pptv over the North Pacific, Alaska, Greenland, North Atlantic and Central Atlantic, respectively, and lower than the observed with an RMSE of 7, 11 and 5 over the Central Pacific, South Pacific and South-East Atlantic.

Relative to the CHEM run, in February the MARI run explains a larger proportion of the observed MeONO<sub>2</sub> variability in all regions but Alaska and the Central Atlantic and has higher RMSEs in all regions but the Central and South Pacific. In August, the MARI run shows a similar increase in R<sup>2</sup> for all regions but Greenland and a decrease in RMSEs. This general increase in R<sup>2</sup> in the MARI run relative to the CHEM run implies that an oceanic source of MeONO<sub>2</sub> plays a substantial role in determining MeONO<sub>2</sub> concentrations in our selected regions. Although, the remaining differences between the observations and the model indicate that having only an oceanic source of MeONO<sub>2</sub> in the model is not enough to reproduce observations.

In the FIRE run, modelled MeONO<sub>2</sub> concentrations are much smaller than the observed and R<sup>2</sup> for the profiles are lower than 0.6 in all regions but the North Atlantic in February (R<sup>2</sup>=0.76) and Greenland in August (R<sup>2</sup>=0.80). This indicates that a biomass burning source of MeONO<sub>2</sub> plays a minor role in determining MeONO<sub>2</sub> concentrations and having only this source in the model is also not enough to reproduce observations.

Relative to the CHEM and MARI runs in February, the FULL run explains the largest proportion of the observed MeONO<sub>2</sub> variability in all regions but the North Atlantic and has the smallest RMSEs in all regions but the North, Central and South East Atlantic. Relative to the CHEM run in August, the FULL run explains a larger proportion of the observed variability in all regions but Greenland and has higher RMSEs in all regions but the Central and South Pacific. Relative to the MARI run in August, the FULL run explains a smaller proportion of the observed variability in all regions but the South Pacific, Central Atlantic and Greenland and has higher RMSEs. This deterioration in model's skill to capture MeONO<sub>2</sub> profiles in August in the FULL run relative to the CHEM and MARI runs is linked to a positive model bias in MeONO<sub>2</sub> in the CHEM run.

FIGURE 3.12: As in Fig. 3.7 but for MeONO<sub>2</sub>.

A positive model bias in MeONO<sub>2</sub> in the CHEM run in August over the North Pacific, Alaska, Greenland, North Atlantic and Central Atlantic is likely linked to UM-UKCA's boreal summertime positive bias in CH<sub>4</sub> in the Northern Hemisphere. To confirm this, let us examine the seasonal changes in MeONO<sub>2</sub> concentrations as a function of MeONO<sub>2</sub> photochemical production and loss, generically expressed by the following equation:

$$\frac{d[\text{MeONO}_2]}{dt} = k_1[\text{MeOO}][\text{NO}] - k_2[\text{MeONO}_2][\text{OH}] - j[\text{MeONO}_2] \quad (3.1)$$

If we assume that the winter and summer surface mean temperatures are equal to 0°C and 20°C, respectively, then  $k_1$  is smaller in summer than in winter (by 9%).  $k_2$  follows the opposite trend and is higher in summer than in winter (by 19%), as well as [OH] and  $j$ . That means that in order to get maximum MeONO<sub>2</sub> concentrations in summer instead of winter, modelled MeONO<sub>2</sub> photochemical production must have been much higher than loss despite the fact that theoretically MeONO<sub>2</sub> photochemical production is slower at higher temperatures. That is only possible if [MeOO] or [NO] were overestimated by the model. From the previous section about NO<sub>x</sub> we know that NO<sub>x</sub> was generally underestimated by the model. Therefore, it is a combination of UM-UKCA's known positive biases in CH<sub>4</sub> and OH that must have lead to an overproduction of MeOO radicals during boreal summer. This circumstance is also reinforced by the fact MeOO sink is smaller in summer than in winter due to a slower rate of formation of MeOO reservoirs (formaldehyde (HCHO), methanol (CH<sub>3</sub>OH) and methyl hydroperoxide (CH<sub>3</sub>OOH)). As a result, MeONO<sub>2</sub> photochemical production is overestimated by the model in the Northern Hemisphere during boreal summer, leading to the fact that modelled MeONO<sub>2</sub> seasonality in the Northern Hemisphere is the opposite of the observed.

A negative model bias in C<sub>1</sub>-C<sub>3</sub> RONO<sub>2</sub> in the MARI and FULL runs in August over the South Pacific is clearly caused by an underestimation of the seasonal variability in C<sub>1</sub>-C<sub>3</sub> RONO<sub>2</sub> oceanic emissions (by about a factor of 2). This outcome was expected because in this region the Fisher et al. (2018) emissions depended on a single, fixed value of seawater nitrite, and it also highlights the need for more seawater nitrite and alkyl nitrate saturation measurements in the Southern Ocean in different seasons.

### Ethyl nitrate

EtONO<sub>2</sub> is one of the three new species that we introduced into UM-UKCA for the first time in this study. EtONO<sub>2</sub> is formed in a minor channel of the EtOO radical reaction with NO at a yield of 0.9% and is destroyed by photolysis and OH oxidation, producing acetaldehyde (CH<sub>3</sub>CHO), HO<sub>2</sub> and NO<sub>2</sub>. Knowing that the vertical profiles of the EtONO<sub>2</sub> parent alkane, C<sub>2</sub>H<sub>6</sub>, are predominantly not captured by the model,

we were surprised to see that the FULL run captures the observed EtONO<sub>2</sub> profiles rather well (Figure 3.13, Table C.7).

Let us start with a comparison of the CHEM run with ATom. The CHEM run explains 74% and 79% of the observed EtONO<sub>2</sub> profile over the Central Atlantic in February and over Greenland in August, respectively, but generates R<sup>2</sup> lower than 0.6 for all other regions. In contrast to MeONO<sub>2</sub>, modelled EtONO<sub>2</sub> concentrations are higher during boreal and austral winter and lower during boreal and austral summer, meaning that EtONO<sub>2</sub> seasonality is captured by the model.

Relative to the CHEM run, in February the MARI run explains a larger proportion of the observed EtONO<sub>2</sub> variability in all regions but the North Pacific and Central Atlantic and has higher RMSEs in all regions but the South Pacific. In August, R<sup>2</sup> increase and RMSEs decrease only for the profiles over the Central Pacific, South Pacific and South East Atlantic, implying that an oceanic source of EtONO<sub>2</sub> plays a substantial role in determining EtONO<sub>2</sub> concentrations only in these three regions.

In the FIRE run, modelled EtONO<sub>2</sub> concentrations are much smaller than the observed and R<sup>2</sup> for the profiles are lower than 0.6 in all regions but the North Atlantic (R<sup>2</sup>=0.62) and Central Atlantic (R<sup>2</sup>=0.69) in February and Greenland in August (R<sup>2</sup>=0.77). This indicates that a biomass burning source of EtONO<sub>2</sub> plays a minor role in determining EtONO<sub>2</sub> concentrations and having only this source in the model is not enough to reproduce observations.

Relative to the CHEM and MARI runs in February, the FULL run explains the largest proportion of EtONO<sub>2</sub> variability and has the smallest RMSEs over the Central and South Pacific. Also, the FULL run has the smallest RMSEs over Alaska and Greenland and explains a larger proportion of EtONO<sub>2</sub> variability than the CHEM run but a smaller proportion than the MARI run. Relative to the CHEM and MARI runs in August, the FULL run explains the largest or a similar proportion of EtONO<sub>2</sub> variability over the North, Central and South Pacific and the North Atlantic and has predominantly the highest RMSEs.

An explanation for an unexpectedly good model performance in simulating EtONO<sub>2</sub> in the FULL run in both months in the Northern Hemisphere is likely linked to a negative model bias in C<sub>2</sub>H<sub>6</sub>. It could be that (a) the secondary production of EtOO radicals was high enough to compensate for a negative bias in the primary production of these radicals from the C<sub>2</sub>H<sub>6</sub>+OH reaction or (b) EtOO sinks were too small in the model. The first hypothesis is viable because EtOO radicals are produced from C<sub>3</sub>H<sub>8</sub> oxidation in the UKCA's CheST chemical mechanism<sup>6</sup>, and it would be useful to test this hypothesis in the future by calculating the C<sub>2</sub>H<sub>6</sub>+OH fluxes from UM-UKCA v10.6 run with hourly resolution and comparing the results with C<sub>2</sub>H<sub>6</sub> and OH data from ATom. The second hypothesis is difficult to test because of the absence of RO<sub>2</sub> measurements in ATom.

---

<sup>6</sup>EtOO radicals are not produced from C<sub>5</sub>H<sub>8</sub> oxidation in the UKCA's CheST chemical mechanism.

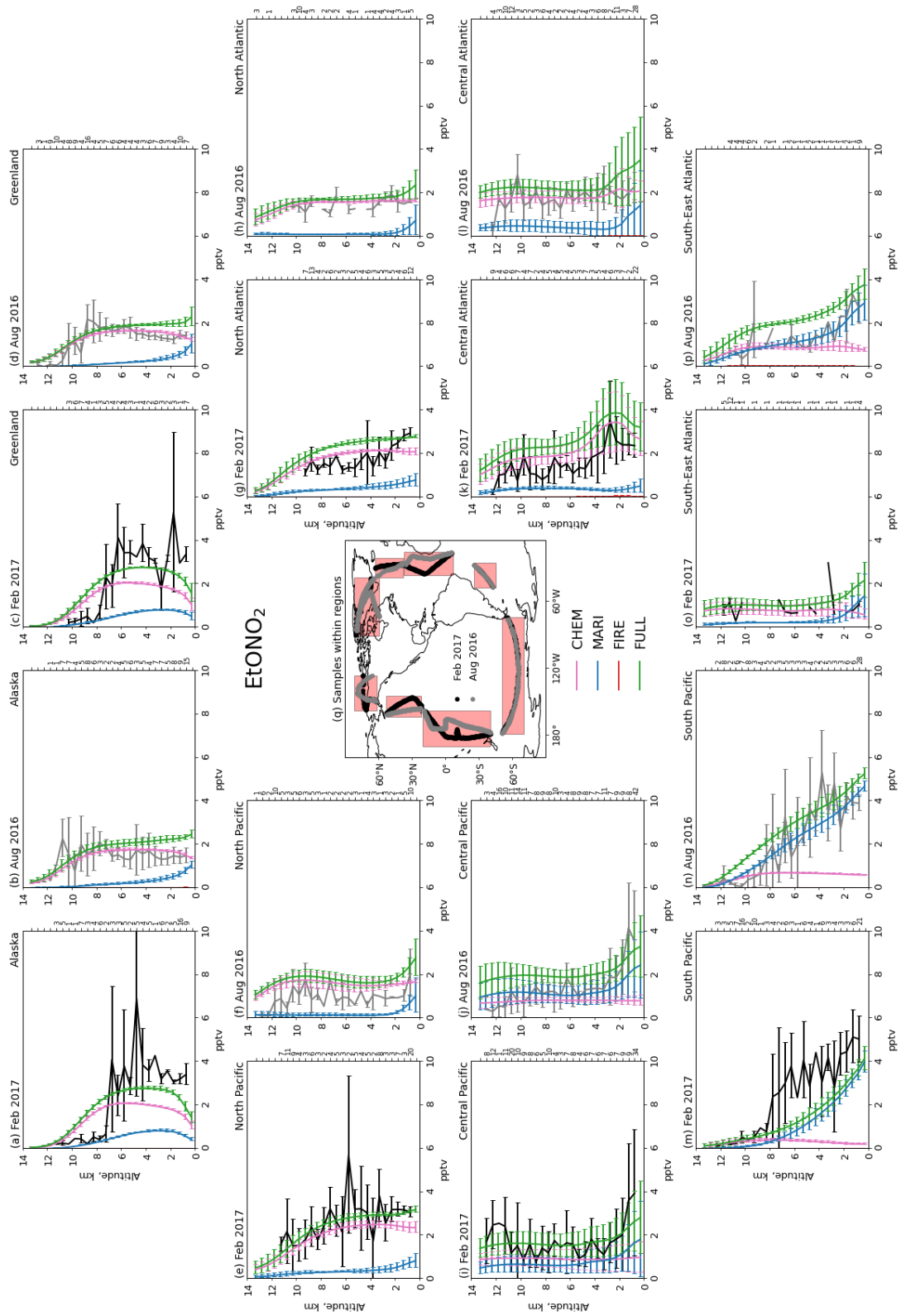


FIGURE 3.13: As in Fig. 3.7 but for EtONO<sub>2</sub>.



## Propyl nitrates

nPrONO<sub>2</sub> and iPrONO<sub>2</sub> are the other two new species that we introduced into UM-UKCA for the first time in this study. They are produced in a minor channel of the nPrOO and iPrOO reactions with NO at yields of 2% and 4.2%, respectively, and are destroyed by photolysis and OH oxidation, producing propionaldehyde (C<sub>2</sub>H<sub>5</sub>CHO), HO<sub>2</sub> and NO<sub>2</sub> in the case of nPrONO<sub>2</sub>, and acetone (CH<sub>3</sub>COCH<sub>3</sub>), HO<sub>2</sub> and NO<sub>2</sub> in the case of iPrONO<sub>2</sub>.

In contrast to EtONO<sub>2</sub>, model biases in C<sub>3</sub> RONO<sub>2</sub> reflect those of their parent alkane, C<sub>3</sub>H<sub>8</sub> (Figures 3.14-3.15 and C.10-C.11 with differing x-axis, Tables C.8-C.9).

The CHEM run predominantly underestimates C<sub>3</sub> RONO<sub>2</sub> concentrations in both months in all regions and explains more than 60% of C<sub>3</sub> RONO<sub>2</sub> profiles only over the Central Atlantic in February. In contrast to MeONO<sub>2</sub>, modelled C<sub>3</sub> RONO<sub>2</sub> concentrations are higher during boreal and austral winter and lower during boreal and austral summer, meaning that C<sub>3</sub> RONO<sub>2</sub> seasonality is captured by the model.

Relative to the CHEM run, the MARI run explains a larger proportion of C<sub>3</sub> RONO<sub>2</sub> variability over the North Atlantic in February, Central Pacific in August and South Pacific in both months and has higher RMSEs for these regions but the South Pacific.

In the FIRE run, modelled C<sub>3</sub> RONO<sub>2</sub> concentrations are much smaller than the observed and R<sup>2</sup> for the profiles are higher than 0.6 only for the North and Central Atlantic in February and Greenland in August.

Relative to the CHEM and MARI runs, the FULL run explains the largest or a similar proportion of C<sub>3</sub> RONO<sub>2</sub> variability and has the smallest RMSEs over the Central Atlantic in February and the South Pacific in both month, but the model performs worse in other regions.

In all sensitivity runs, modelled iPrONO<sub>2</sub> concentrations are generally higher than nPrONO<sub>2</sub> concentrations, which agrees with the observations.



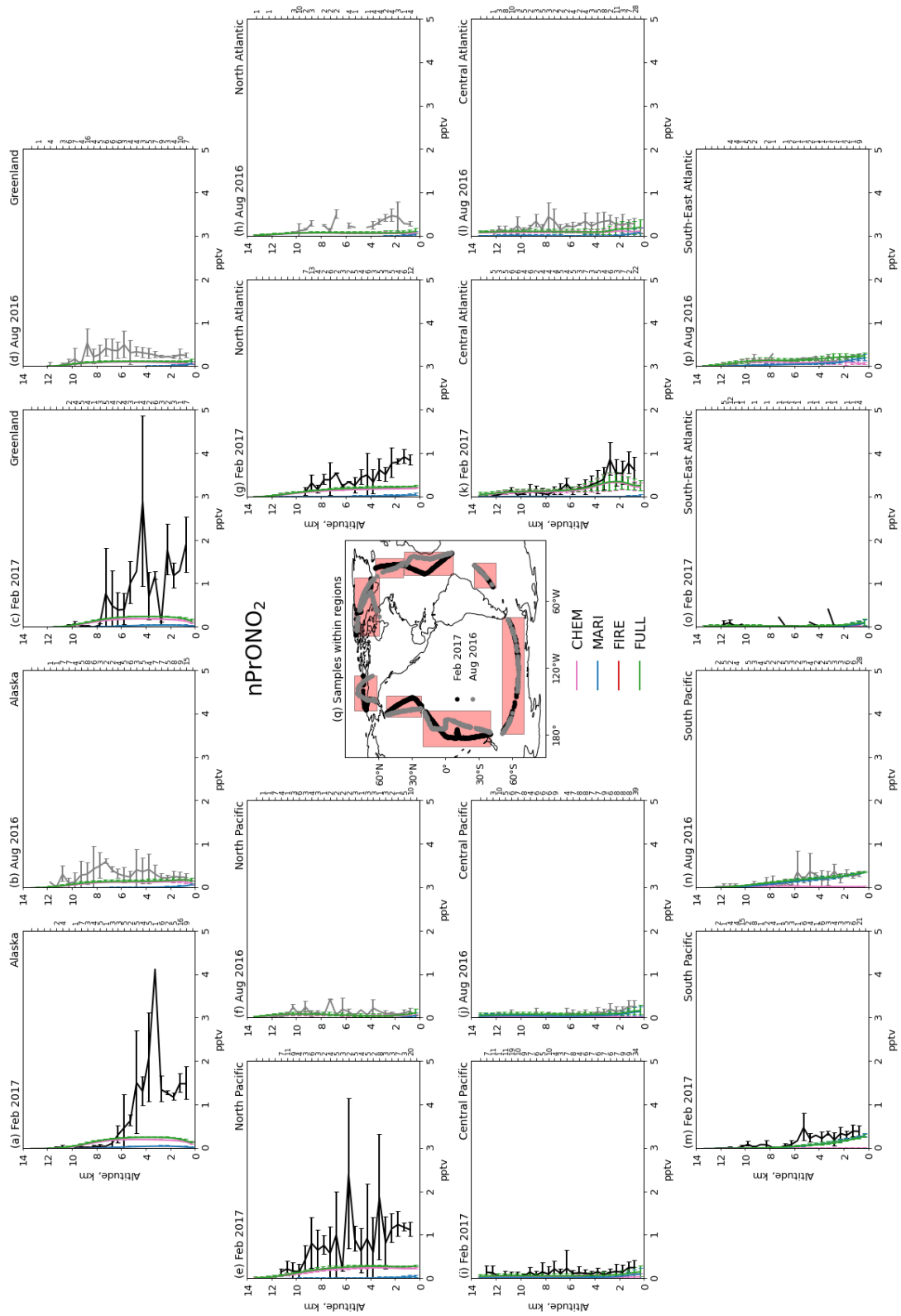


FIGURE 3.14: As in Fig. 3.7 but for nPrONO<sub>2</sub>.

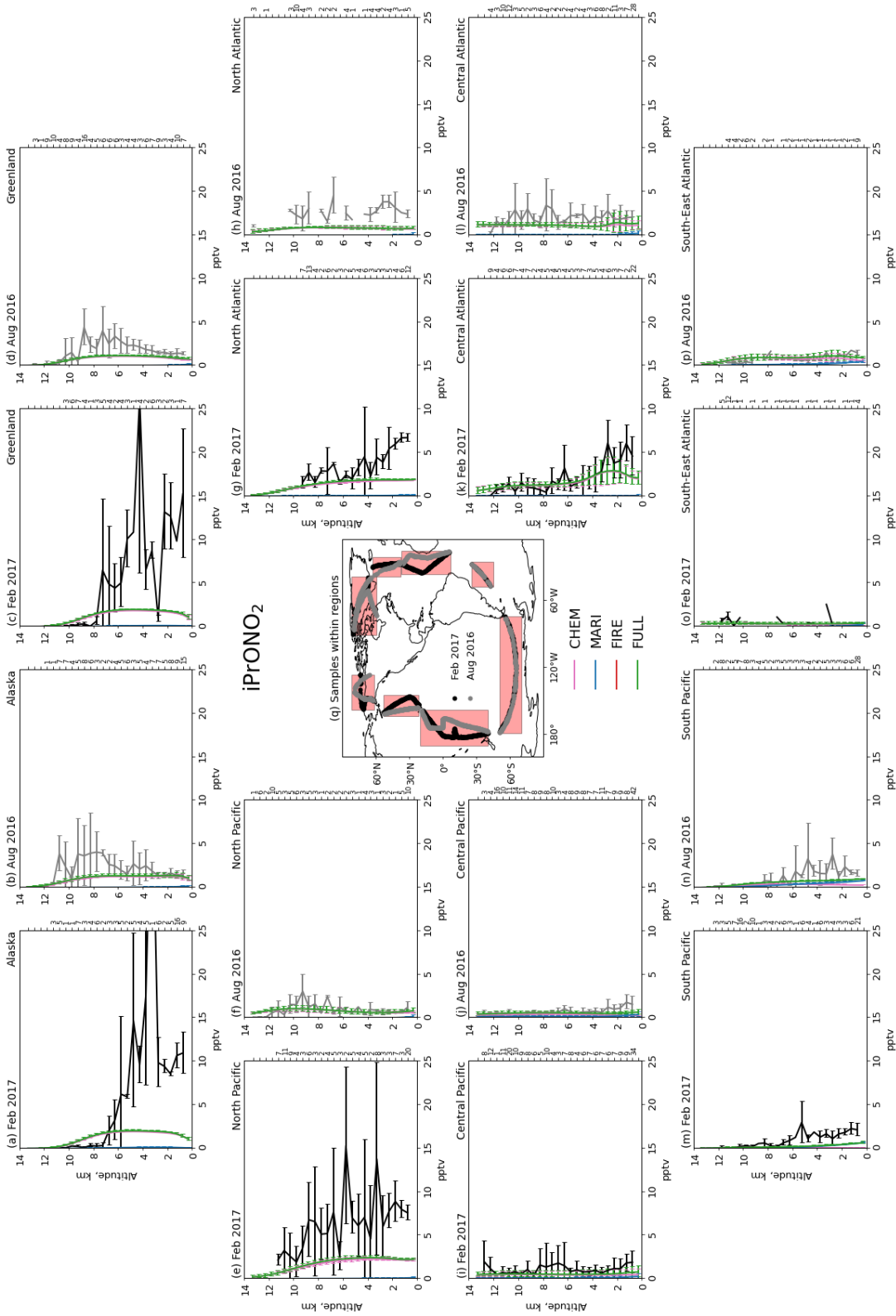


FIGURE 3.15: As in Fig. 3.7 but for  $iPrONO_2$ .

### 3.4 Summary

We implemented the new C<sub>2</sub>-C<sub>3</sub> RONO<sub>2</sub> chemistry and C<sub>1</sub>-C<sub>3</sub> RONO<sub>2</sub> oceanic and biomass burning emissions into a global 3D chemistry-climate model UM-UKCA. We performed six 10-year-long perpetual year 2000 simulations with UM-UKCA, testing the sensitivity of C<sub>1</sub>-C<sub>3</sub> RONO<sub>2</sub> atmospheric concentrations to the processes that control their abundance. We also compared the regional mean vertical profiles of CH<sub>4</sub>, C<sub>2</sub>H<sub>6</sub>, C<sub>3</sub>H<sub>8</sub>, NO<sub>x</sub>, O<sub>3</sub>, MeONO<sub>2</sub>, EtONO<sub>2</sub>, nPrONO<sub>2</sub> and iPrONO<sub>2</sub> observed during the Atmospheric Tomography mission with those simulated by the UM-UKCA CHEM, MARI, FIRE and FULL runs in 8 remote regions in February and August.

We discovered that UM-UKCA captures the observed CH<sub>4</sub> and O<sub>3</sub> vertical profiles reasonably well, showing a previously known bias in CH<sub>4</sub> likely caused by a misrepresentation of its surface latitudinal gradient by a lower boundary condition. NO<sub>x</sub> concentrations are generally underestimated by the model as well as C<sub>2</sub>H<sub>6</sub> and C<sub>3</sub>H<sub>8</sub> because of (a) a poor representation of their emissions in the emissions inventories used in our study and (b) a positive model bias in OH in the Northern Hemisphere. Modelled MeONO<sub>2</sub> seasonality in the Northern Hemisphere is the opposite of the observed, showing lower concentrations during boreal winter and higher concentrations during boreal summer likely caused by an overproduction of MeOO radicals during boreal summer. Observed EtONO<sub>2</sub>, nPrONO<sub>2</sub> and iPrONO<sub>2</sub> seasonality is captured well by the model, showing higher concentrations during boreal and austral winter and lower concentrations during boreal and austral summer. The cause of a surprisingly good model performance in the case of EtONO<sub>2</sub> is unclear, but it is likely linked to the bias in the sources or sinks of EtOO radicals. nPrONO<sub>2</sub> and iPrONO<sub>2</sub> concentrations are generally underestimated by the model, but modelled iPrONO<sub>2</sub> concentrations are higher than nPrONO<sub>2</sub> concentrations, which agrees with the observations. An inclusion of direct, especially oceanic, C<sub>1</sub>-C<sub>3</sub> RONO<sub>2</sub> emissions helps to explain a larger proportion of the observed C<sub>1</sub>-C<sub>3</sub> RONO<sub>2</sub> variability and reduce root-mean-square errors between the observations and the model over the Central and South Pacific, with other regions showing a mixed response. However, a negative model bias in C<sub>1</sub>-C<sub>3</sub> RONO<sub>2</sub> concentrations in the MARI and FULL runs in August over the South Pacific indicates that the seasonal variability in C<sub>1</sub>-C<sub>3</sub> RONO<sub>2</sub> oceanic emissions is underestimated in this region by about a factor of 2.

Being aware of the UM-UKCA biases, we may now proceed to the evaluation of the impact of C<sub>1</sub>-C<sub>3</sub> RONO<sub>2</sub> chemistry and direct emissions on tropospheric chemistry.



# 4

## Impact of C<sub>1</sub>-C<sub>3</sub> alkyl nitrates on tropospheric ozone chemistry

### 4.1 Introduction

To understand what impact of C<sub>1</sub>-C<sub>3</sub> alkyl nitrates have on tropospheric ozone chemistry, one should first understand what photochemical conditions trigger and sustain alkyl nitrate chemistry, or organic nitrate chemistry in general. According to [Perring et al. \(2013\)](#), photochemical production of alkyl and multifunctional organic nitrates is maximised at intermediate NO<sub>x</sub>, where O<sub>3</sub> production is maximised too as OH reacts more often with VOCs rather than with NO<sub>2</sub> (Figure 4.1). According to [Browne and Cohen \(2012\)](#), photochemical production of biogenic nitrates accounts for the majority of the instantaneous NO<sub>x</sub> sink in low NO<sub>x</sub> environments with high concentrations of biogenic VOCs (Figure 4.2). Based on these studies, one would expect that photochemical production of organic nitrates has the largest impact on tropospheric ozone chemistry in areas with intermediate to low NO<sub>x</sub> and high VOCs. This agrees well with the results of [Fisher et al. \(2018\)](#), who found that organic nitrates (namely, C<sub>1</sub>-C<sub>3</sub> and ≥C<sub>4</sub> alkyl nitrates, isoprene hydroxynitrates and monoterpene hydroxynitrates) are net NO<sub>x</sub> sinks over the continents and the northern mid-latitude oceans in regions of continental outflow (Figure 4.3). [Fisher et al. \(2018\)](#) also found that organic nitrates are net NO<sub>x</sub> sources over the oceans in the tropics and the Southern Hemisphere largely due to the presence of oceanic emissions of shorter-chain alkyl nitrates in these regions.

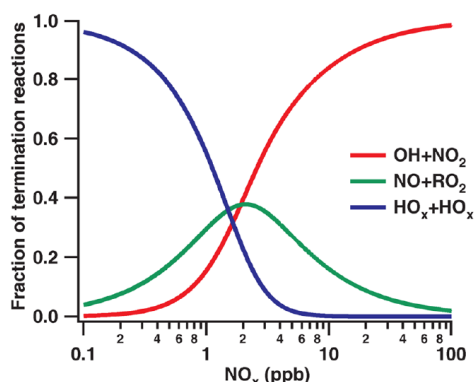


FIGURE 4.1: The relative importance of three possible chain termination reactions as a function of  $\text{NO}_x$  for a VOC reactivity of  $5 \text{ s}^{-1}$  and an OH production rate of  $10^6 \text{ molecules cm}^{-3} \text{ s}^{-1}$ : (blue) formation of peroxides, (green) formation of alkyl nitrates and (red) formation of  $\text{HNO}_3$ . From Perring et al. (2013).

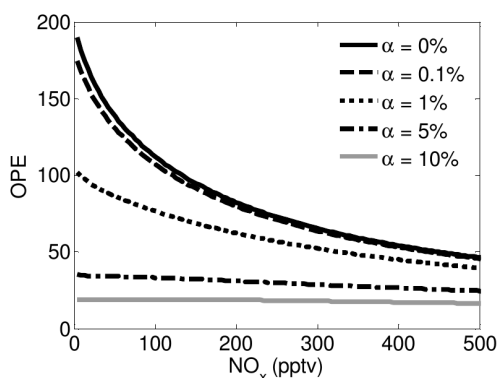


FIGURE 4.2: Steady state box model results for  $\text{O}_3$  production efficiency (OPE) versus  $\text{NO}_x$  concentration.  $\alpha$  is the “effective branching ratio” of  $\text{RONO}_2$  formation:  $\alpha=0$ -0.1% represents remote ocean conditions,  $\alpha=5$ -10% represents areas highly influenced by BVOCs (e.g. isoprene). From Browne and Cohen (2012).

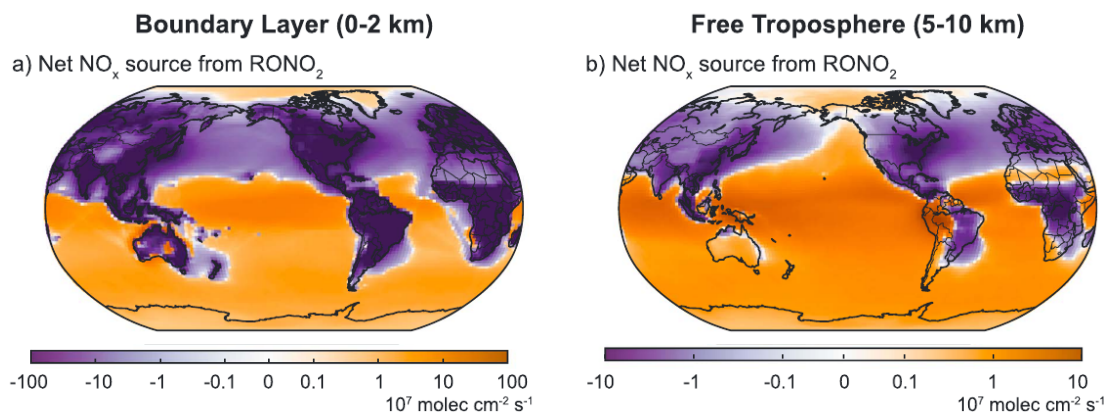


FIGURE 4.3: Impact of  $\text{RONO}_2$  chemistry on  $\text{NO}_x$  export in the boundary layer (0–2 km, left) and free troposphere (5–10 km, right). The net  $\text{NO}_x$  source from  $\text{RONO}_2$  is calculated as the difference between  $\text{NO}_2$  release during  $\text{RONO}_2$  decomposition and  $\text{NO}$  consumption during  $\text{RONO}_2$  formation, and summed over model levels within the given altitude range. Orange areas indicate net  $\text{NO}_x$  release and purple indicate net  $\text{NO}_x$  loss.  $\text{RONO}_2$  include  $C_1$ - $C_3$  and  $\geq C_4$  alkyl nitrates, isoprene hydroxynitrates and monoterpene hydroxynitrates. From Fisher et al. (2018).

In this chapter, we estimate the global and localised impacts of all known sources of  $C_1$ - $C_3$   $\text{RONO}_2$ , i.e. photochemical production and oceanic and biomass burning emissions, on tropospheric ozone chemistry. We do it separately for each source and for a combination of sources through a series of sensitivity simulations performed with a global 3D chemistry-climate model. To provide context, we also compare our results with similar studies conducted by Neu et al. (2008), Williams et al. (2014), Khan et al. (2015) and Fisher et al. (2018).

TABLE 4.1: Percentage change in the annual mean tropospheric ozone burden and methane lifetime due to the addition of alkyl nitrate chemistry and/or direct emissions. The error given in brackets was calculated as  $\sqrt{x^2 + y^2}$  (in %), where x and y are the standard errors of the mean from the control and sensitivity run, respectively.

Study	CHEM	MARI	FIRE	FULL
<i>%<math>\Delta</math> O<sub>3</sub> burden</i>				
Neu et al. (2008)		+1.28 <sup>a</sup>		
Williams et al. (2014)		+0.30 <sup>b</sup>		+0.09 <sup>d</sup>
this study	+0.48 (0.19)	+0.95 (0.25)	+0.18 (0.20) <sup>c</sup>	+1.09 (0.25)
<i>%<math>\Delta</math> CH<sub>4</sub> lifetime</i>				
Neu et al. (2008)		-1.69		
Williams et al. (2014)		-0.24 <sup>b</sup>		+0.35 <sup>d</sup>
this study	-0.68 (0.42)	-1.44 (0.39)	-0.12 (0.65) <sup>c</sup>	-1.56 (0.37)

<sup>a</sup> Neu et al. (2008) reported that an increase in the global tropospheric ozone column varied from 0.35 to 0.42 DU between seasons. On average it is 0.385 DU, which is 1.28% if we assume that the tropospheric ozone column is equal to 30 DU (Xia et al., 2017).

<sup>b</sup> Williams et al. (2014) EMISS run: without MeONO<sub>2</sub> photochemical production but with the Neu et al. (2008) MeONO<sub>2</sub> oceanic emissions between 10°S-10°N.

<sup>c</sup> The difference between the SSAN and FIRE runs, in both of which MeONO<sub>2</sub> concentration was initialised with a steady state value instead of a zero.

<sup>d</sup> Williams et al. (2014) FULL run: with MeONO<sub>2</sub> photochemical production at a branching ratio of 0.3% and the Neu et al. (2008) MeONO<sub>2</sub> oceanic emissions between 10°S-10°N halved.

## 4.2 Global impact of alkyl nitrates

Let us compare the results from our UM-UKCA SSAN, BASE, CHEM, MARI, FIRE and FULL runs with those from analogous runs from Neu et al. (2008), Williams et al. (2014), Khan et al. (2015) and Fisher et al. (2018) and focus on the global impacts of alkyl nitrate chemistry and/or direct emissions on tropospheric ozone burden and tropospheric methane lifetime. The description of the models used in the aforementioned studies was given in Tables 1.5-1.6. Each of these studies used a different definition of the troposphere, which in our study was defined as one where O<sub>3</sub> concentration is less than 125 ppbv. To calculate CH<sub>4</sub> lifetime, we used the following expression:

$$\tau_{\text{CH}_4} = \frac{\sum[\text{CH}_4]}{k_{\text{OH}}[\text{CH}_4][\text{OH}]} \quad (4.1)$$

where  $\sum[\text{CH}_4]$  is the tropospheric methane burden and  $k_{\text{OH}}$  is a reaction rate coefficient of the CH<sub>4</sub>+OH reaction. The global impact of C<sub>1</sub>-C<sub>3</sub> RONO<sub>2</sub> chemistry and/or direct emissions appears to be rather small (Table 4.1).

### 4.2.1 CHEM

We found that the addition of  $C_1$ - $C_3$   $\text{RONO}_2$  photochemical production and loss increases tropospheric ozone burden by  $1.30 \pm 0.53$  Tg ( $0.48 \pm 0.19\%$ ) and decreases methane lifetime by  $0.066 \pm 0.041$  yr ( $0.68 \pm 0.42\%$ ) in the model. An increase in tropospheric ozone burden was unexpected as it is generally thought that alkyl nitrate formation suppresses the tropospheric ozone production. However, knowing that UM-UKCA has a positive bias in  $\text{MeONO}_2$  in the Northern Hemisphere during boreal summer (see Chapter 3) likely explains this increase in ozone, because an excess in  $\text{MeONO}_2$  could have served as an extra  $\text{NO}_x$  source for the tropospheric ozone production. We could not compare our estimates of the change in tropospheric ozone burden and methane lifetime with other studies, because the only study that had equivalents of our BASE and CHEM runs, Williams et al. (2014) and their BASE and LOWBR runs, did not report these estimates. However, we can compare our CHEM run results with the results from the Khan et al. (2015) BASE run, which is equivalent to our CHEM run.

STOCHEM-CRI and UM-UKCA simulate the lowest alkyl nitrate concentrations over the oceans in the Southern Hemisphere (Figure 4.4), i.e. far away from alkyl nitrate precursor emissions. The largest concentrations of alkyl nitrates are simulated over the tropics and the northern mid-latitudes. The major difference between the STOCHEM-CRI and UM-UKCA alkyl nitrate distributions is that UM-UKCA does not simulate an alkyl nitrate maxima over the east coast of North America, while STOCHEM-CRI does despite both models having a similar  $\text{NO}_x$  distribution<sup>1</sup>. UM-UKCA  $\text{MeONO}_2$  and  $\text{EtONO}_2$  concentrations are generally lower than those in STOCHEM-CRI. In fact, the UM-UKCA  $\text{MeONO}_2$  maxima over the Amazon region and equatorial Africa are almost two times smaller than those in STOCHEM-CRI. This might indicate that the contribution of isoprene as a source of  $\text{MeOO}$  radicals (via the conversion of the acetyl peroxy radicals ( $\text{MeCO}_3$ ) to  $\text{MeOO}$  radicals) to  $\text{MeONO}_2$  production is smaller in UM-UKCA than in STOCHEM-CRI. UM-UKCA  $\text{nPrONO}_2$  and  $\text{iPrONO}_2$  concentrations are higher than those in STOCHEM-CRI over the Middle East, India and East Asia. This might reflect the differences in  $\text{C}_3\text{H}_8$  emissions used by the models.

### 4.2.2 MARI

Two studies performed an equivalent of our MARI run exploring the impact of photochemical processing of alkyl nitrate oceanic emissions on tropospheric chemistry. Neu et al. (2008) found that including  $\text{MeONO}_2$  and  $\text{EtONO}_2$  oceanic emissions of a total of  $0.35$  ( $\pm 0.2$ - $0.6$ ) Tg N  $\text{yr}^{-1}$  (82% of which was  $\text{MeONO}_2$ ) over the tropical oceans ( $10^\circ\text{S}$ - $10^\circ\text{N}$ ) and the Southern Ocean (south of  $45^\circ\text{S}$ ) increased the tropospheric ozone column on average by 0.385 Dobson units, with a 1 Dobson unit increase over the Western Pacific, and decreased methane lifetime by 0.16 yr (1.69%, from 9.44 to 9.28 years).

---

<sup>1</sup>Not shown here, but both have maxima over the east coast of North America, Europe and East Asia.



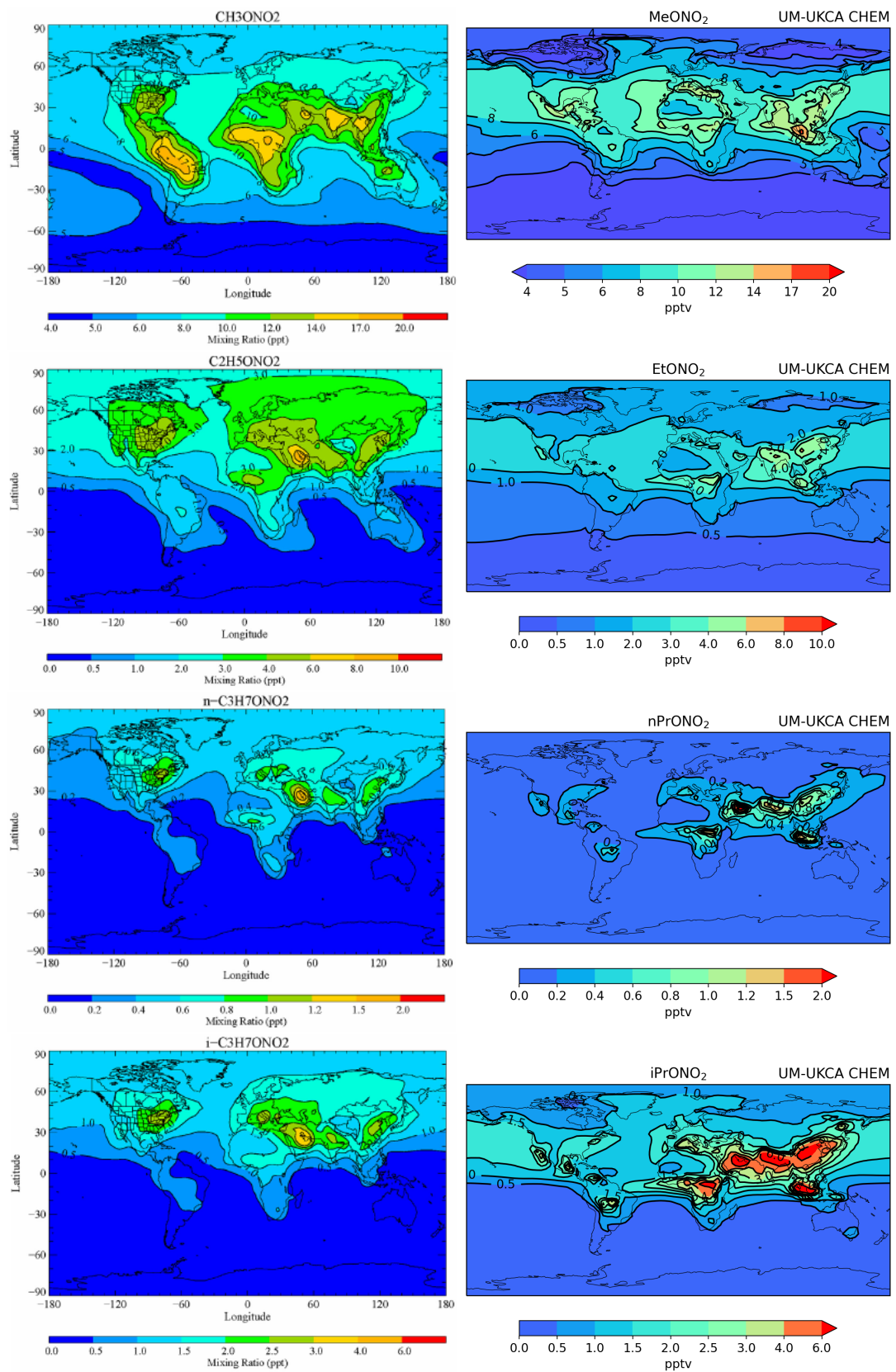


FIGURE 4.4: (Left) Annual mean surface level distribution of MeONO<sub>2</sub>, EtONO<sub>2</sub>, nPrONO<sub>2</sub> and iPrONO<sub>2</sub> from the STOCHEM-CRI BASE run from Khan et al. (2015). (Right) Same but from the UM-UKCA CHEM run. Note the non-uniform colour scales.

Williams et al. (2014) found that including MeONO<sub>2</sub> oceanic emissions of 0.3 Tg N yr<sup>-1</sup> over the tropical oceans (10°S-10°N) increased tropospheric ozone burden by 1.0 Tg (0.30%, from 334.3 to 335.3 Tg) and decreased methane lifetime by 0.02 yr (0.24%, from 8.42 to 8.40 years). We found that including C<sub>1</sub>-C<sub>3</sub> RONO<sub>2</sub> oceanic emissions of a total of 0.17 Tg N yr<sup>-1</sup> over the tropical and high latitude oceans increases tropospheric ozone burden by 2.58±0.68 Tg (0.95±0.25%) and decreases methane lifetime by 0.140±0.037 yr (1.44±0.39%). All above studies agree that the addition of alkyl nitrate oceanic emissions increases tropospheric ozone burden and via an associated increase in OH decreases methane lifetime. The magnitude of these changes varies between studies, with our study being somewhere in-between despite having the smallest total alkyl nitrate oceanic emissions.

### 4.2.3 FIRE

We found that the photochemical processing of C<sub>1</sub>-C<sub>3</sub> RONO<sub>2</sub> biomass burning emissions increases tropospheric ozone burden by 0.49±0.55 Tg (0.18±0.20%) and decreases methane lifetime by 0.012±0.063 (0.12±0.65%). The only study that had a similar run to our FIRE run, Khan et al. (2015) and their STOCHEM-BB run, did not report these estimates, but their run was not directly comparable because it had both photochemical production and biomass burning emissions of C<sub>1</sub>-C<sub>3</sub> RONO<sub>2</sub>.

### 4.2.4 FULL

No other studies performed an equivalent of our FULL run exploring the combined impact of C<sub>1</sub>-C<sub>3</sub> RONO<sub>2</sub> chemistry and oceanic and biomass burning emissions on tropospheric chemistry. However, two studies had runs similar to our FULL run. The Williams et al. (2014) FULL run had MeONO<sub>2</sub> photochemical production and loss and MeONO<sub>2</sub> oceanic emissions of 0.15 Tg N yr<sup>-1</sup> (the Neu et al. (2008) estimate halved) over the tropical oceans. The Fisher et al. (2018) “new” run had organic nitrate<sup>2</sup> photochemical production and loss and C<sub>1</sub>-C<sub>2</sub> RONO<sub>2</sub> oceanic emissions of a total of 0.18 Tg N yr<sup>-1</sup> over the tropical and high latitude oceans. Since we found that the global impact of biomass burning emissions of C<sub>1</sub>-C<sub>3</sub> RONO<sub>2</sub> is smaller than of their other sources, our FULL run can be compared to the Williams et al. (2014) FULL run and the Fisher et al. (2018) “new” run.

Williams et al. (2014) found that MeONO<sub>2</sub> chemistry and oceanic emissions increased tropospheric ozone burden by 0.3 Tg (0.09%, from 334.3 to 334.6 Tg) and increased methane lifetime by 0.03 yr (0.35%, from 8.42 to 8.45 years). We found that C<sub>1</sub>-C<sub>3</sub> RONO<sub>2</sub> chemistry and oceanic and biomass burning emissions increased tropospheric ozone burden by 2.96±0.69 Tg (1.09±0.25%) and decreased methane lifetime by 0.151±0.036 yr (1.56±0.37%). These estimates are rather different. If we consider the

---

<sup>2</sup>C<sub>1</sub>-C<sub>3</sub> and ≥C<sub>4</sub> alkyl nitrates, isoprene hydroxynitrates and monoterpene hydroxynitrates.

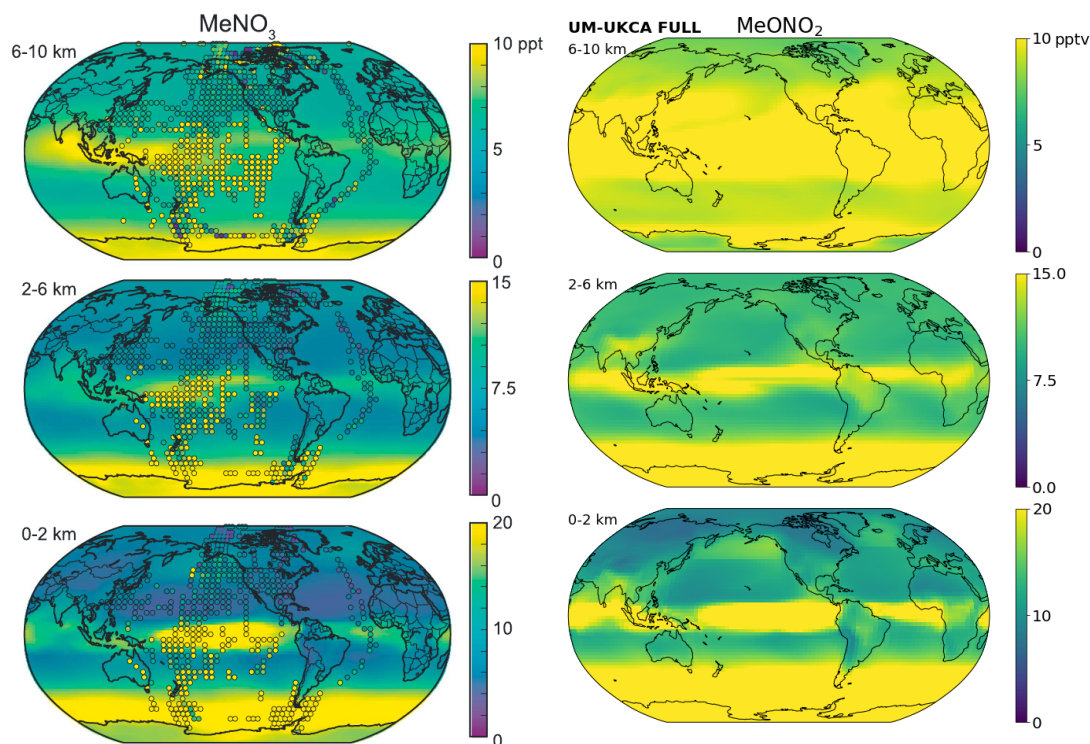
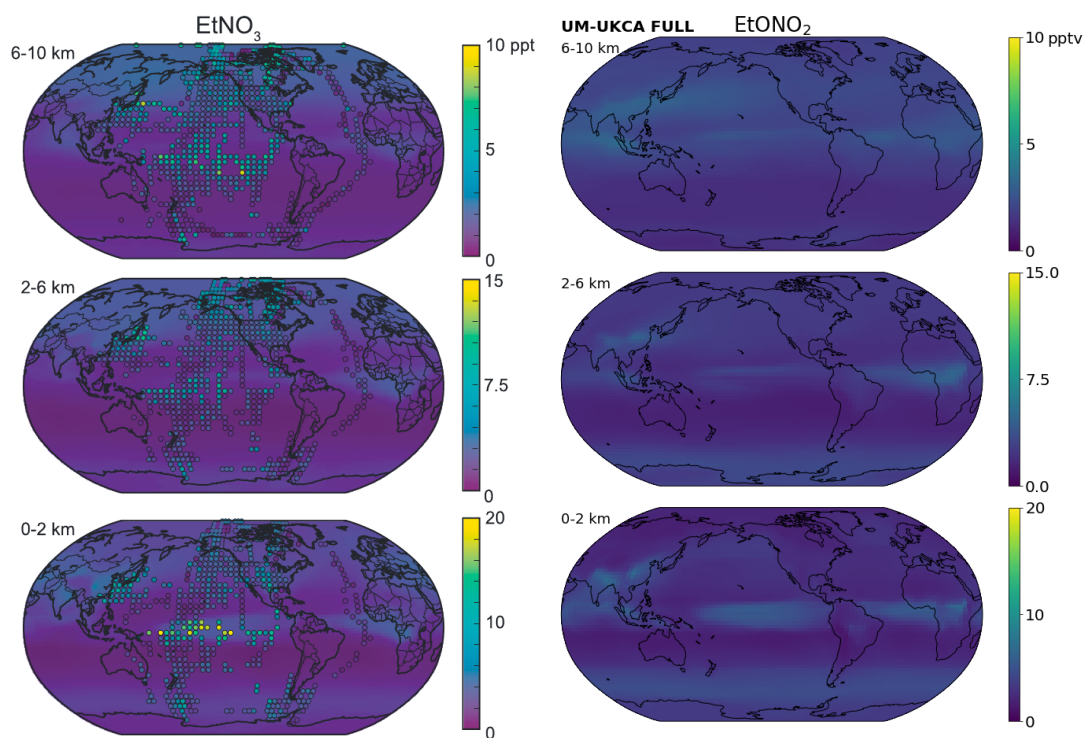
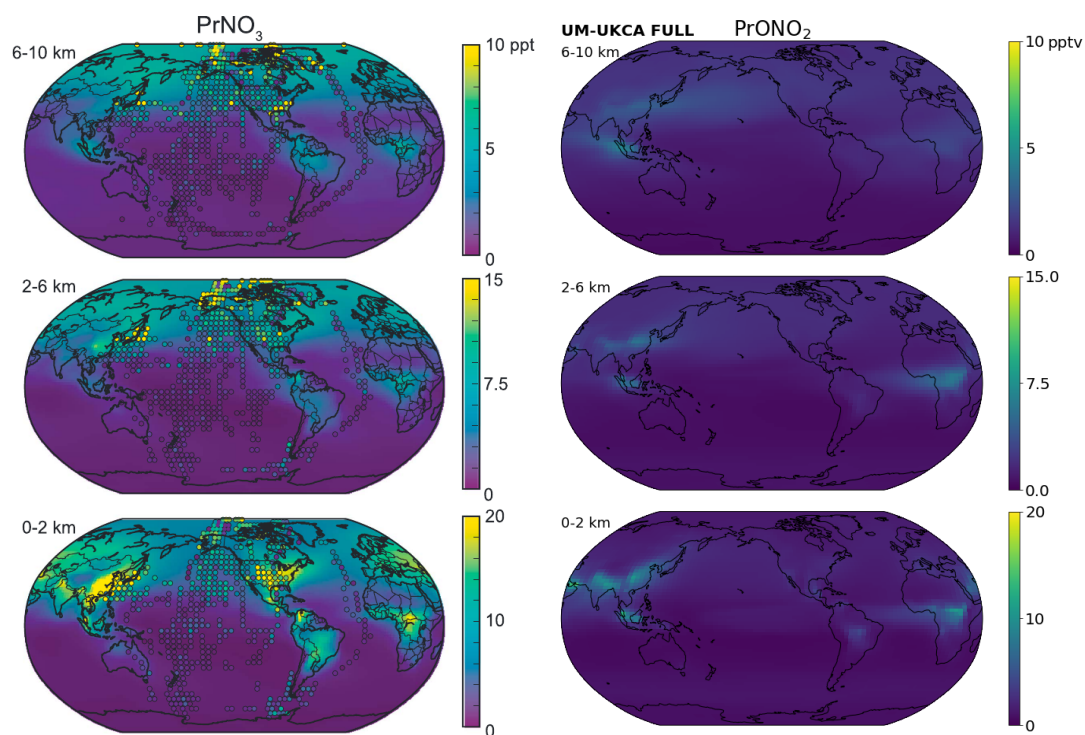


FIGURE 4.5: Annual mean distribution of  $\text{MeONO}_2$  at different altitude ranges: (bottom) 0–2 km, (middle) 2–6 km, (top) 6–10 km. (Left column) Background colours show GEOS-Chem model results from 2013 with aircraft observations from 1996–2017 overlaid as filled circles. Observations have been averaged over all flight days and over a horizontal resolution of  $4^\circ \times 5^\circ$  for visibility. Note the difference in colour scale between different altitude ranges and supersaturated colours in the case of  $\text{MeONO}_2$ . From Fisher et al. (2018). (Right column) Same but from the UM-UKCA FULL run.

distribution of alkyl nitrate oceanic emissions in the runs under comparison, it seems that ozone is less sensitive to alkyl nitrate chemistry in the tropics than in high latitudes. Why the Williams et al. (2014) methane lifetime increased when ozone burden increased is not clear, but all our runs consistently show a decrease in methane lifetime.

Since Fisher et al. (2018) did not report any estimates of the change in tropospheric ozone burden and methane lifetime between their “standard” and “new” runs, but provided other measures of the impact of alkyl nitrates on tropospheric chemistry, we recreated some of the figures from their study using the data from our FULL run.

Figures 4.5–4.7 show that UM-UKCA predicts higher  $\text{MeONO}_2$  concentrations than GEOS-Chem at all altitude ranges, especially at 6–10 km, which is more consistent with the observations. However, the decline in  $\text{MeONO}_2$  concentrations from the equator to the extratropics is more gradual in UM-UKCA than in GEOS-Chem, with UM-UKCA being less consistent with the observations. In the case of  $\text{EtONO}_2$ , both models capture the observed distribution well. In the case of  $\text{C}_3 \text{RONO}_2$ , GEOS-Chem captures the observed distribution better than UM-UKCA, with UM-UKCA maxima being about 2 times lower than the observed because of a negative bias in  $\text{C}_3 \text{RONO}_2$  (see Chapter 3).

FIGURE 4.6: As in Fig. 4.5 but for EtONO<sub>2</sub>.FIGURE 4.7: As in Fig. 4.5 but for the sum of nPrONO<sub>2</sub> and iPrONO<sub>2</sub>.



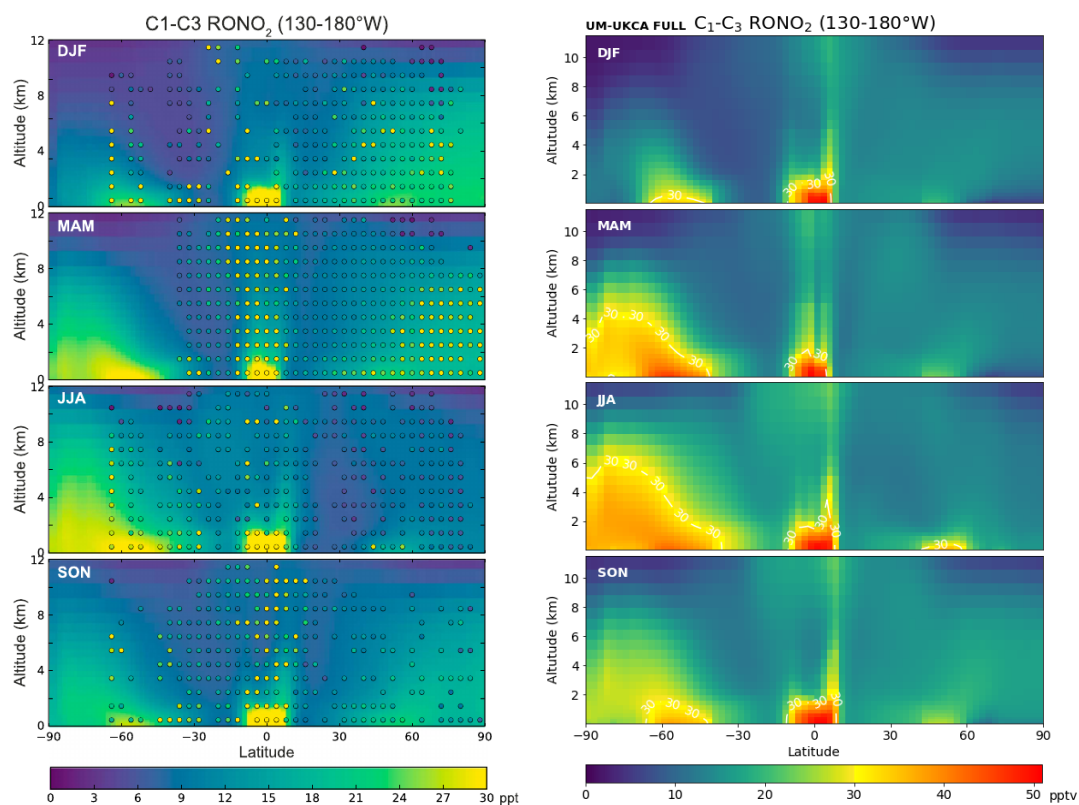


FIGURE 4.8: (Left) Zonal cross sections of seasonal mean distribution of total  $C_1$ - $C_3$   $RONO_2$  over the Pacific ( $180$ - $130^\circ$ W). Background colours show GEOS-Chem model results from 2013 with aircraft observations from 1996-2017 overlaid as filled circles. Observations have been averaged over all flight days and over a horizontal resolution of  $4^\circ \times 5^\circ$  and vertical resolution of 1 km. From Fisher et al. (2018). (Right) Same but from the UM-UKCA FULL run. Note that colour scales are different: values below 30 pptv are coloured using the same colour map, but UM-UKCA values higher than GEOS-Chem ones are coloured using another colour map. 30 pptv isoline is shown in white.

Figure 4.8 shows the zonal cross section of seasonal mean distribution of the sum of  $C_1$ - $C_3$   $RONO_2$  over the Pacific. UM-UKCA simulates higher alkyl nitrate concentrations than the observed or simulated by GEOS-Chem over the equator and in the southern high latitudes in all seasons, especially during boreal spring and summer. UM-UKCA also simulates higher  $C_1$ - $C_3$   $RONO_2$  concentrations than the observed or simulated by GEOS-Chem in the Northern Hemisphere during boreal summer because UM-UKCA has a positive bias in  $MeONO_2$  there during that season (see Chapter 3).

Figure 4.9 shows the relative changes in the annual mean  $NO_x$ ,  $NO_y$ , PAN and  $O_3$  concentrations in the boundary layer and free troposphere caused by adding  $C_1$ - $C_3$   $RONO_2$  chemistry to GEOS-Chem and UM-UKCA. The spatial distribution of these changes is similar between models, however, UM-UKCA generally shows a less uniform response. In both models, the impacts of alkyl nitrates are most prominent in the boundary layer over the tropical Pacific and the Southern Ocean, i.e. in areas with alkyl nitrate oceanic emissions.

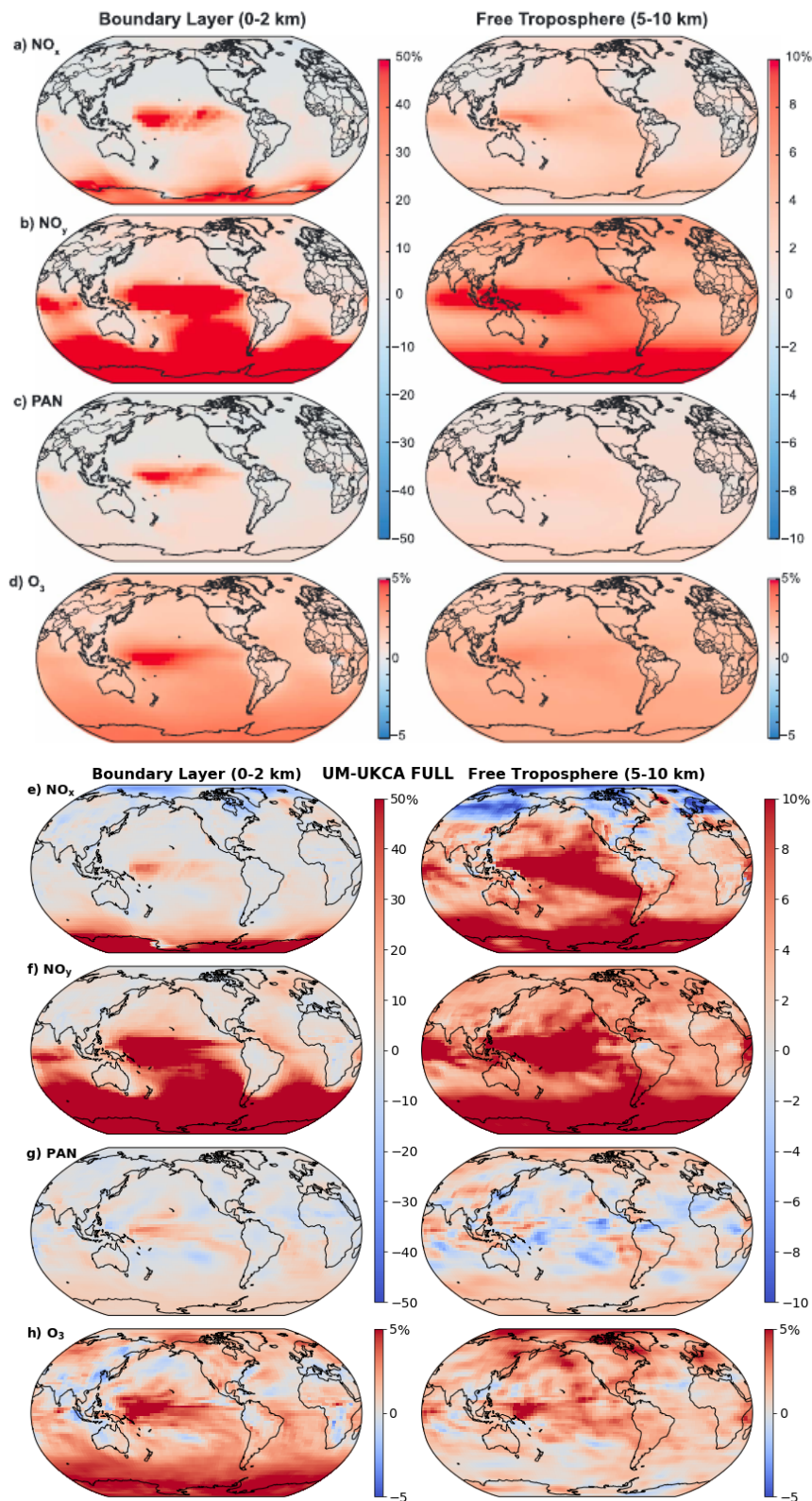


FIGURE 4.9: (Top) Relative change in annual mean  $NO_x$ ,  $NO_y$ , PAN and  $O_3$  caused by adding  $C_1$ - $C_3$  RONO<sub>2</sub> chemistry to GEOS-Chem. Changes are expressed as percent change from the standard simulation (no  $C_1$ - $C_3$  RONO<sub>2</sub>) and shown separately for the boundary layer (0-2 km, left panels) and free troposphere (5-10 km, right panels). From Fisher et al. (2018). (Bottom) Same but UM-UKCA FULL minus BASE. Note that in GEOS-Chem  $NO_y = NO_x + HNO_3 + PANs + RONO_2 + \text{aerosol nitrate} + \text{other nitrogen species}$ , in UM-UKCA  $NO_y = NO_x + HNO_3 + PAN + PPAN + RONO_2 + HONO + HO_2NO_2 + N_2O_5$ . Note that all colour scales are supersaturated.

**NO<sub>x</sub>**. In the tropical Pacific boundary layer, UM-UKCA shows a smaller increase in NO<sub>x</sub> (10-35%) than GEOS-Chem (up to 50%). In the tropical Pacific free troposphere, however, UM-UKCA shows a larger NO<sub>x</sub> increase (up to 25%) than GEOS-Chem (up to 10%). The latter might mean that alkyl nitrate destruction is a stronger NO<sub>x</sub> source in UM-UKCA than in GEOS-Chem, likely because UM-UKCA has higher alkyl nitrate concentrations in the tropical Pacific boundary layer. In the southern high-latitude boundary layer, UM-UKCA shows a larger increase in NO<sub>x</sub> (50-80%) than GEOS-Chem (up to 50%), with this increase still being larger in UM-UKCA (up to 30%) than in GEOS-Chem (0-4%) in the southern high-latitude free troposphere. In the Arctic, UM-UKCA shows a decrease in NO<sub>x</sub> in the boundary layer (up to -30%) and free troposphere (up to -14%), while GEOS-Chem shows a decrease in NO<sub>x</sub> in the North Atlantic boundary layer (up to -5...-10%) and an increase over the Chukchi Sea area (up to 5-10%), but an increase in the free troposphere.

**NO<sub>y</sub>**. In the boundary layer, UM-UKCA NO<sub>y</sub> concentrations increased by up to 140% in the tropical Pacific and by up to 220% in the southern high-latitudes, while in GEOS-Chem they “more than doubled from a baseline” (Fisher et al. (2018), p.13). In the free troposphere, UM-UKCA NO<sub>y</sub> concentrations increased by up to 40% in the tropical Pacific and by up to 10-24% the southern high-latitudes, while in GEOS-Chem they increased by no more than 10%.

**PAN**. PAN concentrations seem to be less sensitive to the addition of C<sub>1</sub>-C<sub>3</sub> RONO<sub>2</sub> chemistry to UM-UKCA than to GEOS-Chem. In the boundary layer, UM-UKCA PAN concentrations increased up to 30% over the tropical Pacific, while in GEOS-Chem they increased by up to 40-50%. In the free troposphere, however, the changes in PAN stayed below 10% in both models.

**O<sub>3</sub>**. The impact of alkyl nitrates on ozone concentrations is similar in GEOS-Chem and UM-UKCA. Both models agree that in the tropical Pacific ozone increases by less than 10% (up to 6.2% in GEOS-Chem and 9.4% in UM-UKCA) in the boundary layer and by less than 7% (up to 3% and 6.9%, respectively) in the free troposphere. This localised increase in ozone concentrations is caused by the fact that (a) the Walker circulation helps to sustain ozone loss over this area, but (b) it also helps to accumulate emissions of alkyl nitrates and destroy them, the net result being an increase in NO<sub>x</sub> and ozone concentrations. This UM-UKCA result is more consistent with the findings of Williams et al. (2014) and Fisher et al. (2018), the former of which reported an increase in ozone of up to 5% in the tropical Pacific from their EMISS run, and is less consistent with the findings of Neu et al. (2008), who reported an ozone increase of up to 20% in the same area. Both UM-UKCA and GEOS-Chem show an increase in ozone concentrations in the southern high-latitude boundary layer of up to 5-6%.

### 4.3 Localised impacts of alkyl nitrates

To see if the localised changes in the tropospheric composition due to the addition of  $C_1$ - $C_3$   $\text{RONO}_2$  chemistry and/or direct emissions are statistically significant in UM-UKCA, we performed the following statistical analysis.

#### 4.3.1 Statistical analysis

First, we ran all UM-UKCA simulations as 10-year-long perpetual year 2000 simulations in order to collect data for statistical analysis. We discarded the first 2 years of data from each simulation as a spin-up, as it was the amount of time needed for alkyl nitrate concentrations to rise from zero to a stable non-zero concentration. The remaining 8 years of data were not enough for a proper statistical analysis, but we used it for such an analysis anyway, because running the model for a longer time period was impractical.

Next, we analysed the seasonal mean distribution of the key species in the boundary layer (0-2 km) and the free troposphere (5-10 km) as well as the zonal cross sections of seasonal mean distribution. To see if the differences in the seasonal means between the BASE run and a sensitivity run were statistically significant, we performed the following statistical tests:

1. Shapiro-Wilk test to check if the data were normally distributed.
2. Paired samples t-test or Wilcoxon signed-rank test, depending on the outcome of the Shapiro-Wilk test, to check if the data sampled at individual grid points from the BASE run and a sensitivity run had an identical average. If the data were normally distributed, we used the paired samples t-test. If the data were not normally distributed, we used the Wilcoxon signed-rank test, because it is a non-parametric version of the paired samples t-test.
3. “Field significance” test to evaluate the collective significance of the paired samples t-tests or the Wilcoxon signed-rank tests at individual grid points. This test is a procedure known as the control of the false discovery rate (Wilks, 2006; Wilks, 2016), which protects the analysis against overstatement and overinterpretation of multiple testing results.

The significance level in all aforementioned statistical tests was set to 5%.

#### 4.3.2 Impact of $C_1$ - $C_3$ alkyl nitrate photochemical production

When  $C_1$ - $C_3$   $\text{RONO}_2$  photochemical production and loss are included into UM-UKCA, the changes in the seasonal mean ozone concentrations in the boundary layer (Figure 4.10), the free troposphere (not shown) and in the zonal seasonal means (Figure 4.14) are present, but none of them are statistically significant.



### 4.3.3 Impact of C<sub>1</sub>-C<sub>3</sub> alkyl nitrate oceanic emissions

When C<sub>1</sub>-C<sub>3</sub> RONO<sub>2</sub> oceanic emissions and photochemical loss are included into UM-UKCA, NO<sub>x</sub> and ozone concentrations show a statistically significant increase over the Southern Ocean. NO<sub>x</sub> (not shown) increases by no more than 1 pptv (180%) in the boundary layer in all seasons, with a maximum increase during boreal winter. Ozone (Figure 4.11) increases by up to 1-2 ppbv (20%) in the boundary layer during boreal winter and by ≤1 ppbv (≤5%) in other seasons. While increases in NO<sub>x</sub> are statistically significant during boreal winter, spring and autumn, increases in ozone are statistically significant only in boreal winter and autumn.

The zonal mean ozone concentrations (Figure 4.15) show a statistically significant increase (a) of up to 2 ppbv within 0-5 km over the Southern Ocean during boreal winter and autumn, and (b) of up to 1 ppbv within 0-10 km near the equator also during boreal winter and autumn.

### 4.3.4 Impact of C<sub>1</sub>-C<sub>3</sub> alkyl nitrate biomass burning emissions

When C<sub>1</sub>-C<sub>3</sub> RONO<sub>2</sub> biomass burning emissions and photochemical loss are included into UM-UKCA, NO<sub>x</sub> shows a statistically significant increase in the boundary layer over equatorial Africa during boreal autumn. An associated increase in ozone (Figure 4.12) is not statistically significant.

The zonal mean ozone concentrations (Figure 4.16) show a statistically significant increase of up to 2 ppbv within 0-5 km near the equator during boreal winter.

### 4.3.5 Impact of C<sub>1</sub>-C<sub>3</sub> alkyl nitrate photochemical production and direct emissions

When C<sub>1</sub>-C<sub>3</sub> RONO<sub>2</sub> photochemical production and loss and oceanic and biomass burning emissions are included into UM-UKCA, NO<sub>x</sub> and ozone concentrations show a statistically significant increase mostly over the Southern Ocean. NO<sub>x</sub> increases by no more than 1 pptv (185%) in the boundary layer in all seasons, with a maximum increase during boreal winter. Ozone (Figure 4.13) increases by up to 1-2 ppbv (20%) in the boundary layer during boreal winter and by ≤1 ppbv (≤5%) in other seasons.

The zonal mean ozone concentrations (Figure 4.17) show a statistically significant increase mostly in the regions where the addition of C<sub>1</sub>-C<sub>3</sub> RONO<sub>2</sub> direct emissions also has an impact.

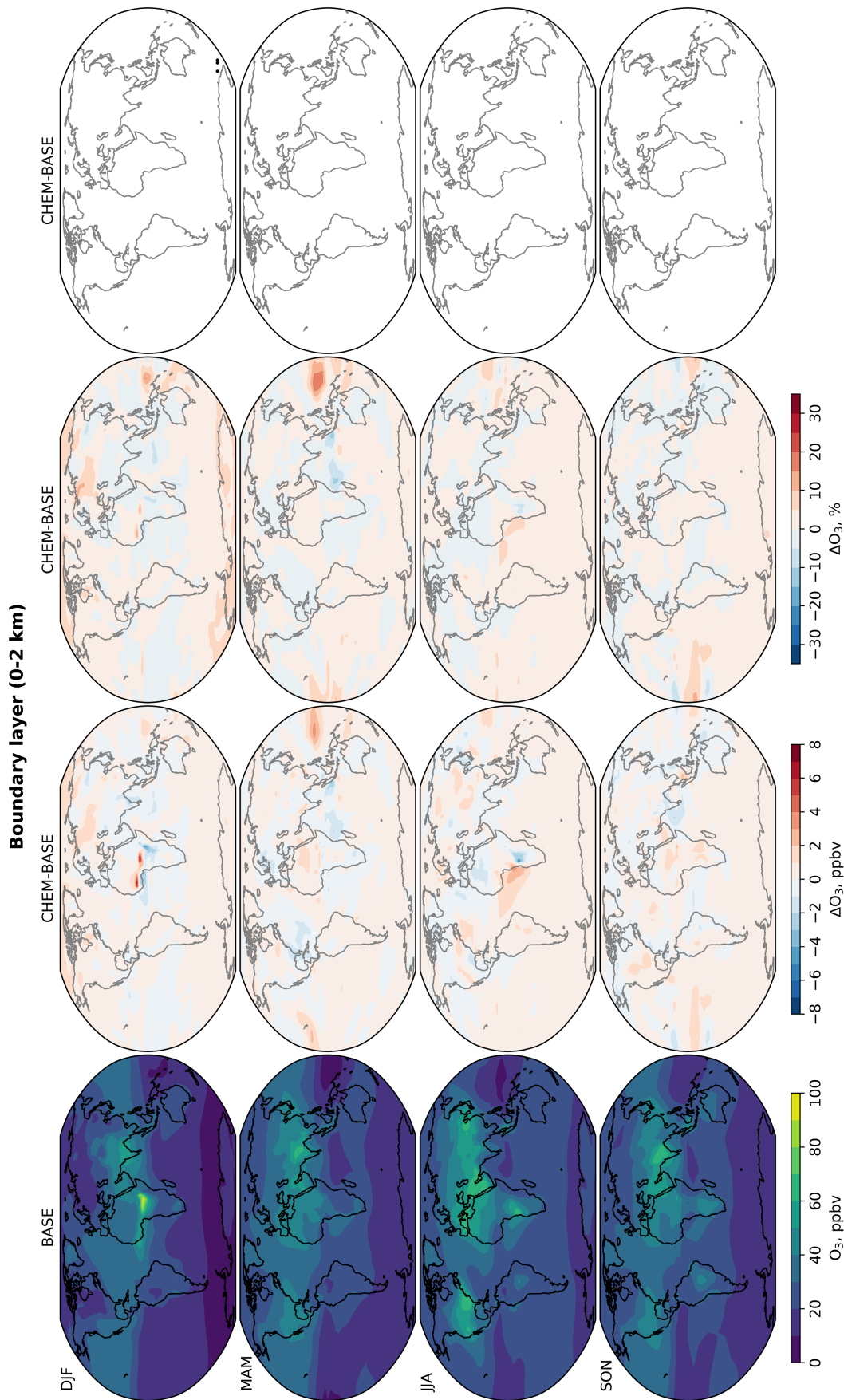


FIGURE 4.10: Seasonal mean distribution of  $O_3$  in the boundary layer (0-2 km) in the UM-UKCA BASE and CHEM runs. Stippling highlights the areas where the difference in concentrations is statistically significant.

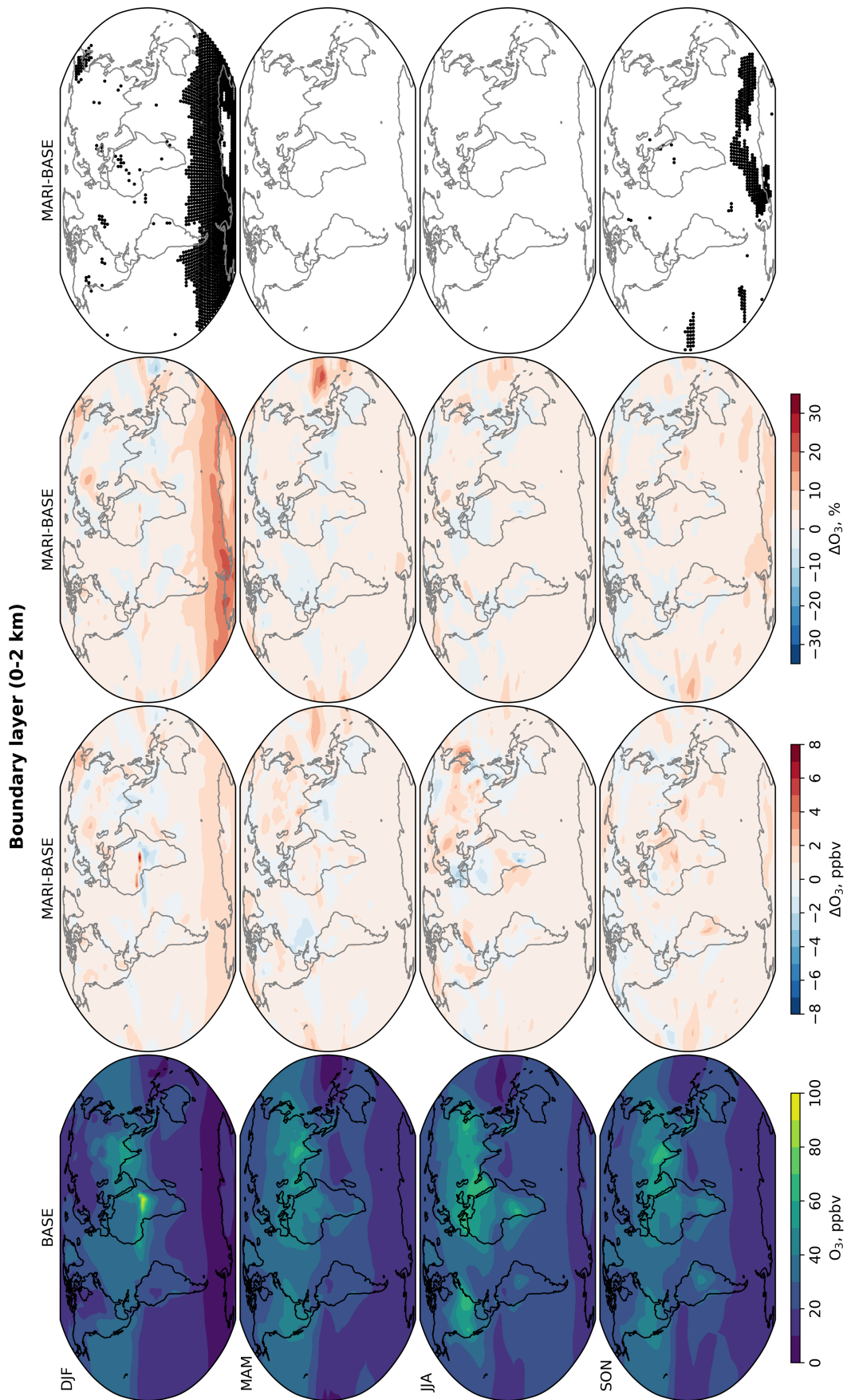


FIGURE 4.11: As in Fig. 4.10 but in the UM-UKCA BASE and MARI runs.

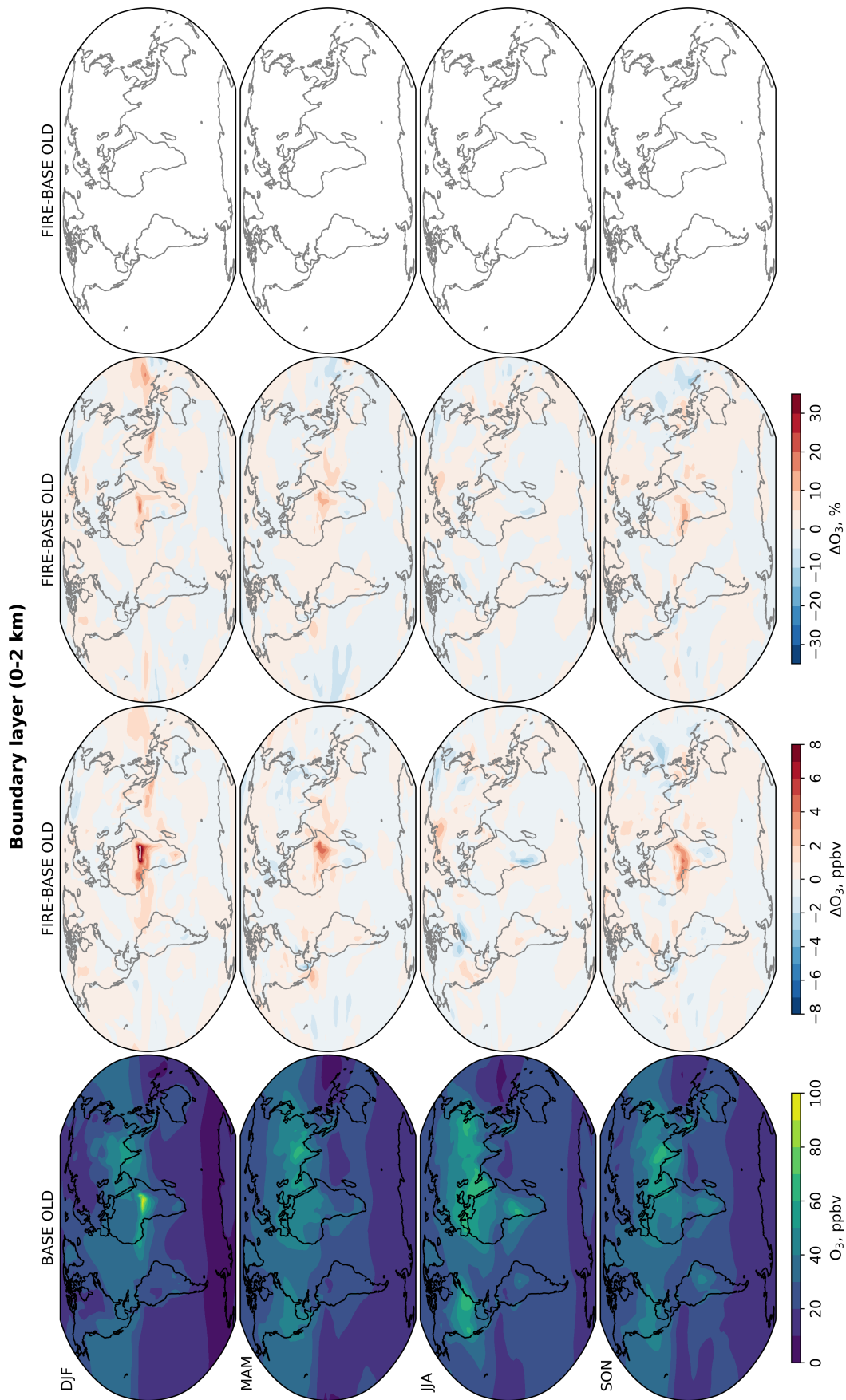


FIGURE 4.12: As in Fig. 4.10 but in the UM-UKCA SSAN (BASE OLD) and FIRE runs.



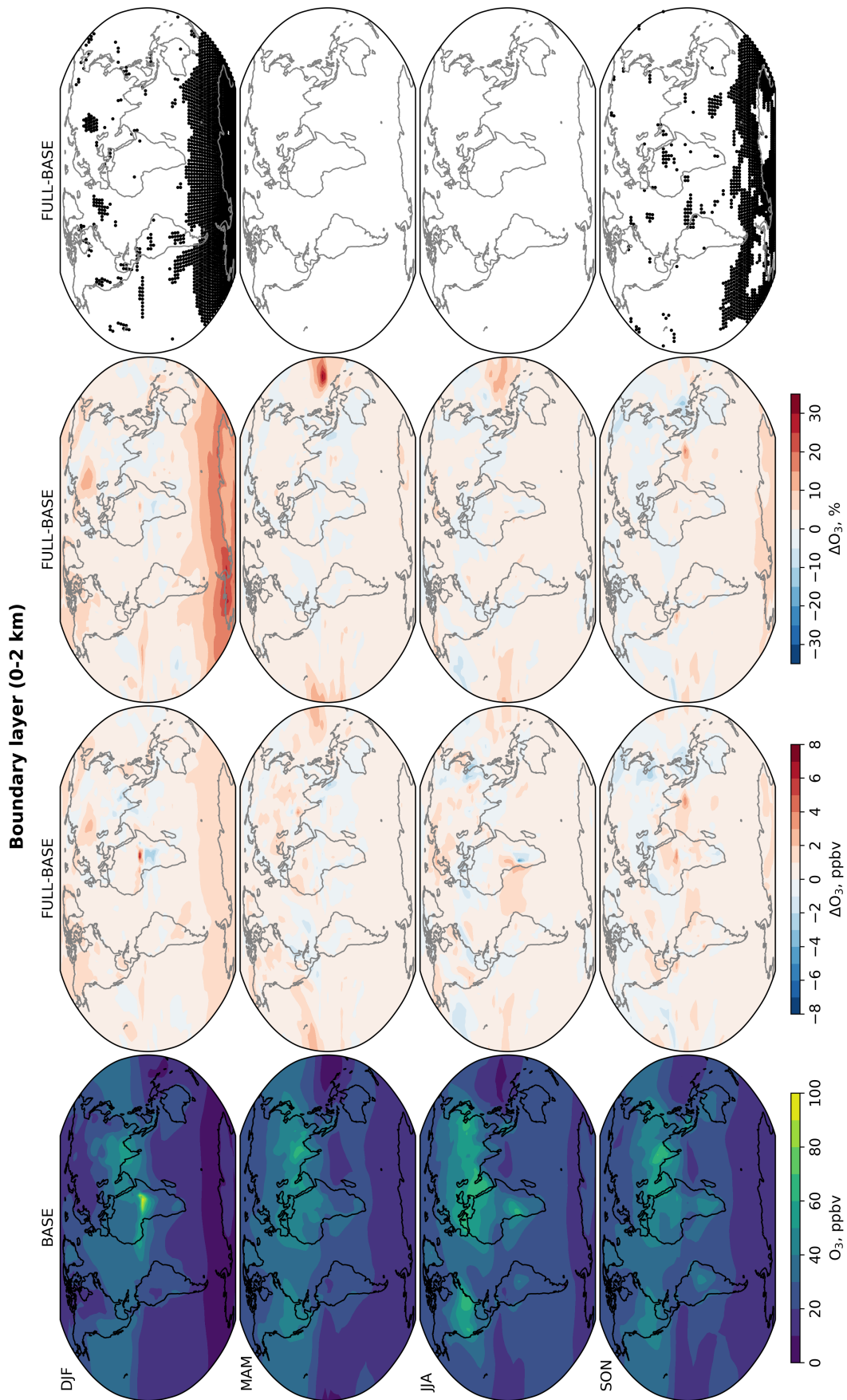


FIGURE 4.13: As in Fig. 4.10 but in the UM-UKCA BASE and FULL runs.

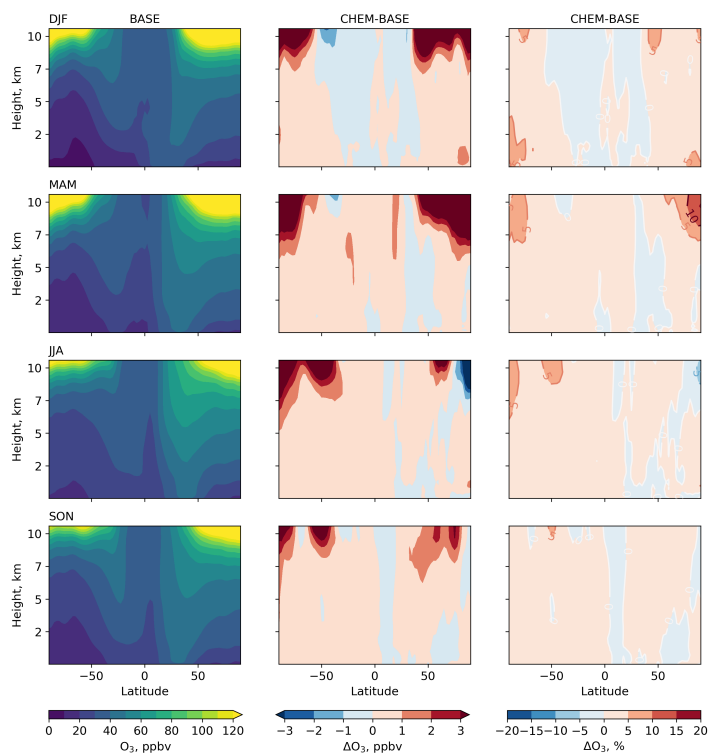


FIGURE 4.14: Zonal seasonal mean distribution of  $O_3$  in the troposphere (0–10 km) in the UM-UKCA BASE and CHEM runs. Stippling highlights the areas where the difference in concentrations is statistically significant.

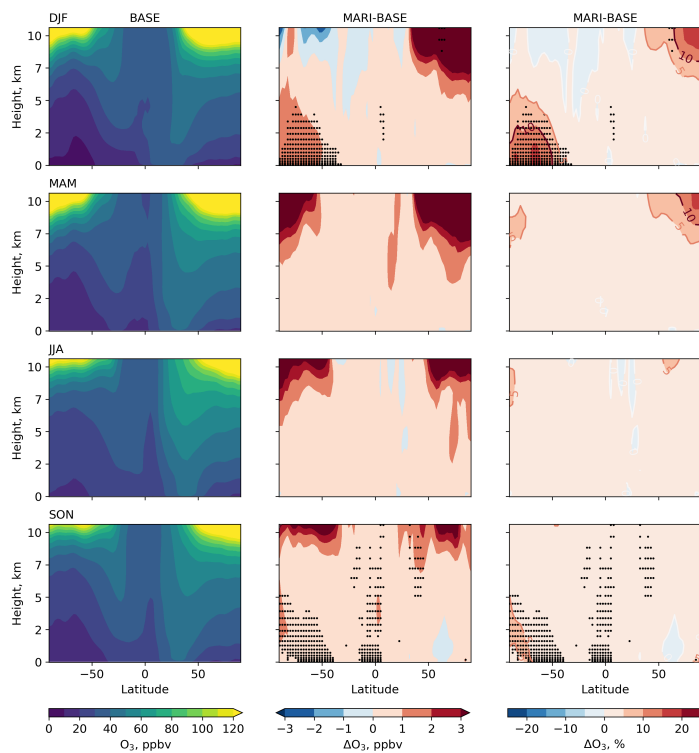


FIGURE 4.15: As in Fig. 4.14 but in the UM-UKCA BASE and MARI runs.

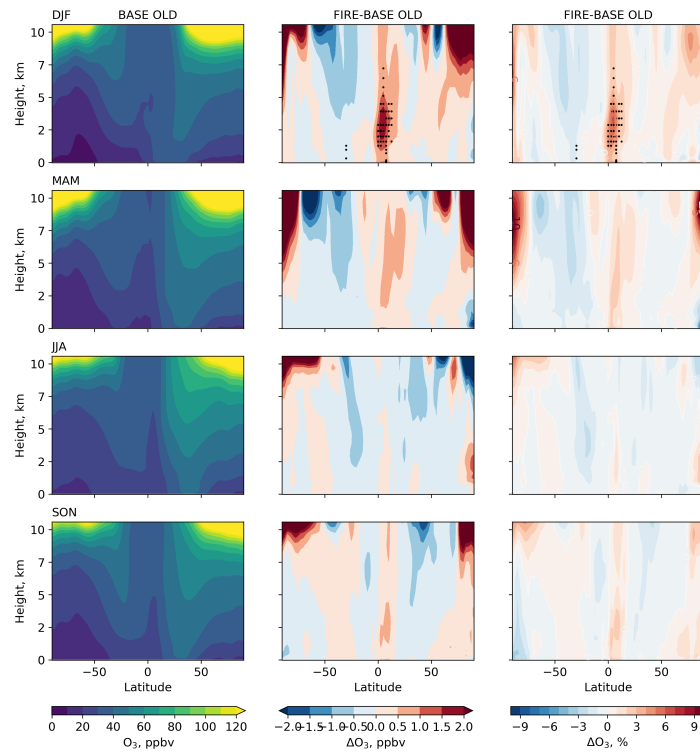


FIGURE 4.16: As in Fig. 4.14 but in the UM-UKCA SSAN (BASE OLD) and FIRE runs.

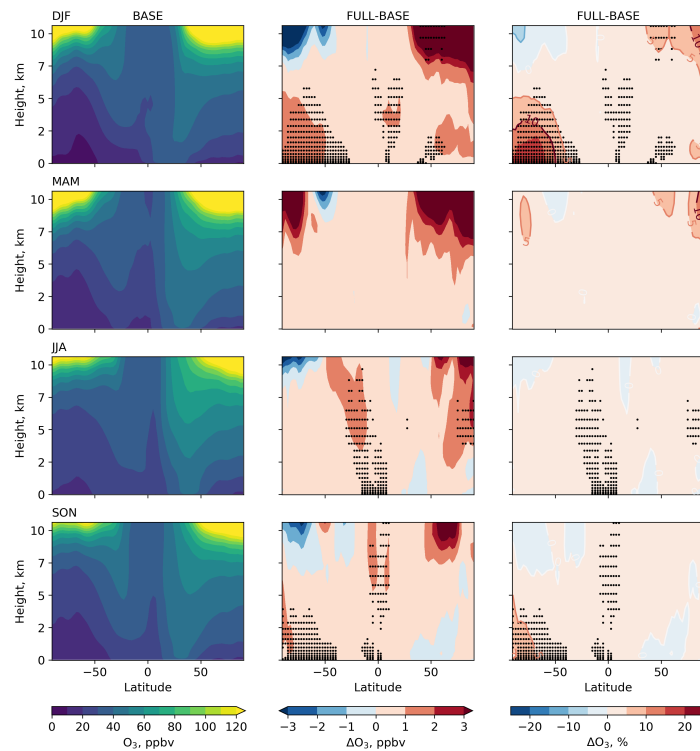


FIGURE 4.17: As in Fig. 4.14 but in the UM-UKCA BASE and FULL runs.

TABLE 4.2: Global mean tropospheric ozone and methane burdens, methane lifetime and interhemispheric annual mean OH ratio computed for 90°N-90°S using 125 ppbv ozonepause and averaged over 8 years of UM-UKCA perpetual year 2000 simulation. The standard error of the mean is given in brackets.

Experiment	$O_3$ Tg yr <sup>-1</sup>	$CH_4$ Tg yr <sup>-1</sup>	$\tau_{CH_4}$ yr	NH/SH OH
SSAN	272.50 (0.30)	4357.49 (26.38)	9.652 (0.037)	1.364 (0.004)
BASE	271.89 (0.47)	4367.93 (25.79)	9.700 (0.027)	1.367 (0.005)
CHEM	273.19 (0.24)	4355.96 (24.35)	9.634 (0.031)	1.358 (0.003)
MARI	274.47 (0.49)	4343.19 (24.91)	9.560 (0.026)	1.340 (0.005)
FIRE	272.99 (0.46)	4349.43 (51.08)	9.640 (0.051)	1.366 (0.006)
FULL	274.85 (0.50)	4340.52 (23.19)	9.549 (0.024)	1.345 (0.005)

TABLE 4.3: Global mean tropospheric MeONO<sub>2</sub>, EtONO<sub>2</sub>, nPrONO<sub>2</sub> and iPrONO<sub>2</sub> burdens computed for 90°N-90°S using 125 ppbv ozonepause and averaged over 8 years of UM-UKCA perpetual year 2000 simulation. The standard error of the mean is given in brackets.

Experiment	MeONO <sub>2</sub> Gg yr <sup>-1</sup>	EtONO <sub>2</sub> Gg yr <sup>-1</sup>	nPrONO <sub>2</sub> Gg yr <sup>-1</sup>	iPrONO <sub>2</sub> Gg yr <sup>-1</sup>
CHEM	76.69 (0.21)	19.36 (0.02)	1.740 (0.004)	15.873 (0.029)
MARI	65.64 (0.08)	11.55 (0.02)	0.792 (0.001)	2.051 (0.003)
FIRE	0.19 (0.01)	0.11 (0.00)	0.004 (0.000)	0.032 (0.000)
FULL	144.52 (0.25)	31.12 (0.03)	2.508 (0.004)	17.916 (0.025)

## 4.4 Summary

We explored the global and localised impacts of  $C_1$ - $C_3$  RONO<sub>2</sub> chemistry and oceanic and biomass burning emissions on tropospheric ozone chemistry in a series of sensitivity simulations with the UM-UKCA model. To see if the localised impacts of  $C_1$ - $C_3$  RONO<sub>2</sub> were statistically significant, we also performed a number of statistical tests.

We found that  $C_1$ - $C_3$  RONO<sub>2</sub> photochemical production and loss increase tropospheric ozone burden by  $1.30 \pm 0.53$  Tg ( $0.48 \pm 0.19\%$ ) and decrease methane lifetime by  $0.066 \pm 0.041$  yr ( $0.68 \pm 0.42\%$ ). An increase in tropospheric ozone burden was unexpected as it is generally thought that alkyl nitrate formation suppresses the tropospheric ozone production. However, a now known UM-UKCA positive bias in MeONO<sub>2</sub> in the Northern Hemisphere during boreal summer likely explains this increase in ozone, because an excess in MeONO<sub>2</sub> could have served as an extra NO<sub>x</sub> source for the tropospheric ozone production.  $C_1$ - $C_3$  RONO<sub>2</sub> chemistry also changes NO<sub>x</sub> and ozone seasonal mean concentrations between the UM-UKCA BASE and CHEM runs, but none of these changes are statistically significant.

$C_1$ - $C_3$  RONO<sub>2</sub> oceanic emissions have the largest global impact on tropospheric ozone chemistry among all alkyl nitrate sources considered in this study. Tropospheric ozone burden increases by  $2.58 \pm 0.68$  Tg ( $0.95 \pm 0.25\%$ ) and methane lifetime decreases by  $0.140 \pm 0.037$  yr ( $1.44 \pm 0.39\%$ ), which is within range of previously reported estimates.



UM-UKCA  $\text{NO}_x$  and ozone seasonal mean concentrations show a statistically significant increase of up to 1 pptv and 2 ppbv, respectively, over the Southern Ocean within 0-5 km during boreal winter and autumn. This is expected as photochemical processing of alkyl nitrate oceanic emissions releases  $\text{NO}_x$  into a typically low  $\text{NO}_x$  environment during the most photochemically active seasons of the Southern Hemisphere. Therefore,  $\text{C}_1\text{-C}_3$   $\text{RONO}_2$  are a very important component of  $\text{NO}_y$  budget in the Southern Hemisphere, where they comprise up to 80% of  $\text{NO}_y$  according to UM-UKCA (not shown).

$\text{C}_1\text{-C}_3$   $\text{RONO}_2$  biomass burning emissions have the smallest global impact on tropospheric ozone chemistry among all alkyl nitrate sources considered in this study. Tropospheric ozone burden increases by  $0.49 \pm 0.55$  Tg ( $0.18 \pm 0.20\%$ ) and methane lifetime decreases by  $0.012 \pm 0.063$  ( $0.12 \pm 0.65\%$ ). Although, in the free troposphere over the equatorial Africa,  $\text{C}_1\text{-C}_3$   $\text{RONO}_2$  biomass burning emissions cause a statistically significant increase in zonal mean ozone concentrations of up to 2 ppbv during boreal winter.

The combination of  $\text{C}_1\text{-C}_3$   $\text{RONO}_2$  photochemical production and loss and oceanic and biomass burning emissions increases tropospheric ozone burden by  $2.96 \pm 0.69$  Tg ( $1.09 \pm 0.25\%$ ) and decreases methane lifetime by  $0.151 \pm 0.036$  yr ( $1.56 \pm 0.37\%$ ). Statistically significant increases in seasonal mean ozone concentrations of up to 2 ppbv ( $\leq 5\%$ ) are located within 0-5 km over the Southern Ocean during boreal winter and autumn and within 0-10 km near the equator during boreal winter, summer and autumn.



## Synthesis and conclusions

C<sub>1</sub>-C<sub>3</sub> alkyl nitrates (RONO<sub>2</sub>) are important reservoirs of tropospheric reactive nitrogen. They are produced from the oxidation of their parent alkanes in the presence of NO<sub>x</sub> and emitted from oceanic and biomass burning sources. Due to their relatively long lifetime, they can be destroyed far away from their sources and change ozone concentrations at regional levels, altering the oxidising capacity of the atmosphere.

The chemistry of C<sub>1</sub>-C<sub>3</sub> RONO<sub>2</sub> is rather well known, but information about their oceanic and biomass burning sources is limited. We derived a new estimate of C<sub>1</sub>-C<sub>3</sub> RONO<sub>2</sub> biomass burning emissions from the Global Fire Emissions Database and implemented these emissions into a global 3D chemistry-climate model UM-UKCA, along with C<sub>1</sub>-C<sub>3</sub> RONO<sub>2</sub> chemistry from the Master Chemical Mechanism, dry deposition (as PAN) and oceanic emissions based on the data from [Fisher et al. \(2018\)](#).

We performed six 10-year-long perpetual year 2000 simulations with UM-UKCA, testing the sensitivity of C<sub>1</sub>-C<sub>3</sub> RONO<sub>2</sub> atmospheric concentrations to the processes that control their abundance. These simulations were designed to explore the statistical significance of the global and localised impacts of C<sub>1</sub>-C<sub>3</sub> RONO<sub>2</sub> chemistry and oceanic and biomass burning emissions on the composition of the troposphere. We also compared the regional mean vertical profiles of CH<sub>4</sub>, C<sub>2</sub>H<sub>6</sub>, C<sub>3</sub>H<sub>8</sub>, NO<sub>x</sub>, O<sub>3</sub>, MeONO<sub>2</sub>, EtONO<sub>2</sub>, nPrONO<sub>2</sub> and iPrONO<sub>2</sub> observed during the Atmospheric Tomography mission and simulated by UM-UKCA in 8 remote regions in February and August.

We discovered that UM-UKCA captures the observed CH<sub>4</sub> and O<sub>3</sub> vertical profiles reasonably well, showing a previously known bias in CH<sub>4</sub> likely caused by a misrepresentation of its surface latitudinal gradient by a lower boundary condition. NO<sub>x</sub> concentrations are generally underestimated by the model as well as C<sub>2</sub>H<sub>6</sub> and C<sub>3</sub>H<sub>8</sub>

because of (a) a poor representation of their emissions in the emissions inventories used in our study and (b) a positive model bias in OH in the Northern Hemisphere. Modelled MeONO<sub>2</sub> seasonality in the Northern Hemisphere is the opposite of the observed, showing lower concentrations during boreal winter and higher concentrations during boreal summer likely caused by an overproduction of MeOO radicals during boreal summer. Observed EtONO<sub>2</sub>, nPrONO<sub>2</sub> and iPrONO<sub>2</sub> seasonality is captured well by the model, showing higher concentrations during boreal and austral winter and lower concentrations during boreal and austral summer. The cause of a surprisingly good model performance in the case of EtONO<sub>2</sub> is unclear, but it is likely linked to the bias in the sources or sinks of the EtOO radicals. nPrONO<sub>2</sub> and iPrONO<sub>2</sub> concentrations are generally underestimated by the model, but modelled iPrONO<sub>2</sub> concentrations are higher than nPrONO<sub>2</sub> concentrations, which agrees with the observations. An inclusion of direct, especially oceanic, C<sub>1</sub>-C<sub>3</sub> RONO<sub>2</sub> emissions helps to explain a larger proportion of the observed C<sub>1</sub>-C<sub>3</sub> RONO<sub>2</sub> variability and reduces the root-mean-square errors between the observations and the model over the Central and South Pacific, with other regions showing a mixed response. However, a negative model bias in C<sub>1</sub>-C<sub>3</sub> RONO<sub>2</sub> concentrations in the MARI and FULL runs in August over the South Pacific indicates that the seasonal variability in C<sub>1</sub>-C<sub>3</sub> RONO<sub>2</sub> oceanic emissions is underestimated in this region by about a factor of 2.

We found that C<sub>1</sub>-C<sub>3</sub> RONO<sub>2</sub> photochemical production and loss increase tropospheric ozone burden by  $1.30 \pm 0.53$  Tg ( $0.48 \pm 0.19\%$ ) and decrease methane lifetime by  $0.066 \pm 0.041$  yr ( $0.68 \pm 0.42\%$ ). An increase in tropospheric ozone burden was unexpected as it is generally thought that alkyl nitrate formation suppresses the tropospheric ozone production. However, a now known UM-UKCA positive bias in MeONO<sub>2</sub> in the Northern Hemisphere during boreal summer likely explains this increase in ozone, because an excess in MeONO<sub>2</sub> could have served as an extra NO<sub>x</sub> source for the tropospheric ozone production. C<sub>1</sub>-C<sub>3</sub> RONO<sub>2</sub> chemistry also changes NO<sub>x</sub> and ozone seasonal mean concentrations between the UM-UKCA BASE and CHEM runs, but none of these changes are statistically significant.

C<sub>1</sub>-C<sub>3</sub> RONO<sub>2</sub> oceanic emissions have the largest global impact on tropospheric ozone chemistry among all alkyl nitrate sources considered in this study. Tropospheric ozone burden increases by  $2.58 \pm 0.68$  Tg ( $0.95 \pm 0.25\%$ ) and methane lifetime decreases by  $0.140 \pm 0.037$  yr ( $1.44 \pm 0.39\%$ ), which is within range of previously reported estimates. UM-UKCA NO<sub>x</sub> and ozone seasonal mean concentrations show a statistically significant increase of up to 1 pptv and 2 ppbv, respectively, over the Southern Ocean within 0-5 km during boreal winter and autumn. This is expected as photochemical processing of alkyl nitrate oceanic emissions releases NO<sub>x</sub> into a typically low NO<sub>x</sub> environment during the most photochemically active seasons of the Southern Hemisphere. Therefore, C<sub>1</sub>-C<sub>3</sub> RONO<sub>2</sub> are a very important component of NO<sub>y</sub> budget in the Southern Hemisphere, where they comprise up to 80% of NO<sub>y</sub> according to UM-UKCA.

$C_1$ - $C_3$   $\text{RONO}_2$  biomass burning emissions have the smallest global impact on tropospheric ozone chemistry among all alkyl nitrate sources considered in this study. Tropospheric ozone burden increases by  $0.49 \pm 0.55$  Tg ( $0.18 \pm 0.20\%$ ) and methane lifetime decreases by  $0.012 \pm 0.063$  ( $0.12 \pm 0.65\%$ ). Although, in the free troposphere over the equatorial Africa,  $C_1$ - $C_3$   $\text{RONO}_2$  biomass burning emissions cause a statistically significant increase in zonal mean ozone concentrations of up to 2 ppbv during boreal winter.

The combination of  $C_1$ - $C_3$   $\text{RONO}_2$  photochemical production and loss and oceanic and biomass burning emissions increases tropospheric ozone burden by  $2.96 \pm 0.69$  Tg ( $1.09 \pm 0.25\%$ ) and decreases methane lifetime by  $0.151 \pm 0.036$  yr ( $1.56 \pm 0.37\%$ ). Statistically significant increases in seasonal mean ozone concentrations of up to 2 ppbv ( $\leq 5\%$ ) are located within 0-5 km over the Southern Ocean during boreal winter and autumn and within 0-10 km near the equator during boreal winter, summer and autumn.

Our study shows that the change in tropospheric ozone burden caused by  $C_1$ - $C_3$   $\text{RONO}_2$  chemistry and emissions ( $1.09 \pm 0.25\%$ ) is of the same order of magnitude as the projected future change in tropospheric ozone burden modelled using emissions and climate projections from the Representative Concentration Pathways (RCPs) for 2030 (2100): -4% (-16%) for RCP2.6, 2% (-7%) for RCP4.5, 1% (-9%) for RCP6.0 and 7% (18%) for RCP8.5 (Young et al., 2013), but this change is smaller than (a) the 10% uncertainty in tropospheric ozone burden caused by the uncertainties across the JPL and IUPAC recommended inorganic reaction rate coefficients for  $\text{O}_x$ - $\text{HO}_x$ - $\text{NO}_x$ - $\text{CO}$ - $\text{CH}_4$  chemistry (Newsome and Evans, 2017), and (b) the 19% change<sup>1</sup> in present day tropospheric ozone burden caused by halogen chemistry (Sherwen et al., 2017).

## 5.1 Future work

This thesis progresses our understanding of the impacts of  $C_1$ - $C_3$   $\text{RONO}_2$  chemistry and emissions on tropospheric ozone chemistry. However, there are still some issues and open questions that future studies can address.

1. To better simulate  $\text{MeONO}_2$  concentrations, UM-UKCA v7.3 boreal summertime positive bias in the Northern Hemisphere needs to be addressed. One could try using a latitude varying methane lower boundary condition or methane emissions and do a series of perturbation experiments exploring the sensitivity of  $\text{MeONO}_2$  concentrations to changes in methane. A similar approach could be used for emissions of hydrocarbons included in the UM-UKCA ethane and propane species and would help to model  $\text{EtONO}_2$ ,  $\text{nPrONO}_2$  and  $\text{iPrONO}_2$  concentrations better too.

---

<sup>1</sup>339 Tg with halogens and 416 Tg without halogens according to GEOS-Chem.

2. A more extensive validation of UM-UKCA C<sub>1</sub>-C<sub>3</sub> RONO<sub>2</sub> chemistry is needed, especially for the seasons not covered in this thesis. It could be accomplished by comparing UM-UKCA data with ATom-3 and ATom-4 data when they are released, as well as by comparing UM-UKCA data with an assemble of C<sub>1</sub>-C<sub>3</sub> RONO<sub>2</sub> airborne observations collected between 1996 and 2017 and prepared by [Fisher et al. \(2018\)](#).
3. More concurrent measurements of chlorophyll *a* and seawater nitrite in the tropics are needed to better understand the relationship between these species, as well as more seawater nitrite and C<sub>1</sub>-C<sub>3</sub> RONO<sub>2</sub> saturation measurements (especially in the Southern Ocean in different seasons) to better constrain C<sub>1</sub>-C<sub>3</sub> RONO<sub>2</sub> oceanic source.
4. Future modelling studies would benefit from incorporating the [Simpson et al. \(2002\)](#) estimates of emission ratios of C<sub>1</sub>-C<sub>4</sub> RONO<sub>2</sub> relative to CO<sub>2</sub> and CO during different stages of savannah fires (flaming and smoldering) originally sampled in Australia. It is especially relevant for the studies investigating the photochemical footprint of the recent 2019-2020 Australian bushfire season, colloquially known as the black summer.
5. Building upon our box modelling work that showed that unifying the inorganic and C<sub>1</sub>-C<sub>3</sub> alkane chemistry from the Master Chemical Mechanism and the UM-UKCA's CheST chemical mechanism eliminates the differences in the steady state ozone, OH and HO<sub>2</sub> concentrations predicted by our box model, one could conduct a similar analysis for UM-UKCA using the output from the UMUI jobs xolnb (with the original CheST mechanism) and xolna (with the revised CheST mechanism: updated inorganic and C<sub>1</sub>-C<sub>3</sub> alkane chemistry). The outcome of this work would be similar in scope to the [Newsome and Evans \(2017\)](#) work for GEOS-Chem, but estimating the sensitivity and uncertainty of UM-UKCA annual mean tropospheric ozone burden, surface ozone, tropospheric OH concentrations and methane lifetime caused by the differences in JPL and IUPAC recommended reaction rate coefficients.

# 6

## Contribution to the OXBUDS project

Over the course of my PhD, I have been contributing to the Oxidant Budgets of the Northern Hemisphere Troposphere Since 1950 (OXBUDS) project. This project aimed to use long-term trends of C<sub>4</sub>-C<sub>5</sub> alkane and alkyl nitrate concentrations to determine the impact of changing anthropogenic emissions on the ozone and hydroxyl radical budgets of the Northern Hemisphere troposphere since 1950. The project was led by the principal investigator Prof. Claire E. Reeves (UEA) in close collaboration with the co-investigator Dr Alex T. Archibald (University of Cambridge). They oversaw the work of the following members of staff: Dr Paul T. Griffiths (University of Cambridge), Dr Marcus O. Köhler (UEA) and Dr Mike J. Newland (UEA, involved only at the beginning of the project). I was supervised by Prof. Claire E. Reeves.

Apart from participating in project meetings and discussing results, my contribution to the project included:

1. The development of a reduced version of C<sub>2</sub>-C<sub>5</sub> RONO<sub>2</sub> chemistry from the MCM v3.3.1. This version had to include (a) C<sub>4</sub>-C<sub>5</sub> alkane chemistry and (b) C<sub>2</sub>-C<sub>5</sub> RONO<sub>2</sub> chemistry as this chemistry was absent from the UM-UKCA CheST chemical mechanism. A special requirement was to include the reactions between the RO<sub>2</sub> radicals and NO and the HO<sub>2</sub> radicals as explicitly as possible, because these reactions control the rate of formation of alkyl nitrates.
2. UM-UKCA v10.6 validation against ATom.

As the project evolved, we decided to include C<sub>2</sub>-C<sub>5</sub> RONO<sub>2</sub> chemistry into UM-UKCA in a diagnostic rather than an interactive way, so that the reduced chemical mechanism that I prepared and tested against the MCM only served as a guide for the development of a simpler chemical mechanism by Dr Marcus O. Köhler. This diagnostic mechanism included the degradation of C<sub>4</sub>-C<sub>4</sub> alkanes and the reactions forming nBuONO<sub>2</sub>, sBuONO<sub>2</sub>, nPeBONO<sub>2</sub>, nPeCONO<sub>2</sub> and iPeBONO<sub>2</sub>. However, all reactants were recovered, such that the formation of the aforementioned alkyl nitrates had no impact on the rest of chemistry in the model.

For UM-UKCA v10.6 validation against ATom, I conducted a similar analysis to the one presented in Chapter 3 but for C<sub>2</sub>H<sub>6</sub>, C<sub>3</sub>H<sub>8</sub>, nC<sub>4</sub>H<sub>10</sub>, iC<sub>4</sub>H<sub>10</sub>, nC<sub>5</sub>H<sub>12</sub>, iC<sub>5</sub>H<sub>12</sub>, MeONO<sub>2</sub>, nBuONO<sub>2</sub>, sBuONO<sub>2</sub>, nPeBONO<sub>2</sub>, nPeCONO<sub>2</sub> and iPeBONO<sub>2</sub> using the output from the UM-UKCA v10.6 (a) long-term global runs with monthly output and (b) a limited area run with hourly output, both provided by Dr Marcus O. Köhler. The results are discussed in Köhler et al. (in prep.), but in brief, C<sub>4</sub>-C<sub>5</sub> RH and RONO<sub>2</sub> are generally underestimated by UM-UKCA, mostly over land and near pollution sources. However, the order of magnitude of C<sub>4</sub>-C<sub>5</sub> RONO<sub>2</sub>/RH ratio is captured reasonably well.



# A

## Appendix to Chapter 1

TABLE A.1: Aircraft and ship measurements of alkyl nitrates, ordered by month. Adapted from Fisher et al. (2018) and extended to include cruises.

Campaign	Platform	Month	Year	Region	Latitudes	Longitudes	Reference
HIPPO-1	aircraft	Jan	2009	Pacific	70°S-60°N	150°E-100°W	Wofsy (2011)
ORCAS	aircraft	Jan-Feb	2016	Southern Ocean	75°S-55°S	91°W-52°W	Stephens et al. (2018)
ATOM-2	aircraft	Feb	2017	Pacific	70°S-60°N	180°W-130°W	Wofsy et al. (2018)
				Atlantic	70°S-60°N	60°W-0°E	
SAGA-3	ship	Feb-Mar	1990	Equatorial Pacific	10°S-15°N	165°W-144°W	Atlas et al. (1993)
TOPSE	aircraft	Feb-May	2000	N. American Arctic	60°N-90°N	104°W-54°W	Atlas et al. (2003)
HIPPO-3	aircraft	Mar-Apr	2010	Pacific	70°S-60°N	150°E-100°W	Wofsy (2011)
PEM-Tropics B	aircraft	Mar-Apr	1999	Tropical Pacific	36°S-40°N	149°E-75°W	Blake et al. (2003)
TRACE-P	aircraft	Mar-Apr	2001	North Pacific	12°N-46°N	120°E-120°W	Jacob et al. (2003)
ARCTAS-A	aircraft	Apr	2008	N. American Arctic	60°N-90°N	175°W-50°W	Jacob et al. (2010)
INTEX-B	aircraft	Apr-May	2006	North Pacific	19°N-60°N	175°E-105°W	Kleb et al. (2011)
ITCT-2K2	aircraft	Apr-May	2002	North Pacific	26°N-48°N	130°W-90°W	Parrish et al. (2004)
SEAREX	ship	Apr-Jul	1986	North Pacific	20°N-55°N	170°W-145°W	Atlas (1988)
DC3	aircraft	May-Jun	2012	Continental US	30°N-42°N	105°W-80°W	Barth et al. (2015)
PHASE-1	ship	May-Jun	2004	Equatorial Pacific	0°-20°N	165°E-155°W	Dahl et al. (2005)
HIPPO-4	aircraft	Jun-Jul	2010	Pacific	70°S-60°N	150°E-100°W	Wofsy (2011)
FRAPPE	aircraft	Jul-Aug	2014	Continental US	37°N-42°N	110°W-100°W	Flocke et al. (2019)
ITOP	aircraft	Jul-Aug	2004	North Atlantic	33°N-47°N	20°W-40°W	Reeves et al. (2007)
ATOM-1	aircraft	Aug	2016	Pacific	70°S-60°N	180°W-130°W	Wofsy et al. (2018)
				Atlantic	70°S-60°N	60°W-0°E	
HIPPO-5	aircraft	Aug-Sep	2011	Pacific	70°S-60°N	150°E-100°W	Wofsy (2011)
SEAC4RS	aircraft	Aug-Sep	2013	Continental US	19°N-55°N	130°W-75°W	Toon et al. (2016)
PEM-Tropics A	aircraft	Aug-Oct	1996	Pacific	72°S-45°N	153°E-75°W	Talbot et al. (2000)
AMT-9	ship	Sep-Oct	1999	Atlantic	35°S-54°N	56°W-0°	Chuck et al. (2002)
ANT-XVIII/1	ship	Sep-Oct	2000	Atlantic	34°S-54°N	20°W-19°E	Chuck et al. (2002)
TEXAQS	aircraft	Sep-Oct	2006	Continental US	28°N-35°N	100°W-93°W	Parrish et al. (2009)
WIFE	aircraft	Sep-Oct	1998	Western US	32°N-49°N	124°W-0°	Friedli et al. (2001)
Albatross	ship	Oct-Nov	1996	Atlantic	50°S-67°N	68°W-25°W	Fischer et al. (2000)
HIPPO-2	aircraft	Oct-Nov	2009	Pacific	70°S-60°N	150°E-100°W	Wofsy (2011)
ACE-1	aircraft	Nov-Dec	1995	Pacific, S. Ocean	60°S-76°N	147°E-149°W	Blake et al. (1999)
JR124	ship	Nov-Dec	2004	Southern Ocean	36°S-65°S	30°W-70°W	Hughes et al. (2008)

TABLE A.2: Ground-based measurements of alkyl nitrates, ordered by month.

Site	Month	Year	Environment	Reference
Ulm, Germany	winter, summer	1992-1993	rural	Hauff et al. (1998)
Thompson Farm, NH, US	Jan-Feb	2002	suburban	Russo et al. (2010)
Neumayer, Antarctica	Jan-Mar	1997	background	Jones et al. (1999)
Alert, Canada	Jan-Apr	1992	background	Muthuramu et al. (1994)
Thompson Farm, NH, US	Jan 2004 - Feb 2008		suburban	Russo et al. (2010)
Boulder, CO, US	Feb-Mar	2011	semi rural	Abeira et al. (2018)
Boulder, CO, US	Mar-May	2015	semi rural	Abeira et al. (2018)
Mauna Loa, Hawaii	May-Jun	1988	background	Walega et al. (1992)
Ulm, Germany	May-Jun	1998	rural	Fischer et al. (2000)
Cape Recife, South Africa	Jun, Aug-Oct	1992-1993	coastal, suburban	Kock and Anderson (1994)
Kinterbish, AL, US	Jun-Jul	1992	rural	Bertman et al. (1995)
Thompson Farm, NH, US	Jun-Aug	2002	suburban	Russo et al. (2010)
Schauinsland, Germany	Jun 1990 - May 1991		rural	Flocke et al. (1998)
Summit, Greenland	Jun 1997 - Jun 1998		background	Swanson et al. (2003)
Boulder, CO, US	Jul-Aug	2015	semi rural	Abeira et al. (2018)
Scotia, PA, US	Jul-Aug	1988	rural/suburban	Bertman et al. (1995)
Thompson Farm, NH, US	Jul-Aug	2004	suburban	Russo et al. (2010)
Ulm, Germany	Jul, Sep	1997	rural	Fischer et al. (2000)
Granite Bay, CA, US	Jul-Sep	2001	urban	Day et al. (2003)
Chebogue Point, Canada	Aug, Sep	1993	rural	Roberts et al. (1998)
La Porte, TX, US	Aug-Sep	2000	urban	Day et al. (2003)
Tai O, China	Aug 2001 - Dec 2002		suburban	Simpson et al. (2006)
Blodgett Forest, CA, US	Oct 2000 - Dec 2001		urban	Day et al. (2003)

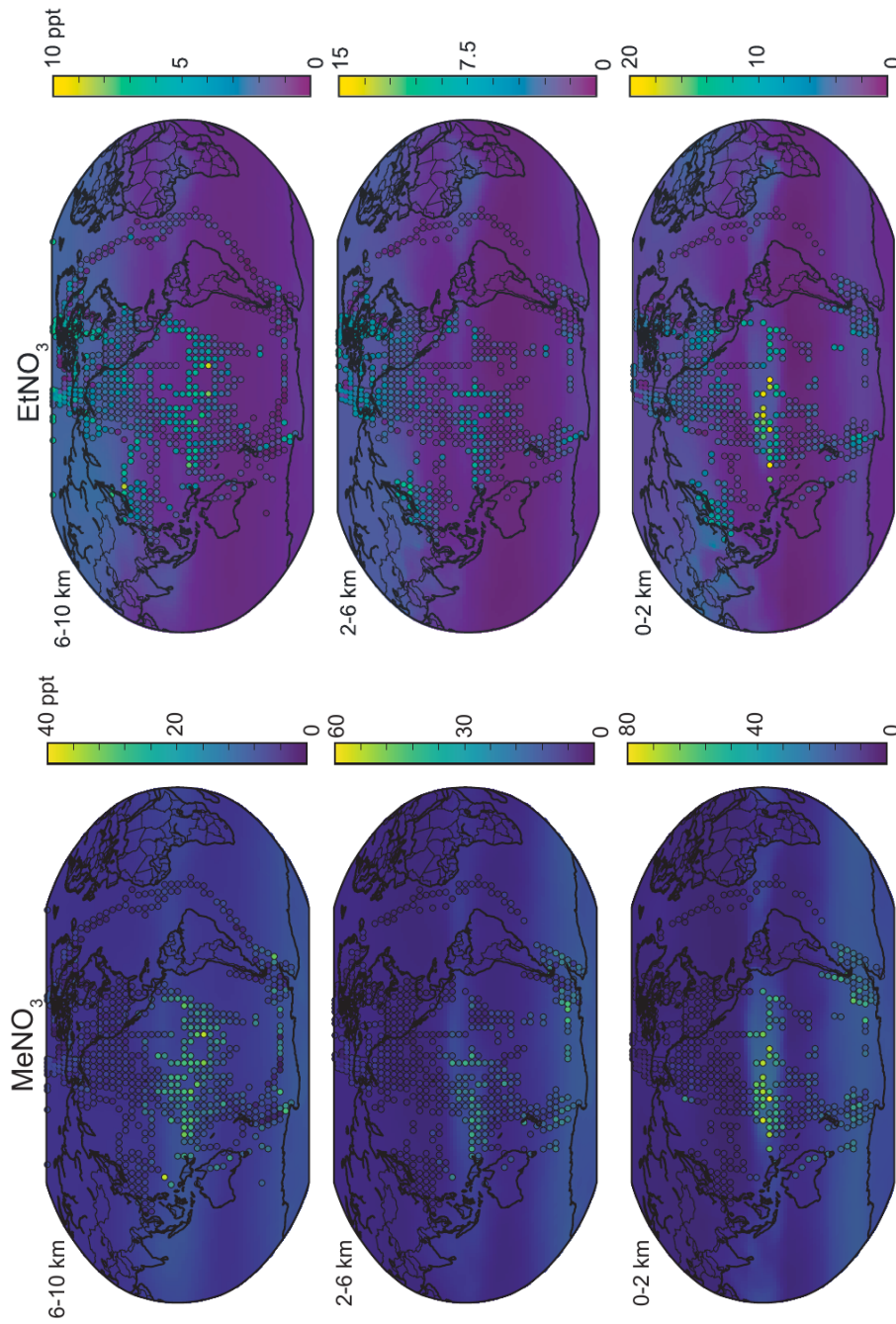


FIGURE A.1: Annual mean distribution of (left)  $\text{MeNO}_2$  and (right)  $\text{EtNO}_3$  at different altitude ranges: (bottom) 0–2 km, (middle) 2–6 km, (top) 6–10 km. Background colours show GEOS-Chem model results from 2013 with aircraft observations from 1996–2017 overlaid as filled circles. Observations have been averaged over all flight days and over a horizontal resolution of  $4^\circ \times 5^\circ$  for visibility. Note the difference in colour scale between different altitude ranges. From Fisher et al. (2018).

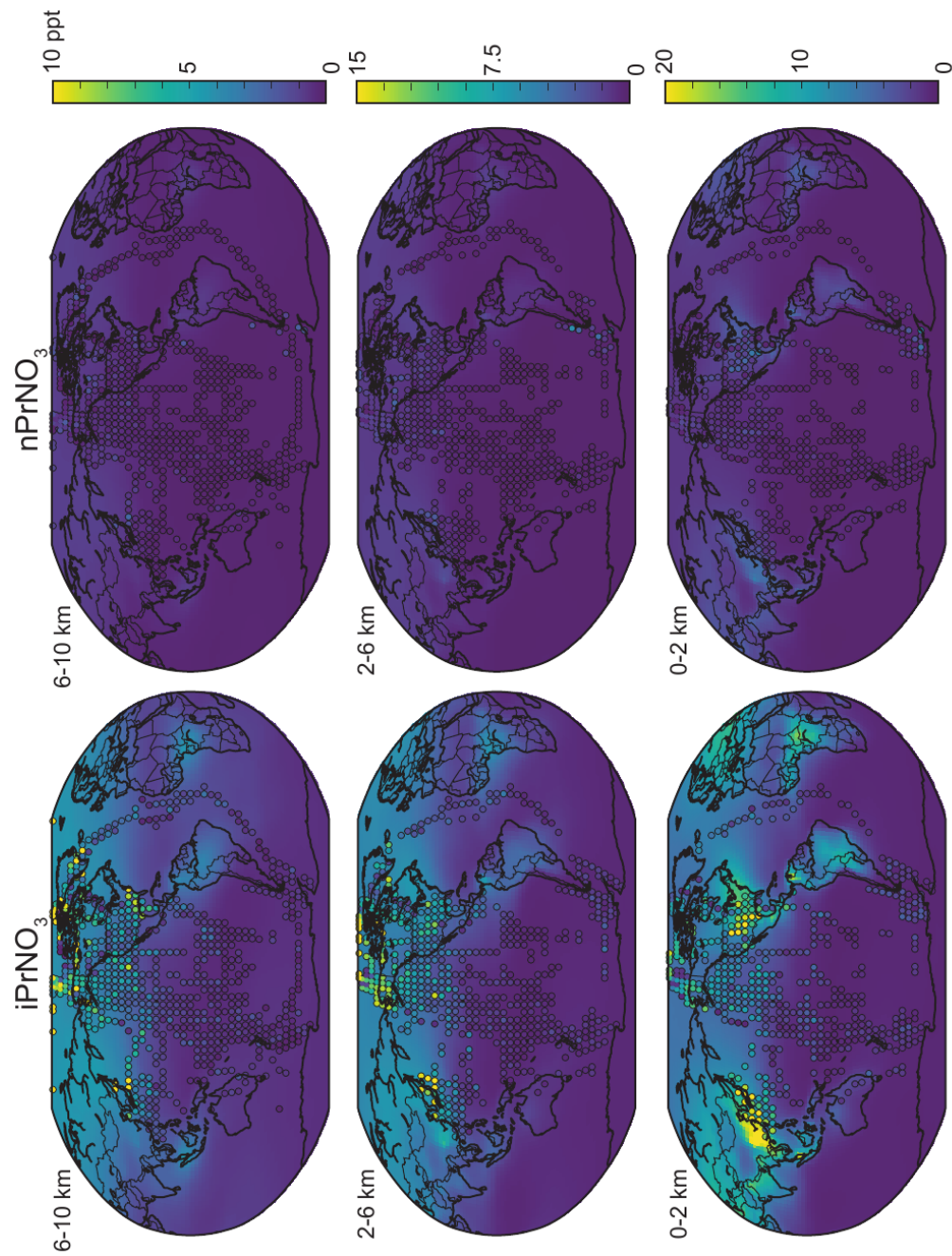


FIGURE A.2: As in Fig. A.1 but for (left)  $iPrONO_2$  and (right)  $nPrONO_2$ .



# B

## Appendix to Chapter 2

## B.1 Figures

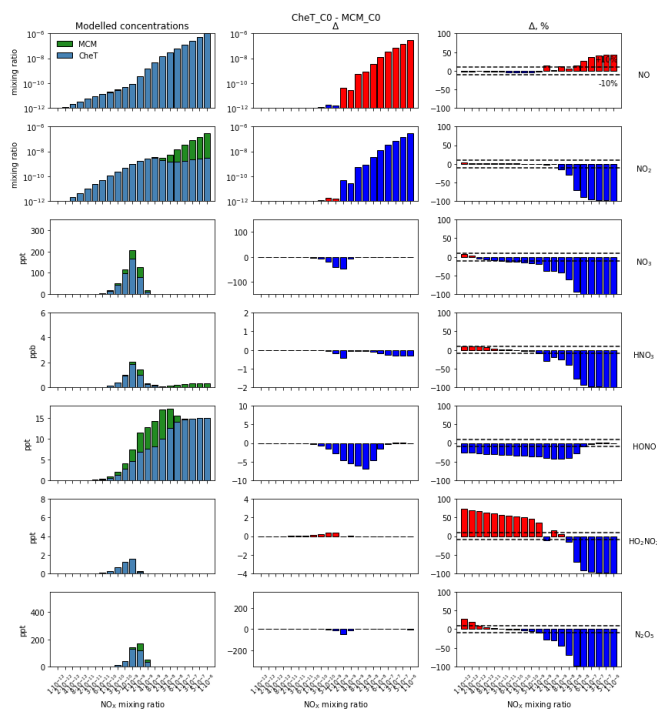


FIGURE B.1: As in Fig. 2.5 but for NO, NO<sub>2</sub>, NO<sub>3</sub>, HNO<sub>3</sub>, HONO, HO<sub>2</sub>NO<sub>2</sub> and N<sub>2</sub>O<sub>5</sub> before unification.

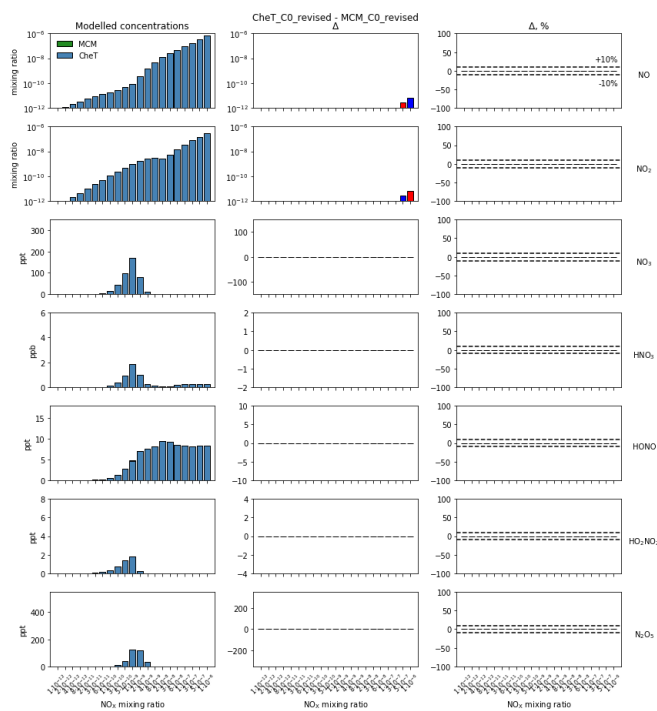


FIGURE B.2: As in Fig. B.1 but after unification.



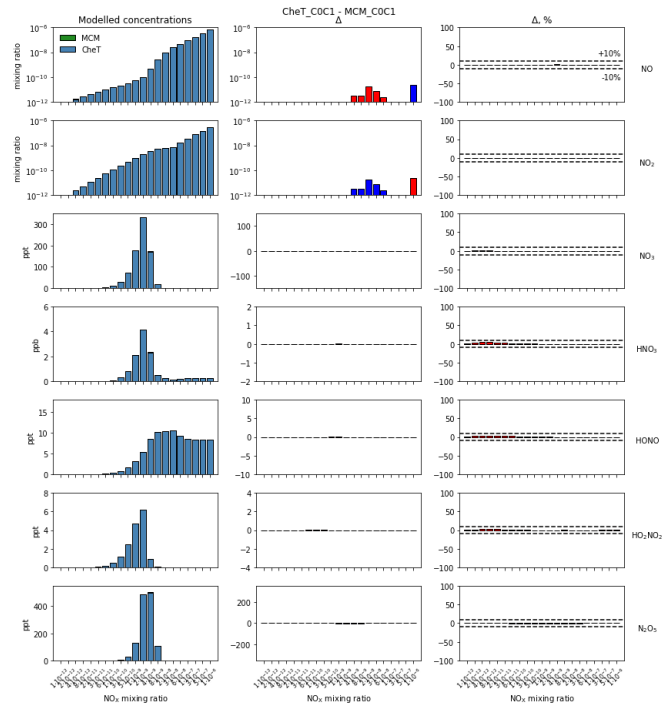


FIGURE B.3: As in Fig. B.1 but for the inorganic and  $\text{CH}_4$  chemistry before unification.

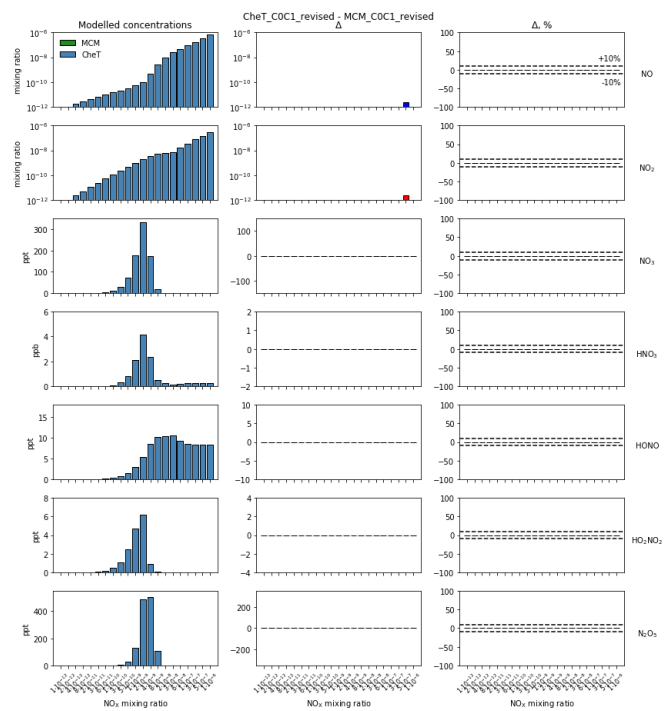


FIGURE B.4: As in Fig. B.3 but after unification.

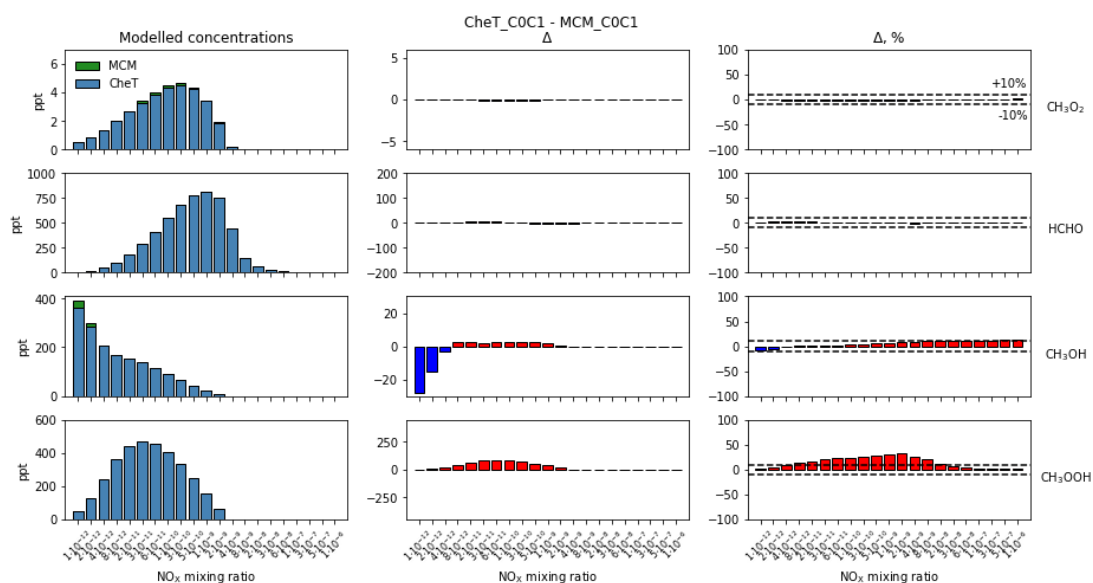


FIGURE B.5:  $\text{CH}_3\text{O}_2$ ,  $\text{HCHO}$ ,  $\text{CH}_3\text{OH}$  and  $\text{CH}_3\text{OOH}$  in steady state box model runs with the inorganic and  $\text{CH}_4$  chemistry. (Left) steady state concentrations; (middle) absolute and (right) relative differences between mechanisms (CheT minus MCM) before unification. Dashed lines mark  $\pm 10\%$  difference.

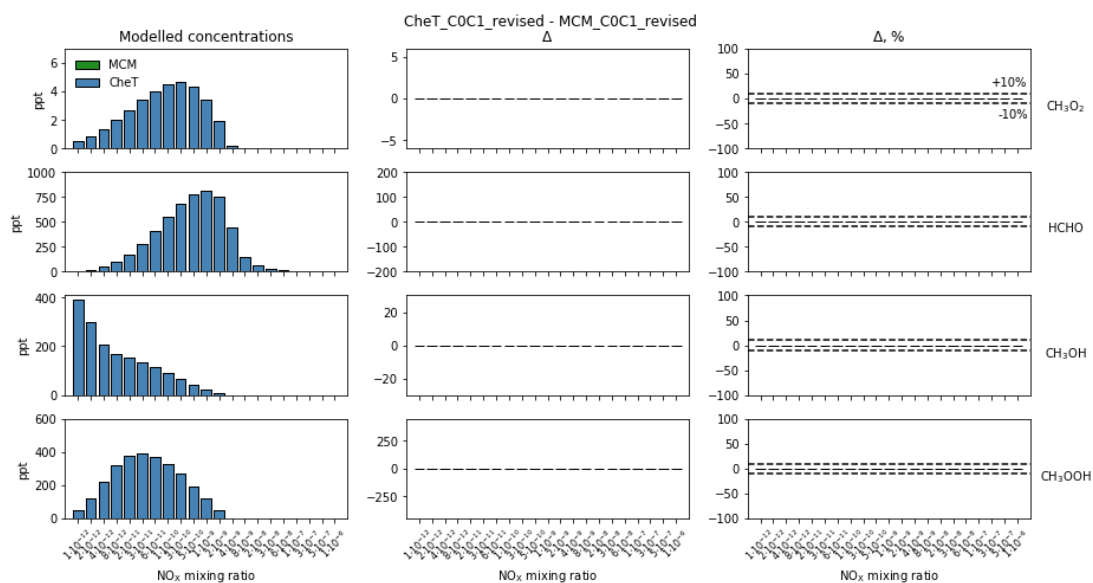


FIGURE B.6: As in Fig. B.5 but after unification.

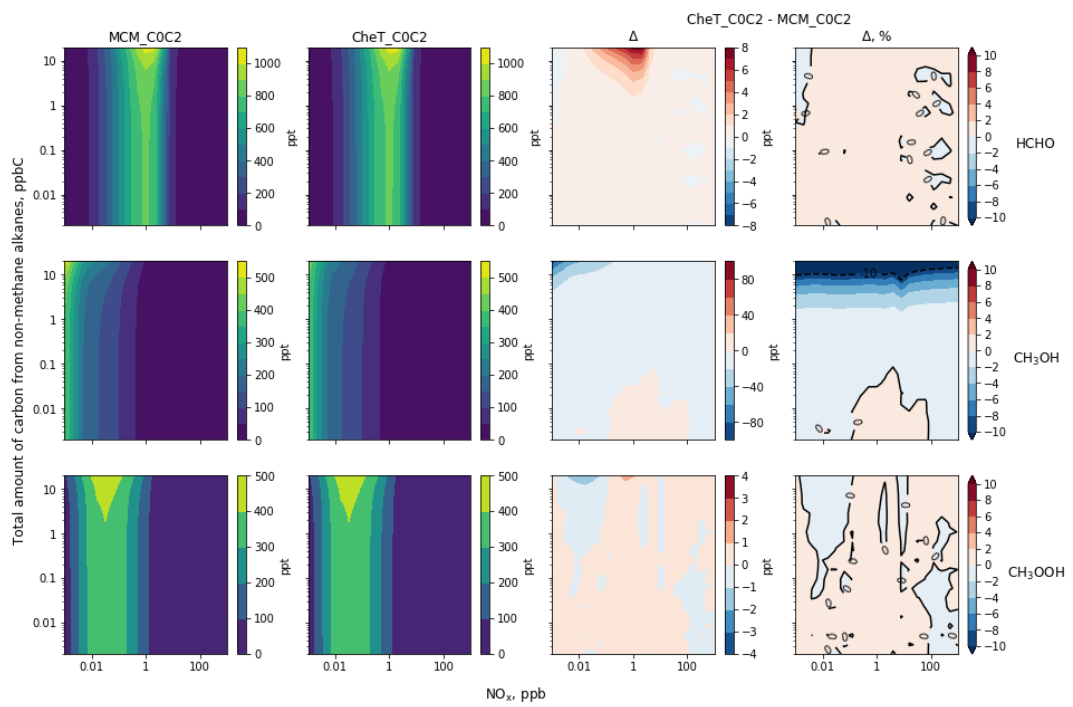


FIGURE B.7: As in Fig. 2.9 for HCHO,  $\text{CH}_3\text{OH}$  and  $\text{CH}_3\text{OOH}$  but before unification.

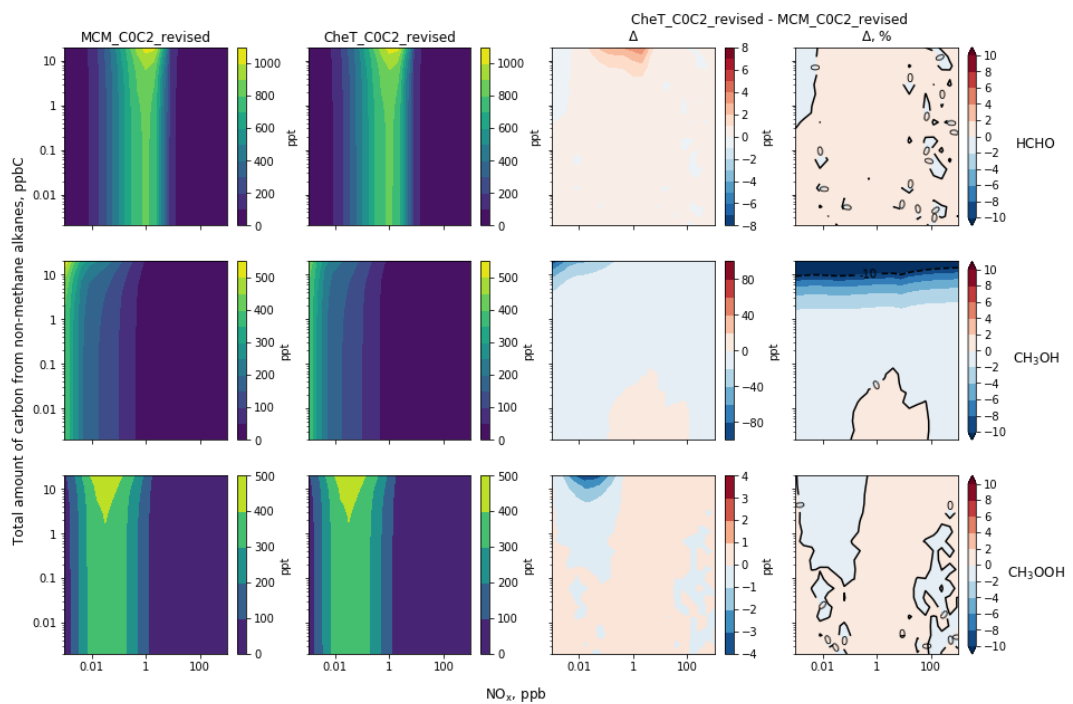


FIGURE B.8: As in Fig. B.7 but after unification.

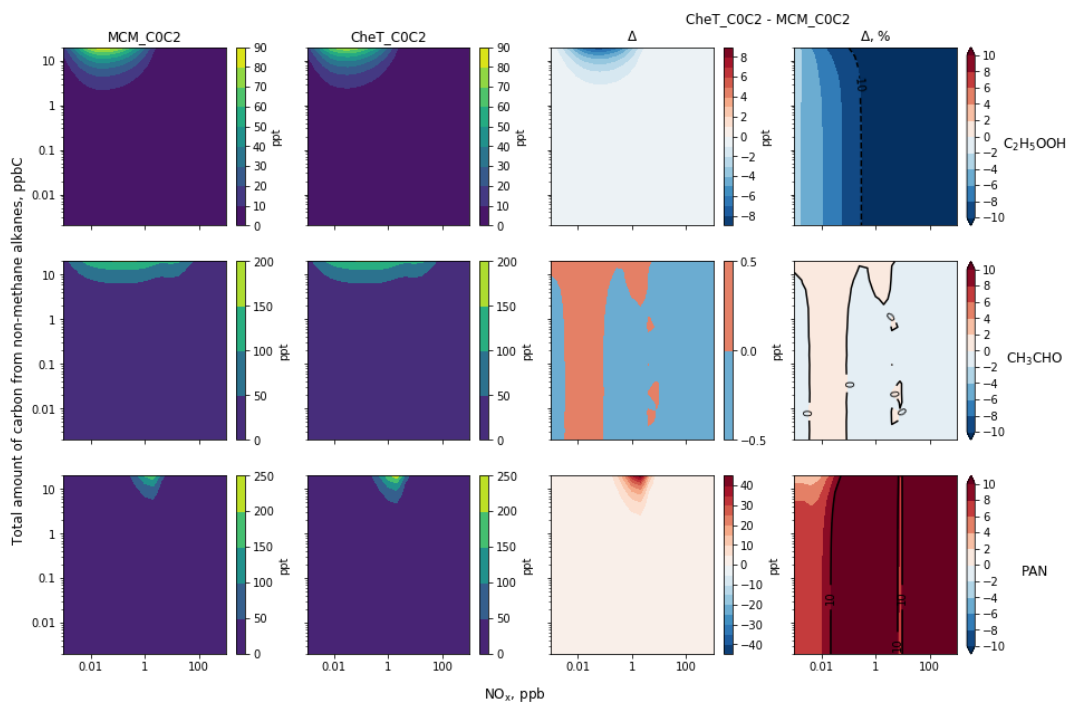


FIGURE B.9: As in Fig. 2.9 but for  $C_2H_5OOH$ ,  $CH_3CHO$  and PAN before unification.

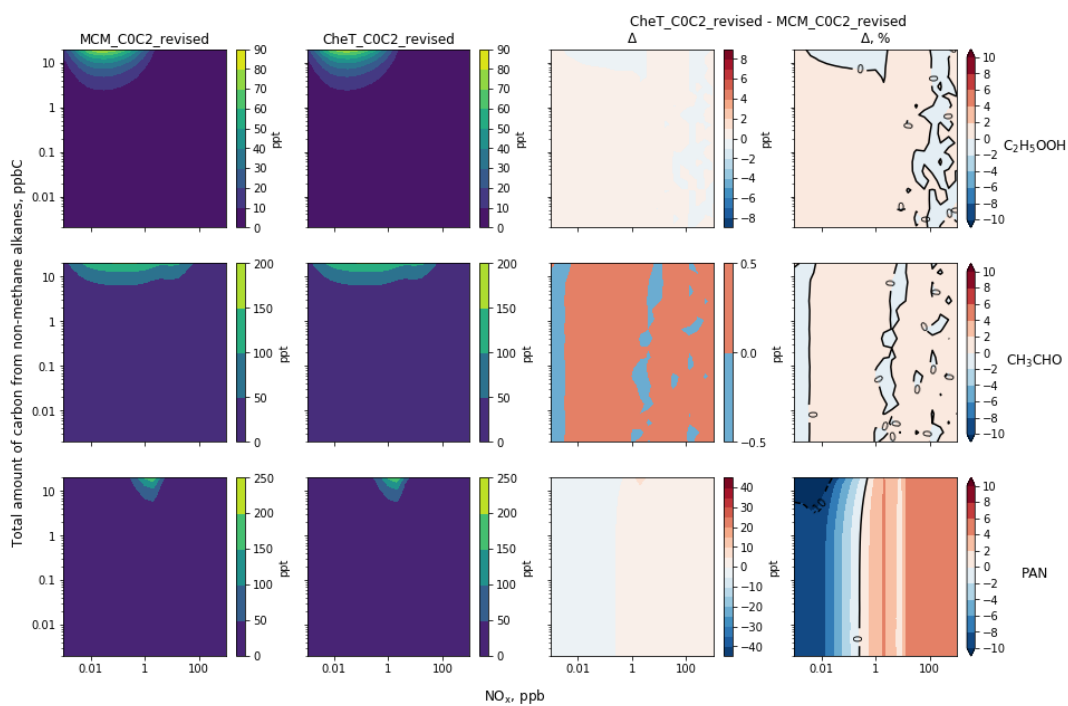


FIGURE B.10: As in Fig. B.9 but after unification.

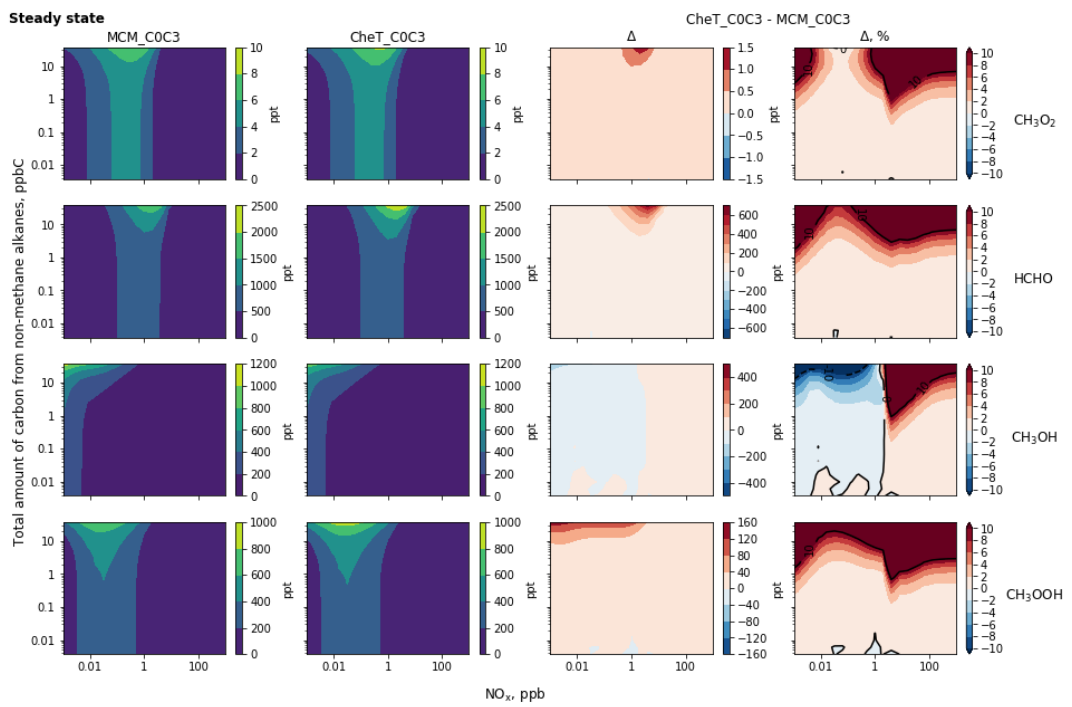


FIGURE B.11: As in Fig. 2.11 but for  $\text{CH}_2\text{O}_2$ , HCHO,  $\text{CH}_3\text{OH}$  and  $\text{CH}_3\text{OOH}$  before unification.

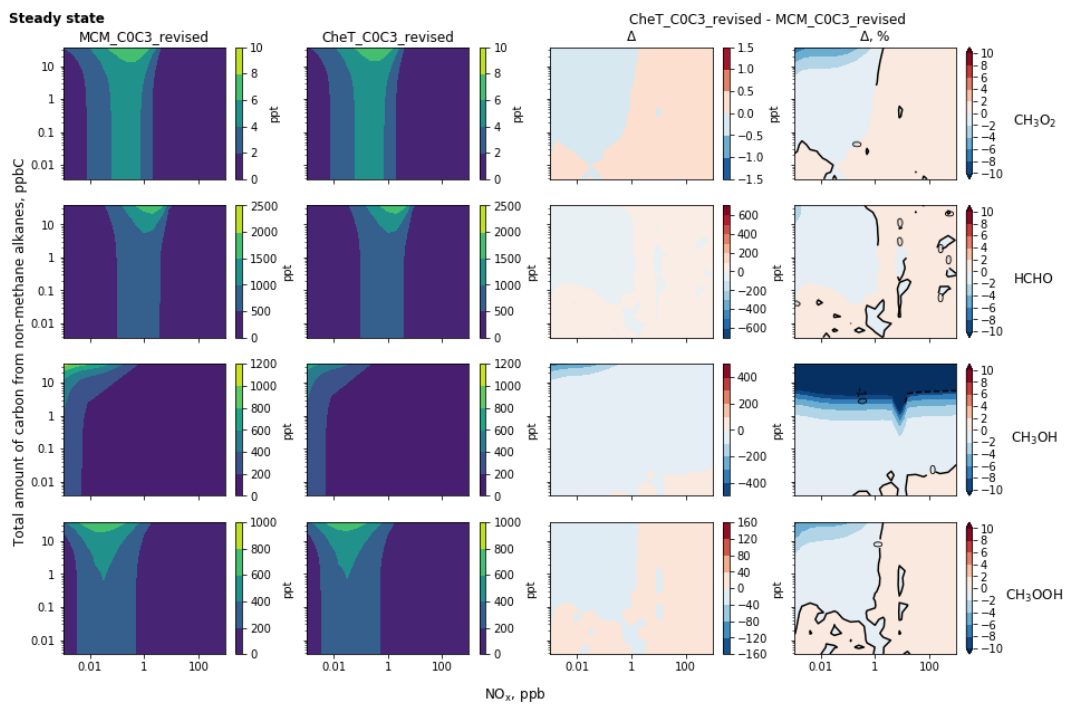


FIGURE B.12: As in Fig. B.11 but after unification.

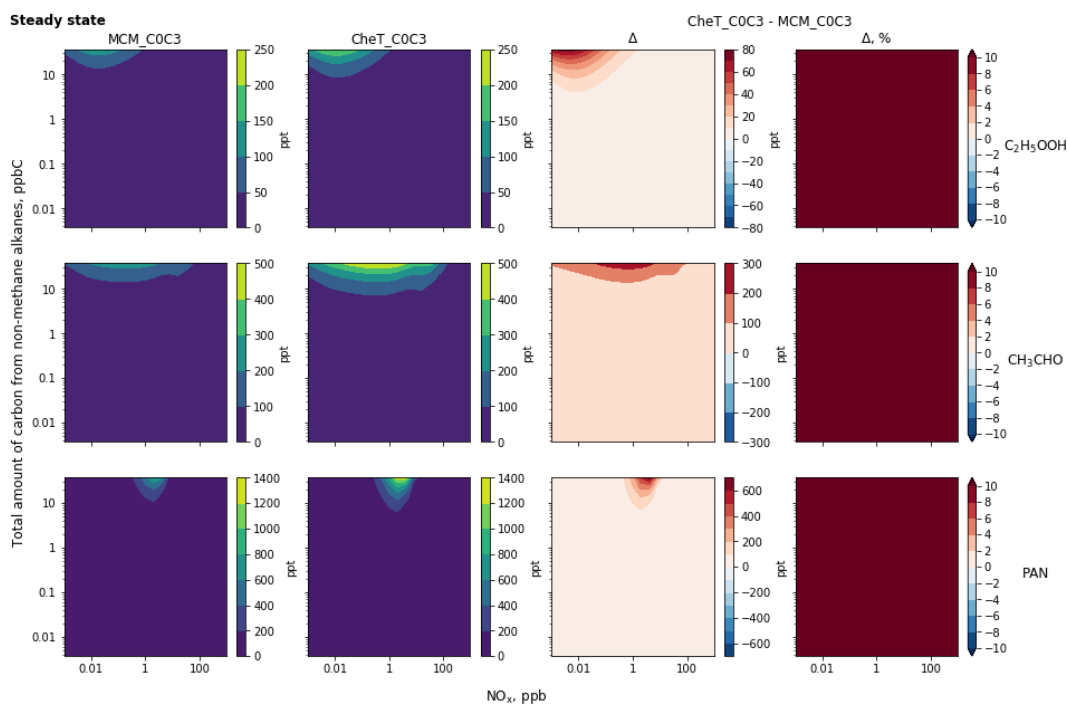


FIGURE B.13: As in Fig. 2.11 but for C<sub>2</sub>H<sub>5</sub>OOH, CH<sub>3</sub>CHO and PAN before unification.

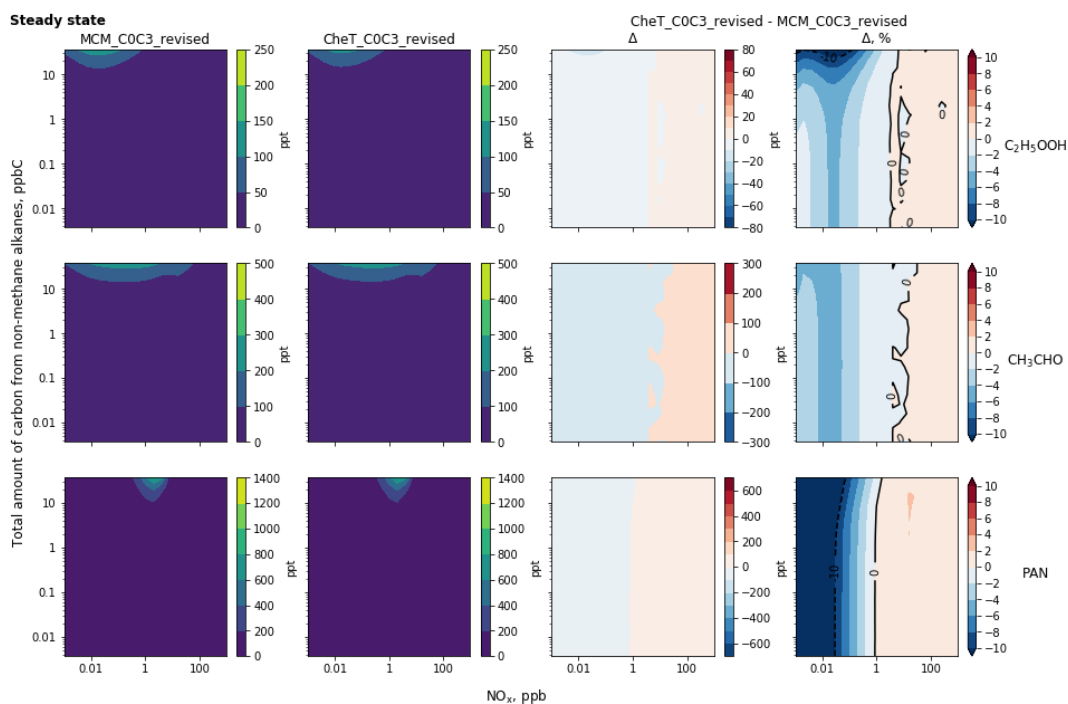


FIGURE B.14: As in Fig. B.13 but after unification.

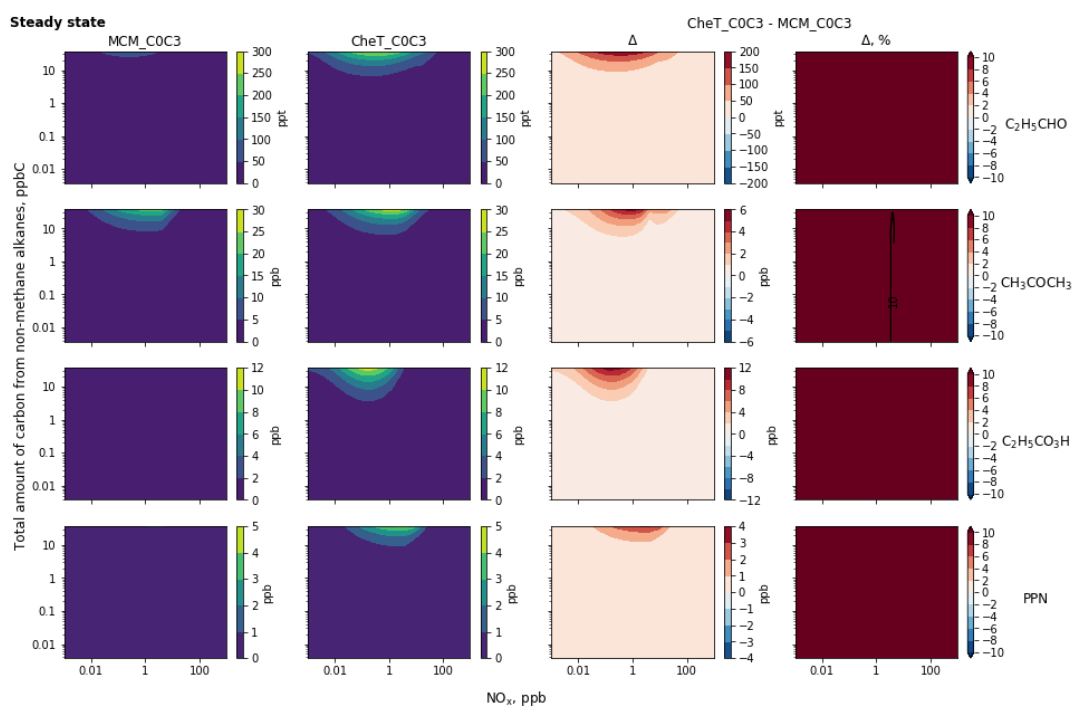


FIGURE B.15: As in Fig. 2.11 for C<sub>2</sub>H<sub>5</sub>CHO, CH<sub>3</sub>COCH<sub>3</sub>, C<sub>2</sub>H<sub>5</sub>CO<sub>3</sub>H and PPN but before unification.

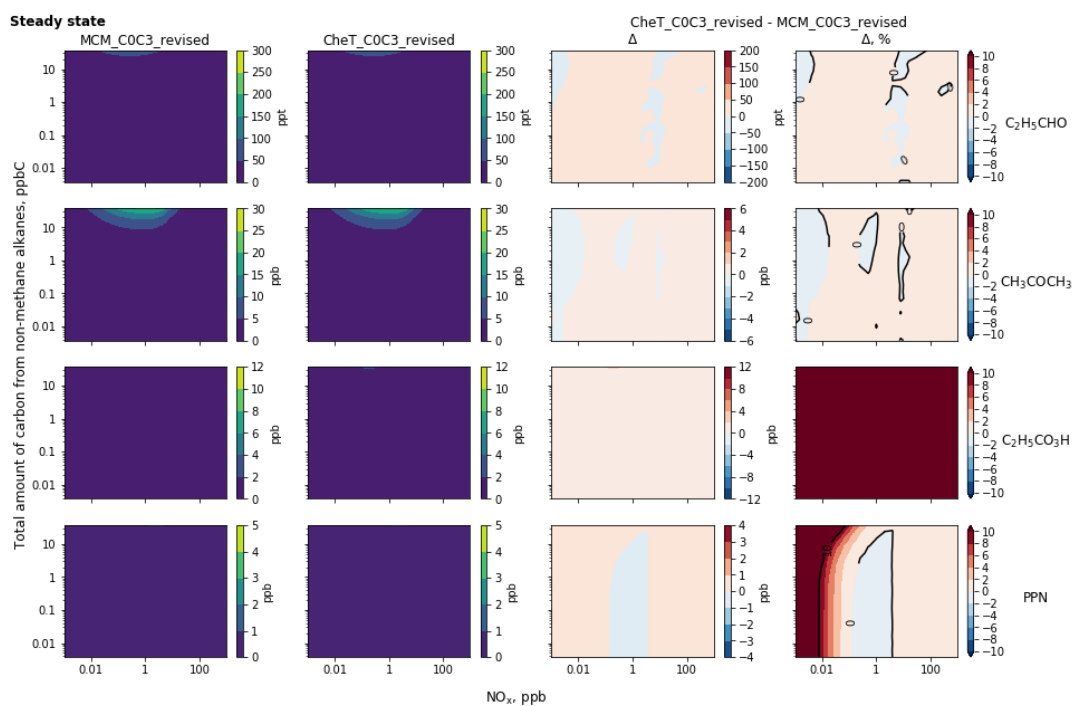


FIGURE B.16: As in Fig. B.15 but after unification.

## B.2 Code

An example of an .eqn file (in this case called stat\_emissions.eqn) that contains the equations describing an artificial NO<sub>x</sub> emission (<R1>) and the release of NO and NO<sub>2</sub> from the artificial NO<sub>x</sub> (<R2>, <R3>).

```
#EQUATIONS
<R1> EMITTER_NOX=NOX_fake:nox_tend(nox,C(ind_NO),C(ind_NO2),VAR,ind_NOX_fake);
<R2> NOX_fake = NO : no_tend(nox,C(ind_NO),C(ind_NO2));
<R3> NOX_fake = NO2 : no2_tend(nox,C(ind_NO),C(ind_NO2));
```

An example of a .def file (in this case called MCM\_COC3\_revised\_stat\_0.def) that contains information used to run a steady state box model experiment with the MCM.

```
#INCLUDE ../eqn/MCM_COC3_stat.spc
#INCLUDE ../eqn/MCM_COC3_revised.eqn
#INCLUDE ../eqn/dummy.eqn
#INCLUDE ../eqn/stat_emissions.eqn
#INCLUDE ../eqn/stat_deposition.eqn
#LOOKATALL
#INITVALUES
CFACTOR = 1.;
ALL_SPEC = 0.0;
{Variable species}
O3 = 9.73e+11;
NO = 2.43e+07;
{Fixed species}
M = 2.43e+19;
N2 = 1.90e+19;
O2 = 5.06e+18;
H2O = 2.44e+17;
EMITTER_NOX = 1.00; ! artificial emission of NOx
CO = 2.44e+12;
CH4 = 4.376e+13;
C2H6 = 2.43e+07;
C3H8 = 1.41e+07;
#INLINE F90_INIT
TSTART = 0.0D0*3600.D0
TEND = TSTART + 4320.0D0*3600.D0 ! 6 months
DT = 3600.00D0 ! 1 hour
TEMP = 298.0D0
#ENDINLINE
#INLINE F90_GLOBAL
REAL(dp) :: M, N2, O2, R02, H2O
REAL(dp) :: nox = 2.43e+07
REAL(dp) :: zmb1 = 1e5
REAL(dp) :: cair
#ENDINLINE
```



```

#INLINE F90_RCONST
  USE constants
  R02 = &
  C(ind_CH3O2) + C(ind_C2H5O2) + C(ind_IC3H7O2) + C(ind_NC3H7O2) + &
  C(ind_HOCH2CH2O2) + C(ind_CH3CO3) + C(ind_HCOCH2O2) + &
  C(ind_CH3COCH2O2) + C(ind_IPROPOL02) + C(ind_C2H5CO3) + C(ind_HO1C3O2) &
  + C(ind_HYPROP02) + C(ind_HOCH2CO3) + C(ind_CH3CHOHC03) + &
  C(ind_HOC2H4CO3) + C(ind_HCOC03)
  N2 = C(ind_N2)
  O2 = C(ind_O2)
  H2O = C(ind_H2O)
  M = N2 + O2 + H2O
  CALL mcm_constants()
#ENDINLINE
#INLINE F90_RATES
function k3rd_order (temp, cair, Fc, klow, &
                    alpha_low, beta_low, khigh, &
                    alpha_high, beta_high)
  real(8)           :: k3rd_order
  real(4), intent(in) :: Fc, klow, alpha_low, &
                    beta_low, khigh, alpha_high, beta_high
  real(8), intent(in) :: temp, cair
  real(4)           :: k_low, k_high, Ffac, Wfac, Nfac, logF, &
                    nf, zr, zo, zi, zfc
  k_low = klow *(temp/300.)**(alpha_low) *exp(-beta_low/temp)*cair
  k_high = khigh*(temp/300.)**(alpha_high)*exp(-beta_high/temp)
  if (FC<0.1 ) then
    k3rd_order = k_low
  else
    if (FC>1.0) then
      zfc = exp(-temp/FC)
      nf = 0.75 - 1.27*log10(zfc)
    else
      zfc=Fc
      nf = 0.75 - 1.27*log10(zfc)
    endif
    zo = k_low
    zi = k_high
    zr = zo / zi
    k3rd_order = (zo/(1.0_dp+zr)) *
                 zfc**(1.0_dp/(1.0_dp + (LOG10(zr))**2.))
  endif
end function k3rd_order
! Calculate the tendencies in NO, NO2 and NOx and
! the contribution of NO and NO2 into NOx
REAL FUNCTION nox_tend(nox, no, no2, VAR, ind_NOX_fake)

```

```
USE MCM_COC3_revised_stat_Parameters, ONLY: NVAR
REAL(8), INTENT(INOUT) :: VAR(NVAR)
INTEGER, INTENT(IN) :: ind_NOX_fake
REAL(dp) :: nox, no, no2
VAR(ind_NOX_fake) = nox - no - no2
END FUNCTION nox_tend
REAL FUNCTION no_tend(nox, no, no2)
REAL(dp) :: nox, no, no2
no_tend = no / (no + no2)
END FUNCTION no_tend
REAL FUNCTION no2_tend(nox, no, no2)
REAL(dp) :: nox, no, no2
no2_tend = no2 / (no + no2)
END FUNCTION no2_tend
#ENDINLINE
```

### B.3 MCM-CheT reaction comparison

TABLE B.1: Comparison of the MCM and CheT inorganic reactions and rate coefficients. If the rate coefficient depends on N<sub>2</sub>, O<sub>2</sub>, H<sub>2</sub>O or M, the number densities of these species were taken into account when the coefficient at 298 K was calculated.

#	Reaction	Rate coefficient	Value at 298K	Source	Comments	Decision
	MCM					
	HO <sub>2</sub> NO <sub>2</sub> =HO <sub>2</sub> +NO <sub>2</sub>	KMT10	0.06	IUPAC 2012		leave unchanged
	CheT					
3	HO <sub>2</sub> NO <sub>2</sub> =HO <sub>2</sub> +NO <sub>2</sub>	kloss_HO2NO2_a	Incl. SUN	IUPAC 2001		leave unchanged in UKCA, use KMT10 in box
		no data		JPL 2015		
	MCM					
	N <sub>2</sub> O <sub>5</sub> =NO <sub>2</sub> +NO <sub>3</sub>	KMT04	0.04	IUPAC 2012		leave unchanged
	CheT					
5	N <sub>2</sub> O <sub>5</sub> =NO <sub>2</sub> +NO <sub>3</sub>	kloss_N2O5	Incl. SUN	IUPAC 2002	In UKCA some code in asad_trimol.F90 looks for this reaction and modifies the rate by an extra factor	leave unchanged in UKCA, use KMT04 in box
		no data		JPL 2015		
	MCM					
	HO <sub>2</sub> +HO <sub>2</sub> =H <sub>2</sub> O <sub>2</sub>	2.20D-13*KMT06*EXP(600/TEMP)+ 1.90D-33*M*KMT06*EXP(980/TEMP)	4.47 × 10 <sup>-12</sup>	IUPAC 2001		update to JPL 2015
	CheT					
11	HO <sub>2</sub> +HO <sub>2</sub> =H <sub>2</sub> O <sub>2</sub> +O <sub>2</sub>	3.00E-13*EXP(460.0/temp)*	3.91 × 10 <sup>-12</sup>	JPL 2011		

		(1+1.4E-21*c(ind_H2O)*EXP(2200./temp))			In UKCA the rate is modified in the presence of H <sub>2</sub> O in asad_bimol.f90	leave unchanged	
34	HO2+HO2=H2O2+O2+M	k3rd_order(temp,c(ind_M), 0.,2.10E-33,0.,-920.,0.,0.,0.)* (1+1.4E-21*c(ind_H2O)*exp(2200./temp))				In UKCA the rate is modified in the presence of H <sub>2</sub> O in asad_trimol.f90	leave unchanged
		----- same as JPL 2011 -----		JPL 2015	-----		
	MCM						
	HO2+NO=OH+NO2	3.45D-12*EXP(270/TEMP)	$8.54 \times 10^{-12}$	IUPAC 2008		update to JPL 2015	
	CheT						
12	HO2+NO=OH+NO2	3.30E-12*EXP(270.0/temp)	$8.17 \times 10^{-12}$	JPL 2011		leave unchanged	
		----- same as JPL 2011 -----		JPL 2015	-----		
	MCM						
	HO2+NO3=OH+NO2	4.0D-12	$4.0 \times 10^{-12}$	IUPAC 2008		update to JPL 2015	
	CheT						
13	HO2+NO3=OH+NO2+O2	3.50E-12	$3.5 \times 10^{-12}$	JPL 2011		leave unchanged	
		----- same as JPL 2011 -----		JPL 2015	-----		
	MCM						
	HO2+O3=OH	2.03D-16*(TEMP/300)**4.57* EXP(693/TEMP)	$2.01 \times 10^{-15}$	IUPAC 2001			
	CheT						
14	HO2+O3=OH+O2+O2	2.03E-16*(temp/300.）**4.57* EXP(693.0/temp)	$2.01 \times 10^{-15}$	IUPAC 2001			
		----- 1.0e-14*exp(-490/T) -----	$1.93 \times 10^{-15}$	JPL 2015		update both to JPL 2015	
	MCM						
	NO+NO3=NO2+NO2	1.8D-11*EXP(110/TEMP)	$2.60 \times 10^{-11}$	IUPAC 2002		update to JPL 2015	

CheT					
15	NO+NO3=NO2+NO2	1.50E-11*EXP(170.0/temp)	$2.65 \times 10^{-11}$	JPL 2011	leave unchanged
		same as JPL 2011		JPL 2015	
MCM					
	NO+O3=NO2	1.4D-12*EXP(-1310/TEMP)	$1.73 \times 10^{-14}$	IUPAC 2008	update to JPL 2015
CheT					
16	NO+O3=NO2+O2	3.00E-12*EXP(-1500.0/temp)	$1.95 \times 10^{-14}$	JPL 2011	leave unchanged
		same as JPL 2011		JPL 2015	
MCM					
	NO2+O3=NO3	1.4D-13*EXP(-2470/TEMP)	$3.52 \times 10^{-17}$	IUPAC 2008	update to JPL 2015
CheT					
18	NO2+O3=NO3+O2	1.20E-13*EXP(-2450.0/temp)	$3.23 \times 10^{-17}$	JPL 2011	leave unchanged
		same as JPL 2011		JPL 2015	
MCM					
	O1D=OH+OH	2.14D-10*H2O	$5.22 \times 10^7$	IUPAC 2007	update to JPL 2015 taking H <sub>2</sub> O into account
CheT					
19	O1D+H2O=OH+OH	1.63E-10*EXP(60.0/temp)	$4.86 \times 10^7$	JPL 2011	leave unchanged
		same as JPL 2011		JPL 2015	
MCM					
	O1D=O	2.0D-11*EXP(130/TEMP)*N2+ 3.2D-11*EXP(67/TEMP)*O2	$7.91 \times 10^8$	IUPAC 2001	update to JPL 2015
CheT					
20	O1D+N2=O3P+N2	2.15E-11*EXP(110.0/temp)	$7.92 \times 10^8$	JPL 2011	leave unchanged
21	O1D+O2=O3P+O2	3.30E-11*EXP(55.0/temp)			
		same as JPL 2011		JPL 2015	
MCM					
	O+NO2=NO	5.5D-12*EXP(188/TEMP)	$1.03 \times 10^{-11}$	IUPAC 2001	update to JPL 2015
CheT					
22	O3P+NO2=NO+O2	5.10E-12*EXP(210.0/temp)	$1.03 \times 10^{-11}$	JPL 2011	leave unchanged

	same as JPL 2011		JPL 2015	
MCM				
OH+H2=HO2	7.7D-12*EXP(-2100/TEMP)	$6.70 \times 10^{-15}$	IUPAC 2001	update to JPL 2015
CheT				
25 OH+H2=HO2	2.80E-12*EXP(-1800.0/temp)	$6.67 \times 10^{-15}$	JPL 2011	leave unchanged
	same as JPL 2011		JPL 2015	
MCM				
OH+HNO3=NO3	K1 = 2.40D-14*EXP(460/TEMP) K3 = 6.50D-34*EXP(1335/TEMP) K4 = 2.70D-17*EXP(2199/TEMP) K2 = (K3*M)/(1+(K3*M/K4)) KMT11 = K1 + K2	$1.54 \times 10^{-13}$	IUPAC 2007	leave unchanged
CheT				
27 OH+HNO3=H2O+NO3	z1 = 2.4e-14*EXP(460.0/temp) z3 = (6.5e-34*EXP(1335.0/temp))* *c(ind_M) z4 = 2.7e-17*EXP(2199.0/temp) z2 = z3*c(ind_M)/(1.+z3*c(ind_M)/z4) kloss_HO_HNO3_bimol = z1 + z2	$1.56 \times 10^{-13}$	IUPAC 2004	In UKCA density dependence is calculated in asad_bimol.f90
	same as IUPAC 2007	$1.54 \times 10^{-13}$	JPL 2015	
MCM				
OH+HO2NO2=NO2	3.2D-13*EXP(690/TEMP)*1.0	$3.24 \times 10^{-12}$	IUPAC 2007	
CheT				
29 OH+HO2NO2=H2O+NO2+O2	3.20E-13*EXP(690.0/temp)	$3.24 \times 10^{-12}$	IUPAC 2007	
	1.3e-12*exp(380/T)	$4.65 \times 10^{-12}$	JPL 2015	update both to JPL 2015
MCM				
OH+HONO=NO2	2.5D-12*EXP(260/TEMP)	$5.98 \times 10^{-12}$	IUPAC 2007	
CheT				

30	OH+HONO=H2O+NO2	2.50E-12*EXP(260.0/temp) 1.8e-11*exp(-390/T)	$5.98 \times 10^{-12}$ $4.86 \times 10^{-12}$	IUPAC 2004 JPL 2015		update both to JPL 2015
	MCM					
	OH+NO3=HO2+NO2	2.0D-11	$2.00 \times 10^{-11}$	IUPAC 2008		update to JPL 2015
	CheT					
31	OH+NO3=HO2+NO2	2.20E-11 same as JPL 2011	$2.20 \times 10^{-11}$	JPL 2011 JPL 2015		leave unchanged
	MCM					
	-					add reaction to MCM using JPL 2015
	CheT					
33	OH+OH=H2O+O3P	6.31E-14*(temp/300)**2.6* EXP(945.0/temp) 1.8e-12	$1.48 \times 10^{-12}$ $1.8 \times 10^{-12}$	IUPAC 2001 JPL 2015	IUPAC 2001 expression: $6.2 \times 10^{-14}(T/298)^{2.6}e^{945/T}$ JPL gives no T dependence	update to JPL 2015
	MCM					
	HO2+NO2=HO2NO2	KMT09	$7.45 \times 10^{-13}$	IUPAC 2012		
	CheT					
35	HO2+NO2=HO2NO2+M	k3rd_order(temp,c(ind_M), 0.6,2.00E-31,-3.4,0.0,2.90E-12,0.0,0.0) #C6: (1.9) (-31) 3.4 (4.0) (-12) 0.3	$1.13 \times 10^{-12}$	JPL 2011 JPL 2015	JPL2015 parameters are closer to IUPAC2012 than JPL2011	update both to JPL 2015
	MCM					
	NO+NO=NO2+NO2	3.3D-39*EXP(530/TEMP)*O2	$9.89 \times 10^{-20}$	IUPAC 2001		leave unchanged
	CheT					
36	-				Present in CheST	add NO+NO=NO2+NO2 to CheT using IUPAC 2001
		no data	-	JPL 2015		

MCM					
NO <sub>2</sub> +NO <sub>3</sub> =N <sub>2</sub> O <sub>5</sub>	KMT03		$1.24 \times 10^{-12}$	IUPAC 2012	
CheT					
37 NO <sub>2</sub> +NO <sub>3</sub> =N <sub>2</sub> O <sub>5</sub> +M	k3rd_order(temp,c(ind_M), 0.35,3.6E-30,-4.1,0.0,1.90E-12,0.2,0.0)		$1.41 \times 10^{-12}$	IUPAC 2002	All parameters except Fc are the same as in JPL2015
		#C7: (2.4) (-30) 3.0 (1.6) (-12) -0.1		JPL 2015	update both to JPL 2015
MCM					
O+NO=NO <sub>2</sub>	KMT01		$2.23 \times 10^{-12}$	IUPAC 2012	update to JPL 2015
CheT					
38 -					Present in CheST add O <sub>3</sub> P+NO=NO <sub>2</sub> +M to CheT using JPL 2015
		#C1: (9.0) (-32) 1.5 (3.0) (-11) 0.0		JPL 2015	
MCM					
O+NO <sub>2</sub> =NO <sub>3</sub>	KMT02		$2.07 \times 10^{-12}$	IUPAC 2005	update to JPL 2015
CheT					
39 -					Present in CheST add O <sub>3</sub> P+NO <sub>2</sub> =NO <sub>3</sub> +M to CheT using JPL 2015
		#C2: (2.5) (-31) 1.8 (2.2) (-11) 0.7		JPL 2015	
MCM					
OH+NO=HONO	KMT07		$9.70 \times 10^{-12}$	IUPAC 2012	update to JPL 2015
CheT					
41 OH+NO=HONO+M	k3rd_order(temp, c(ind_M), 0.6,7.0E-31,-2.6,0.0,3.60E-11,-0.1,0.0)		$7.35 \times 10^{-12}$	JPL 2011	leave unchanged
		#C3: (7.0) (-31) 2.6 (3.6) (-11) 0.1		JPL 2015	
MCM					
OH+NO <sub>2</sub> =HNO <sub>3</sub>	KMT08		$9.83 \times 10^{-12}$	IUPAC 2012	update to JPL 2015
CheT					
42 OH+NO <sub>2</sub> =HNO <sub>3</sub> +M	k3rd_order(temp,c(ind_M),		$1.05 \times 10^{-11}$	JPL 2011	leave unchanged



	0.6,1.8E-30,-3.0,0.0,2.80E-11,0.0,0.0)				
	#C4: (1.8) (-30) 3.0 (2.8) (-11) 0		JPL 2015		
MCM					
-					add OH+OH=H2O2 to MCM using JPL 2015
CheT					
43 OH+OH=H2O2+M	k3rd_order(temp, c(ind_M), 0.6,6.90E-31,-1.0,0.0,2.60E-11,0.0,0.0)	$6.25 \times 10^{-12}$	JPL 2011	Absent from CRI, present in MOZART	leave unchanged
	#B2: (6.9) (-31) 1.0 (2.6) (-11) 0		JPL 2015		
	9.0e-31*(T/300)[N2] over 200-700 K	$1.70 \times 10^{-11}$	IUPAC 2012		

TABLE B.2: As in Table B.1 but for methane chemistry.

#	Reaction	Rate coefficient	Value at 298K	Source	Comments	Decision
	MCM					
	CH3O2=CH3O	2*KCH3O2*RO2* 7.18*EXP(-885/TEMP)	$2.58 \times 10^{-13}$	MCM 3.3.1		leave unchanged
	CheT					
	MeOO+MeOO=HO2+HO2+HCHO+HCHO	k_MeOO_MeOO_b	$1.18 \times 10^{-12}$	IUPAC 2002	Adjust reactants and products for a new reaction rate	
49	MeOO=HO2+HCHO	2*KCH3O2*C(ind_MeOO)* 7.18*EXP(-885/TEMP)	$2.58 \times 10^{-13}$	MCM 3.3.1		update to MCM 3.3.1
	MCM					
	CH3O2=CH3OH	2*KCH3O2*RO2* 0.5*(1-7.18*EXP(-885/TEMP))	$2.21 \times 10^{-13}$	MCM 3.3.1		leave unchanged
	CH3O2=HCHO	2*KCH3O2*RO2* 0.5*(1-7.18*EXP(-885/TEMP))	$2.21 \times 10^{-13}$	MCM 3.3.1		leave unchanged
	CheT					
	MeOO+MeOO=MeOH+HCHO+O2	k_MeOO_MeOO_a	$-8.33 \times 10^{-13}$	IUPAC 2002	Split into 2 reactions	
50	MeOO=MeOH	2*KCH3O2*C(ind_MeOO)* 0.5*(1-7.18*EXP(-885/TEMP))	$2.21 \times 10^{-13}$	MCM 3.3.1		update to MCM 3.3.1
51	MeOO=HCHO	2*KCH3O2*C(ind_MeOO)* 0.5*(1-7.18*EXP(-885/TEMP))	$2.21 \times 10^{-13}$	MCM 3.3.1		update to MCM 3.3.1
	MCM					
	CH3O2+NO=CH3O+NO2	2.3D-12*EXP(360/TEMP)	$7.70 \times 10^{-12}$	MCM v3.3.1	Multiply the rate by 0.001 when CH3NO3 is present in a subset	leave unchanged
	CheT					
52	MeOO+NO=HO2+HCHO+NO2	2.30E-12*EXP(360.0/temp)	$7.70 \times 10^{-12}$	IUPAC 2005	Multiply the rate by 0.001 when CH3NO3 is present in a subset	leave unchanged

MCM					
NO <sub>3</sub> +HCHO=HNO <sub>3</sub> +CO+HO <sub>2</sub>	5.5D-16	$5.50 \times 10^{-16}$	IUPAC 2007		leave unchanged
CheT					
54 NO <sub>3</sub> +HCHO=HNO <sub>3</sub> +HO <sub>2</sub> +CO	2.00E-12*EXP(-2440.0/temp)	$5.56 \times 10^{-16}$	IUPAC 2007	No direct measurements of T dependence. Infer from T dependence of MeCHO+NO <sub>3</sub>	update to MCM 3.3.1
MCM					add O1D+CH <sub>4</sub> =HCHO+H <sub>2</sub> using JPL 2011
-					
55 O1D+CH <sub>4</sub> =HCHO+H <sub>2</sub>	9.00E-12	$9.00 \times 10^{-12}$	JPL 2011		leave unchanged
MCM					add O1D+CH <sub>4</sub> = HCHO+HO <sub>2</sub> +HO <sub>2</sub> using JPL 2011
-					
56 O1D+CH <sub>4</sub> =HCHO+HO <sub>2</sub> +HO <sub>2</sub>	3.45E-11	$3.45 \times 10^{-11}$	JPL 2011		leave unchanged
MCM					add O1D+CH <sub>4</sub> =OH+CH <sub>3</sub> O <sub>2</sub> using JPL 2015
-					
57 O1D+CH <sub>4</sub> =OH+MeOO	1.31E-10	$1.31 \times 10^{-10}$	JPL 2011		leave unchanged
MCM					
OH+CH <sub>4</sub> =CH <sub>3</sub> O <sub>2</sub>	1.85D-12*EXP(-1690/TEMP)	$6.37 \times 10^{-15}$	IUPAC 2007		leave unchanged
CheT					
58 OH+CH <sub>4</sub> =H <sub>2</sub> O+MeOO	2.45E-12*EXP(-1775.0/temp)	$6.34 \times 10^{-15}$	JPL 2001		update to IUPAC 2007
MCM					
OH+CH <sub>3</sub> OOH=CH <sub>3</sub> O <sub>2</sub>	5.3D-12*EXP(190/TEMP)*0.6	$6.02 \times 10^{-12}$	MCM 3.3.1		leave unchanged
CheT					

62	OH+MeOOH=H2O+MeOO	$1.89\text{E-}12*\text{EXP}(190.0/\text{temp})$	$3.58 \times 10^{-12}$	IUPAC 2007	$5.3\text{e-}12*0.6=3.18\text{e-}12$ , mistake in UKCA code	update to MCM v3.3.1
MCM	CH3O2+NO2=CH3O2NO2	KMT13	$5.85 \times 10^{-12}$	IUPAC 2003		remove reaction
-						
MCM	CH3O2NO2=CH3O2+NO2	KMT14	1.49	IUPAC 2003		remove reaction
-						

TABLE B.3: As in Table B.1 but for ethane chemistry.

#	Reaction	Rate coefficient	Value at 298K	Source	Comments	Decision
	MCM					
	CH3CHO+hv=CH3O2+HO2+CO	J(13)		MCM v3.3.1		add CH3CHO=CH4+CO using CheT J value
	CheT					
64	MeCHO+hv=CH4+CO	J(13)*4.4e-04		CheT		leave unchanged
65	MeCHO+hv=MeOO+HO2+CO	J(13)		CheT		leave unchanged
	MCM					
	PAN=CH3CO3+NO2	KBPAN	$4.30 \times 10^{-4}$	IUPAC 2014		leave unchanged
	CheT					
67	PAN=MeCO3+NO2	kloss_PAN	Incl. SUN	MCM v3.2		leave unchanged in UKCA, use KBPAN in box
	MCM					
	C2H5O2+HO2=C2H5OOH	4.3D-13*EXP(870/TEMP)	$7.97 \times 10^{-12}$	IUPAC 2006		update to IUPAC 2011
	CheT					
71	HO2+EtOO=EtOOH+O2	6.40E-13*EXP(710.0/temp)	$6.93 \times 10^{-12}$	IUPAC 2011		leave unchanged
	MCM					
	PAN+OH=HCHO+CO+NO2	3D-14	$3.00 \times 10^{-14}$	IUPAC 2007		leave unchanged
	CheT					
86	OH+PAN=HCHO+NO2+H2O	3.00E-14	$3.00 \times 10^{-14}$	MCM v3.2	CO is missing	add CO to products
	MCM					
	CH3CO3+NO2=PAN	KFPAN	$8.94 \times 10^{-12}$	IUPAC 2014		leave unchanged
	CheT					
87	MeCO3+NO2=PAN+M	k3rd_order(temp,c(ind_M), 0.3,2.70E-28,-7.1,0.0,1.20E-11,- 0.9,0.0)	$1.05 \times 10^{-11}$	MCM v3.2		update to IUPAC 2014

TABLE B.4: As in Table B.1 but for propane chemistry.

#	Reaction	Rate coefficient	Value at 298K	Source	Comments	Decision
	MCM					
	C2H5CO3+HO2=C2H5O2+OH	5.2D-13*EXP(980/TEMP)*0.44	$6.13 \times 10^{-12}$	IUPAC 2017	In MCM there are 3 C2H5CO3+HO2 channels	leave unchanged
96	-					add HO2+EtCO3=EtOO+OH+CO2 to CheT using IU- PAC 2017 (2.29E- 13*EXP(980.0/temp))
	MCM					
	C2H5CO3+HO2=PERPROACID	5.2D-13*EXP(980/TEMP)*0.41	$5.71 \times 10^{-12}$	IUPAC 2017	In MCM there are 3 C2H5CO3+HO2 channels	leave unchanged
97	CheT HO2+EtCO3=O2+EtCO3H	4.40E-13*EXP(980.0/temp)	$1.18 \times 10^{-11}$	MCM v3.2	CheT rate is a combined rate for 2 channels that give EtOO+OH and EtCO3H products	update to IU- PAC 2017 (2.13E- 13*EXP(980.0/temp))
	MCM					
	CH3COCH2O2+HO2=HYPERACET	1.36D-13*EXP(1250/TEMP)*0.85	$7.67 \times 10^{-12}$	MCM v3.3.1		update to IUPAC 2009
	CheT					

100	HO <sub>2</sub> +MeCOCH <sub>2</sub> OO=MeCOCH <sub>2</sub> OOH	9.00E-12		$9.00 \times 10^{-12}$	IUPAC 2009	Use measured value rather than the expression from the MCM (which does include T dependence)	leave unchanged
<hr/>							
	MCM IC <sub>3</sub> H <sub>7</sub> O <sub>2</sub> +NO <sub>3</sub> =IC <sub>3</sub> H <sub>7</sub> O+NO <sub>2</sub>	2.3D-12		$2.30 \times 10^{-12}$	MCM v3.3.1		leave unchanged
	CheT						
103	iPrOO+NO <sub>3</sub> =Me <sub>2</sub> CO+HO <sub>2</sub> +NO <sub>2</sub>	2.70E-12*EXP(360.0/temp)		$9.04 \times 10^{-12}$	MCM v3.2	CheT uses the same rate as for iPrOO+NO	update to MCM v3.3.1
<hr/>							
	MCM C <sub>2</sub> H <sub>5</sub> CHO+NO <sub>3</sub> =C <sub>2</sub> H <sub>5</sub> CO <sub>3</sub> +HNO <sub>3</sub>	3.24D-12*EXP(-1860/TEMP)		$6.31 \times 10^{-15}$	MCM v3.3.1		update to IUPAC 2007
	CheT						
106	NO <sub>3</sub> +EtCHO=HNO <sub>3</sub> +EtCO <sub>3</sub>	6.30E-15		$6.30 \times 10^{-15}$	IUPAC 2007		leave unchanged
<hr/>							
	MCM -						add reaction using IUPAC 2007
	CheT						
107	NO <sub>3</sub> +Me <sub>2</sub> CO=HNO <sub>3</sub> +MeCOCH <sub>2</sub> OO	3.00E-17		$3.00 \times 10^{-17}$	IUPAC 2007		leave unchanged
<hr/>							
	MCM NC <sub>3</sub> H <sub>7</sub> O <sub>2</sub> +NO <sub>3</sub> =NC <sub>3</sub> H <sub>7</sub> O+NO <sub>2</sub>	2.3D-12		$2.30 \times 10^{-12}$	MCM v3.3.1		leave unchanged
	CheT						
110	nPrOO+NO <sub>3</sub> =EtCHO+HO <sub>2</sub> +NO <sub>2</sub>	2.70E-12*EXP(360.0/temp)		$9.04 \times 10^{-12}$	MCM v3.2	CheT uses the same rate as for nPrOO+NO	update to MCM v3.3.1
<hr/>							
	MCM OH+C <sub>3</sub> H <sub>8</sub> =IC <sub>3</sub> H <sub>7</sub> O <sub>2</sub>	7.6D-12*EXP(-585/TEMP)*0.736		$7.85 \times 10^{-13}$	IUPAC 2007		leave unchanged
	CheT						

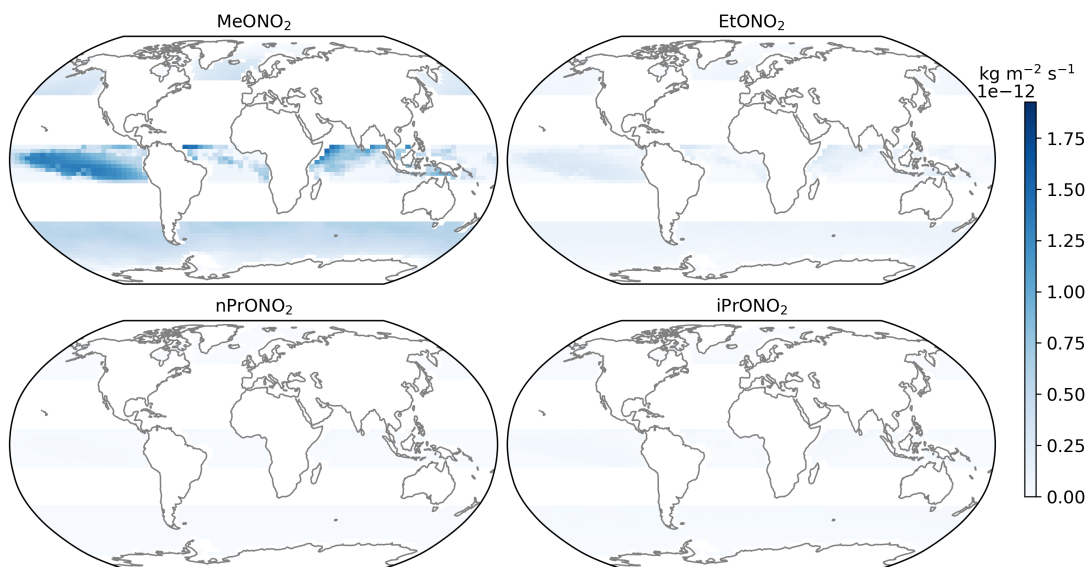
111	OH+C3H8=iPrOO+H2O	7.60E-12*EXP(-585.0/temp)	$1.07 \times 10^{-12}$	IUPAC 2007	In asad_bimol.f90 is used for splitting the channels, didn't understand if they use the right yields	UKCA update in the box model: include branching ratio
	MCM OH+C3H8=NC3H7O2 CheT	7.6D-12*EXP(-585/TEMP)*0.264	$2.82 \times 10^{-13}$	IUPAC 2007		leave unchanged
112	OH+C3H8=nPrOO+H2O	7.60E-12*EXP(-585.0/temp)	$1.07 \times 10^{-12}$	IUPAC 2007	In asad_bimol.f90 is used for splitting the channels, didn't understand if they use the right yields	UKCA update in the box model: include branching ratio
	MCM OH+MGLYOX=CH3CO3+CO CheT	1.9D-12*EXP(575/TEMP)	$1.31 \times 10^{-11}$	IUPAC 2008		leave unchanged
120	OH+MGLY=MeCO3+CO+H2O	1.90E-11*EXP(575.0/temp)	$1.31 \times 10^{-10}$	IUPAC 2008		update, correct power
	MCM PPN+OH=CH3CHO+CO+NO2 CheT	1.27D-12	$1.27 \times 10^{-12}$	MCM v3.3.1		leave unchanged
123	OH+PPAN=MeCHO+NO2+H2O	1.27E-12	$1.27 \times 10^{-12}$	MCM v3.2	CO is missing from products	add CO to products
	MCM C2H5CO3+NO2=PPN CheT	KFPAN	???	IUPAC 2014		leave unchanged
125	EtCO3+NO2=PPAN+M	k3rd_order(temp, c(ind_M), 0.3,2.70E-28,-7.1,0.0,1.20E-11,-0.9,0.0)	???	MCM v3.2		update to IUPAC 2014



# C

## Appendix to Chapter 3

## Oceanic emissions: DJF



## Oceanic emissions: MAM

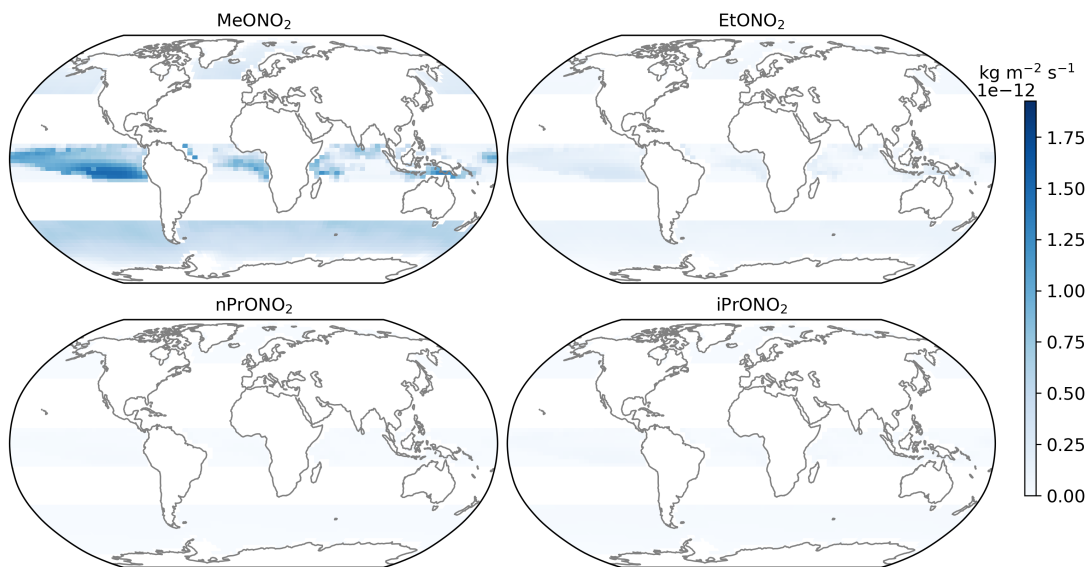


FIGURE C.1: Total  $\text{C}_1\text{-C}_3$   $\text{RONO}_2$  oceanic emissions per season derived from GEOS-Chem and re-gridded onto UM-UKCA grid.

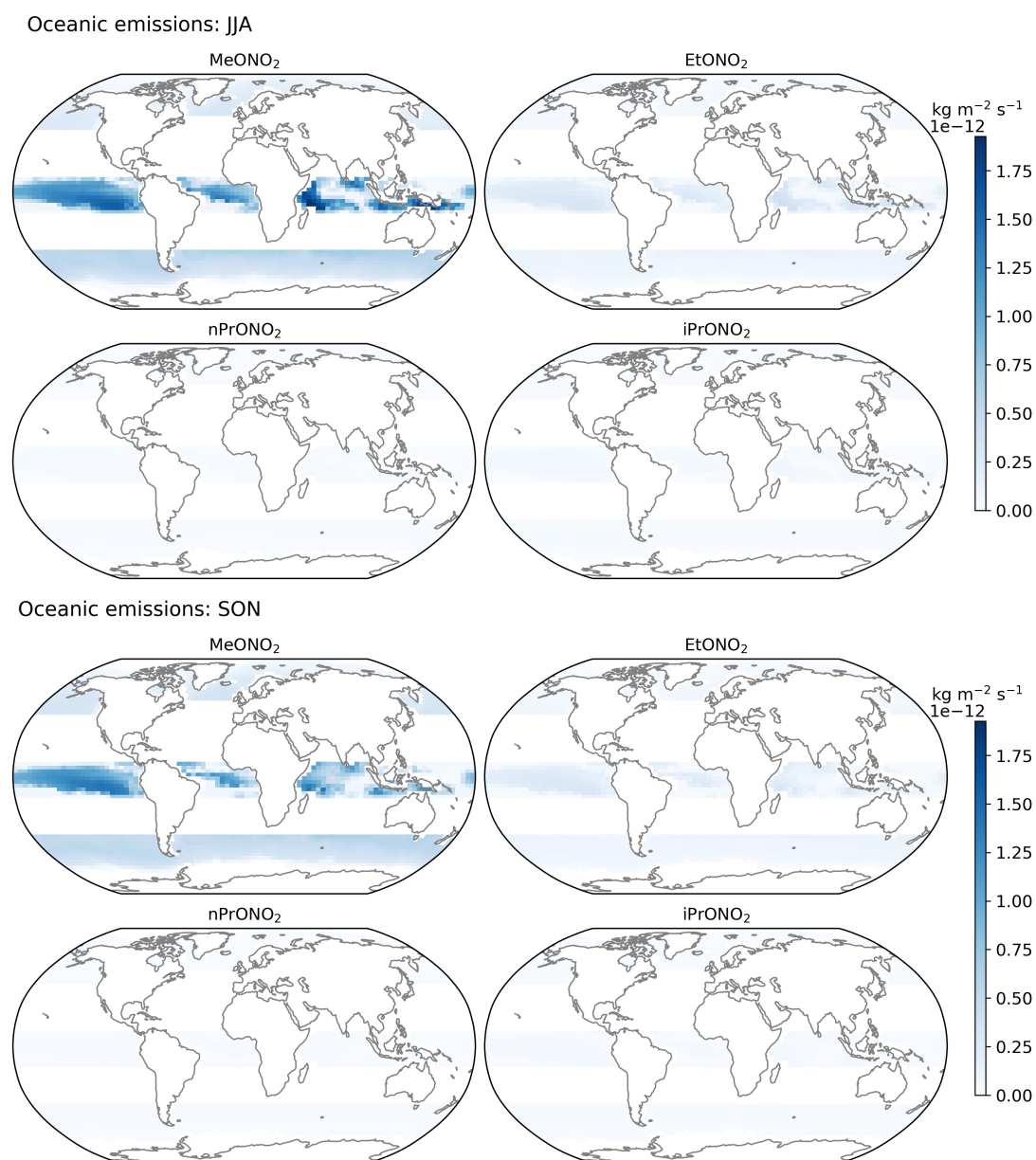
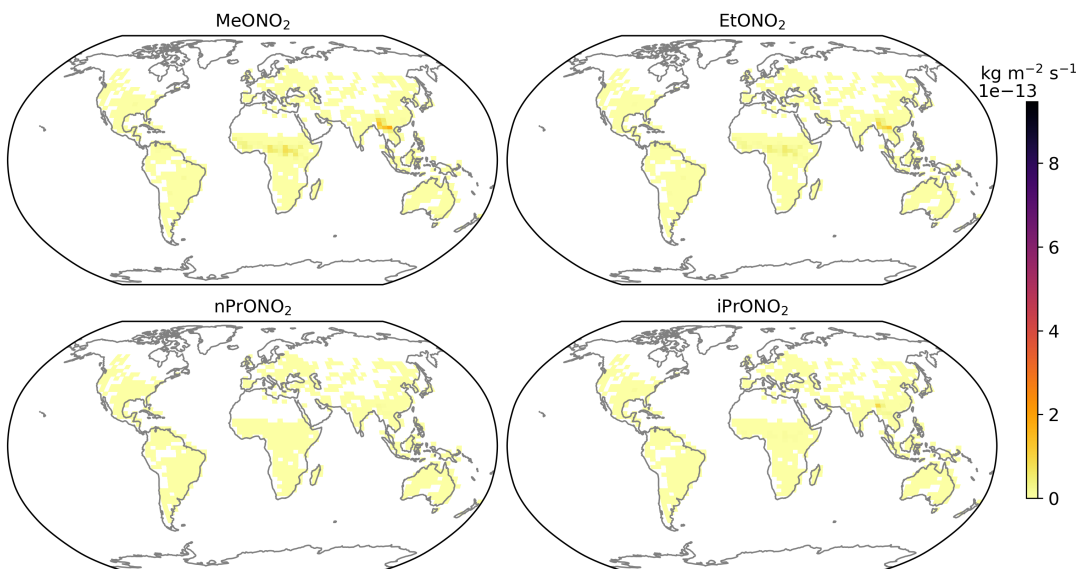


FIGURE C.2: Figure C.1 continued.

## Biomass burning emissions: DJF



## Biomass burning emissions: MAM

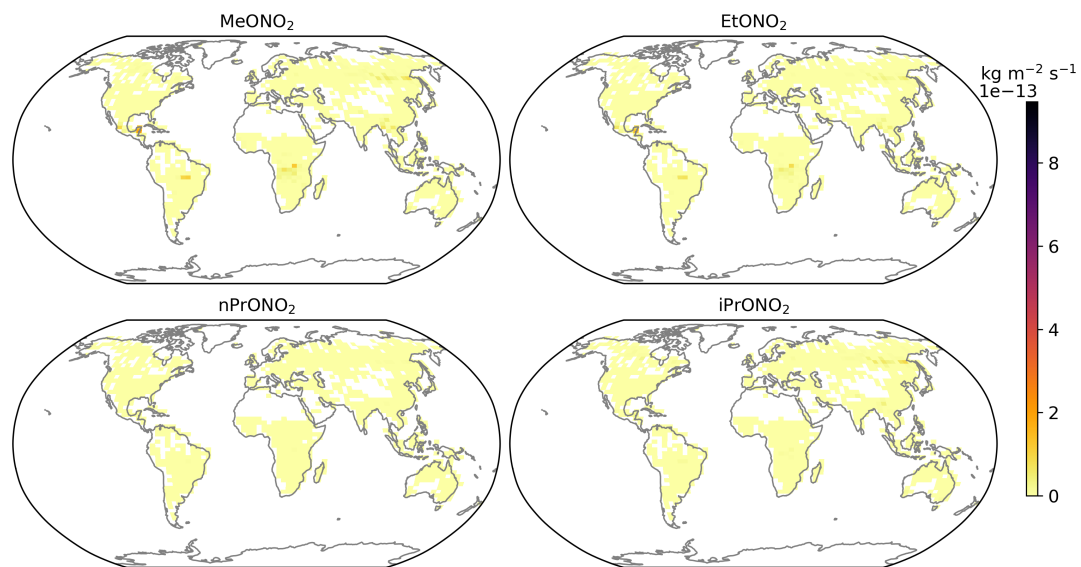


FIGURE C.3: Total C<sub>1</sub>-C<sub>3</sub> RONO<sub>2</sub> biomass burning emissions per season derived from GFEDs and re-gridded onto UM-UKCA grid.

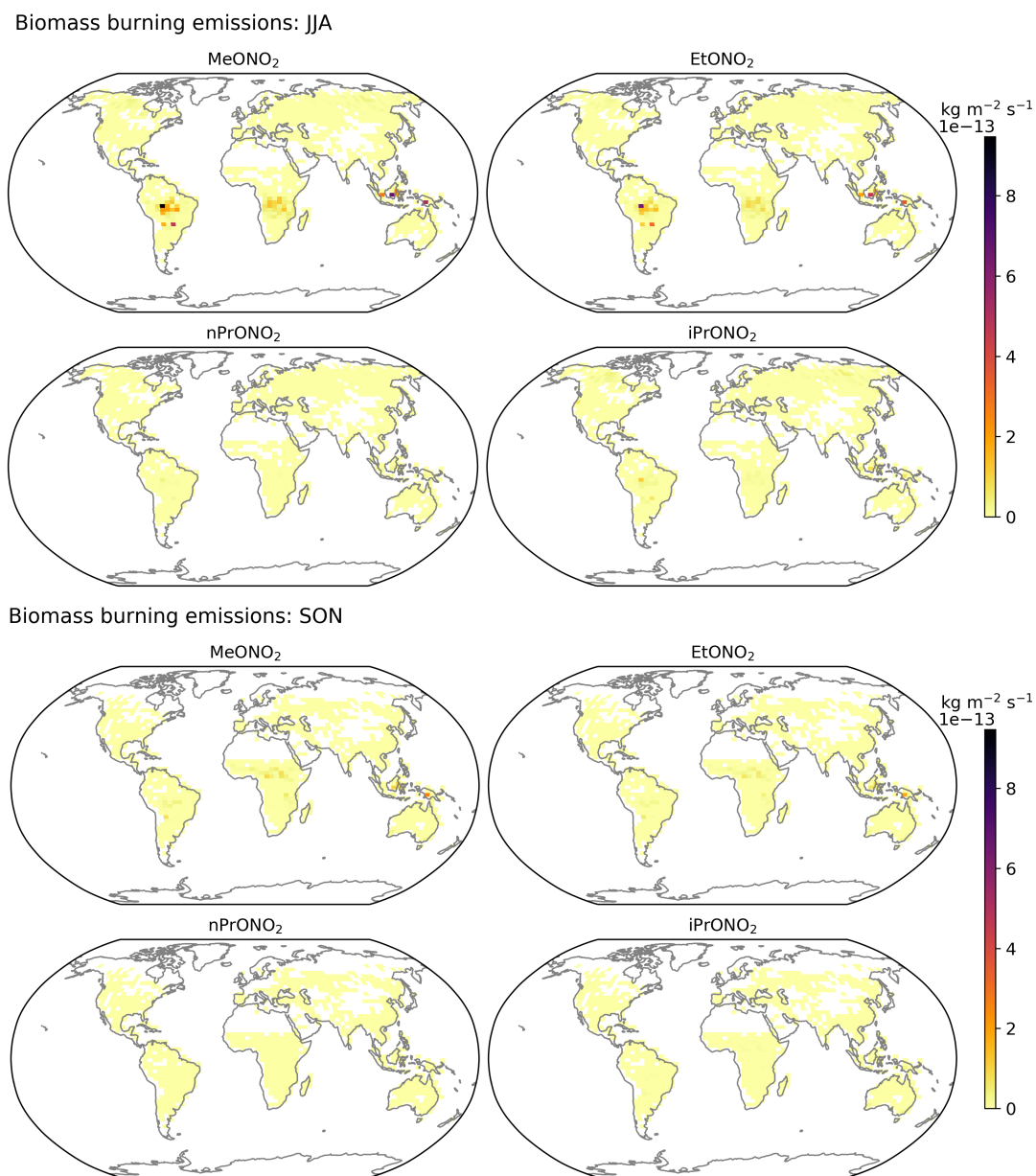
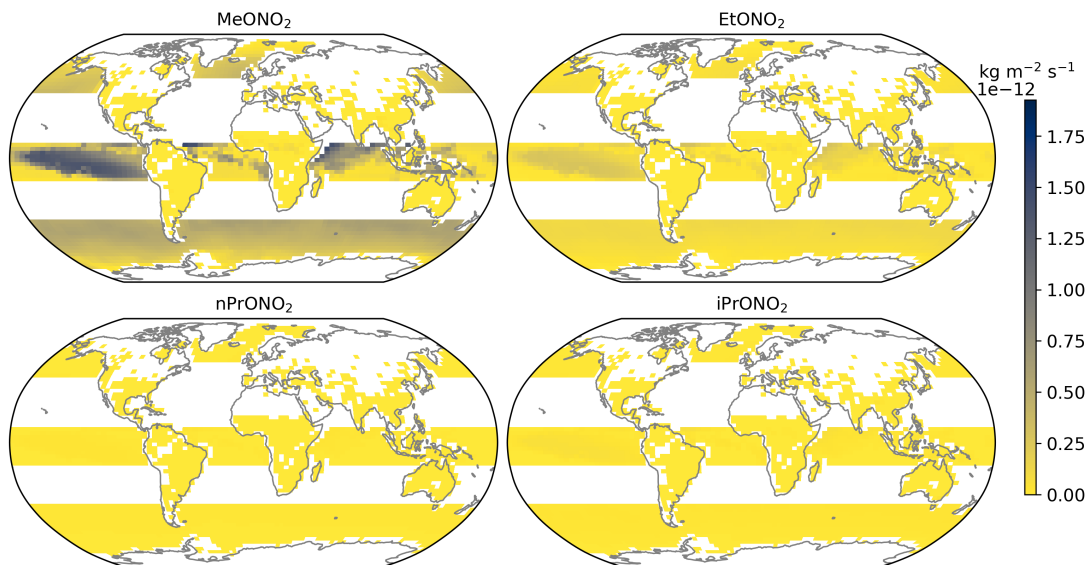


FIGURE C.4: Figure C.3 continued.

Oceanic and biomass burning emissions: DJF



Oceanic and biomass burning emissions: MAM

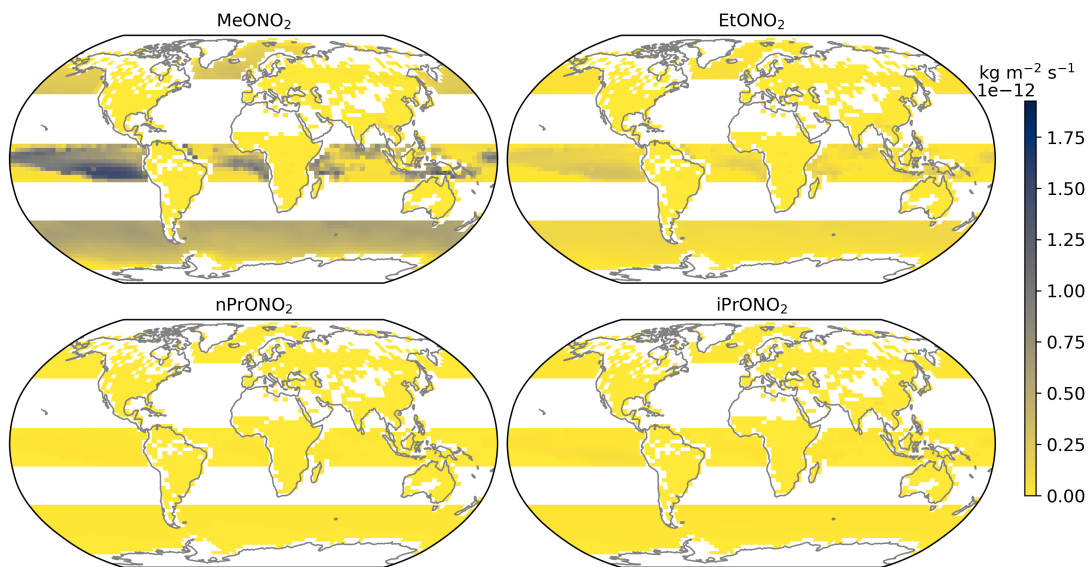


FIGURE C.5: Total C<sub>1</sub>-C<sub>3</sub> RONO<sub>2</sub> oceanic and biomass burning emissions per season.

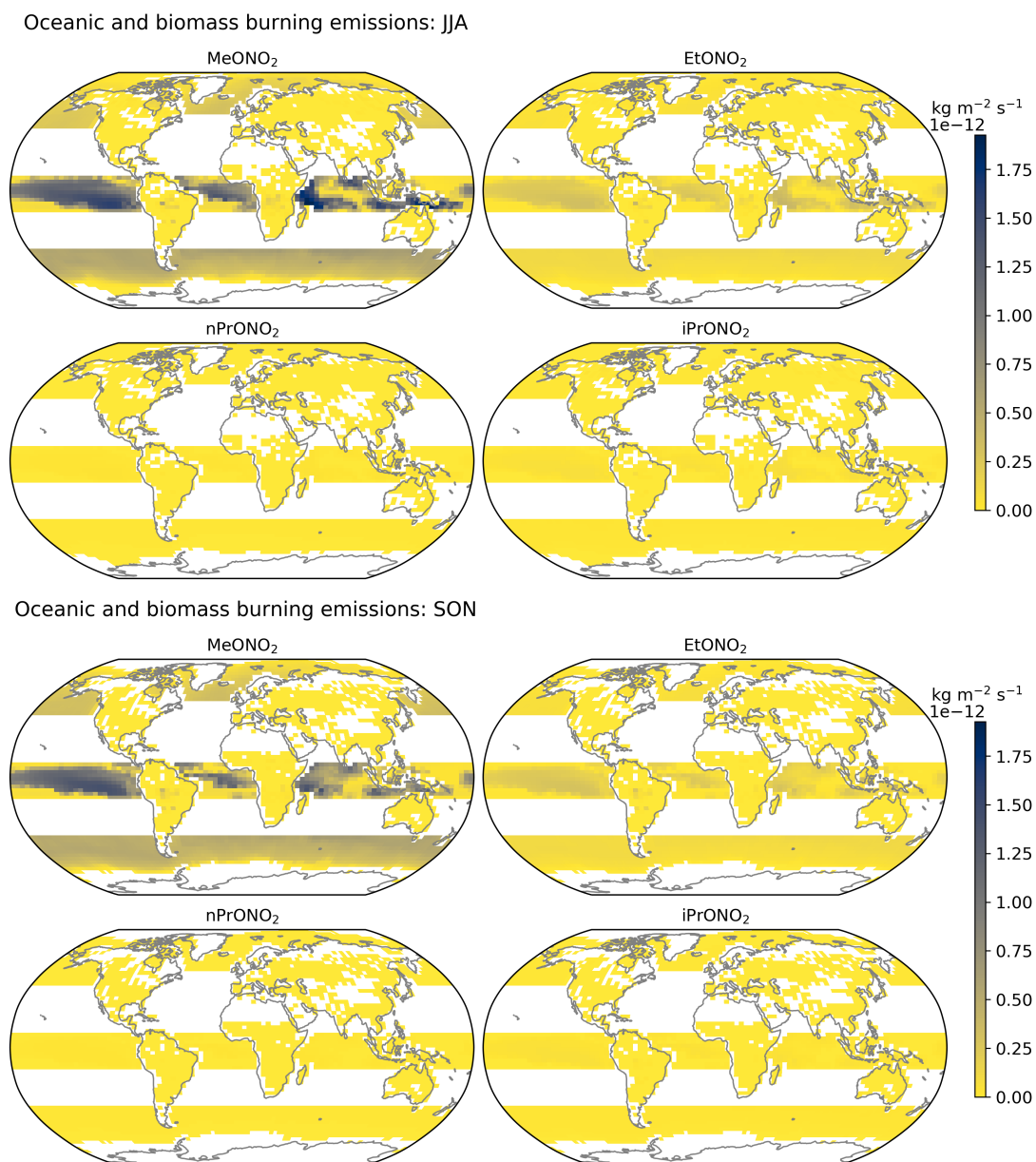


FIGURE C.6: Figure C.5 continued.



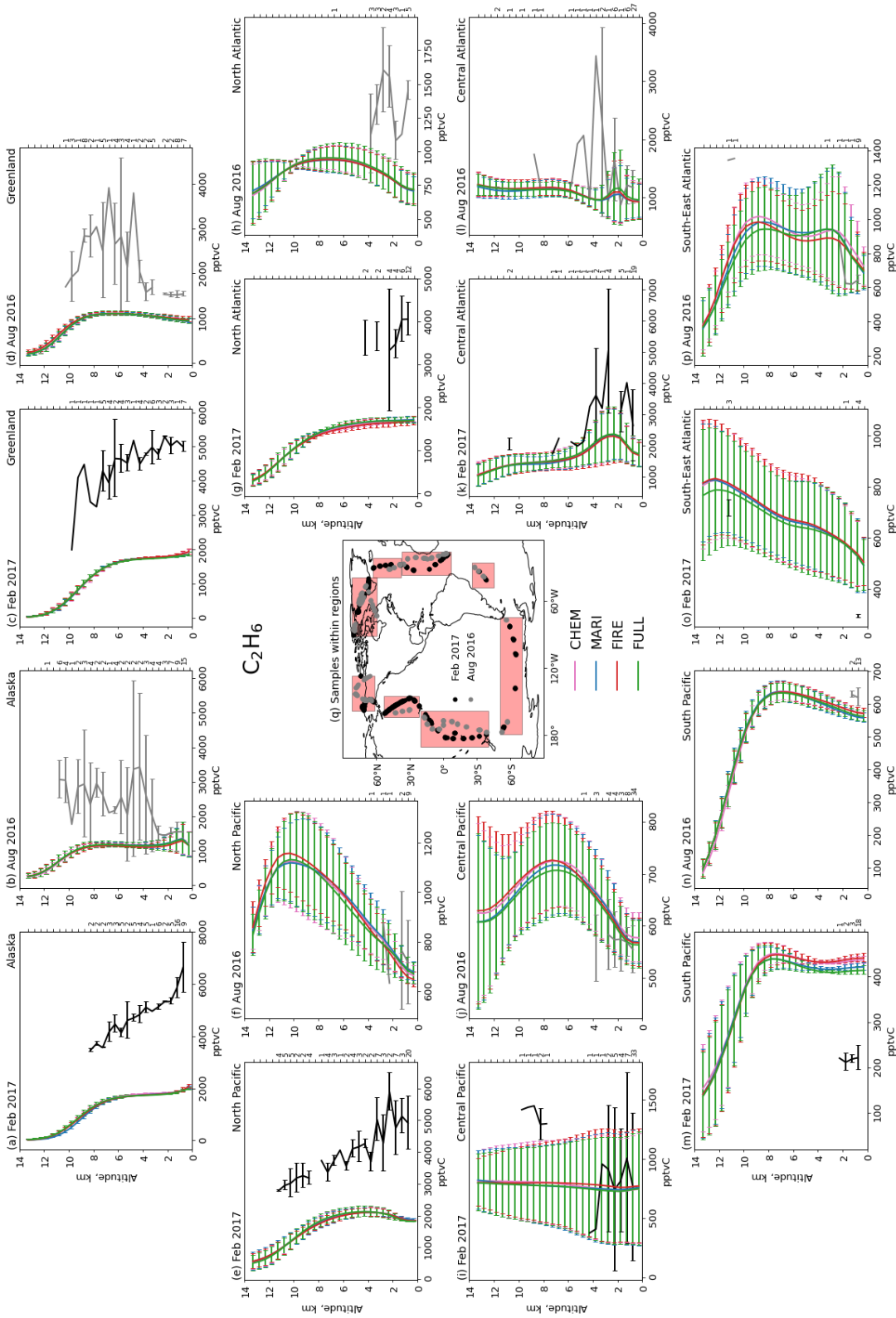


FIGURE C.7: As in Fig. 3.7 but for C<sub>2</sub>H<sub>6</sub> and with differing x-axis.



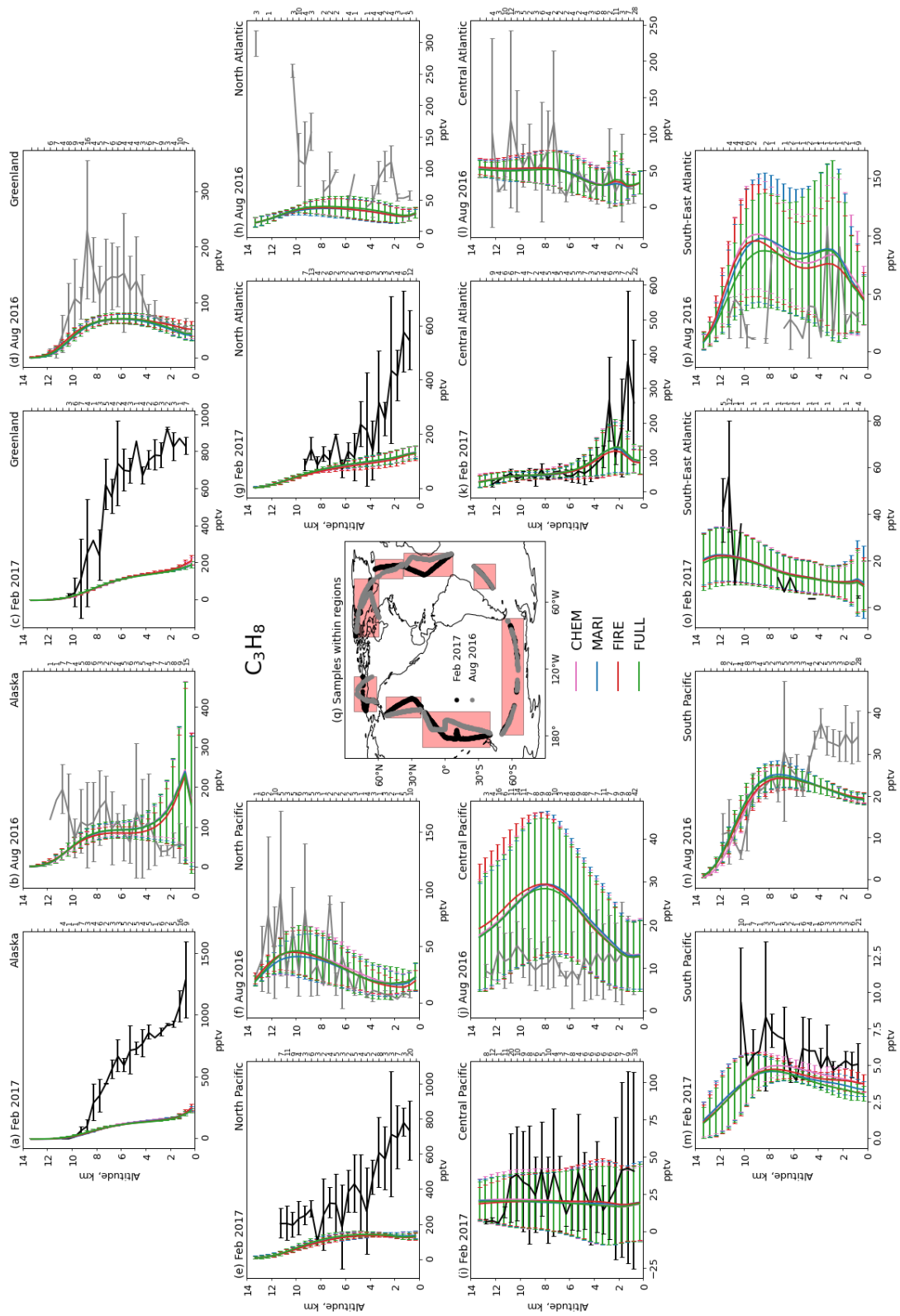


FIGURE C.8: As in Fig. 3.7 but for  $C_3H_8$  and with differing x-axis.

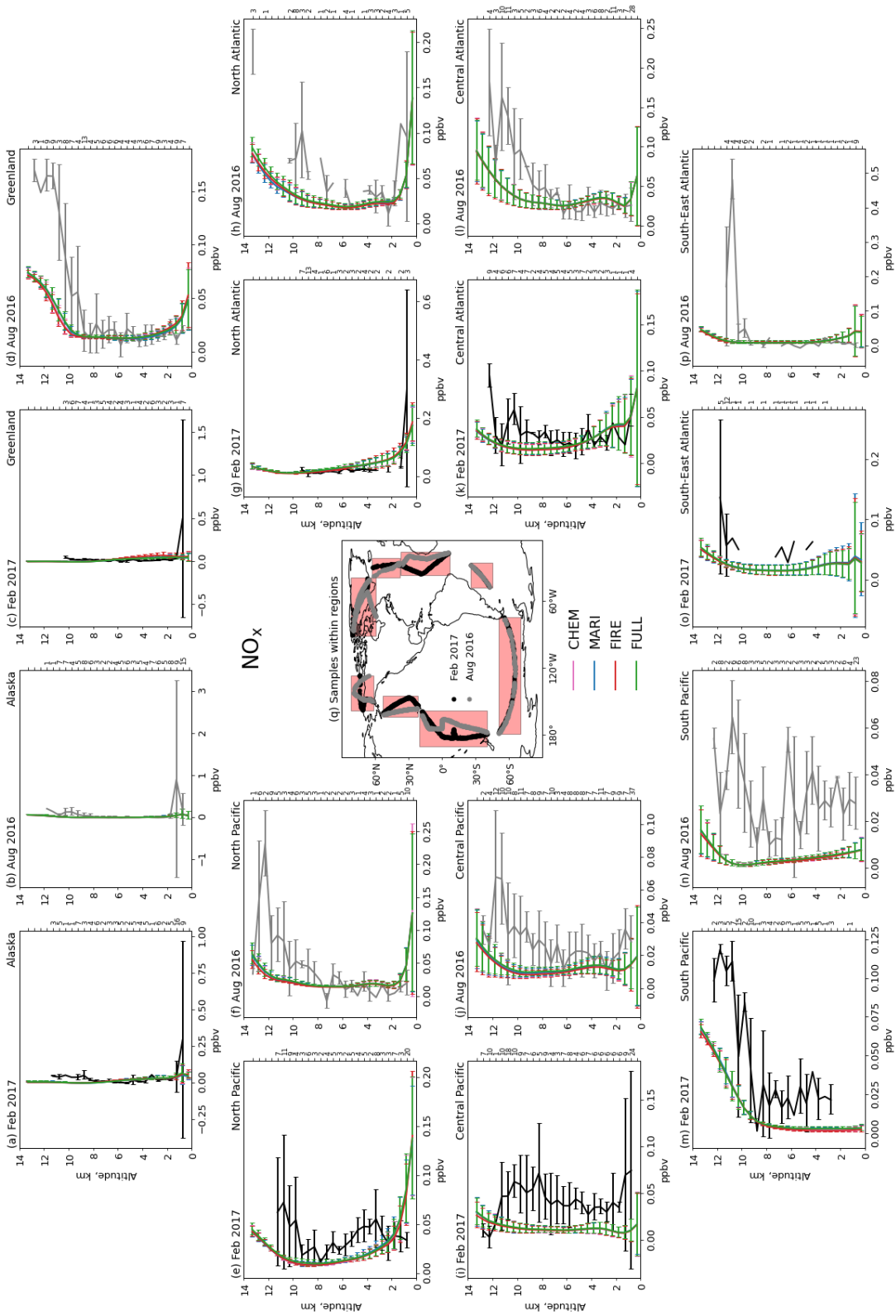


FIGURE C.9: As in Fig. 3.7 but for  $\text{NO}_x$  and with differing x-axis.

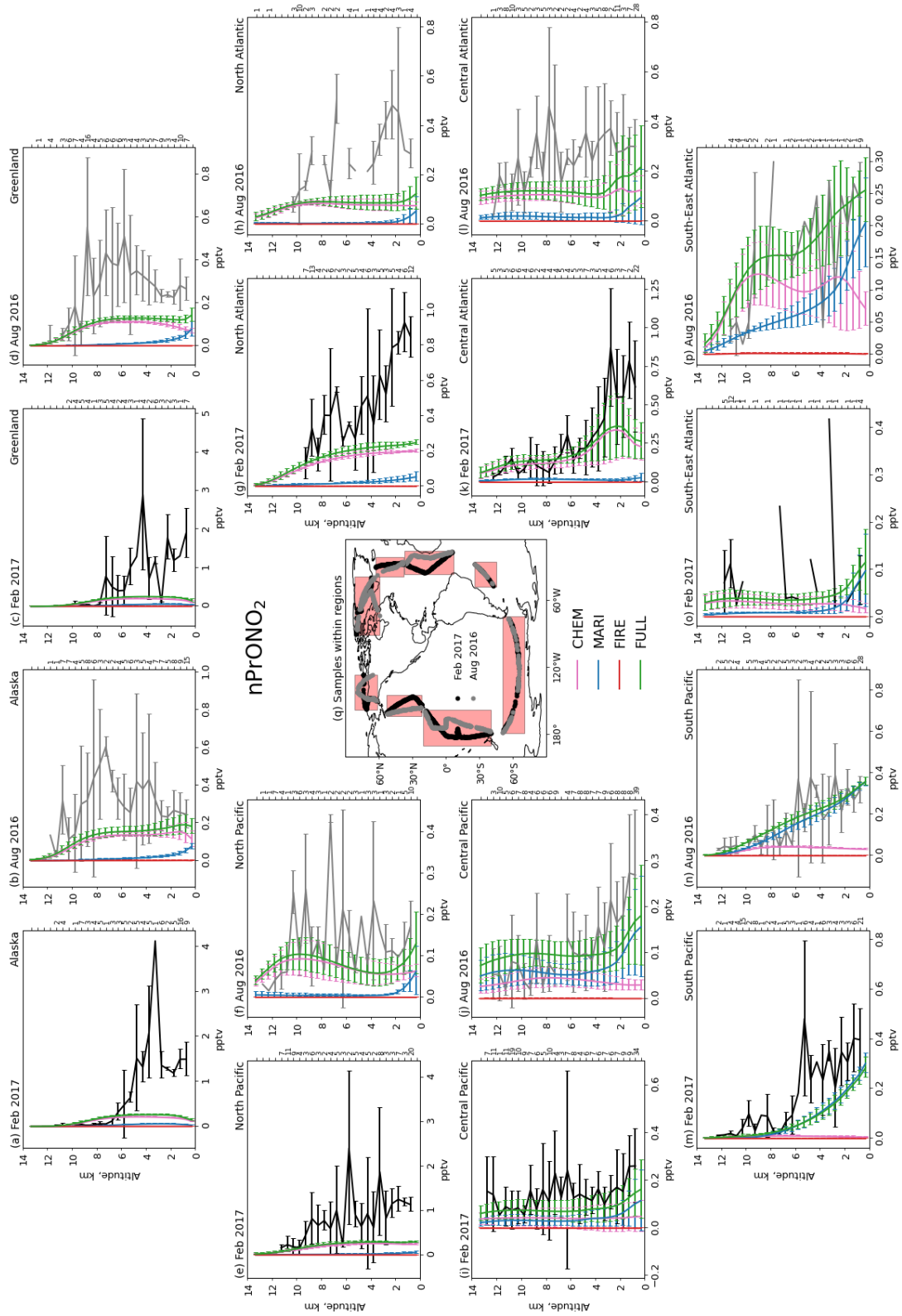


FIGURE C.10: As in Fig. 3.7 but for nPrONO<sub>2</sub> and with differing x-axis.

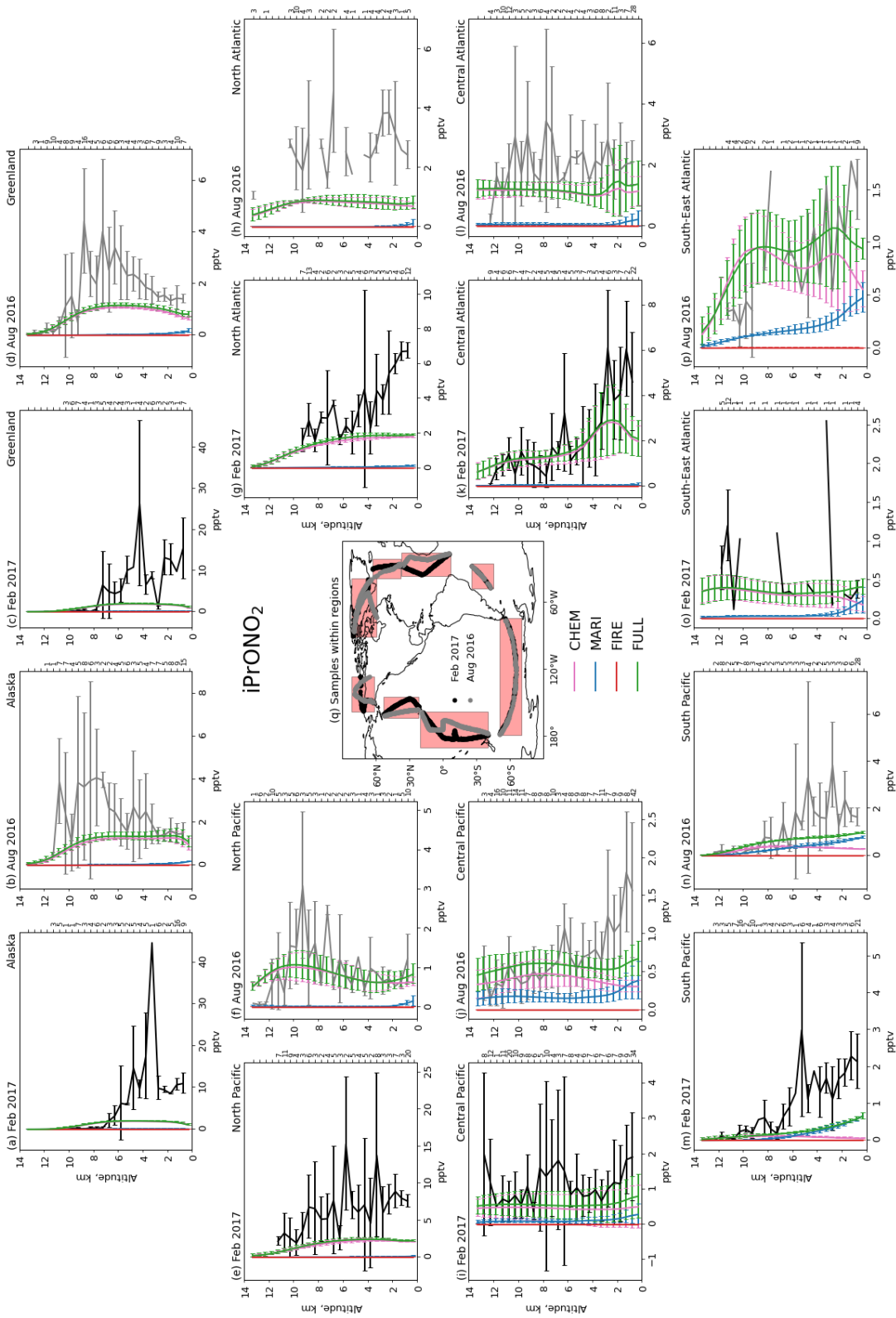


FIGURE C.11: As in Fig. 3.7 but for  $iPrONO_2$  and with differing x-axis.

TABLE C.1: Correlation coefficient (R), correlation of determination ( $R^2$ ) and root-mean-square error (RMSE) derived from a simple linear regression for  $\text{CH}_4$  vertical profiles.

Region	Experiment	R		$R^2$		RMSE, ppbv	
		Feb   Aug	Feb   Aug	Feb   Aug	Feb   Aug		
North Pacific	CHEM	0.69   0.12	0.47   0.02	35.50   24.79			
	MARI	0.69   0.12	0.47   0.02	38.67   26.92			
	FIRE	0.69   0.15	0.48   0.02	32.50   26.47			
	FULL	0.67   0.14	0.44   0.02	42.77   28.31			
Central Pacific	CHEM	0.19   -0.47	0.04   0.22	11.88   7.99			
	MARI	-0.01   -0.45	0.00   0.20	14.40   11.08			
	FIRE	0.14   -0.43	0.02   0.19	10.63   7.63			
	FULL	0.05   -0.47	0.00   0.22	15.26   11.36			
South Pacific	CHEM	0.85   0.21	0.73   0.04	42.00   69.46			
	MARI	0.85   0.22	0.73   0.05	44.43   66.41			
	FIRE	0.85   0.22	0.73   0.05	43.64   61.44			
	FULL	0.85   0.22	0.73   0.05	45.15   66.86			
South East Atlantic	CHEM	0.86   -0.74	0.75   0.55	13.58   16.67			
	MARI	0.87   -0.74	0.76   0.54	13.93   19.03			
	FIRE	0.86   -0.75	0.75   0.56	12.69   14.72			
	FULL	0.86   -0.73	0.74   0.53	17.13   19.60			
Central Atlantic	CHEM	0.73   0.15	0.53   0.02	9.71   9.27			
	MARI	0.72   0.10	0.53   0.01	12.28   8.84			
	FIRE	0.75   0.18	0.56   0.03	9.19   11.83			
	FULL	0.72   0.07	0.52   0.01	12.21   9.79			
North Atlantic	CHEM	0.65   -0.09	0.43   0.01	18.18   49.31			
	MARI	0.63   -0.09	0.40   0.01	16.84   45.12			
	FIRE	0.66   -0.08	0.44   0.01	18.07   50.00			
	FULL	0.62   -0.09	0.38   0.01	17.14   48.35			
Greenland	CHEM	0.96   0.97	0.92   0.94	46.76   83.20			
	MARI	0.96   0.97	0.92   0.94	52.90   91.05			
	FIRE	0.96   0.97	0.92   0.94	41.56   83.06			
	FULL	0.96   0.97	0.92   0.93	53.05   89.45			
Alaska	CHEM	0.99   0.38	0.98   0.14	61.25   93.04			
	MARI	0.99   0.37	0.98   0.14	80.93   90.72			
	FIRE	0.99   0.39	0.98   0.15	61.57   91.27			
	FULL	0.99   0.38	0.98   0.15	69.80   88.98			

TABLE C.2: Correlation coefficient (R), correlation of determination ( $R^2$ ) and root-mean-square error (RMSE) derived from a simple linear regression for  $C_2H_6$  vertical profiles.

Region	Experiment	R		$R^2$		RMSE, pptvC	
		Feb	Aug	Feb	Aug	Feb	Aug
North Pacific	CHEM	0.68	-0.10	0.47	0.01	2246.58	121.45
	MARI	0.70	-0.10	0.49	0.01	2255.06	123.65
	FIRE	0.70	-0.11	0.49	0.01	2265.11	118.83
	FULL	0.64	-0.11	0.41	0.01	2251.25	111.90
Central Pacific	CHEM	0.74	0.68	0.55	0.46	400.12	56.28
	MARI	0.78	0.66	0.61	0.43	412.31	52.83
	FIRE	0.59	0.67	0.35	0.45	403.96	48.98
	FULL	0.76	0.67	0.58	0.45	414.12	45.26
South Pacific	CHEM	0.22	1.00	0.05	1.00	216.08	47.32
	MARI	0.25	1.00	0.06	1.00	201.31	61.66
	FIRE	0.19	1.00	0.03	1.00	220.08	48.08
	FULL	0.24	1.00	0.06	1.00	193.92	56.61
South East Atlantic	CHEM	1.00	-0.10	1.00	0.01	201.76	330.05
	MARI	1.00	-0.11	1.00	0.01	196.99	347.24
	FIRE	1.00	0.16	1.00	0.03	204.25	325.37
	FULL	1.00	-0.23	1.00	0.05	193.76	364.24
Central Atlantic	CHEM	0.84	-0.26	0.70	0.07	1207.80	820.14
	MARI	0.84	-0.25	0.71	0.06	1222.94	827.68
	FIRE	0.84	-0.28	0.70	0.08	1242.34	820.54
	FULL	0.83	-0.43	0.69	0.18	1192.63	823.85
North Atlantic	CHEM	0.49	0.30	0.24	0.09	2033.45	566.05
	MARI	0.38	0.29	0.14	0.09	2020.89	571.45
	FIRE	0.54	0.30	0.29	0.09	2068.86	570.01
	FULL	0.22	0.29	0.05	0.09	2028.80	560.08
Greenland	CHEM	0.81	0.52	0.65	0.27	2958.01	1457.55
	MARI	0.80	0.50	0.64	0.25	2962.36	1460.11
	FIRE	0.81	0.50	0.65	0.25	2952.94	1444.91
	FULL	0.80	0.50	0.65	0.25	2968.58	1454.69
Alaska	CHEM	0.87	-0.38	0.76	0.15	3132.99	1472.27
	MARI	0.89	-0.37	0.79	0.14	3164.61	1456.53
	FIRE	0.90	-0.34	0.81	0.12	3163.19	1477.88
	FULL	0.90	-0.35	0.80	0.12	3161.09	1455.33

TABLE C.3: Correlation coefficient (R), correlation of determination ( $R^2$ ) and root-mean-square error (RMSE) derived from a simple linear regression for  $C_3H_8$  vertical profiles.

Region	Experiment	R		$R^2$		RMSE, pptv	
		Feb	Aug	Feb	Aug	Feb	Aug
North Pacific	CHEM	0.63	0.60	0.39	0.36	333.73	22.83
	MARI	0.65	0.60	0.43	0.37	333.54	23.24
	FIRE	0.61	0.64	0.37	0.41	337.10	22.08
	FULL	0.55	0.60	0.30	0.36	332.09	22.65
Central Pacific	CHEM	-0.28	-0.30	0.08	0.09	13.99	12.57
	MARI	-0.40	-0.31	0.16	0.09	13.99	12.61
	FIRE	-0.09	-0.26	0.01	0.07	13.56	12.85
	FULL	-0.21	-0.28	0.04	0.08	14.14	12.06
South Pacific	CHEM	0.11	0.67	0.01	0.45	1.93	8.17
	MARI	0.29	0.57	0.08	0.32	2.19	8.38
	FIRE	0.14	0.65	0.02	0.42	2.08	8.19
	FULL	0.34	0.60	0.11	0.35	2.27	8.33
South East Atlantic	CHEM	0.79	-0.02	0.62	0.00	12.70	55.25
	MARI	0.80	0.03	0.64	0.00	12.78	55.54
	FIRE	0.80	-0.07	0.63	0.00	12.82	50.97
	FULL	0.79	0.09	0.63	0.01	12.91	50.24
Central Atlantic	CHEM	0.71	0.53	0.50	0.28	72.68	26.63
	MARI	0.70	0.52	0.48	0.27	73.66	26.83
	FIRE	0.70	0.55	0.49	0.30	75.32	26.29
	FULL	0.71	0.53	0.51	0.29	72.14	27.05
North Atlantic	CHEM	0.86	-0.53	0.74	0.28	199.12	116.89
	MARI	0.84	-0.53	0.71	0.28	198.54	117.40
	FIRE	0.86	-0.49	0.74	0.24	202.54	116.87
	FULL	0.83	-0.56	0.70	0.32	198.32	116.13
Greenland	CHEM	0.95	0.69	0.89	0.48	531.08	60.58
	MARI	0.96	0.70	0.91	0.49	532.58	61.17
	FIRE	0.94	0.65	0.89	0.42	529.26	59.36
	FULL	0.95	0.69	0.91	0.48	532.77	60.15
Alaska	CHEM	0.99	-0.68	0.98	0.46	561.93	88.37
	MARI	0.99	-0.67	0.99	0.45	563.16	86.78
	FIRE	0.99	-0.66	0.99	0.43	565.02	83.26
	FULL	0.99	-0.67	0.99	0.45	566.69	85.51

TABLE C.4: Correlation coefficient (R), correlation of determination ( $R^2$ ) and root-mean-square error (RMSE) derived from a simple linear regression for  $\text{NO}_x$  vertical profiles.

Region	Experiment	R		$R^2$		RMSE, ppbv	
		Feb   Aug	Feb   Aug	Feb   Aug	Feb   Aug		
North Pacific	CHEM	0.08   0.47	0.01   0.22	0.03   0.05	0.03   0.05		
	MARI	0.09   0.48	0.01   0.23	0.03   0.05	0.03   0.05		
	FIRE	0.10   0.44	0.01   0.19	0.03   0.05	0.03   0.05		
	FULL	0.08   0.49	0.01   0.24	0.03   0.05	0.03   0.05		
Central Pacific	CHEM	-0.61   0.25	0.37   0.06	0.04   0.02	0.04   0.02		
	MARI	-0.61   0.22	0.37   0.05	0.04   0.02	0.04   0.02		
	FIRE	-0.62   0.24	0.39   0.06	0.04   0.02	0.04   0.02		
	FULL	-0.61   0.29	0.37   0.08	0.04   0.02	0.04   0.02		
South Pacific	CHEM	0.88   0.12	0.78   0.02	0.04   0.03	0.04   0.03		
	MARI	0.89   0.12	0.78   0.01	0.04   0.03	0.04   0.03		
	FIRE	0.89   0.12	0.79   0.01	0.04   0.03	0.04   0.03		
	FULL	0.88   0.11	0.78   0.01	0.04   0.03	0.04   0.03		
South East Atlantic	CHEM	0.54   -0.10	0.29   0.01	0.05   0.11	0.05   0.11		
	MARI	0.51   -0.11	0.26   0.01	0.05   0.11	0.05   0.11		
	FIRE	0.52   -0.12	0.27   0.01	0.05   0.11	0.05   0.11		
	FULL	0.55   -0.10	0.31   0.01	0.05   0.11	0.05   0.11		
Central Atlantic	CHEM	0.15   0.82	0.02   0.67	0.02   0.04	0.02   0.04		
	MARI	0.13   0.79	0.02   0.63	0.02   0.04	0.02   0.04		
	FIRE	0.16   0.80	0.03   0.64	0.02   0.04	0.02   0.04		
	FULL	0.15   0.79	0.02   0.63	0.02   0.04	0.02   0.04		
North Atlantic	CHEM	0.76   0.88	0.58   0.77	0.05   0.05	0.05   0.05		
	MARI	0.78   0.87	0.60   0.75	0.05   0.05	0.05   0.05		
	FIRE	0.77   0.88	0.59   0.78	0.05   0.05	0.05   0.05		
	FULL	0.78   0.88	0.61   0.78	0.05   0.05	0.05   0.05		
Greenland	CHEM	0.28   0.90	0.08   0.81	0.10   0.05	0.10   0.05		
	MARI	0.15   0.93	0.02   0.87	0.10   0.05	0.10   0.05		
	FIRE	0.16   0.88	0.03   0.77	0.10   0.05	0.10   0.05		
	FULL	0.23   0.93	0.05   0.86	0.10   0.05	0.10   0.05		
Alaska	CHEM	0.50   0.58	0.25   0.33	0.06   0.19	0.06   0.19		
	MARI	0.43   0.59	0.19   0.34	0.06   0.19	0.06   0.19		
	FIRE	0.48   0.58	0.23   0.33	0.06   0.19	0.06   0.19		
	FULL	0.57   0.58	0.32   0.34	0.05   0.19	0.05   0.19		



TABLE C.5: Correlation coefficient (R), correlation of determination ( $R^2$ ) and root-mean-square error (RMSE) derived from a simple linear regression for  $O_3$  vertical profiles.

Region	Experiment	R		$R^2$		RMSE, ppbv	
		Feb   Aug	Feb   Aug	Feb   Aug	Feb   Aug		
North Pacific	CHEM	0.66   0.66	0.44   0.44	28.95   26.15			
	MARI	0.66   0.66	0.44   0.43	30.76   27.63			
	FIRE	0.66   0.65	0.44   0.42	26.44   26.87			
	FULL	0.66   0.65	0.44   0.43	34.10   28.38			
Central Pacific	CHEM	0.27   0.36	0.07   0.13	10.95   15.81			
	MARI	0.23   0.34	0.05   0.12	11.21   15.79			
	FIRE	0.27   0.36	0.07   0.13	10.82   15.57			
	FULL	0.24   0.35	0.06   0.13	11.20   15.60			
South Pacific	CHEM	0.95   0.82	0.90   0.68	46.37   56.26			
	MARI	0.95   0.82	0.90   0.68	46.96   52.30			
	FIRE	0.95   0.82	0.90   0.68	46.08   53.97			
	FULL	0.95   0.82	0.90   0.68	47.48   46.78			
South East Atlantic	CHEM	0.66   0.56	0.43   0.32	17.01   19.37			
	MARI	0.66   0.56	0.44   0.31	16.78   19.32			
	FIRE	0.65   0.56	0.43   0.31	17.00   18.08			
	FULL	0.65   0.56	0.42   0.32	17.40   19.80			
Central Atlantic	CHEM	0.58   0.77	0.34   0.60	12.56   11.18			
	MARI	0.58   0.77	0.34   0.60	12.03   11.30			
	FIRE	0.58   0.77	0.33   0.60	12.18   11.15			
	FULL	0.58   0.77	0.33   0.60	12.95   11.27			
North Atlantic	CHEM	0.12   0.56	0.01   0.31	16.51   37.77			
	MARI	0.12   0.56	0.01   0.31	16.82   35.56			
	FIRE	0.12   0.56	0.01   0.31	14.39   36.16			
	FULL	0.12   0.56	0.01   0.32	17.38   37.42			
Greenland	CHEM	0.91   0.99	0.84   0.98	28.92   18.21			
	MARI	0.91   0.99	0.84   0.98	28.54   14.78			
	FIRE	0.91   0.99	0.83   0.98	30.73   24.09			
	FULL	0.92   0.99	0.84   0.98	28.38   16.14			
Alaska	CHEM	0.99   0.67	0.98   0.45	26.36   45.56			
	MARI	0.99   0.67	0.98   0.45	18.24   46.05			
	FIRE	0.99   0.69	0.98   0.47	26.72   42.97			
	FULL	0.99   0.67	0.98   0.45	23.07   44.86			

TABLE C.6: Correlation coefficient (R), correlation of determination ( $R^2$ ) and root-mean-square error (RMSE) derived from a simple linear regression for MeONO<sub>2</sub> vertical profiles.

Region	Experiment	R		$R^2$		RMSE, pptv	
		Feb   Aug	Feb   Aug	Feb   Aug	Feb   Aug	Feb   Aug	Feb   Aug
North Pacific	CHEM	0.47   0.66	0.22   0.43	1.81   5.04			
	MARI	0.51   0.93	0.26   0.86	4.79   2.56			
	FIRE	-0.05   0.02	0.00   0.00	7.10   4.31			
	FULL	0.55   0.83	0.30   0.69	1.12   6.60			
Central Pacific	CHEM	-0.05   0.57	0.00   0.32	12.16   6.89			
	MARI	0.66   0.86	0.43   0.75	11.19   3.80			
	FIRE	-0.77   -0.56	0.59   0.31	16.39   12.05			
	FULL	0.68   0.86	0.47   0.74	7.58   4.34			
South Pacific	CHEM	-0.53   0.82	0.28   0.68	24.45   11.43			
	MARI	0.87   0.85	0.76   0.72	17.94   4.40			
	FIRE	0.34   0.51	0.12   0.26	26.45   15.43			
	FULL	0.88   0.87	0.78   0.75	15.56   5.82			
South East Atlantic	CHEM	-0.34   0.58	0.11   0.34	1.74   5.35			
	MARI	0.64   0.93	0.41   0.87	3.63   1.61			
	FIRE	-0.31   -0.65	0.10   0.43	6.07   10.10			
	FULL	0.65   0.92	0.43   0.85	2.84   5.47			
Central Atlantic	CHEM	0.71   0.38	0.51   0.14	1.06   4.81			
	MARI	0.14   0.43	0.02   0.18	3.58   2.50			
	FIRE	0.63   0.36	0.39   0.13	6.06   6.00			
	FULL	0.79   0.47	0.62   0.22	3.34   8.46			
North Atlantic	CHEM	-0.22   -0.03	0.05   0.00	1.03   6.96			
	MARI	0.86   0.41	0.74   0.17	3.49   2.86			
	FIRE	-0.87   -0.23	0.76   0.05	6.03   4.03			
	FULL	0.70   0.07	0.49   0.01	1.85   8.21			
Greenland	CHEM	0.68   0.92	0.47   0.85	2.80   4.79			
	MARI	0.73   0.45	0.53   0.20	3.85   2.17			
	FIRE	0.31   0.90	0.10   0.80	6.69   3.45			
	FULL	0.83   0.84	0.69   0.71	1.63   6.41			
Alaska	CHEM	0.82   0.11	0.68   0.01	2.67   5.47			
	MARI	0.80   0.62	0.64   0.38	3.58   2.00			
	FIRE	0.49   0.36	0.24   0.13	6.31   3.51			
	FULL	0.86   0.38	0.74   0.15	2.06   7.63			

TABLE C.7: Correlation coefficient (R), correlation of determination ( $R^2$ ) and root-mean-square error (RMSE) derived from a simple linear regression for EtONO<sub>2</sub> vertical profiles.

Region	Experiment	R		$R^2$		RMSE, pptv	
		Feb   Aug	Feb   Aug	Feb   Aug	Feb   Aug	Feb   Aug	Feb   Aug
North Pacific	CHEM	0.60   0.63	0.36   0.40	0.95   0.73			
	MARI	0.39   0.44	0.15   0.19	2.49   0.86			
	FIRE	0.14   0.45	0.02   0.21	2.85   1.05			
	FULL	0.59   0.73	0.35   0.53	0.78   0.89			
Central Pacific	CHEM	0.39   0.40	0.15   0.16	1.11   1.04			
	MARI	0.71   0.87	0.50   0.75	1.14   0.65			
	FIRE	-0.72   -0.44	0.52   0.19	1.91   1.65			
	FULL	0.73   0.91	0.53   0.83	0.59   0.89			
South Pacific	CHEM	-0.16   0.56	0.02   0.32	2.74   2.19			
	MARI	0.86   0.89	0.74   0.78	1.71   0.79			
	FIRE	0.52   0.22	0.27   0.05	2.99   2.68			
	FULL	0.87   0.88	0.76   0.77	1.46   0.97			
South East Atlantic	CHEM	0.08   0.32	0.01   0.10	0.58   0.95			
	MARI	0.02   0.81	0.00   0.66	0.85   0.48			
	FIRE	-0.10   -0.48	0.01   0.23	1.10   1.63			
	FULL	0.05   0.81	0.00   0.65	0.66   0.91			
Central Atlantic	CHEM	0.86   0.29	0.74   0.08	0.77   0.46			
	MARI	-0.09   0.19	0.01   0.04	1.43   1.37			
	FIRE	0.83   0.26	0.69   0.07	1.74   1.83			
	FULL	0.86   0.26	0.74   0.07	1.16   0.76			
North Atlantic	CHEM	0.47   0.68	0.23   0.46	0.52   0.27			
	MARI	0.87   0.25	0.75   0.06	1.43   1.29			
	FIRE	-0.79   0.59	0.62   0.35	1.88   1.44			
	FULL	0.63   0.69	0.39   0.47	0.78   0.37			
Greenland	CHEM	0.70   0.89	0.49   0.79	1.42   0.33			
	MARI	0.83   0.39	0.69   0.15	2.25   1.20			
	FIRE	0.08   0.88	0.01   0.77	2.81   1.39			
	FULL	0.78   0.84	0.61   0.71	1.10   0.45			
Alaska	CHEM	0.69   0.38	0.48   0.14	1.68   0.43			
	MARI	0.84   0.01	0.71   0.00	2.45   1.33			
	FIRE	0.15   0.25	0.02   0.06	2.98   1.55			
	FULL	0.76   0.30	0.58   0.09	1.35   0.62			

TABLE C.8: Correlation coefficient (R), correlation of determination ( $R^2$ ) and root-mean-square error (RMSE) derived from a simple linear regression for nPrONO<sub>2</sub> vertical profiles.

Region	Experiment	R		$R^2$		RMSE, pptv	
		Feb	Aug	Feb	Aug	Feb	Aug
North Pacific	CHEM	0.63	0.19	0.39	0.04	0.80	0.11
	MARI	0.45	0.03	0.20	0.00	0.97	0.16
	FIRE	0.04	0.31	0.00	0.09	0.99	0.16
	FULL	0.63	0.17	0.39	0.03	0.78	0.10
Central Pacific	CHEM	0.25	-0.51	0.06	0.26	0.11	0.10
	MARI	0.57	0.79	0.33	0.62	0.11	0.07
	FIRE	0.17	-0.70	0.03	0.49	0.15	0.13
	FULL	0.56	0.79	0.31	0.63	0.08	0.06
South Pacific	CHEM	0.02	0.41	0.00	0.17	0.22	0.18
	MARI	0.83	0.80	0.68	0.64	0.14	0.08
	FIRE	0.66	0.16	0.44	0.03	0.23	0.21
	FULL	0.82	0.79	0.67	0.63	0.14	0.08
South East Atlantic	CHEM	0.01	0.08	0.00	0.01	0.12	0.10
	MARI	-0.09	0.56	0.01	0.31	0.12	0.11
	FIRE	-0.06	-0.22	0.00	0.05	0.13	0.18
	FULL	-0.10	0.62	0.01	0.38	0.11	0.07
Central Atlantic	CHEM	0.90	0.20	0.80	0.04	0.19	0.18
	MARI	-0.07	0.08	0.00	0.01	0.35	0.25
	FIRE	0.90	0.35	0.80	0.12	0.36	0.27
	FULL	0.90	0.19	0.80	0.04	0.18	0.16
North Atlantic	CHEM	0.74	0.44	0.55	0.19	0.38	0.23
	MARI	0.89	0.23	0.78	0.05	0.51	0.29
	FIRE	-0.83	0.53	0.68	0.29	0.54	0.29
	FULL	0.76	0.49	0.58	0.24	0.35	0.22
Greenland	CHEM	0.55	0.76	0.30	0.58	0.97	0.21
	MARI	0.69	0.16	0.47	0.03	1.07	0.29
	FIRE	-0.33	0.73	0.11	0.54	1.10	0.30
	FULL	0.58	0.73	0.34	0.53	0.94	0.20
Alaska	CHEM	0.54	0.53	0.29	0.28	1.18	0.22
	MARI	0.77	0.00	0.59	0.00	1.27	0.32
	FIRE	-0.46	0.26	0.21	0.07	1.30	0.33
	FULL	0.58	0.47	0.33	0.22	1.15	0.20

TABLE C.9: Correlation coefficient (R), correlation of determination ( $R^2$ ) and root-mean-square error (RMSE) derived from a simple linear regression for iPrONO<sub>2</sub> vertical profiles.

Region	Experiment	R		$R^2$		RMSE, pptv	
		Feb   Aug	Feb   Aug	Feb   Aug	Feb   Aug	Feb   Aug	Feb   Aug
North Pacific	CHEM	0.61   0.52	0.38   0.27	5.43   0.64			
	MARI	0.41   -0.01	0.17   0.00	7.11   1.16			
	FIRE	0.08   0.62	0.01   0.38	7.16   1.18			
	FULL	0.61   0.54	0.37   0.29	5.32   0.63			
Central Pacific	CHEM	0.01   -0.56	0.00   0.32	0.80   0.52			
	MARI	0.34   0.79	0.12   0.63	1.10   0.63			
	FIRE	-0.07   -0.57	0.01   0.33	1.21   0.81			
	FULL	0.35   0.26	0.12   0.07	0.71   0.41			
South Pacific	CHEM	-0.30   0.41	0.09   0.17	1.22   1.29			
	MARI	0.79   0.74	0.63   0.55	1.07   1.19			
	FIRE	0.70   0.18	0.49   0.03	1.28   1.53			
	FULL	0.80   0.71	0.64   0.50	1.03   1.02			
South East Atlantic	CHEM	0.20   -0.06	0.04   0.00	0.66   0.48			
	MARI	-0.20   0.70	0.04   0.48	0.83   0.79			
	FIRE	0.14   -0.40	0.02   0.16	0.86   0.99			
	FULL	0.02   0.55	0.00   0.30	0.64   0.41			
Central Atlantic	CHEM	0.84   -0.12	0.70   0.01	1.28   1.13			
	MARI	-0.07   -0.01	0.00   0.00	2.67   2.07			
	FIRE	0.86   0.15	0.73   0.02	2.71   2.14			
	FULL	0.83   -0.10	0.70   0.01	1.24   1.09			
North Atlantic	CHEM	0.67   0.49	0.44   0.24	2.53   2.00			
	MARI	0.89   0.03	0.79   0.00	3.91   2.71			
	FIRE	-0.87   0.52	0.75   0.27	3.97   2.73			
	FULL	0.62   0.49	0.38   0.24	2.44   1.96			
Greenland	CHEM	0.56   0.77	0.32   0.59	8.34   1.31			
	MARI	0.68   0.11	0.47   0.01	9.44   2.05			
	FIRE	-0.27   0.71	0.07   0.51	9.52   2.08			
	FULL	0.56   0.76	0.31   0.58	8.26   1.27			
Alaska	CHEM	0.50   0.24	0.25   0.06	11.03   1.66			
	MARI	0.67   -0.30	0.45   0.09	11.98   2.53			
	FIRE	-0.33   -0.07	0.11   0.01	12.05   2.56			
	FULL	0.49   0.25	0.24   0.06	10.98   1.58			



## Bibliography

- Abeleira, A., B. Sive, R. F. Swarthout, E. V. Fischer, Y. Zhou, and D. K. Farmer (2018). “Seasonality, sources and sinks of C1–C5 alkyl nitrates in the Colorado Front Range”. In: *Elementa: Science of the Anthropocene* 6.1, p. 45. DOI: [10.1525/elementa.299](https://doi.org/10.1525/elementa.299).
- Akagi, S. K., R. J. Yokelson, C. Wiedinmyer, M. J. Alvarado, J. S. Reid, T. Karl, J. D. Crouse, and P. O. Wennberg (2011). “Emission factors for open and domestic biomass burning for use in atmospheric models”. In: *Atmospheric Chemistry and Physics* 11.9, pp. 4039–4072. DOI: [10.5194/acp-11-4039-2011](https://doi.org/10.5194/acp-11-4039-2011).
- Archer-Nicholls, S., N. Abraham, P. Griffiths, D. Lowe, S. Utembe, F. O. Connor, O. Wild, and A. Archibald (2019). “The impacts of VOCs on atmospheric chemistry : The Common Representatives Intermediates Chemical Mechanism in UKCA”. In: *Geophysical Research Abstracts*. Vol. 21, p. 16717.
- Archibald, A. T., M. A. H. Khan, L. A. Watson, S. R. Utembe, D. E. Shallcross, K. C. Clemitshaw, and M. E. Jenkin (2007). “Comment on ‘Long-term atmospheric measurements of C1-C5 alkyl nitrates in the Pearl River Delta region of southeast China’ by Simpson et al.” In: *Atmospheric Environment* 41.34, pp. 7369–7370. DOI: [10.1016/j.atmosenv.2007.08.004](https://doi.org/10.1016/j.atmosenv.2007.08.004).
- Archibald, A. T., M. E. Jenkin, and D. E. Shallcross (2010). “An isoprene mechanism intercomparison”. In: *Atmospheric Environment* 44.40, pp. 5356–5364. DOI: [10.1016/j.atmosenv.2009.09.016](https://doi.org/10.1016/j.atmosenv.2009.09.016).
- Arribas, A., M. Glover, A. Maidens, K. Peterson, M. Gordon, C. MacLachlan, R. Graham, D. Fereday, J. Camp, A. A. Scaife, P. Xavier, P. McLean, A. Colman, and S. Cusack (2011). “The GloSea4 ensemble prediction system for seasonal forecasting”. In: *Monthly Weather Review* 139.6, pp. 1891–1910. DOI: [10.1175/2010MWR3615.1](https://doi.org/10.1175/2010MWR3615.1).
- Aschmann, S. M., E. C. Tuazon, J. Arey, and R. Atkinson (2011). “Products of the OH radical-initiated reactions of 2-propyl nitrate, 3-methyl-2-butyl nitrate and 3-methyl-2-pentyl nitrate”. In: *Atmospheric Environment* 45.9, pp. 1695–1701. DOI: [10.1016/j.atmosenv.2010.12.061](https://doi.org/10.1016/j.atmosenv.2010.12.061).
- Atherton, C. S. (1989). “Organic nitrates in remote marine environments: Evidence for long range transport”. In: *Geophysical Research Letters* 16.11, pp. 1289–1292. DOI: [10.1029/GL016i011p01289](https://doi.org/10.1029/GL016i011p01289).
- Atkinson, R., D. L. Baulch, R. A. Cox, J. N. Crowley, R. F. Hampson, R. G. Hynes, M. E. Jenkin, M. J. Rossi, and J. Troe (2006). “Evaluated kinetic and photochemical

- data for atmospheric chemistry: Volume II – gas phase reactions of organic species”. In: *Atmospheric Chemistry and Physics* 6.11, pp. 3625–4055. DOI: [10.5194/acp-6-3625-2006](https://doi.org/10.5194/acp-6-3625-2006).
- Atkinson, R. and J. Arey (2003). “Atmospheric Degradation of Volatile Organic Compounds”. In: *Chemical Reviews* 103.12, pp. 4605–4638. DOI: [10.1021/cr0206420](https://doi.org/10.1021/cr0206420).
- Atkinson, R., S. M. Aschmann, W. P. L. Carter, A. M. Wlner, and J. N. Pitts (1982). “Alkyl Nitrate Formation from the NO<sub>x</sub>-Air Photooxidations of C<sub>2</sub>-C<sub>8</sub> n-Alkanes”. In: *Journal of Physical Chemistry* 86.23, pp. 4563–4569. DOI: [10.1021/j100220a022](https://doi.org/10.1021/j100220a022).
- Atlas, E. L., W. Pollock, J. Greenberg, L. Heidt, and A. M. Thompson (1993). “Alkyl nitrates, nonmethane hydrocarbons, and halocarbon gases over the equatorial Pacific Ocean during SAGA 3”. In: *Journal of Geophysical Research* 98.D9, pp. 16933–16947. DOI: [10.1029/93JD01005](https://doi.org/10.1029/93JD01005).
- Atlas, E. (1988). “Evidence for  $\geq$ C<sub>3</sub> alkyl nitrates in rural and remote atmospheres”. In: *Nature* 331, pp. 426–428. DOI: [10.1038/331426a0](https://doi.org/10.1038/331426a0).
- Atlas, E. L., B. A. Ridley, and C. A. Cantrell (2003). “The Tropospheric Ozone Production about the Spring Equinox (TOPSE) Experiment: Introduction”. In: *Journal of Geophysical Research D: Atmospheres* 108.4, pp. 1–1. DOI: [10.1029/2002jd003172](https://doi.org/10.1029/2002jd003172).
- Aumont, B., S. Szopa, and S. Madronich (2005). “Modelling the evolution of organic carbon during its gas-phase tropospheric oxidation: development of an explicit model based on a self generating approach”. In: *Atmospheric Chemistry and Physics* 5.9, pp. 2497–2517. DOI: [10.5194/acp-5-2497-2005](https://doi.org/10.5194/acp-5-2497-2005).
- Baker, A. K., A. J. Beyersdorf, L. A. Doezema, A. Katzenstein, S. Meinardi, I. J. Simpson, D. R. Blake, and F. Sherwood Rowland (2008). “Measurements of non-methane hydrocarbons in 28 United States cities”. In: *Atmospheric Environment* 42.1, pp. 170–182. DOI: [10.1016/j.atmosenv.2007.09.007](https://doi.org/10.1016/j.atmosenv.2007.09.007).
- Ballschmiter, K. (2002). “A marine source for alkyl nitrates”. In: *Science* 297.16 August, pp. 1127–1128. DOI: [10.1126/science.1075470](https://doi.org/10.1126/science.1075470).
- Banerjee, A., A. T. Archibald, A. C. Maycock, P. Telford, N. L. Abraham, X. Yang, P. Braesicke, and J. A. Pyle (2014). “Lightning NO<sub>x</sub>, a key chemistry-climate interaction: Impacts of future climate change and consequences for tropospheric oxidising capacity”. In: *Atmospheric Chemistry and Physics* 14.18, pp. 9871–9881. DOI: [10.5194/acp-14-9871-2014](https://doi.org/10.5194/acp-14-9871-2014).
- Barth, M. C., C. A. Cantrell, W. H. Brune, S. A. Rutledge, J. H. Crawford, H. Huntrieser, L. D. Carey, D. MacGorman, M. Weisman, K. E. Pickering, E. Bruning, B. Anderson, E. Apel, M. Biggstaff, T. Campos, P. Campuzano-Jost, R. Cohen, J. Crouse, D. A. Day, G. Diskin, F. Flocke, A. Fried, C. Garland, B. Heikes, S. Honomichl, R. Hornbrook, L. Gregory Huey, J. L. Jimenez, T. Lang, M. Lichtenstern, T. Mikoviny, B. Nault, D. O’Sullivan, L. L. Pan, J. Peischl, I. Pollack, D. Richter, D. Riemer, T. Ryerson, H. Schlager, J. St. Clair, J. Walega, P. Weibring, A. Weinheimer, P. Wennberg, A. Wisthaler, P. J. Wooldridge, and C. Ziegler (2015). “The



- Deep Convective Clouds and Chemistry (DC3) field campaign”. In: *Bulletin of the American Meteorological Society* 96.8, pp. 1281–1310. DOI: [10.1175/BAMS-D-13-00290.1](https://doi.org/10.1175/BAMS-D-13-00290.1).
- Bertman, S. B., J. M. Roberts, D. D. Parrish, M. P. Buhr, P. D. Goldan, W. C. Kuster, F. C. Fehsenfeld, S. A. Montzka, and H. Westberg (1995). “Evolution of alkyl nitrates with air mass age”. In: *Journal of Geophysical Research* 100.D11, pp. 22805–22813. DOI: [10.1029/95JD02030](https://doi.org/10.1029/95JD02030).
- Blake, N. J., D. R. Blake, O. W. Wingenter, B. C. Sive, C. H. Kang, D. C. Thornton, A. R. Bandy, E. Atlas, F. Flocke, J. M. Harris, and F. S. Rowland (1999). “Air-craft measurements of the latitudinal, vertical, and seasonal variations of NMHCs, methyl nitrate, methyl halides, and DMS during the First Aerosol Characterization Experiment (ACE 1)”. In: *Journal of Geophysical Research* 104.D17, pp. 21803–21817. DOI: [10.1029/1999JD900238](https://doi.org/10.1029/1999JD900238).
- Blake, N. J., D. R. Blake, and A. L. Swanson (2003). “Latitudinal, vertical, and seasonal variations of C1-C4 alkyl nitrates in the troposphere over the Pacific Ocean during PEM-Tropics A and B: Oceanic and continental sources”. In: *Journal of Geophysical Research* 108.D2, p. 8242. DOI: [10.1029/2001JD001444](https://doi.org/10.1029/2001JD001444).
- Browne, E. C. and R. C. Cohen (2012). “Effects of biogenic nitrate chemistry on the NO<sub>x</sub> lifetime in remote continental regions”. In: *Atmospheric Chemistry and Physics* 12.24, pp. 11917–11932. DOI: [10.5194/acp-12-11917-2012](https://doi.org/10.5194/acp-12-11917-2012).
- Burkholder, J. B., S. P. Sander, J. Abbatt, J. R. Barker, R. E. Huie, C. E. Kolb, M. J. Kurylo, V. L. Orkin, D. M. Wilmouth, and P. H. Wine (2015). *Chemical Kinetics and Photochemical Data for Use in Atmospheric Studies, Evaluation Number 18*. Tech. rep. Pasadena: Jet Propulsion Laboratory.
- Chipperfield, M. P. and S. R. Arnold (2015). *NUMERICAL MODELS | Chemistry Models*. Elsevier, pp. 135–143. DOI: [10.1016/B978-0-12-382225-3.00249-8](https://doi.org/10.1016/B978-0-12-382225-3.00249-8).
- Chuck, A. L., S. M. Turner, and P. S. Liss (2002). “Direct evidence for a marine source of C1 and C2 alkyl nitrates”. In: *Science* 297.5584, pp. 1151–1154. DOI: [10.1126/science.1073896](https://doi.org/10.1126/science.1073896).
- Clemitshaw, K. C., J. Williams, O. V. Rattigan, D. E. Shallcross, K. S. Law, and R. Anthony Cox (1997). “Gas-phase ultraviolet absorption cross-sections and atmospheric lifetimes of several C2-C5 alkyl nitrates”. In: *Journal of Photochemistry and Photobiology A: Chemistry* 102.2-3, pp. 117–126. DOI: [10.1016/S1010-6030\(96\)04458-9](https://doi.org/10.1016/S1010-6030(96)04458-9).
- Collins, J. W., J. F. Lamarque, M. Schulz, O. Boucher, V. Eyring, I. M. Hegglin, A. Maycock, G. Myhre, M. Prather, D. Shindell, and J. S. Smith (2017). “AerChem-MIP: Quantifying the effects of chemistry and aerosols in CMIP6”. In: *Geoscientific Model Development* 10.2, pp. 585–607. DOI: [10.5194/gmd-10-585-2017](https://doi.org/10.5194/gmd-10-585-2017).
- Cooper, O. R., D. D. Parrish, J. Ziemke, N. V. Balashov, M. Cupeiro, I. E. Galbally, S. Gilge, L. Horowitz, N. R. Jensen, J.-F. Lamarque, V. Naik, S. J. Oltmans, J.

- Schwab, D. T. Shindell, A. M. Thompson, V. Thouret, Y. Wang, and R. M. Zbinden (2014). “Global distribution and trends of tropospheric ozone: An observation-based review”. In: *Elementa: Science of the Anthropocene* 2.000029, pp. 1–28. DOI: [10.12952/journal.elementa.000029](https://doi.org/10.12952/journal.elementa.000029).
- Dahl, E. E., S. A. Yvon-Lewis, and E. S. Saltzman (2007). “Alkyl nitrate (C1-C3) depth profiles in the tropical Pacific Ocean”. In: *Journal of Geophysical Research* 112.C01012. DOI: [10.1029/2006JC003471](https://doi.org/10.1029/2006JC003471).
- Dahl, E. E. and E. S. Saltzman (2003). “The aqueous phase yield of alkyl nitrates from ROO + NO: Implications for photochemical production in seawater”. In: *Geophysical Research Letters* 30.6, p. 1271. DOI: [10.1029/2002GL016811](https://doi.org/10.1029/2002GL016811).
- Dahl, E. E. and E. S. Saltzman (2008). “Alkyl nitrate photochemical production rates in North Pacific seawater”. In: *Marine Chemistry* 112.3-4, pp. 137–141. DOI: [10.1016/j.marchem.2008.10.002](https://doi.org/10.1016/j.marchem.2008.10.002).
- Dahl, E. E., S. A. Yvon-Lewis, and E. S. Saltzman (2005). “Saturation anomalies of alkyl nitrates in the tropical Pacific Ocean”. In: *Geophysical Research Letters* 32.L20817, pp. 1–4. DOI: [10.1029/2005GL023896](https://doi.org/10.1029/2005GL023896).
- Dahl, E. E., E. M. Heiss, and K. Murawski (2012). “The effects of dissolved organic matter on alkyl nitrate production during GOMECC and laboratory studies”. In: *Marine Chemistry* 142-144, pp. 11–17. DOI: [10.1016/j.marchem.2012.08.001](https://doi.org/10.1016/j.marchem.2012.08.001).
- Dalsøren, S. B., G. Myhre, O. Hodnebrog, C. L. Myhre, A. Stohl, I. Pissò, S. Schwietzke, L. Höglund-Isaksson, D. Helmig, S. Reimann, S. Sauvage, N. Schmidbauer, K. A. Read, L. J. Carpenter, A. C. Lewis, S. Punjabi, and M. Wallasch (2018). “Discrepancy between simulated and observed ethane and propane levels explained by underestimated fossil emissions”. In: *Nature Geoscience* 11.3, pp. 178–184. DOI: [10.1038/s41561-018-0073-0](https://doi.org/10.1038/s41561-018-0073-0).
- Damian, V., A. Sandu, M. Damian, F. Potra, and G. R. Carmichael (2002). “The kinetic preprocessor KPP - A software environment for solving chemical kinetics”. In: *Computers and Chemical Engineering* 26.11, pp. 1567–1579. DOI: [10.1016/S0098-1354\(02\)00128-X](https://doi.org/10.1016/S0098-1354(02)00128-X).
- Davies, T., M. J. Cullen, A. J. Malcolm, M. H. Mawson, A. Staniforth, A. A. White, and N. Wood (2005). “A new dynamical core of the Met Office’s global and regional modelling of the atmosphere”. In: *Quarterly Journal of the Royal Meteorological Society* 131.608, pp. 1759–1782. DOI: [10.1256/qj.04.101](https://doi.org/10.1256/qj.04.101).
- Day, D. A., M. B. Dillon, P. J. Wooldridge, J. A. Thornton, R. S. Rosen, E. C. Wood, and R. C. Cohen (2003). “On alkyl nitrates, O<sub>3</sub>, and the “missing NO<sub>y</sub>””. In: *Journal of Geophysical Research* 108.D16, p. 4501. DOI: [10.1029/2003JD003685](https://doi.org/10.1029/2003JD003685).
- Dlugokencky, E. and S. Houweling (2015). *CHEMISTRY OF THE ATMOSPHERE / Chemical Kinetics*. Second. Vol. 1. Elsevier, pp. 363–371. DOI: [10.1016/B978-0-12-382225-3.00223-1](https://doi.org/10.1016/B978-0-12-382225-3.00223-1).

- Eastham, S. D. and D. J. Jacob (2017). “Limits on the ability of global Eulerian models to resolve intercontinental transport of chemical plumes”. In: *Atmospheric Chemistry and Physics* 17.4, pp. 2543–2553. DOI: [10.5194/acp-17-2543-2017](https://doi.org/10.5194/acp-17-2543-2017).
- Ehhalt, D. H., F. Rohrer, and A. Wahner (2015). “TROPOSPHERIC CHEMISTRY AND COMPOSITION | Oxidizing Capacity”. In: *Encyclopedia of Atmospheric Sciences*. 2nd ed. Vol. 6. Elsevier, pp. 243–250. DOI: [10.1016/B978-0-12-382225-3.00437-0](https://doi.org/10.1016/B978-0-12-382225-3.00437-0).
- Emmerson, K. M. and M. J. Evans (2009). “Comparison of tropospheric gas-phase chemistry schemes for use within global models”. In: *Atmospheric Chemistry and Physics* 9.5, pp. 1831–1845. DOI: [10.5194/acp-9-1831-2009](https://doi.org/10.5194/acp-9-1831-2009).
- Eyring, V., J.-F. Lamarque, P. Hess, F. Arfeuille, K. Bowman, M. P. Chipperfield, B. Duncan, A. Fiore, A. Gettelman, M. A. Giorgetta, C. Granier, M. Hegglin, D. Kinnison, M. Kunze, U. Langematz, B. Luo, R. Martin, K. Matthes, P. A. Newman, T. Peter, A. Robock, T. Ryerson, A. Saiz-Lopez, R. Salawitch, M. Schultz, T. G. Shepherd, D. Shindell, J. Staehelin, S. Tegtmeier, L. Thomason, S. Tilmes, J.-P. Vernier, D. W. Waugh, and P. J. Young (2013). “Overview of IGAC/SPARC Chemistry-Climate Model Initiative (CCMI) Community Simulations in Support of Upcoming Ozone and Climate Assessments”. In: *SPARC Newsletter No. 40* January, pp. 48–66.
- Farmer, D. K., A. E. Perring, P. J. Wooldridge, D. R. Blake, A. Baker, S. Meinardi, L. G. Huey, D. Tanner, O. Vargas, and R. C. Cohen (2011). “Impact of organic nitrates on urban ozone production”. In: *Atmospheric Chemistry and Physics* 11.9, pp. 4085–4094. DOI: [10.5194/acp-11-4085-2011](https://doi.org/10.5194/acp-11-4085-2011).
- Fischer, R., R. Weller, H.-W. Jacobi, and K. Ballschmiter (2002). “Levels and pattern of volatile organic nitrates and halocarbons in the air at Neumayer Station (70 degrees S), Antarctic”. In: *Chemosphere* 48.9, pp. 981–992. DOI: [10.1016/S0045-6535\(02\)00110-8](https://doi.org/10.1016/S0045-6535(02)00110-8).
- Fischer, R. G., J. Kastler, and K. Ballschmiter (2000). “Levels and pattern of alkyl nitrates, multifunctional alkyl nitrates, and halocarbons in the air over the Atlantic Ocean”. In: *Journal of Geophysical Research* 105.D11, pp. 14473–14494. DOI: [10.1029/1999JD900780](https://doi.org/10.1029/1999JD900780).
- Fisher, J. A., D. J. Jacob, M. T. Purdy, M. Kopacz, P. Le Sager, C. Carouge, C. D. Holmes, R. M. Yantosca, R. L. Batchelor, K. Strong, G. S. Diskin, H. E. Fuelberg, J. S. Holloway, E. J. Hyer, W. W. McMillan, J. Warner, D. G. Streets, Q. Zhang, Y. Wang, and S. Wu (2010). “Source attribution and interannual variability of Arctic pollution in spring constrained by aircraft (ARCTAS, ARCPAC) and satellite (AIRS) observations of carbon monoxide”. In: *Atmospheric Chemistry and Physics* 10.3, pp. 977–996. DOI: [10.5194/acp-10-977-2010](https://doi.org/10.5194/acp-10-977-2010).
- Fisher, J. A., E. L. Atlas, B. Barletta, S. Meinardi, D. R. Blake, C. R. Thompson, T. B. Ryerson, J. Peischl, Z. A. Tzompa-Sosa, and L. T. Murray (2018). “Methyl, ethyl,

- and propyl nitrates: global distribution and impacts on reactive nitrogen in remote marine environments”. In: *Journal of Geophysical Research: Atmospheres* 123. DOI: [10.1029/2018JD029046](https://doi.org/10.1029/2018JD029046).
- Flocke, F., A. Volz-Thomas, H.-J. Buers, W. Pätz, H.-J. Garthe, and D. Kley (1998). “Long-term measurements of alkyl nitrates in southern Germany: 1. General behavior and seasonal and diurnal variation”. In: *Journal of Geophysical Research* 103.D5, pp. 5729–5746. DOI: [10.1029/97JD03461](https://doi.org/10.1029/97JD03461).
- Flocke, F., G. Pfister, J. H. Crawford, K. E. Pickering, G. Pierce, D. Bon, and P. Reddy (2019). “Air Quality in the Northern Colorado Front Range Metro Area: The Front Range Air Pollution and Photochemistry Experiment (FRAPPÉ)”. In: *Journal of Geophysical Research: Atmospheres* 125.2. DOI: [10.1029/2019JD031197](https://doi.org/10.1029/2019JD031197).
- Friedli, H. R., E. Atlas, V. R. Stroud, L. Giovanni, T. Campos, and L. F. Radke (2001). “Volatile organic trace gases emitted from North American wildfires”. In: *Global Biogeochemical Cycles* 15.2, pp. 435–452. DOI: [10.1029/2000GB001328](https://doi.org/10.1029/2000GB001328).
- Gaudel, A., O. R. Cooper, G. Ancellet, B. Barret, A. Boynard, J. P. Burrows, C. Clerbaux, P.-F. Coheur, J. Cuesta, E. Cuevas, S. Doniki, G. Dufour, F. Ebojje, G. Foret, O. Garcia, M. J. G. Munos, J. W. Hannigan, F. Hase, G. Huang, B. Hasler, D. Hurtmans, D. A. Jaffe, N. Jones, P. Kalabokas, B. Kerridge, S. Kulawik, B. Latter, T. Leblanc, E. Le Flochmoën, W. Lin, J. Liu, X. Liu, E. Mahieu, A. McClure-Begley, J. Neu, M. Osman, M. Palm, H. Petetin, I. Petropavlovskikh, R. Querel, N. Rappoe, A. Rozanov, M. G. Schultz, J. Schwab, R. Siddans, D. Smale, M. Steinbacher, H. Tanimoto, D. W. Tarasick, V. Thouret, A. M. Thompson, T. Trickl, E. Weatherhead, C. Wespes, H. M. Worden, C. Vigouroux, X. Xu, G. Zeng, and J. R. Ziemke (2018). “Tropospheric Ozone Assessment Report : Present-day distribution and trends of tropospheric ozone relevant to climate and global atmospheric chemistry model evaluation”. In: *Elementa: Science of the Anthropocene*. DOI: <http://doi.org/10.1525/elementa.291>.
- González Sánchez, J. M., S. Khemiri, S. Ravier, A. Durand, J.-L. Clément, and A. Monod (2018). “Study of the reactivity of the isobutyl nitrate in the aqueous phase of the atmosphere: Development of a methodology for studying the fate of polyfunctional organic nitrates”. In: *Geophysical Research Abstracts*. Vol. 20. Vienna, Austria: EGU General Assembly 2018, EGU2018–9376.
- Guenther, A. B., X. Jiang, C. L. Heald, T. Sakulyanontvittaya, T. Duhl, L. K. Emissions, and X. Wang (2012). “The model of emissions of gases and aerosols from nature version 2.1 (MEGAN2.1): An extended and updated framework for modeling biogenic emissions”. In: *Geoscientific Model Development* 5.6, pp. 1471–1492. DOI: [10.5194/gmd-5-1471-2012](https://doi.org/10.5194/gmd-5-1471-2012).
- Hauff, K., R. G. Fischer, and K. Ballschmiter (1998). “Determination of C1-C5 alkyl nitrates in rain, snow, white frost, lake, and tap water by a combined codistillation head-space gas chromatography technique. Determination of Henry’s law constants

- by head-space GC". In: *Chemosphere* 37.13, pp. 2599–615. DOI: [10.1016/s0045-6535\(98\)00159-3](https://doi.org/10.1016/s0045-6535(98)00159-3).
- Helmig, D., S. Rossabi, J. Hueber, P. Tans, S. A. Montzka, K. Masarie, K. Thoning, C. Plass-duelmer, A. Claude, L. J. Carpenter, A. C. Lewis, S. Punjabi, S. Reimann, M. K. Vollmer, R. Steinbrecher, J. W. Hannigan, L. K. Emmons, E. Mahieu, B. Franco, D. Smale, and A. Pozzer (2016). "Reversal of global atmospheric ethane and propane trends largely due to US oil and natural gas production". In: *Nature Geoscience* 9.July, pp. 490–498. DOI: [10.1038/NGE02721](https://doi.org/10.1038/NGE02721).
- Hewitt, H. T., D. Copsey, I. D. Culverwell, C. M. Harris, R. S. Hill, A. B. Keen, A. J. McLaren, and E. C. Hunke (2011). "Design and implementation of the infrastructure of HadGEM3: The next-generation Met Office climate modelling system". In: *Geoscientific Model Development* 4.2, pp. 223–253. DOI: [10.5194/gmd-4-223-2011](https://doi.org/10.5194/gmd-4-223-2011).
- Hughes, C., A. L. Chuck, S. M. Turner, and P. S. Liss (2008). "Methyl and ethyl nitrate saturation anomalies in the Southern Ocean (36–65°S, 30–70°W)". In: *Environmental Chemistry* 5.1, pp. 11–15. DOI: [10.1071/EN07083](https://doi.org/10.1071/EN07083).
- Hungate, B. A. and G. W. Koch (2015). *Global Change: Biospheric Impacts and Feedbacks*. Second Edi. Vol. 3. 4. Elsevier, pp. 132–140. DOI: [10.1016/B978-0-12-382225-3.00472-2](https://doi.org/10.1016/B978-0-12-382225-3.00472-2).
- Inomata, S., H. Yamada, and H. Tanimoto (2016). "Investigation on VOC Emissions from Automobile Sources by Means of Online Mass Spectrometry". In: *Current Pollution Reports* 2.3, pp. 188–199. DOI: [10.1007/s40726-016-0032-6](https://doi.org/10.1007/s40726-016-0032-6).
- Jacob, D. J., J. H. Crawford, H. Maring, A. D. Clarke, J. E. Dibb, L. K. Emmons, R. A. Ferrare, C. A. Hostetler, P. B. Russell, H. B. Singh, A. M. Thompson, G. E. Shaw, E. McCauley, J. R. Pederson, and J. A. Fisher (2010). "The Arctic Research of the Composition of the Troposphere from Aircraft and Satellites (ARCTAS) mission: design, execution, and first results". In: *Atmospheric Chemistry and Physics* 10.11, pp. 5191–5212. DOI: [10.5194/acp-10-5191-2010](https://doi.org/10.5194/acp-10-5191-2010).
- Jacob, D. J. (1999). *Introduction to Atmospheric Chemistry*. Princeton, New Jersey: Princeton University Press, p. 280. DOI: [10.1029/01E000292](https://doi.org/10.1029/01E000292).
- Jacob, D. J., J. H. Crawford, M. M. Kleb, V. S. Connors, R. J. Bendura, J. L. Raper, G. W. Sachse, J. C. Gille, L. Emmons, and C. L. Heald (2003). "Transport and Chemical Evolution over the Pacific (TRACE-P) aircraft mission: Design, execution, and first results". In: *Journal of Geophysical Research Atmospheres* 108.20. DOI: [10.1029/2002JD003276](https://doi.org/10.1029/2002JD003276).
- Jenkin, M. E., L. A. Watson, S. R. Utembe, and D. E. Shallcross (2008). "A Common Representative Intermediates (CRI) mechanism for VOC degradation. Part 1: Gas phase mechanism development". In: *Atmospheric Environment* 42.31, pp. 7185–7195. DOI: [10.1016/j.atmosenv.2008.07.028](https://doi.org/10.1016/j.atmosenv.2008.07.028).

- Jenkin, M. E., J. C. Young, and A. R. Rickard (2015). “The MCM v3.3.1 degradation scheme for isoprene”. In: *Atmospheric Chemistry and Physics* 15.20, pp. 11433–11459. DOI: [10.5194/acp-15-11433-2015](https://doi.org/10.5194/acp-15-11433-2015).
- Jenkin, M. E., S. M. Saunders, and M. J. Pilling (1997). “The tropospheric degradation of volatile organic compounds: A protocol for mechanism development”. In: *Atmospheric Environment* 31.1, pp. 81–104. DOI: [10.1016/S1352-2310\(96\)00105-7](https://doi.org/10.1016/S1352-2310(96)00105-7).
- Johnson, M. T. (2010). “A numerical scheme to calculate temperature and salinity dependent air-water transfer velocities for any gas”. In: *Ocean Science* 6.4, pp. 913–932. DOI: [10.5194/os-6-913-2010](https://doi.org/10.5194/os-6-913-2010).
- Jones, A. E., R. Weller, A. Minikin, E. W. Wolff, W. T. Sturges, H. P. McIntyre, S. R. Leonard, O. Schrems, and S. Bauguitte (1999). “Oxidized nitrogen chemistry and speciation in the Antarctic troposphere”. In: *Journal of Geophysical Research* 104.D17, pp. 21355–21366. DOI: [10.1029/1999JD900362](https://doi.org/10.1029/1999JD900362).
- Khan, M. A. H., M. C. Cooke, S. R. Utembe, W. C. Morris, A. T. Archibald, R. G. Derwent, M. E. Jenkin, A. J. Orr-ewing, C. M. Higgins, C. J. Percival, K. E. Leather, and D. E. Shallcross (2015). “Global modeling of the C1-C3 alkyl nitrates using STOCHEM-CRI”. In: *Atmospheric Environment* 123, pp. 256–267. DOI: [10.1016/j.atmosenv.2015.10.088](https://doi.org/10.1016/j.atmosenv.2015.10.088).
- Kim, M. J., J. M. Michaud, R. Williams, B. P. Sherwood, R. Pomeroy, F. Azam, M. Burkart, and T. H. Bertram (2015). “Bacterial-driven production of nitrates in seawater”. In: *Geophysical Research Letters* 42.2, pp. 1–8. DOI: [10.1002/2014GL062865](https://doi.org/10.1002/2014GL062865).
- Kleb, M. M., G. Chen, J. H. Crawford, F. M. Flocke, and C. C. Brown (2011). “An overview of measurement comparisons from the INTEX-B/MILAGRO airborne field campaign”. In: *Atmospheric Measurement Techniques* 4.1, pp. 9–27. DOI: [10.5194/amt-4-9-2011](https://doi.org/10.5194/amt-4-9-2011).
- Kock, A. C. de and C. R. Anderson (1994). “The measurement of C3-C5 alkyl nitrates at a coastal sampling site in the southern hemisphere”. In: *Chemosphere* 29.2, pp. 299–310. DOI: [10.1016/0045-6535\(94\)90106-6](https://doi.org/10.1016/0045-6535(94)90106-6).
- Krol, M and J. Lelieveld (2003). “Can the variability in tropospheric OH be deduced from measurements of 1,1,1-trichloroethane (methyl chloroform)?” In: *Journal of Geophysical Research* 108.D3, p. 4125. DOI: [doi:10.1029/2002JD002423](https://doi.org/10.1029/2002JD002423).
- Lamarque, J. F., D. T. Shindell, B. Josse, P. J. Young, I. Cionni, V. Eyring, D. Bergmann, P. Cameron-Smith, W. J. Collins, R. Doherty, S. Dalsoren, G. Faluvegi, G. Folberth, S. J. Ghan, L. W. Horowitz, Y. H. Lee, I. A. MacKenzie, T. Nagashima, V. Naik, D. Plummer, M. Righi, S. T. Rumbold, M. Schulz, R. B. Skeie, D. S. Stevenson, S. Strode, K. Sudo, S. Szopa, A. Voulgarakis, and G. Zeng (2013). “The atmospheric chemistry and climate model intercomparison Project (ACCMIP): Overview and description of models, simulations and climate diagnostics”. In: *Geoscientific Model Development* 6.1, pp. 179–206. DOI: [10.5194/gmd-6-179-2013](https://doi.org/10.5194/gmd-6-179-2013).



- Law, K. S., P. H. Plantevin, D. E. Shallcross, H. L. Rogers, J. A. Pyle, C. Grouhel, V. Thouret, and A. Marenco (1998). “Evaluation of modeled O<sub>3</sub> using Measurement of Ozone by Airbus In-Service Aircraft (MOZAIC) data”. In: *Journal of Geophysical Research* 103.D19, pp. 25721–25737. DOI: [10.1029/98JD01482](https://doi.org/10.1029/98JD01482).
- Lee, D. S., I. Köhler, E. Grobler, F. Rohrer, R. Sausen, L. Gallardo-Klenner, J. G. Olivier, F. J. Dentener, and A. F. Bouwman (1997). “Estimations of global NO<sub>x</sub> emissions and their uncertainties”. In: *Atmospheric Environment* 31.12, pp. 1735–1749. DOI: [10.1016/S1352-2310\(96\)00327-5](https://doi.org/10.1016/S1352-2310(96)00327-5).
- Malkin, T. L., D. E. Heard, C. Hood, J. Stocker, D. Carruthers, I. A. MacKenzie, R. M. Doherty, M. Vieno, J. Lee, J. Kleffmann, S. Laufs, and L. K. Whalley (2016). “Assessing chemistry schemes and constraints in air quality models used to predict ozone in London against the detailed Master Chemical Mechanism”. In: *Faraday Discussions* 189, pp. 589–616. DOI: [10.1039/C5FD00218D](https://doi.org/10.1039/C5FD00218D).
- Monks, P. S., A. T. Archibald, A. Colette, O. Cooper, M. Coyle, R. Derwent, D. Fowler, C. Granier, K. S. Law, G. E. Mills, D. S. Stevenson, O. Tarasova, V. Thouret, E. von Schneidmesser, R. Sommariva, O. Wild, and M. L. Williams (2015). “Tropospheric ozone and its precursors from the urban to the global scale from air quality to short-lived climate forcer”. In: *Atmospheric Chemistry and Physics* 15.15, pp. 8889–8973. DOI: [10.5194/acp-15-8889-2015](https://doi.org/10.5194/acp-15-8889-2015).
- Moore, R. M. and N. V. Blough (2002). “A marine source of methyl nitrate”. In: *Geophysical Research Letters* 29.15, pp. 27–1–27–4. DOI: [10.1029/2002gl014989](https://doi.org/10.1029/2002gl014989).
- Morgenstern, O., P. Braesicke, F. M. O’Connor, A. C. Bushell, C. E. Johnson, S. M. Osprey, and J. A. Pyle (2009). “Evaluation of the new UKCA climate-composition model – Part 1: The stratosphere”. In: *Geoscientific Model Development* 2.1, pp. 43–57. DOI: [10.5194/gmd-2-43-2009](https://doi.org/10.5194/gmd-2-43-2009).
- Morgenstern, O., M. Hegglin, E. Rozanov, F. O’Connor, N. Luke Abraham, H. Akiyoshi, A. Archibald, S. Bekki, N. Butchart, M. Chipperfield, M. Deushi, S. Dhomse, R. Garcia, S. Hardiman, L. Horowitz, P. Jöckel, B. Josse, D. Kinnison, M. Lin, E. Mancini, M. Manyin, M. Marchand, V. Marécal, M. Michou, L. Oman, G. Pitari, D. Plummer, L. Revell, D. Saint-Martin, R. Schofield, A. Stenke, K. Stone, K. Sudo, T. Tanaka, S. Tilmes, Y. Yamashita, K. Yoshida, and G. Zeng (2017). “Review of the global models used within phase 1 of the Chemistry-Climate Model Initiative (CCMI)”. In: *Geoscientific Model Development* 10.2, pp. 639–671. DOI: [10.5194/gmd-10-639-2017](https://doi.org/10.5194/gmd-10-639-2017).
- Muthuramu, K., P. B. Shepson, J. W. Bottenheim, B. T. Jobson, H. Niki, and K. G. Anlauf (1994). “Relationships between organic nitrates and surface ozone destruction during Polar Sunrise Experiment 1992”. In: *Journal of Geophysical Research* 99.D12, pp. 25369–25378. DOI: [10.1029/94JD01309](https://doi.org/10.1029/94JD01309).
- Myhre, G., D. T. Shindell, F.-M. Bréon, W. J. Collins, J. Fuglestedt, J. Huang, D. Koch, J.-F. Lamarque, D. Lee, B. Mendoza, T. Nakajima, A. Robock, G. Stephens,

- T Takemura, and H Zhan (2013). “Anthropogenic and Natural Radiative Forcing”. In: *Climate Change 2013: The Physical Science Basis. Contribution of Working Group I to the Fifth Assessment Report of the Intergovernmental Panel on Climate Change*. Ed. by T. Stocker, D Qin, G.-K. Plattner, M Tignor, S. Allen, J Boschung, A Nauels, Y Xia, V Bex, and P. Midgley. Cambridge, United Kingdom and New York, NY, USA: Cambridge University Press. Chap. 8, pp. 659–740. DOI: [10.1017/CB09781107415324.018](https://doi.org/10.1017/CB09781107415324.018).
- Naik, V., A. Voulgarakis, A. M. Fiore, L. W. Horowitz, J. F. Lamarque, M. Lin, M. J. Prather, P. J. Young, D. Bergmann, P. J. Cameron-Smith, I. Cionni, W. J. Collins, S. B. Dalsøren, R. Doherty, V. Eyring, G. Faluvegi, G. A. Folberth, B. Josse, Y. H. Lee, I. A. MacKenzie, T. Nagashima, T. P. C. Van Noije, D. A. Plummer, M. Righi, S. T. Rumbold, R. Skeie, D. T. Shindell, D. S. Stevenson, S. Strode, K. Sudo, S. Szopa, and G. Zeng (2013). “Preindustrial to present-day changes in tropospheric hydroxyl radical and methane lifetime from the Atmospheric Chemistry and Climate Model Intercomparison Project (ACCMIP)”. In: *Atmospheric Chemistry and Physics* 13.10, pp. 5277–5298. DOI: [10.5194/acp-13-5277-2013](https://doi.org/10.5194/acp-13-5277-2013).
- Nault, B. A., J. L. Laughner, P. J. Wooldridge, J. D. Crouse, J. Dibb, G. Diskin, J. Peischl, J. R. Podolske, I. B. Pollack, T. B. Ryerson, E. Scheuer, P. O. Wennberg, and R. C. Cohen (2017). “Lightning NO<sub>x</sub> Emissions: Reconciling Measured and Modeled Estimates With Updated NO<sub>x</sub> Chemistry”. In: *Geophysical Research Letters* 44.18, pp. 9479–9488. DOI: [10.1002/2017GL074436](https://doi.org/10.1002/2017GL074436).
- Neu, J. L., M. J. Lawler, M. J. Prather, and E. S. Saltzman (2008). “Oceanic alkyl nitrates as a natural source of tropospheric ozone”. In: *Geophysical Research Letters* 35.L13814, pp. 1–6. DOI: [10.1029/2008GL034189](https://doi.org/10.1029/2008GL034189).
- Newsome, B. and M. Evans (2017). “Impact of uncertainties in inorganic chemical rate constants on tropospheric composition and ozone radiative forcing”. In: *Atmospheric Chemistry and Physics* 17.23, pp. 14333–14352. DOI: [10.5194/acp-17-14333-2017](https://doi.org/10.5194/acp-17-14333-2017).
- Nicely, J. M., R. J. Salawitch, T. Canty, D. C. Anderson, S. R. Arnold, M. P. Chipperfield, L. K. Emmons, J. Flemming, V. Huijnen, D. E. Kinnison, J. Lamarque, J. Mao, S. A. Monks, S. D. Steenrod, S. Tilmes, and S. Turquety (2017). “Quantifying the causes of differences in tropospheric OH within global models”. In: *Journal of Geophysical Research: Atmospheres* 122, pp. 1983–2007. DOI: [10.1002/2016JD026239](https://doi.org/10.1002/2016JD026239).
- O’Connor, F. M., C. E. Johnson, O Morgenstern, N. L. Abraham, P Braesicke, M Dalvi, G. A. Folberth, M. G. Sanderson, P. J. Telford, A Voulgarakis, P. J. Young, G Zeng, W. J. Collins, and J. A. Pyle (2014). “Evaluation of the new UKCA climate-composition model – Part 2: The Troposphere”. In: *Geoscientific Model Development* 7, pp. 41–91. DOI: [10.5194/gmd-7-41-2014](https://doi.org/10.5194/gmd-7-41-2014).
- Parrish, D. D., Y. Kondo, O. R. Cooper, C. A. Brock, D. A. Jaffe, M. Trainer, T. Ogawa, G. Hübler, and F. C. Fehsenfeld (2004). “Intercontinental Transport and



- Chemical Transformation 2002 (ITCT 2K2) and Pacific Exploration of Asian Continental Emission (PEACE) experiments: An overview of the 2002 winter and spring intensives”. In: *Journal of Geophysical Research D: Atmospheres* 109.23, pp. 1–13. DOI: [10.1029/2004JD004980](https://doi.org/10.1029/2004JD004980).
- Parrish, D. D., D. T. Allen, T. S. Bates, M. Estes, F. C. Fehsenfeld, G. Feingold, R. Ferrare, R. M. Hardesty, J. F. Meagher, J. W. Nielsen-Gammon, R. B. Pierce, T. B. Ryerson, J. H. Seinfeld, and E. J. Williams (2009). “Overview of the Second Texas Air Quality Study (TexAQS II) and the Gulf of Mexico Atmospheric Composition and Climate Study (GoMACCS)”. In: *Journal of Geophysical Research Atmospheres* 114.D00F13, pp. 1–28. DOI: [10.1029/2009JD011842](https://doi.org/10.1029/2009JD011842).
- Passant, N. R. (2002). “Speciation of UK emissions of non-methane volatile organic compounds”. In: *AEA Technology Report ENV-0545* 1, pp. 1–289.
- Patra, P. K., M. C. Krol, S. A. Montzka, T. Arnold, E. L. Atlas, B. R. Lintner, B. B. Stephens, B. Xiang, J. W. Elkins, P. J. Fraser, A. Ghosh, E. J. Hintsa, D. F. Hurst, K. Ishijima, P. B. Krummel, B. R. Miller, K. Miyazaki, F. L. Moore, J. Mühle, S. O’Doherty, R. G. Prinn, L. P. Steele, M. Takigawa, H. J. Wang, R. F. Weiss, S. C. Wofsy, and D. Young (2014). “Observational evidence for interhemispheric hydroxyl-radical parity”. In: *Nature* 513.7517, pp. 219–223. DOI: [10.1038/nature13721](https://doi.org/10.1038/nature13721).
- Perring, A. E., S. E. Pusede, and R. C. Cohen (2013). “An observational perspective on the atmospheric impacts of alkyl and multifunctional nitrates on ozone and secondary organic aerosol”. In: *Chemical Reviews* 113.8, pp. 5848–5870. DOI: [10.1021/cr300520x](https://doi.org/10.1021/cr300520x).
- Pöschl, U., R. Von Kuhlmann, N. Poisson, and P. J. Crutzen (2000). “Development and intercomparison of condensed isoprene oxidation mechanisms for global atmospheric modeling”. In: *Journal of Atmospheric Chemistry* 37.1, pp. 29–52. DOI: [10.1023/A:1006391009798](https://doi.org/10.1023/A:1006391009798).
- Prather, M. J., X. Zhu, C. M. Flynn, S. A. Strode, J. M. Rodriguez, S. D. Steenrod, J. Liu, J. F. Lamarque, A. M. Fiore, L. W. Horowitz, J. Mao, L. T. Murray, D. T. Shindell, and S. C. Wofsy (2017). “Global atmospheric chemistry - Which air matters”. In: *Atmospheric Chemistry and Physics* 17.14, pp. 9081–9102. DOI: [10.5194/acp-17-9081-2017](https://doi.org/10.5194/acp-17-9081-2017).
- Radenac, M. H., F. Léger, A. Singh, and T. Delcroix (2012). “Sea surface chlorophyll signature in the tropical Pacific during eastern and central Pacific ENSO events”. In: *Journal of Geophysical Research: Oceans* 117.4, pp. 1–15. DOI: [10.1029/2011JC007841](https://doi.org/10.1029/2011JC007841).
- Rayner, N. A., D. E. Parker, E. B. Horton, C. K. Folland, L. V. Alexander, D. P. Rowell, E. C. Kent, and A. Kaplan (2003). “Global analyses of sea surface temperature, sea ice, and night marine air temperature since the late nineteenth century”. In: *Journal of Geophysical Research* 108.D14, p. 4407. DOI: [10.1029/2002JD002670](https://doi.org/10.1029/2002JD002670).

- Reeves, C. E., J. Slemr, D. E. Oram, D. R. Worton, S. A. Penkett, D. J. Stewart, R. M. Purvis, N. Watson, J. Hopkins, A. Lewis, J. Methven, D. R. Blake, and E. Atlas (2007). “Alkyl nitrates in outflow from North America over the North Atlantic during Intercontinental Transport of Ozone and Precursors 2004”. In: *Journal of Geophysical Research* 112.D10S37. DOI: [10.1029/2006JD007567](https://doi.org/10.1029/2006JD007567).
- Rhew, R. C., M. J. Deventer, A. A. Turnipseed, C. Warneke, J. Ortega, S. Shen, L. Martinez, A. Koss, B. M. Lerner, J. B. Gilman, J. N. Smith, A. B. Guenther, and J. A. De Gouw (2017). “Ethene, propene, butene and isoprene emissions from a ponderosa pine forest measured by relaxed eddy accumulation”. In: *Atmospheric Chemistry and Physics* 17.21, pp. 13417–13438. DOI: [10.5194/acp-17-13417-2017](https://doi.org/10.5194/acp-17-13417-2017).
- Roberts, J. M. (1990). “The atmospheric chemistry of organic nitrates”. In: *Atmospheric Environment* 24A.2, pp. 243–287. DOI: [10.1016/0960-1686\(90\)90108-Y](https://doi.org/10.1016/0960-1686(90)90108-Y).
- Roberts, J. M., S. B. Bertman, D. D. Parrish, F. C. Fehsenfeld, B. T. Jobson, and H. Niki (1998). “Measurement of alkyl nitrates at Chebogue Point, Nova Scotia during the 1993 North Atlantic Regional Experiment (NARE) intensive”. In: *Journal of Geophysical Research* 103.D11, pp. 13569–13580. DOI: [10.1029/98JD00266](https://doi.org/10.1029/98JD00266).
- Robertson, R. E., K. M. Koshy, A. Annessa, J. N. Ong, J. M. W. Scott, and M. J. Blandamer (1982). “Kinetics of solvolysis in water of four secondary alkyl nitrates”. In: *Canadian Journal of Chemistry* 60, pp. 1780–1785. DOI: [10.1139/v82-244](https://doi.org/10.1139/v82-244).
- Russo, R. S., Y. Zhou, K. B. Haase, O. W. Wingenter, E. K. Frinak, H. Mao, R. W. Talbot, and B. C. Sive (2010). “Temporal variability, sources, and sinks of C1-C5 alkyl nitrates in coastal New England”. In: *Atmospheric Chemistry and Physics* 10.4, pp. 1865–1883. DOI: [10.5194/acp-10-1865-2010](https://doi.org/10.5194/acp-10-1865-2010).
- Sander, R. (2015). “Compilation of Henry’s law constants (version 4.0) for water as solvent”. In: *Atmospheric Chemistry and Physics* 15.8, pp. 4399–4981. DOI: [10.5194/acp-15-4399-2015](https://doi.org/10.5194/acp-15-4399-2015).
- Sathyendranath, S., R. J. Brewin, C. Brockmann, V. Brotas, B. Calton, A. Chuprin, P. Cipollini, A. B. Couto, J. Dingle, R. Doerffer, C. Donlon, M. Dowell, A. Farman, M. Grant, S. Groom, A. Horseman, T. Jackson, H. Krasemann, S. Lavender, V. Martinez-Vicente, C. Mazeran, F. Mélin, T. S. Moore, D. Müller, P. Regner, S. Roy, C. J. Steele, F. Steinmetz, J. Swinton, M. Taberner, A. Thompson, A. Valente, M. Zühlke, V. E. Brando, H. Feng, G. Feldman, B. A. Franz, R. Frouin, R. W. Gould, S. B. Hooker, M. Kahru, S. Kratzer, B. G. Mitchell, F. E. Muller-Karger, H. M. Sosik, K. J. Voss, J. Werdell, and T. Platt (2019). “An ocean-colour time series for use in climate studies: The experience of the ocean-colour climate change initiative (OC-CCI)”. In: *Sensors (Switzerland)* 19.19. DOI: [10.3390/s19194285](https://doi.org/10.3390/s19194285).

- Saunders, S. M., M. E. Jenkin, R. G. Derwent, and M. J. Pilling (2003). “Protocol for the development of the Master Chemical Mechanism, MCM v3 (Part A): tropospheric degradation of non-aromatic volatile organic compounds”. In: *Atmospheric Chemistry and Physics* 3.1, pp. 161–180. DOI: [10.5194/acp-3-161-2003](https://doi.org/10.5194/acp-3-161-2003).
- Sherwen, T., M. J. Evans, L. J. Carpenter, J. A. Schmidt, and L. J. Mickley (2017). “Halogen chemistry reduces tropospheric O<sub>3</sub> radiative forcing”. In: *Atmospheric Chemistry and Physics* 17.2, pp. 1557–1569. DOI: [10.5194/acp-17-1557-2017](https://doi.org/10.5194/acp-17-1557-2017).
- Shindell, D. T., M. Chin, F. Dentener, R. M. Doherty, G. Faluvegi, A. M. Fiore, P. Hess, and D. M. Koch (2008). “A multi-model assessment of pollution transport to the Arctic”. In: *Atmospheric Chemistry and Physics* 8.17, pp. 5353–5372. DOI: [10.5194/acp-8-5353-2008](https://doi.org/10.5194/acp-8-5353-2008).
- Sillman, S. (1999). “The relation between ozone, NO<sub>x</sub> and hydrocarbons in urban and polluted rural environments”. In: *Atmospheric Environment* 33.12, pp. 1821–1845. DOI: [10.1016/S1352-2310\(98\)00345-8](https://doi.org/10.1016/S1352-2310(98)00345-8).
- Simpson, I. J., S. Meinardi, D. R. Blake, N. J. Blake, and F. S. Rowland (2002). “A biomass burning source of C<sub>1</sub>–C<sub>4</sub> alkyl nitrates”. In: *Geophysical Research Letters* 29.24, p. 2168. DOI: [10.1029/2002GL016290](https://doi.org/10.1029/2002GL016290).
- Simpson, I. J., T. Wang, H. Guo, Y. H. Kwok, F. Flocke, E. Atlas, S. Meinardi, F. S. Rowland, and D. R. Blake (2006). “Long-term atmospheric measurements of C<sub>1</sub>–C<sub>5</sub> alkyl nitrates in the Pearl River Delta region of southeast China”. In: *Atmospheric Environment* 40.9, pp. 1619–1632. DOI: [10.1016/j.atmosenv.2005.10.062](https://doi.org/10.1016/j.atmosenv.2005.10.062).
- Simpson, I. J., F. Flocke, E. Atlas, F. S. Rowland, S. Meinardi, T. Wang, H. Guo, Y. H. Kwok, and D. R. Blake (2007). “Reply to ‘Comment on ‘Long-term atmospheric measurements of C<sub>1</sub>–C<sub>5</sub> alkyl nitrates in the Pearl River Delta region of southeast China’””. In: *Atmospheric Environment* 41.34, pp. 7371–7372. DOI: [10.1016/j.atmosenv.2007.07.016](https://doi.org/10.1016/j.atmosenv.2007.07.016).
- Sommariva, R., M. Trainer, J. A. de Gouw, J. M. Roberts, C. Warneke, E. Atlas, F. Flocke, P. D. Goldan, W. C. Kuster, A. L. Swanson, and F. C. Fehsenfeld (2008). “A study of organic nitrates formation in an urban plume using a Master Chemical Mechanism”. In: *Atmospheric Environment* 42.23, pp. 5771–5786. DOI: [10.1016/j.atmosenv.2007.12.031](https://doi.org/10.1016/j.atmosenv.2007.12.031).
- Spivakovsky, C. M., J. A. Logan, S. A. Montzka, Y. J. Balkanski, M. Foreman-Fowler, D. B. Jones, L. W. Horowitz, A. C. Fusco, C. A. Brenninkmeijer, M. J. Prather, S. C. Wofsy, and M. B. McElroy (2000). “Three-dimensional climatological distribution of tropospheric OH: Update and evaluation”. In: *Journal of Geophysical Research* 105.D7, pp. 8931–8980. DOI: [10.1029/1999JD901006](https://doi.org/10.1029/1999JD901006).
- Squire, O. J., A. T. Archibald, N. L. Abraham, D. J. Beerling, C. N. Hewitt, J. Lathière, R. C. Pike, P. J. Telford, and J. A. Pyle (2014). “Influence of future climate and cropland expansion on isoprene emissions and tropospheric ozone”. In: *Atmospheric Chemistry and Physics* 14.2, pp. 1011–1024. DOI: [10.5194/acp-14-1011-2014](https://doi.org/10.5194/acp-14-1011-2014).

- Squire, O. J., A. T. Archibald, P. T. Griffiths, M. E. Jenkin, D. Smith, and J. A. Pyle (2015). “Influence of isoprene chemical mechanism on modelled changes in tropospheric ozone due to climate and land use over the 21st century”. In: *Atmospheric Chemistry and Physics* 15.9, pp. 5123–5143. DOI: [10.5194/acp-15-5123-2015](https://doi.org/10.5194/acp-15-5123-2015).
- Stephens, B. B., M. C. Long, R. F. Keeling, E. A. Kort, C. Sweeney, E. C. Apel, E. L. Atlas, S. Beaton, J. D. Bent, N. J. Blake, J. F. Bresch, J. Casey, B. C. Daube, M. Diao, E. Diaz, H. Dierssen, V. Donets, B. C. Gao, M. Gierach, R. Green, J. Haag, M. Hayman, A. J. Hills, M. S. Hoecker-Martínez, S. B. Honomichl, R. S. Hornbrook, J. B. Jensen, R. R. Li, I. McCubbin, K. McKain, E. J. Morgan, S. Nolte, J. G. Powers, B. Rainwater, K. Randolph, M. Reeves, S. M. Schauffler, K. Smith, M. Smith, J. Stith, G. Stossmeister, D. W. Toohey, and A. S. Watt (2018). “The O<sub>2</sub>/N<sub>2</sub> ratio and CO<sub>2</sub> airborne Southern Ocean study”. In: *Bulletin of the American Meteorological Society* 99.2, pp. 381–402. DOI: [10.1175/BAMS-D-16-0206.1](https://doi.org/10.1175/BAMS-D-16-0206.1).
- Stockwell, W. R., C. V. Lawson, E. Saunders, and W. S. Goliff (2012). “A Review of Tropospheric Atmospheric Chemistry and Gas-Phase Chemical Mechanisms for Air Quality Modeling”. In: *Atmosphere* 3, pp. 1–32. DOI: [10.3390/atmos3010001](https://doi.org/10.3390/atmos3010001).
- Stone, D., L. K. Whalley, and D. E. Heard (2012). “Tropospheric OH and HO<sub>2</sub> radicals: field measurements and model comparisons”. In: *Chemical Society Reviews* 41, pp. 6348–6404. DOI: [10.1039/c2cs35140d](https://doi.org/10.1039/c2cs35140d).
- Strode, S. A., J. Liu, L. Lait, R. Commane, B. Daube, S. Wofsy, A. Conaty, P. Newman, and M. Prather (2018). “Forecasting carbon monoxide on a global scale for the ATom-1 aircraft mission: Insights from airborne and satellite observations and modeling”. In: *Atmospheric Chemistry and Physics* 18.15, pp. 10955–10971. DOI: [10.5194/acp-18-10955-2018](https://doi.org/10.5194/acp-18-10955-2018).
- Swanson, A. L., N. J. Blake, E. Atlas, F. Flocke, D. R. Blake, and F. S. Rowland (2003). “Seasonal variations of C<sub>2</sub>–C<sub>4</sub> nonmethane hydrocarbons and C<sub>1</sub>–C<sub>4</sub> alkyl nitrates at the Summit research station in Greenland”. In: *Journal of Geophysical Research* 108.D2, p. 4065. DOI: [10.1029/2001JD001445](https://doi.org/10.1029/2001JD001445).
- Szopa, S., B. Aumont, and S. Madronich (2005). “Assessment of the reduction methods used to develop chemical schemes: building of a new chemical scheme for VOC oxidation suited to three-dimensional multiscale HO<sub>x</sub>-NO<sub>x</sub>-VOC chemistry simulations”. In: *Atmospheric Chemistry and Physics* 5.9, pp. 2519–2538. DOI: [10.5194/acp-5-2519-2005](https://doi.org/10.5194/acp-5-2519-2005).
- Talbot, R. W., J. E. Dibb, E. M. Scheuer, J. D. Bradshaw, S. T. Sandholm, H. B. Singh, D. R. Blake, N. J. Blake, E. Atlas, and F. Flocke (2000). “Tropospheric reactive odd nitrogen over the South Pacific in austral springtime”. In: *Journal of Geophysical Research* 105.D5, pp. 6681–6694. DOI: [10.1029/1999JD901114](https://doi.org/10.1029/1999JD901114).
- Talukdar, K. R., C. S. Herndon, B. J. Burkholder, M. J. Roberts, and R. A. Ravishankara (1997a). “Atmospheric fate of several alkyl nitrates Part 1 Rate coefficients

- of the reactions of alkyl nitrates with isotopically labelled hydroxyl radicals”. In: *Faraday Transactions* 93.16, p. 2787. DOI: [10.1039/a701780d](https://doi.org/10.1039/a701780d).
- Talukdar, R. K., J. B. Burkholder, A.-M. Schmoltner, J. M. Roberts, R. R. Wilson, and A. R. Ravishankara (1995). “Investigation of the loss processes for peroxyacetyl nitrate in the atmosphere: UV photolysis and reaction with OH”. In: *Journal of Geophysical Research* 100.D7, pp. 14163–14173. DOI: [10.1029/95JD00545](https://doi.org/10.1029/95JD00545).
- Talukdar, R. K., J. B. Burkholder, M. Hunter, M. K. Gilles, J. M. Roberts, and A. R. Ravishankara (1997b). “Atmospheric fate of several alkyl nitrates Part 2 UV absorption cross-sections and photodissociation quantum yields Ranajit”. In: *Faraday Transactions* 93.16, pp. 2797–2805. DOI: [10.1039/A701781B](https://doi.org/10.1039/A701781B).
- Tarasick, D. W. and R Slater (2008). “Ozone in the troposphere: Measurements, climatology, budget, and trends”. In: *Atmosphere-Ocean* 46.1, pp. 93–115. DOI: [10.3137/ao.460105](https://doi.org/10.3137/ao.460105).
- Tarasick, D., I. E. Galbally, O. R. Cooper, M. G. Schultz, G. Ancellet, T. Leblanc, T. J. Wallington, J. Ziemke, X. Liu, M. Steinbacher, J. Staehelin, C. Vigouroux, J. W. Hannigan, O. García, G. Foret, P. Zanis, E. Weatherhead, I. Petropavlovskikh, H. Worden, M. Osman, J. Liu, K.-L. Chang, A. Gaudel, M. Lin, M. Granados-Muñoz, A. M. Thompson, S. J. Oltmans, J. Cuesta, G. Dufour, V. Thouret, B. Hassler, T. Trickl, and J. L. Neu (2019). “Tropospheric Ozone Assessment Report: Tropospheric ozone from 1877 to 2016, observed levels, trends and uncertainties”. In: *Elementa: Science of the Anthropocene* 7.1, p. 39. DOI: [10.1525/elementa.376](https://doi.org/10.1525/elementa.376).
- Telford, P. J., N. L. Abraham, A. T. Archibald, P. Braesicke, M. Dalvi, O. Morgenstern, F. M. O’Connor, N. A. D. Richards, and J. A. Pyle (2013). “Implementation of the Fast-JX Photolysis scheme (v6.4) into the UKCA component of the MetUM chemistry-climate model (v7.3)”. In: *Geoscientific Model Development* 6.1, pp. 161–177. DOI: [10.5194/gmd-6-161-2013](https://doi.org/10.5194/gmd-6-161-2013).
- The Royal Society (2008). *Ground-level ozone in the 21st century: future trends, impacts and policy implications*. Tech. rep. Royal Society policy document 15/08. London: The Royal Society.
- Toon, O. B., H. Maring, J. Dibb, R. Ferrare, D. J. Jacob, E. J. Jensen, Z. J. Luo, G. G. Mace, L. L. Pan, L. Pfister, K. H. Rosenlof, J. Redemann, J. S. Reid, H. B. Singh, A. M. Thompson, R. Yokelson, P. Minnis, G. Chen, K. W. Jucks, and A. Pszenny (2016). “Planning, implementation, and scientific goals of the Studies of Emissions and Atmospheric Composition, Clouds and Climate Coupling by Regional Surveys (SEAC4RS) field mission”. In: *Journal of Geophysical Research: Atmospheres* 121, pp. 4967–5009. DOI: [10.1002/2015JD024297](https://doi.org/10.1002/2015JD024297).
- Turberg, M., D. Giolando, C Tilt, T Soper, S Mason, M Davies, P Klingensmith, and G. Takacs (1990). “Atmospheric photochemistry of alkyl nitrates”. In: *Journal of Photochemistry and Photobiology A: Chemistry* 51, pp. 281–292. DOI: [10.1016/1010-6030\(90\)87063-H](https://doi.org/10.1016/1010-6030(90)87063-H).

- Vingarzan, R. (2004). “A review of surface ozone background levels and trends”. In: *Atmospheric Environment* 38.21, pp. 3431–3442. DOI: [10.1016/j.atmosenv.2004.03.030](https://doi.org/10.1016/j.atmosenv.2004.03.030).
- Volz, A. and D. Kley (1988). “Evaluation of the Montsouris series of ozone measurements made in the nineteenth century”. In: *Nature* 332.17, pp. 240–242. DOI: [10.1038/332240a0](https://doi.org/10.1038/332240a0).
- Walega, J. G., B. A. Ridley, S. Madronich, F. E. Grahek, J. D. Shetter, T. D. Sauvain, C. J. Hahn, J. T. Merrill, B. A. Bodhaine, and E. Robinson (1992). “Observations of peroxyacetyl nitrate, peroxypropionyl nitrate, methyl nitrate and ozone during the Mauna Loa Observatory Photochemistry Experiment”. In: *Journal of Geophysical Research* 97.D10, pp. 10311–10330. DOI: [10.1029/91JD02288](https://doi.org/10.1029/91JD02288).
- Walters, D. N., M. J. Best, A. C. Bushell, D. Copsey, J. M. Edwards, P. D. Falloon, C. M. Harris, A. P. Lock, J. C. Manners, C. J. Morcrette, M. J. Roberts, R. A. Stratton, S. Webster, J. M. Wilkinson, M. R. Willett, I. A. Boutle, P. D. Earnshaw, P. G. Hill, C. MacLachlan, G. M. Martin, W. Moufouma-Okia, M. D. Palmer, J. C. Petch, G. G. Rooney, A. A. Scaife, and K. D. Williams (2011). “The Met Office Unified Model Global Atmosphere 3.0/3.1 and JULES Global Land 3.0/3.1 configurations”. In: *Geoscientific Model Development* 4.4, pp. 919–941. DOI: [10.5194/gmd-4-919-2011](https://doi.org/10.5194/gmd-4-919-2011).
- Werf, G. R. van der, J. T. Randerson, L. Giglio, T. T. Van Leeuwen, Y. Chen, B. M. Rogers, M. Mu, M. J. Van Marle, D. C. Morton, G. J. Collatz, R. J. Yokelson, and P. S. Kasibhatla (2017). “Global fire emissions estimates during 1997–2016”. In: *Earth System Science Data* 9.2, pp. 697–720. DOI: [10.5194/essd-9-697-2017](https://doi.org/10.5194/essd-9-697-2017).
- Whitehouse, L. E., A. S. Tomlin, and M. J. Pilling (2004). “Systematic reduction of complex tropospheric chemical mechanisms using sensitivity and time-scale analyses”. In: *Atmospheric Chemistry and Physics* 4.7, pp. 2025–2056. DOI: [10.5194/acp-4-2057-2004](https://doi.org/10.5194/acp-4-2057-2004).
- Wild, O., J. K. Sundet, M. J. Prather, I. S. A. Isaksen, H. Akimoto, E. V. Browell, and S. J. Oltmans (2003). “Chemical transport model ozone simulations for spring 2001 over the western Pacific: Comparisons with TRACE-P lidar, ozonesondes, and Total Ozone Mapping Spectrometer columns”. In: *Journal of Geophysical Research* 108.D21, p. 8826. DOI: [10.1029/2002JD003283](https://doi.org/10.1029/2002JD003283).
- Wilks, D. S. (2006). “On “field significance” and the false discovery rate”. In: *Journal of Applied Meteorology and Climatology* 45.9, pp. 1181–1189. DOI: [10.1175/JAM2404.1](https://doi.org/10.1175/JAM2404.1).
- Wilks, D. (2016). “The stippling shows statistically significant grid points”. In: *Bulletin of the American Meteorological Society* 97.December, pp. 2263–2274. DOI: [10.1175/BAMS-D-15-00267.1](https://doi.org/10.1175/BAMS-D-15-00267.1).
- Williams, J., G Le Bras, A Kukui, H Ziereis, and C. Brenninkmeijer (2014). “The impact of the chemical production of methyl nitrate from the NO + CH<sub>3</sub>O<sub>2</sub> reaction on



- the global distributions of alkyl nitrates, nitrogen oxides and tropospheric ozone: a global modelling study”. In: *Atmospheric Chemistry and Physics* 14.5, pp. 2363–2382. DOI: [10.5194/acp-14-2363-2014](https://doi.org/10.5194/acp-14-2363-2014).
- Wofsy, S. C. (2011). “HIAPER Pole-to-Pole Observations (HIPPO): Fine-grained, global-scale measurements of climatically important atmospheric gases and aerosols”. In: *Philosophical Transactions of the Royal Society A: Mathematical, Physical and Engineering Sciences* 369.1943, pp. 2073–2086. DOI: [10.1098/rsta.2010.0313](https://doi.org/10.1098/rsta.2010.0313).
- Wofsy, S. C. et al. (2018). *ATom: Merged Atmospheric Chemistry, Trace Gases, and Aerosols*. DOI: [10.3334/ORNLDAAC/1581](https://doi.org/10.3334/ORNLDAAC/1581).
- Worton, D. R., C. E. Reeves, S. A. Penkett, W. T. Sturges, J. Slemr, D. E. Oram, B. J. Bandy, W. J. Bloss, N. Carslaw, J. Davey, K. M. Emmerson, T. J. Gravestock, J. F. Hamilton, D. E. Heard, J. R. Hopkins, A. Hulse, T. Ingram, M. J. Jacob, J. D. Lee, R. J. Leigh, A. C. Lewis, P. S. Monks, and S. C. Smith (2010). “Alkyl nitrate photochemistry during the tropospheric organic chemistry experiment”. In: *Atmospheric Environment* 44.6, pp. 773–785. DOI: [10.1016/j.atmosenv.2009.11.038](https://doi.org/10.1016/j.atmosenv.2009.11.038).
- Xia, L., J. P. Nowack, S. Tilmes, and A. Robock (2017). “Impacts of stratospheric sulfate geoengineering on tropospheric ozone”. In: *Atmospheric Chemistry and Physics* 17.19, pp. 11913–11928. DOI: [10.5194/acp-17-11913-2017](https://doi.org/10.5194/acp-17-11913-2017).
- Xiao, Y., D. J. Jacob, and S. Turquety (2007). “Atmospheric acetylene and its relationship with CO as an indicator of air mass age”. In: *Journal of Geophysical Research* 112.D12305. DOI: [10.1029/2006JD008268](https://doi.org/10.1029/2006JD008268).
- Xiao, Y., J. A. Logan, D. J. Jacob, R. C. Hudman, R. Yantosca, and D. R. Blake (2008). “Global budget of ethane and regional constraints on U.S. sources”. In: *Journal of Geophysical Research* 113.D21306. DOI: [10.1029/2007JD009415](https://doi.org/10.1029/2007JD009415).
- Yarwood, G., S. Rao, M. Yocke, and G. Z. Whitten (2005). *Updates to the Carbon Bond chemical mechanism: CB05*. Tech. rep., p. 246.
- Yeung, L. Y., L. T. Murray, P. Martinerie, E. Witrant, H. Hu, A. Banerjee, A. Orsi, and J. Chappellaz (2019). “Isotopic constraint on the twentieth-century increase in tropospheric ozone”. In: *Nature* 570.7760, pp. 224–227. DOI: [10.1038/s41586-019-1277-1](https://doi.org/10.1038/s41586-019-1277-1).
- Young, P. J. (2007). “Ph.D thesis”. PhD thesis. University of Cambridge.
- Young, P. J., A. T. Archibald, K. W. Bowman, J.-F. Lamarque, V. Naik, D. S. Stevenson, S. Tilmes, A. Voulgarakis, O. Wild, D. J. Bergmann, P. Cameron-Smith, I. Cionni, W. J. Collins, S. B. Dalsøren, R. M. Doherty, V. Eyring, G. Faluvegi, L. W. Horowitz, B. Josse, Y. H. Lee, I. A. MacKenzie, T. Nagashima, D. A. Plummer, M. Righi, S. T. Rumbold, R. B. Skeie, D. T. Shindell, S. A. Strode, K. Sudo, S. Szopa, and G. Zeng (2013). “Pre-industrial to end 21st century projections of tropospheric ozone

- from the Atmospheric Chemistry and Climate Model Intercomparison Project (ACCMIP)”. In: *Atmospheric Chemistry and Physics* 13, pp. 2063–2090. DOI: [10.5194/acp-13-2063-2013](https://doi.org/10.5194/acp-13-2063-2013).
- Young, P. J., V. Naik, A. M. Fiore, A. Gaudel, J. Guo, M. Y. Lin, J. L. Neu, D. D. Parrish, H. E. Rieder, J. L. Schnell, S. Tilmes, O. Wild, L. Zhang, J. Ziemke, J. Brandt, A. Delcloo, R. M. Doherty, C. Geels, M. I. Hegglin, L. Hu, U. Im, R. Kumar, A. Luhar, L. Murray, D. Plummer, J. Rodriguez, A. Saiz-Lopez, M. G. Schultz, M. T. Woodhouse, and G. Zeng (2018). “Tropospheric ozone assessment report: Assessment of global-scale model performance for global and regional ozone distributions, variability, and trends”. In: *Elementa: Science of the Anthropocene* 6. DOI: [10.1525/elementa.265](https://doi.org/10.1525/elementa.265).
- Zheng, B., F. Chevallier, P. Ciais, Y. Yin, and Y. Wang (2018). “On the Role of the Flaming to Smoldering Transition in the Seasonal Cycle of African Fire Emissions”. In: *Geophysical Research Letters* 45.21, pp. 11,998–12,007. DOI: [10.1029/2018GL079092](https://doi.org/10.1029/2018GL079092).
- Zhu, L. and D. Kellis (1997). “Temperature dependence of the UV absorption cross sections and photodissociation products of C3-C5 alkyl nitrates”. In: *Chemical Physics Letters* 278.1-3, pp. 41–48. DOI: [10.1016/S0009-2614\(97\)01011-7](https://doi.org/10.1016/S0009-2614(97)01011-7).
- Ziska, F., B. Quack, K. Abrahamsson, S. D. Archer, E. Atlas, T. Bell, J. H. Butler, L. J. Carpenter, C. E. Jones, N. R. Harris, H. Hepach, K. G. Heumann, C. Hughes, J. Kuss, K. Krüger, P. Liss, R. M. Moore, A. Orlikowska, S. Raimund, C. E. Reeves, W. Reifenhäuser, A. D. Robinson, C. Schall, T. Tanhua, S. Tegtmeier, S. Turner, L. Wang, D. Wallace, J. Williams, H. Yamamoto, S. Yvon-Lewis, and Y. Yokouchi (2013). “Global sea-to-air flux climatology for bromoform, dibromomethane and methyl iodide”. In: *Atmospheric Chemistry and Physics* 13.17, pp. 8915–8934. DOI: [10.5194/acp-13-8915-2013](https://doi.org/10.5194/acp-13-8915-2013).